frontiers | Research Topics

Innovative drug combinations for enhanced solid tumor treatment efficacy

Edited by
Giovanna Damia and Massimo Broggini

Published in
Frontiers in Oncology

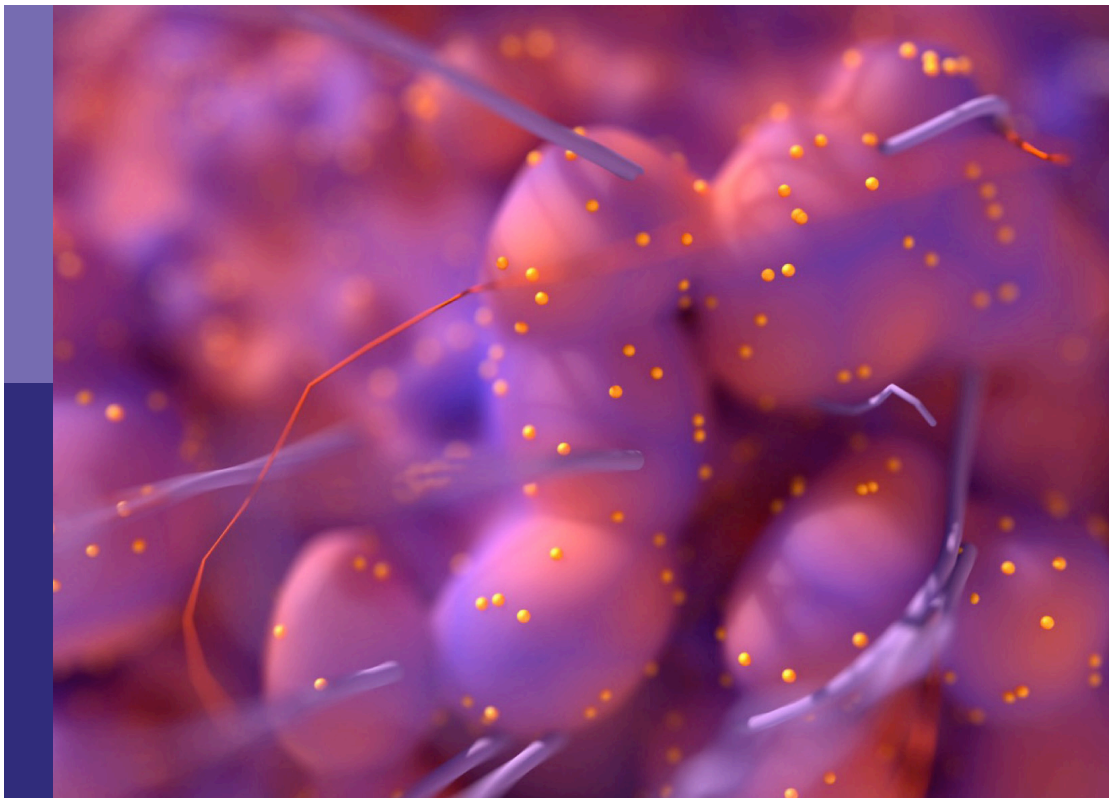

ISSN 1664-8714
ISBN 978-2-8325-7377-8
DOI 10.3389/978-2-8325-7377-8

Generative AI statement
Any alternative text (Alt text) provided alongside figures in the articles in this ebook has been generated by Frontiers with the support of artificial intelligence and reasonable efforts have been made to ensure accuracy, including review by the authors wherever possible. If you identify any issues, please contact us.

About Frontiers

Frontiers is more than just an open access publisher of scholarly articles: it is a pioneering approach to the world of academia, radically improving the way scholarly research is managed. The grand vision of Frontiers is a world where all people have an equal opportunity to seek, share and generate knowledge. Frontiers provides immediate and permanent online open access to all its publications, but this alone is not enough to realize our grand goals.

Frontiers journal series

The Frontiers journal series is a multi-tier and interdisciplinary set of open-access, online journals, promising a paradigm shift from the current review, selection and dissemination processes in academic publishing. All Frontiers journals are driven by researchers for researchers; therefore, they constitute a service to the scholarly community. At the same time, the *Frontiers journal series* operates on a revolutionary invention, the tiered publishing system, initially addressing specific communities of scholars, and gradually climbing up to broader public understanding, thus serving the interests of the lay society, too.

Dedication to quality

Each Frontiers article is a landmark of the highest quality, thanks to genuinely collaborative interactions between authors and review editors, who include some of the world's best academicians. Research must be certified by peers before entering a stream of knowledge that may eventually reach the public - and shape society; therefore, Frontiers only applies the most rigorous and unbiased reviews. Frontiers revolutionizes research publishing by freely delivering the most outstanding research, evaluated with no bias from both the academic and social point of view. By applying the most advanced information technologies, Frontiers is catapulting scholarly publishing into a new generation.

What are Frontiers Research Topics?

Frontiers Research Topics are very popular trademarks of the *Frontiers journals series*: they are collections of at least ten articles, all centered on a particular subject. With their unique mix of varied contributions from Original Research to Review Articles, Frontiers Research Topics unify the most influential researchers, the latest key findings and historical advances in a hot research area.

Find out more on how to host your own Frontiers Research Topic or contribute to one as an author by contacting the Frontiers editorial office: frontiersin.org/about/contact

Innovative drug combinations for enhanced solid tumor treatment efficacy

Topic editors

Giovanna Damia — Mario Negri Institute for Pharmacological Research (IRCCS), Italy

Massimo Broggini — Mario Negri Institute for Pharmacological Research (IRCCS), Italy

Citation

Damia, G., Broggini, M., eds. (2026). *Innovative drug combinations for enhanced solid tumor treatment efficacy*. Lausanne: Frontiers Media SA. doi: 10.3389/978-2-8325-7377-8

Table of contents

frontiers | Frontiers in Oncology

TYPE Editorial
PUBLISHED 06 January 2026
DOI 10.3389/fonc.2025.1763808

OPEN ACCESS

EDITED AND REVIEWED BY
Jonathan W. Song,
The Ohio State University, United States

*CORRESPONDENCE
Massimo Broggini
massimo.broggini@marionegri.it

RECEIVED 09 December 2025
REVISED 16 December 2025
ACCEPTED 16 December 2025
PUBLISHED 06 January 2026

CITATION
Damia G and Broggini M (2026) Editorial: Innovative drug combinations for enhanced solid tumor treatment efficacy.
Front. Oncol. 15:1763808.
doi: 10.3389/fonc.2025.1763808

Editorial: Innovative drug combinations for enhanced solid tumor treatment efficacy

Giovanna Damia[1] and Massimo Broggini[2]*

[1]Laboratory of Preclinical Gynaecological Oncology, Milan, Italy, [2]Laboratory of Molecular Pharmacology, Department of Experimental Oncology, Istituto di Ricerche Farmacologiche Mario Negri IRCCS, Milan, Italy

KEYWORDS

chemotherapy, drug combination, drug resistance, immunotherapy, targeted therapy

Editorial on the Research Topic

Innovative drug combinations for enhanced solid tumor treatment efficacy

Despite substantial advances in recent years, the treatment of solid tumors remains suboptimal. The identification of actionable molecular targets, the development of target-specific agents, and the advent of immunotherapy have not only profoundly reshaped the oncology landscape, but also clearly demonstrated that monotherapies are generally insufficient to elicit durable antitumor responses (1–5). The expanding understanding of the molecular mechanisms underlying tumor initiation, tumor progression and resistance provides an unprecedented foundation for the rational design of more effective treatment strategies, favoring and fostering the transition toward a personalized oncology medicine.

Importantly, this mechanistic knowledge is guiding the rational design of combination therapies, which represent the most promising approach to overcoming the intrinsic heterogeneity of solid tumors with the possibility to achieve more effective and potentially curative outcomes (6–9). Indeed, rationally designed combinations that integrate targeted agents, immunotherapies, or even conventional cytotoxic treatments have the potential to simultaneously suppress parallel oncogenic pathways, prevent compensatory signaling, and enhance antitumor immune responses (2, 7, 10, 11).

Efforts to develop, validate, and clinically implement well-designed combination regimens, based on the molecular characteristics of the tumors, are essential to achieve more effective, durable, and potentially curative outcomes for a broader population of patients. This was the goal of the Research Topic that collected 13 different contributions reporting different strategies converging on the use of new combinations.

In NSCLC the introduction of specific KRAS inhibitor has improved the outcome of patients harboring KRASG12C mutation. In their article, Tubita et al. showed that use of KRAS G12c inhibitors (both sotorasib and adagrasib) was able to enhance the response to conventional chemotherapy in NSCLC harboring this KRAS mutation. Using *in vitro* systems, the authors provide evidence that the superiority of the combination was obtained both using sequential and concurrent treatments and both in 2D and 3D models.

In the same setting (NSCLC), Jin et al. used a tri-specific antibody targeting EGFR, cMET and VEGF. The rationale behind the use of this tri-specific antibody is based on the known crosstalk between the three targeted signaling pathways. This strategy was superior

to the use of single EGFR or bispecific EGFR/cMET antibodies. Furthermore, the authors showed that the strong efficacy of the trsipecific antibody could be even enhanced when combined with chemo or radiotherapy in xenografts models with strong and durable tumor regression without additional toxicity. Dual targeting of EGFR and VEGF has been tested clinically with a new third generation EGFR inhibitor (aumolertinib) in combination with an established anti-VEGF therapy (bevacizumab) in a phase II in patients with EGFR mutated NSCLC. The study (Kong et al.) reached the primary endpoint with an extension of progression free survival (PFS), again indicating the superiority of the simultaneously targeting pathways that are interconnected.

The use of antibodies targeting immune-checkpoint (PD1/PDL1 or CTLA4) has significantly changed the survival of NSCLC and melanoma patients. The combination of different checkpoint inhibitors represents now the standard treatment for these tumors. In a systematic review that included 10 clinical trials with more than 3000 patients, Dai et al. extended these results in gastrointestinal cancers, showing that the combination had strong efficacy in GI cancer and in particular in esophageal cancer again, reinforcing the superiority of combinations over monotherapy.

Two case reports, one in a patient with rare cervical sarcomatoid carcinoma (Zhang et al.) and the other in Grade 2 meningioma (Reusch et al.), highlighted the use of immunotherapy. In the first report, the authors used a combination of permbrolizumab (anti PD-1) with bevacizumab (targeting angiogenesis) that resulted in a prolonged PFS and OS. Interestingly, the combination was rationally designed based on the molecular characteristics of the patient, again supporting the notion that targeted combinations has stronger potential over empirical ones. The second case report indeed used immunotherapy as single therapy, based on the molecular characteristics of the tumor patient bearing a mutation in *PBMR1* (a gene involved in control of genomic stability) that, when mutated, in renal carcinoma associates with response to immune-checkpoint inhibitors.

Combinations of targeted therapy and chemotherapy have been tested in two case reports using as targeted agent anlotinib, a drug hitting several tyrosine kinases including VEGFR, FGFR, PDGFR and c-kit. In the first report (Sun et al.), the authors treated a rare lung NUT carcinoma (a very aggressive tumor with poor prognosis) with this multi-kinase inhibitor in combination with etoposide and cisplatin. The combination significantly prolonged PFS over that previously reported for this kind of tumor. The other case report (Liang et al.) was on a rare, poor prognosis, mesenchymal tumor (pulmonary arterial intima sarcoma) that was treated in a neo-adjuvant setting with the same multikinase inhibitor together with chemotherapy (in this case ifosfamide and pirarubicin). Interestingly, the patient was initially treated with chemotherapy alone, that resulted in a slow progression. Addition of anlotinib in subsequent treatments not only caused a significant tumor reduction, but also ameliorated the general symptoms of the patients.

Another important rational design for combinations includes the use of drugs targeting DNA repair. An interesting report (Zouggari et al.) showed that the addition of the thymidine analogue CldU was able to significantly enhance the response of *BRCA2*-mutated cells to olaparib (a PARP inhibitor). What is even more important, is that the use of CldU was able to overcome resistance to PARP inhibitors. This is particularly important because the efficacy of PARP inhibitors in clinic is hampered by the onset of drug resistance.

The review by Zhou et al. was centered on SLFN11 as a potential biomarker of sensitivity to DNA targeting agents. The authors gave an overview of the functions of SLFN11 but, in the context of the Research Topic, they proposed treatment strategies based on the expression status of SLFN11. This represents an additional way to foster combinations, as already discussed, based on the molecular characteristics of the tumors, and further prove that rational combination could even rise to synthetic lethality sparing normal cells.

Interestingly, in the manuscript by Chen et al. a screening of an in-house panel of small molecules against hepatocellular carcinoma (HCC) cancer stem cells led to the identification of a new compound C504244, able to interfere with the β -catenin signaling. Lenvatinib, a multi-targeted TKI, is approved for first-line treatments for advanced HCC. As resistance to lenvatinib has been associated to overactivation of β-catetin and that cancer stem cell have been implicated in therapy resistance in HHC, the authors combined C504244 and lenvatinib both *in vitro* and *in vivo* models and found how this combination reverted lenvatinib resistance.

A triple combination (palbociclib, a CDK4/6 inhibitor, PF-07104091, a CDK2 inhibitor and SX-682, a dual CXCR1 and CXCR2-CXCR1/2-) was tested as potential new effective treatment in preclinical models of melanoma (Yang et al.). The triple treatment was able not only to reduce melanoma tumor cell viability, to interfere with tumor growth more effectively in BRAF WT NRAS WT melanoma cells, but also induced a less immunosuppressive tumor immune microenvironment opening up the road for the design of clinical trials for immunochekpoint-resistant melanomas without BRAF mutation.

Finally, in the last manuscript (Zhang et al.), trastuzumab combined with low-dose nab-paclitaxel and radiotherapy was able to induce a very good disease control in a 86-years old man with a HER2-positive salivary duct carcinoma (SDC), a rare and aggressive malignancy. This case highlights the efficacy and safety of HER2-targeted combination therapy in elderly SDC patients, offering valuable insights into biomarker-driven personalized treatment strategies for this population.

All the manuscripts presented in this Research Topic support how rational, biology-guided combination strategies represent one of the most promising avenues to improve outcomes in solid tumors. Continued efforts to optimize and validate integrated therapeutic approaches will be crucial to translate these advances into durable and meaningful clinical benefits for patient with solid tumors.

Author contributions

GD: Writing – original draft, Writing – review & editing. MB: Writing – original draft, Writing – review & editing.

Conflict of interest

The author(s) declared that this work was conducted in the absence of any commercial or financial relationships that could be construed as a potential conflict of interest.

The author MB declared that they were an editorial board member of Frontiers, at the time of submission. This had no impact on the peer review process and the final decision.

Generative AI statement

The author(s) declared that generative AI was not used in the creation of this manuscript.

Any alternative text (alt text) provided alongside figures in this article has been generated by Frontiers with the support of artificial intelligence and reasonable efforts have been made to ensure accuracy, including review by the authors wherever possible. If you identify any issues, please contact us.

Publisher's note

All claims expressed in this article are solely those of the authors and do not necessarily represent those of their affiliated organizations, or those of the publisher, the editors and the reviewers. Any product that may be evaluated in this article, or claim that may be made by its manufacturer, is not guaranteed or endorsed by the publisher.

References

1. Fernandes MR, Aggarwal P, Costa RGF, Cole AM, Trinchieri G. Targeting the gut microbiota for cancer therapy. *Nat Rev Cancer*. (2022) 22:703–22. doi: 10.1038/s41568-022-00513-x

2. Yap TA, Parkes EE, Peng W, Moyers JT, Curran MA, Tawbi HA. Development of immunotherapy combination strategies in cancer. *Cancer Discov*. (2021) 11:1368–97. doi: 10.1158/2159-8290.CD-20-1209

3. Zaidi N, Jaffee EM, Yarchoan M. Recent advances in therapeutic cancer vaccines. *Nat Rev Cancer*. (2025) 25:517–33. doi: 10.1038/s41568-025-00820-z

4. Huang L, Zhu H, Shi Y. Immune checkpoint inhibitors for the treatment of solid tumors and lymphoma in the past 26 years (2000-2025). *J Hematol Oncol J Hematol Oncol*. (2025) 18:107. doi: 10.1186/s13045-025-01734-x

5. Di Federico A, Stumpo S, Mantuano F, De Giglio A, Lo Bianco F, Pecci F, et al. Long-term overall survival with dual CTLA-4 and PD-L1 or PD-1 blockade and biomarker-based subgroup analyses in patients with advanced non-small-cell lung cancer: a systematic review and reconstructed individual patient data meta-analysis. *Lancet Oncol*. (2025) 26:1443–53. doi: 10.1016/S1470-2045(25)00429-2

6. Li Y, Zheng R, Pan B, Wang X, Zhang L, Gao H, et al. Beyond monotherapy: multimodal strategies integrating immune checkpoint inhibitors in lymphoma management. *Front Immunol*. (2025) 16:1713199. doi: 10.3389/fimmu.2025.1713199

7. Chiappa M, Decio A, Guarrera L, Mengoli I, Karki A, Yemane D, et al. Onvansertib treatment overcomes olaparib resistance in high-grade ovarian carcinomas. *Cell Death Dis*. (2024) 15:521. doi: 10.1038/s41419-024-06894-1

8. Affatato R, Chiappa M, Guffanti F, Ricci F, Formenti L, Fruscio R, et al. Onvansertib and paclitaxel combined in platinum-resistant ovarian carcinomas. *Ther Adv Med Oncol*. (2022) 14:17588359221095064. doi: 10.1177/17588359221095064

9. Gupta SK, Smith EJ, Mladek AC, Tian S, Decker PA, Kizilbash SH, et al. PARP inhibitors for sensitization of alkylation chemotherapy in glioblastoma: impact of blood-brain barrier and molecular heterogeneity. *Front Oncol*. (2018) 8:670. doi: 10.3389/fonc.2018.00670

10. Stone S, McPherson JP, Kulkarni RP, Young A. The impact of concomitant medications on treatment outcomes in patients with cancer receiving immune checkpoint inhibitors. *Nat Rev Cancer*. (2025). doi: 10.1038/s41568-025-00890-z

11. Junttila MR, de Sauvage FJ. Influence of tumour micro-environment heterogeneity on therapeutic response. *Nature*. (2013) 501:346–54. doi: 10.1038/nature12626

frontiers | Frontiers in Oncology

TYPE Systematic review
PUBLISHED 07 January 2025
DOI 10.3389/fonc.2024.1515992

OPEN ACCESS

EDITED BY
Giovanna Damia,
Mario Negri Institute for Pharmacological Research (IRCCS), Italy

REVIEWED BY
Kang Qin,
University of Texas MD Anderson Cancer Center, United States
Shweta Kamat,
Open Health Company, United States

*CORRESPONDENCE
Zhengchuan Hu
zhengchuanhu09@163.com

RECEIVED 23 October 2024
ACCEPTED 16 December 2024
PUBLISHED 07 January 2025

CITATION
Dai B, Jiang J, Yu X, Zhan H and Hu Z (2025) Efficacy and safety of nivolumab plus ipilimumab in gastrointestinal cancers: a systematic review and meta-analysis. *Front. Oncol.* 14:1515992. doi: 10.3389/fonc.2024.1515992

Efficacy and safety of nivolumab plus ipilimumab in gastrointestinal cancers: a systematic review and meta-analysis

Bowen Dai[1], Jiaping Jiang[1], Xiaoyu Yu[1], Haihua Zhan[1] and Zhengchuan Hu[2*]

[1]Southwest Medical University, Luzhou, China, [2]Department of General Surgery (Gastrointestinal Surgery), The Affiliated Hospital of Southwest Medical University, Luzhou, China

Introduction: Gastrointestinal (GI) cancers represent a significant global health burden, and the need for more effective treatment options is exceptionally pressing. The present meta-analysis aimed to explore the efficacy and safety of the combination of nivolumab and ipilimumab in treating GI cancers.

Methods: A systematic search of four databases (PubMed, Embase, Web of Science, and Cochrane Library) was conducted for articles on the treatment of GI cancers with nivolumab combined with ipilimumab, published from 2014 up to 30 August 2024. The inclusion criteria were designed according to the principles of Participants, Intervention, Control, Outcomes, and Study (PICOS). The control group was chemotherapy or nivolumab monotherapy or nivolumab in combination with other drugs. We extracted data from 10 randomized controlled trials and utilized a random effects model to assess the objective response rate (ORR), median progression-free survival (mPFS), median overall survival (mOS), median duration of response (mDOR), and treatment-related adverse events (TRAEs). The data analysis was conducted using Review Manager version 5.4 and Stata version 12.0.

Results: Overall, the combination of nivolumab and ipilimumab demonstrated superior outcomes, including a higher ORR (OR = 1.69, P = 0.01), prolonged mOS (MD = 1.74, P = 0.04) and extended mDOR (MD = 5.64, P < 0.00001) compared to the control group. Subgroup analysis demonstrated that the ORR (OR = 1.75, P = 0.02) and mOS (MD = 5.02, P = 0.003) were significantly improved in patients with esophageal cancer. Notably, the ORR in patients with biliary cancer was significantly lower (OR = 0.11, P = 0.04). Additionally, the ORR was significantly higher in the NIVO1 + IPI3group (OR = 2.82, P = 0.01) and NIVO3 + IPI1 group (OR = 1.62, P = 0.01). Regarding safety, there was no statistically significant difference between the combination regimen and the control group in terms of any grade (OR = 0.72, P = 0.26) or grade 3-4 TRAEs (OR = 1.36, P = 0.14).

Conclusions: Nivolumab in combination with ipilimumab demonstrated significant efficacy in GI cancers (especially esophageal cancer) without causing more adverse reactions. However, its efficacy in biliary cancer still needs to be further proven.

Systematic review registration: https://www.crd.york.ac.uk/prospero/, identifier CRD42024590994.

KEYWORDS

nivolumab, ipilimumab, gastrointestinal cancer, objective response rate, efficacy, meta-analysis

1 Introduction

Today, the burden of cancer is one of the world's greatest public health problems (1). Gastrointestinal (GI) cancers constitute a significant category of neoplasms, encompassing a range of digestive tract tumors, including those affecting the colon, rectum, esophagus, stomach, liver, pancreas, gallbladder, and bile ducts. These cancers represent a significant global health burden, with a prevalence rate exceeding 26% and a mortality rate exceeding 35% (2). Immunotherapy, particularly immune checkpoint blockade and targeting the tumor immune microenvironment, has been extensively employed in the treatment of numerous GI cancers, including microsatellite instability-high (MSI-H) colorectal cancer, gastric cancer, and hepatocellular carcinoma (3–5). While immunotherapy has demonstrated considerable efficacy in the treatment of numerous tumors, it can also induce adverse events related to the immune system, particularly in the case of immune checkpoint inhibitors (6, 7). Accordingly, there is a clear need to investigate the development of more efficacious and safer immune checkpoint target drugs.

Currently, data from several clinical trials show satisfactory therapeutic effects of immune checkpoint inhibitors in patients with GI cancers, such as HER-2, PD-1/PD-L1, and CTLA4-targeted therapy (8–10). Cytotoxic T-lymphocyte-associated antigen 4 (CTLA4, also designated as CD152) and programmed cell death protein 1 (PD1, also designated as CD279) represented two of the most intensively investigated targets in the domain of clinical immunotherapy. CTLA4 is an immune checkpoint receptor that is predominantly expressed in T cells. It has the same receptor as CD28 but exhibits a higher overall affinity. By inhibiting the CTLA-4 receptor-ligand interaction through the use of an anti-CTLA-4 antibody, the CD28-mediated T cell stimulation signal is enhanced, thereby achieving an anti-tumor immune effect (11, 12). PD-1 is expressed at a greater level than CTLA4 in activated T cells, B cells, and myeloid cells. It inhibits T cell activation, affects the tumor microenvironment and tolerance, and so forth, by interacting with two ligands, PD-L1 and PD-L2, which partially overlap in their functions (13–15). There is mounting evidence that targeting the PD-1/PD-L pathway represents an efficacious treatment strategy for augmenting anti-tumor immune responses. Antibody-mediated PD-1 or PD-L1 blockade held immense clinical promise for a range of advanced tumors (including non-small cell lung cancer, melanoma, gastroesophageal cancer, hepatocellular carcinoma, and others) in comparison to chemotherapy or palliative care (16–19). Concurrently, research has demonstrated that the combination of anti-CTLA-4 and anti-PD-1 therapies is regarded as a more efficacious approach (20). The simultaneous blockade of these two molecules may result in a synergistic effect, whereby they act on CD28 and participate in signal pathways such as T cell activation, thereby enhancing T cell activity. However, the relative contribution of the various known molecular mechanisms of CTLA4 and PD-1 blockade to the therapeutic effect remains to be further explored (21, 22). Nivolumab and ipilimumab are monoclonal antibodies that target PD-1 and CTLA-4, respectively. The combination of anti-PD-1 and anti-CTLA-4 therapy (nivo-ipi) has been officially approved by the US Food and Drug Administration (FDA) for the treatment of a variety of cancers, including colorectal cancer, hepatocellular carcinoma, and other cancers (23, 24). Therefore, the combination of nivolumab and ipilimumab is expected to become a new and more effective treatment option for GI cancers.

Some studies have demonstrated that the combination of nivolumab and ipilimumab yielded promising clinical outcomes in the treatment of GI cancers (including gastroesophageal cancer, esophageal squamous cell carcinoma, pancreatic cancer, and hepatocellular carcinoma) (10, 25–28). Nevertheless, the advantages of this therapeutic approach in the context of other GI cancers (e.g., colorectal and biliary cancers) remain a matter of contention, and the overall efficacy and safety of this regimen in GI cancers has yet to be fully evaluated (29). Although some meta-analyses indicated that the combination of nivolumab and ipilimumab may be an effective treatment for second-line therapy of advanced hepatocellular carcinoma and the third-line treatment of advanced gastric cancer, the current evidence was insufficient to conclude the efficacy of this regimen for all GI cancers (30, 31). Moreover, there is a dearth of direct efficacy assessments of different tumor types and different dose ratios of the combination, which is essential to demonstrate the universality and heterogeneity of treatment options.

In order to ascertain the overall efficacy and safety of this combination in the treatment of GI cancers, as well as variations in efficacy across tumor types and dose ratios, and to enhance the clinical feasibility of this combination in the treatment of GI cancers, we conducted a meta-analysis. The results of the analysis may contribute to the development of clinical decision-making and provide potential new options for the first-line treatment of GI cancers. This will facilitate the development of optimal treatment strategies for future patients undergoing treatment with GI tumors.

2 Method

2.1 Search strategy

This systematic review and meta-analysis followed the PRISMA statement and was registered with PROSPERO (CRD42024590994). A systematic search was conducted in four databases, namely PubMed, Embase, Web of Science, and Cochrane Library to identify relevant articles from 2014 to August 30, 2024, using the following keywords: (Ipilimumab) and (Nivolumab) and (Stomach Neoplasms or Esophageal Neoplasms or Liver Neoplasms or Colonic Neoplasms or Rectal Neoplasms or Colorectal Neoplasms or Pancreatic Neoplasms or Gallbladder Neoplasms or Bile Duct Neoplasms or Gastrointestinal Neoplasms). In addition, we searched the gray literature. The search strategy was constructed following the PICOS framework and comprised the integration of both Medical Subject Headings (MeSH) terms and free-text keywords. For articles with missing or incomplete data, we contacted the authors by email to obtain complete data. Additionally, we sought relevant literature that is not readily available through standard sources by reaching out to subject matter experts in the field.

2.2 Inclusion and exclusion criteria

Inclusion criteria were as follows: (a) patients diagnosed with all GI cancer types; (b) the combination therapy of nivolumab and ipilimumab was used as the experimental group; (c) chemotherapy or monotherapy with nivolumab or combination therapy with nivolumab and other drugs was used as the control group; (d) at least one of the following outcomes was reported: overall survival (OS), progression-free survival (PFS), objective response rate (ORR), duration of response (DOR), and treatment-related adverse events (TRAEs).

Additionally, studies that met the following criteria were excluded: (a) other types of articles, such as observational study designs (retrospective/prospective), single-arm design studies, case reports, publications, animal studies, and conference proceedings; (b) duplicate patient cohorts; (c) cancers that are not GI cancers; (d) other unrelated researches.

2.3 Study selection

All literature was imported into EndNote (Version 20; Clarivate Analytics) and deduplicated using a combination of automatic and manual methods. Subsequently, two reviewers (Bowen Dai, Haihua Zhan) independently screened the titles and abstracts of retrieved articles. Any disagreements were resolved through discussion. In cases of disagreement, a third reviewer took on the role of a mediator.

2.4 Quality assessment

Two authors (Haihua Zhan and Xiaoyu Yu) undertook an independent assessment of the risk of bias of each included randomized controlled trial using the Cochrane Risk of Bias Assessment Tool, which assesses six dimensions: random sequence generation, allocation concealment, blinding of participants and personnel, blinding of outcome assessment, incomplete outcome data, and selective reporting (32). Three levels are defined: 'unclear risk', 'low risk', and 'high risk'. Any disagreements between authors were resolved by discussion with an independent third author.

2.5 Data extraction

The data were extracted by two independent reviewers (Bowen Dai, Jiaping Jiang) and included the following items: the first author, study type, number of participants, sex ratio, median age, primary endpoint, and treatment experimental arm. The following outcome indicators are more appropriate: mOS, mPFS, ORR, mDOR, and TRAEs. To ensure data accuracy, two authors independently performed data extraction. Any discrepancies were resolved through consensus discussions.

2.6 Statistical analysis

Statistical analysis was performed using the Cochrane Review Manager (Review Manager Version 5.4) and Stata 12.0 software. The effect size was calculated using a standardized mean difference, and a 95% confidence interval (CI) was generated. Given that the studies included in the analysis originate from the public literature, it would be more reasonable to select the random effect model as the preliminary model. Furthermore, it was determined that a p-value less than 0.05 would signify statistical significance.

The primary endpoints of this study were mOS, mPFS. Secondary endpoints were ORR, mDOR, and TRAEs. Given the heterogeneity, all pooled analyses were performed using a random effects model. The Cochran Q statistic and the I^2 statistic were employed to assess the presence of heterogeneity. If the Q statistic yielded a statistically significant result ($P < 0.05$), the I^2 statistic quantified the proportion of sample differences attributable to heterogeneity. I^2 values exceeding 25%, 50%, and 75% were considered to be low, medium, and high heterogeneity, respectively (33). Given the considerable heterogeneity observed in mOS and mPFS, we performed a subgroup analysis to investigate potential differences in efficacy across different tumor types. In addition, we conducted a sensitivity analysis to ascertain whether the exclusion of studies exhibiting aberrant characteristics could account for the observed heterogeneity and influence the pooled effect.

3 Results

A total of 1168 published studies were identified through an initial database search. After removing 282 studies using EndNote, the remaining 886 studies were screened. By reading the title and abstract, we excluded 803 unrelated articles. The remaining 83 articles then underwent full-text searching and reading. Of these, 5 could not retrieved, 61 were found to lack data, and 7 could not be located in their entirety. Consequently, a total of 10 studies were ultimately included for data extraction. The complete screening process is illustrated in Figure 1.

3.1 Characteristics of the included studies

Table 1 provides details of each study. In total, 10 trials involving 3056 patients met predefined inclusion criteria. All studies included in this systematic review and meta-analysis were randomized controlled trials (10, 25–29, 34–37). The average age of the included samples was 63.1 years old, with the majority of men (79.08%). One of the studies did not provide information on the age and gender of the population due to differences in its main experimental plan (34). The 10 primary endpoints of the trials include PFS, OS, DOR, ORR, dose-limiting toxicity (DLT), safety, and tolerability. We extracted the ORR, mOS, mPFS, mDOR, and TRAEs reported in the literature for summary analysis.

Of the 10 RCTs included, 3 trials compared the efficacy of nivolumab plus ipilimumab with chemotherapy (10, 34, 35). 2 trials compared the efficacy of nivolumab plus ipilimumab with nivolumab (26, 36). 1 trial compared the efficacy of nivolumab plus ipilimumab plus binimetinib with nivolumab plus binimetinib (37). 1 trial compared the efficacy of nivolumab plus ipilimumab plus cabozantinib with nivolumab plus cabozantinib (27). 2 trials compared the efficacy of nivolumab plus ipilimumab plus stereotactic body radiotherapy (SBRT) with nivolumab plus gemcitabine plus cisplatin plus SBRT (25, 28). 1 trial compared the efficacy of nivolumab plus ipilimumab with nivolumab plus gemcitabine plus cisplatin (29).

3.2 Quality assessment and publication bias

The risk of bias was discussed and assessed according to the Cochrane Collaboration's Risk of Bias tool by two independent investigators (Haihua Zhan, Xiaoyu Yu), the risk of bias of the included literature was assessed in terms of the following six dimensions: random sequence generation (selection bias),

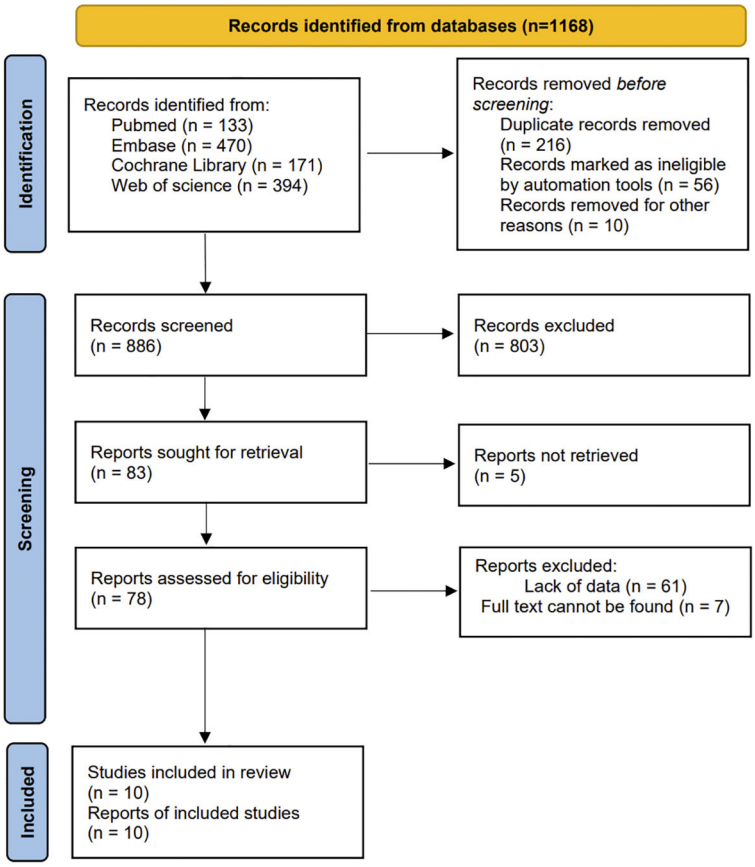

FIGURE 1
Literature screening process.

TABLE 1 Characteristics of studies included in meta-analysis.

Study	Author	Study type	Participants No.	Males (%)	Median age	Primary endpoint	Treatment Experimental Arm
1	Chen 2022	RCT	84	52.4	64.5	CBR	nivolumab plus ipilimumab plus SBRT or nivolumab plus gemcitabine plus cisplatin plus SBRT
2	Elez 2024	RCT	75	64	60.3	DLT ORR	nivolumab plus ipilimumab plus binimetinib or nivolumab plus binimetinib
3	Janjigian 2018	RCT	160	77.5	57.2	ORR	nivolumab plus ipilimumab or nivolumab
4	Juloori 2023	RCT	13	85	67	DLT	nivolumab plus ipilimumab plus SBRT or nivolumab plus gemcitabine plus cisplatin plus SBRT
5	Kaseb 2022	RCT	27	70	63.1	safety tolerability	nivolumab plus ipilimumab or nivolumab
6	Kato 2023	RCT	268	86.6	66.5	OS PFS	nivolumab plus ipilimumab or chemotherapy
7	Kato 2024	RCT	649	83.8	63	OS PFS	nivolumab plus ipilimumab or chemotherapy
8	Sahai 2022	RCT	68	51.4	62.5	PFS	nivolumab plus ipilimumab or nivolumab plus gemcitabine plus cisplatin
9	Shitara 2022	RCT	1641	none	none	OS PFS	nivolumab plus ipilimumab or chemotherapy
10	Yau 2023	RCT	71	87.3	65.7	safety tolerability ORR DOR	nivolumab plus ipilimumab plus cabozantinib or nivolumab plus cabozantinib

CBR, clinical benefit rate; ORR, objective response rate; DLT, dose-limiting toxicity; OS, overall survival; PFS, progression-free survival; DOR, duration of response.

allocation concealment (selection bias), blinding of participants and personnel (performance bias), blinding of outcome assessment (detection bias), incomplete outcome data (attrition bias), and selective reporting (reporting bias), and was categorized into three types: low risk, high risk, and uncertain risk. Data extraction was conducted by mutual agreement and all potential disagreements were resolved by consensus.

Most studies were of good quality. Seven of the studies had a low risk of random sequence generation (selection bias), six had a low risk of allocation concealment (selection bias), nine had a low risk of blinding of participants and personnel (performance bias), eight had a low risk of blinding of outcome assessment (detection bias), four had a low risk of incomplete outcome data (attrition bias) and eight had selective reporting (reporting bias) (Figure 2).

3.3 Meta analysis of ORR

Nine trials reported ORR for 15 cohorts of patients with GI cancers including 2189 patients. There was a significant improvement in ORR in comparison with the control group (OR = 1.69, 95% CI: 1.13-2.52, P = 0.01), and the heterogeneity test showed moderate heterogeneity (I^2 = 54%) (Figure 3). Therefore, the random effects model was adopted. Subsequent sensitivity analysis demonstrated that the removal of any single study did not exert a significant influence on the overall pooled results.

3.4 Meta analysis of mOS

A total of 7 studies comprising 3095 patients reported mOS in 12 groups of patients with GI cancers. The mOS was significantly prolonged compared to the control (MD = 1.74, 95% CI: 0.09-3.38, P = 0.04). And heterogeneity test showed moderate heterogeneity (I^2 = 52%) (Figure 4). Subsequent sensitivity analysis demonstrated that the removal of any single study did not exert a significant influence on the overall pooled results.

3.5 Meta analysis of mPFS

The mPFS in the experimental group was shorter than that in the control group, yet the difference was not statistically significant (MD = -0.94, 95% CI: -1.94-0.06, P = 0.06). Additionally, a high degree of heterogeneity was observed (I^2 = 90%) (Figure 5).

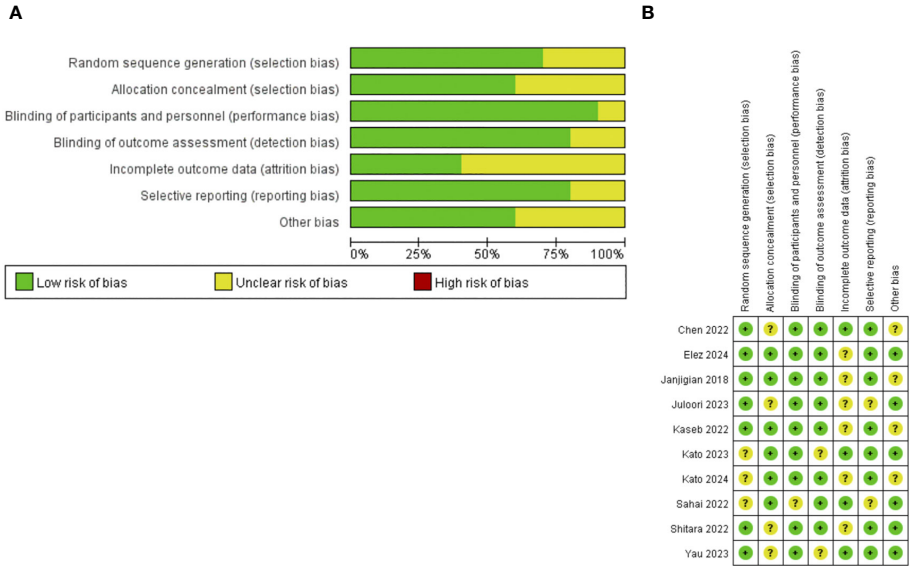

FIGURE 2
(A) Risk of bias graph. **(B)** Risk of bias summary.

Sensitivity analysis demonstrated that no single study significantly influenced the high degree of heterogeneity.

3.6 Meta analysis of mDOR

Two studies, involving 536 patients across 4 groups, reported mDOR for GI cancers. In comparison with the control group, mDOR was significantly extended in the experimental group (MD = 5.64, 95% CI: 3.40-7.88, P < 0.00001). There was no heterogeneity (I^2 = 0%) and publication bias (Figure 6).

3.7 Subgroup analysis

3.7.1 Subgroup analysis of different tumors

Considering the moderate degree of heterogeneity in ORR and mOS observed in the data from the preceding studies, subgroup analyses were conducted to investigate potential differences in efficacy between experimental and control groups across diverse tumor types.

The results showed a significant increase in ORR for esophageal cancer compared to the control group (OR = 1.75, 95% CI: 1.07-2.85, P = 0.02), with moderate heterogeneity (I^2 = 71%). The ORR for biliary cancer was significantly lower, which was statistically significant (OR = 0.11, 95% CI: 0.01-0.90, P = 0.04). There was a relatively significant increase in the objective remission rates of pancreatic cancer, colorectal cancer, gastroesophageal cancer and liver cancer, but none of them were statistically significant (pancreatic cancer: OR = 6.49, 95% CI: 0.75-56.45, P = 0.09; colorectal cancer: OR = 5.39, 95% CI: 0.25-117.77, P = 0.28; gastroesophageal cancer: OR = 1.46, 95% CI: 0.60-3.56, P = 0.40; hepatocellular carcinoma: OR = 1.92, 95% CI: 0.58-6.41, P = 0.29). However, only the heterogeneity in gastroesophageal cancer, esophageal cancer, and liver cancer were measurable, and no significant change was observed. (gastroesophageal cancer: I^2 =

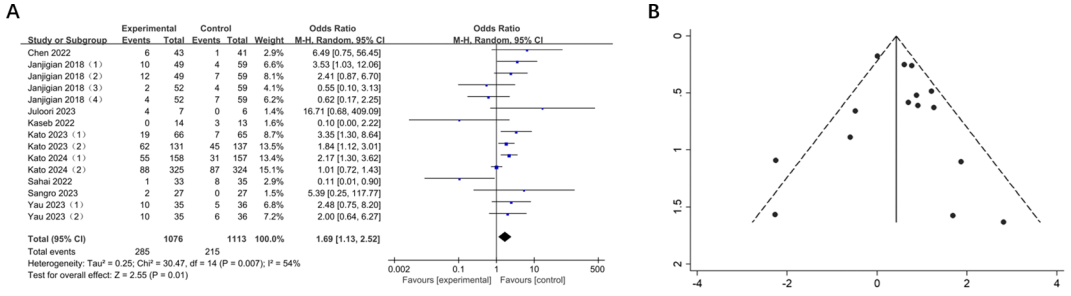

FIGURE 3
(A) Forest plot of ORR in patients with GI cancers treated with and without nivolumab in combination with ipilimumab. **(B)** Funnel plot of ORR in patients with GI cancers treated with and without nivolumab in combination with ipilimumab.

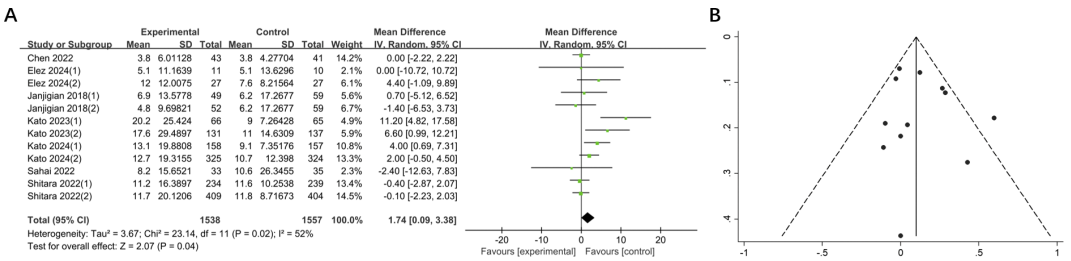

FIGURE 4
(A) Forest plot of mOS in patients with GI cancers treated with regimens containing and without nivolumab in combination with ipilimumab.
(B) Funnel plot of mOS in patients with GI cancers treated with regimens containing and without nivolumab in combination with ipilimumab.

48%; esophageal cancer: I^2 = 71%; hepatocellular carcinoma: I^2 = 45%). A notable disparity in ORR was observed across different subgroups, as indicated by the subgroup differences (Chi^2 = 8.63, df = 5, P = 0.12, I^2 = 42.1%). Moreover, compared with the control group, the mOS of esophageal cancer was significantly prolonged, with a statistically significant difference (esophageal cancer: MD = 5.02, 95% CI: 1.67-8.37, P = 0.003). Conversely, no statistically significant difference was observed for the remaining tumors (Figure 7).

3.7.2 Subgroup analysis of different dose ratios

The NIVO + IPI combination was approved as NIVO 1mg kg^{-1} + IPI 3mg kg^{-1} and NIVO 3mg kg^{-1} + IPI 1mg kg^{-1}. Consequently, we extracted the valid data from six studies and reanalyzed the ORR, mOS, and mPFS of this combination based on the two-dose ratios.

The results showed that the ORR of both the NIVO1 + IPI3 group and the NIVO3 + IPI1 group was higher than that of the control group (NIVO1 + IPI3: OR = 2.82, 95% CI: 1.28-6.18, P = 0.01; NIVO3 + IPI1: OR = 1.62, 95% CI: 1.10-2.38, P = 0.01), and there was low heterogeneity between the subgroups (I^2 = 34.7%). In addition, the mOS and mPFS of the NIVO1 + IPI3 group and the NIVO3 + IPI1 group were not statistically significant (Figure 8).

3.8 Safety

The data on TRAEs were extracted from six studies. The results showed no statistically significant difference in the risk of TRAEs, either of any grade (OR = 0.72, 95% CI: 0.41-1.27, P = 0.26) or grades 3-4 (OR = 1.36, 95% CI: 0.90-2.04, P = 0.14), between the nivolumab-plus-ipilimumab treatment group and the control group (Figure 9).

4 Discussion

GI cancers are among the most lethal forms of cancer globally, accounting for a significant proportion of all tumor-related mortalities (2). As the number of elucidated molecular targets and targeted therapies continues to grow, the prospects and challenges associated with the exploration and identification of more effective immune-targeted therapy regimens become increasingly evident (38). To our knowledge, this is the first meta-analysis evaluating the efficacy and safety of nivolumab in combination with ipilimumab in GI cancers.

The results of the meta-analysis demonstrated that, in comparison with the control group, the combination of nivolumab

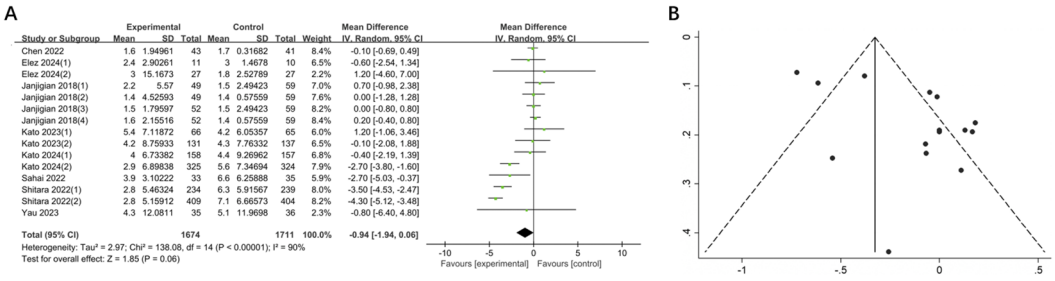

FIGURE 5
(A) Forest plot of mPFS in patients with GI cancers treated with regimens containing and without nivolumab in combination with ipilimumab.
(B) Funnel plot of mPFS in patients with GI cancers treated with regimens containing and without nivolumab in combination with ipilimumab.

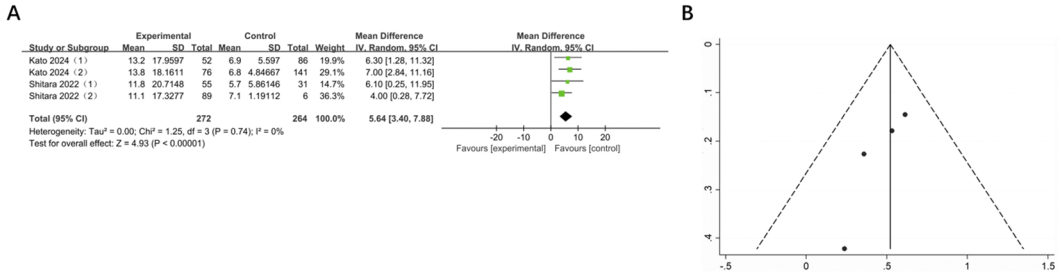

FIGURE 6
(A) Forest plot of mDOR in patients with GI cancers treated with regimens containing and without nivolumab in combination with ipilimumab. **(B)** Funnel plot of mDOR in patients with GI cancers treated with regimens containing and without nivolumab in combination with ipilimumab.

and ipilimumab markedly enhanced the ORR and extended the mOS and mDOR in GI cancers. However, no statistically significant difference was observed in mPFS and the incidence of TRAEs of any grade or grade 3–4 reactions. Due to the moderate heterogeneity observed in ORR and mOS, subgroup analyses were performed based on tumor types. The results of subgroup analyses demonstrated a significant improvement in the ORR for esophageal cancer and a significant decline for biliary cancer. The remaining tumor types exhibited no statistically significant ORR, and the differences between the subgroups demonstrated low heterogeneity. Furthermore, only the mOS of esophageal cancer was significantly improved, and the heterogeneity between subgroups did not change significantly in comparison to the overall result. To gain a more comprehensive understanding of the clinical outcomes associated with this combination regimen, we conducted a subgroup analysis of ORR, mOS, and mPFS based on the dose ratio. The findings revealed that the ORR of both the NIVO1 + IPI3 group and the NIVO3 + IPI1 group was significantly higher than that of the control group, whereas no statistically significant differences were observed in mOS and mPFS.

Part of Our findings are in accordance with those of Parikh et al., who observed that the ORR and OS rate of nivolumab combined with ipilimumab in the treatment of advanced hepatocellular carcinoma were significantly superior to those of nivolumab monotherapy (30). Similarly, the survival benefits and acceptable tolerability observed in the NIVO + IPI therapy in the study by Kato et al. provided strong support for its use as the new standard first-line treatment for Japanese patients with advanced ESCC (10). The lack of a notable extension in mPFS observed in the study may be attributed to tumor heterogeneity and the mechanisms underlying immunotherapy. The effect of immunotherapy typically necessitates a specific period to activate the patient's immune system, and the conventional PFS indicator is unable to fully capture the delayed effect of immunotherapy. As a

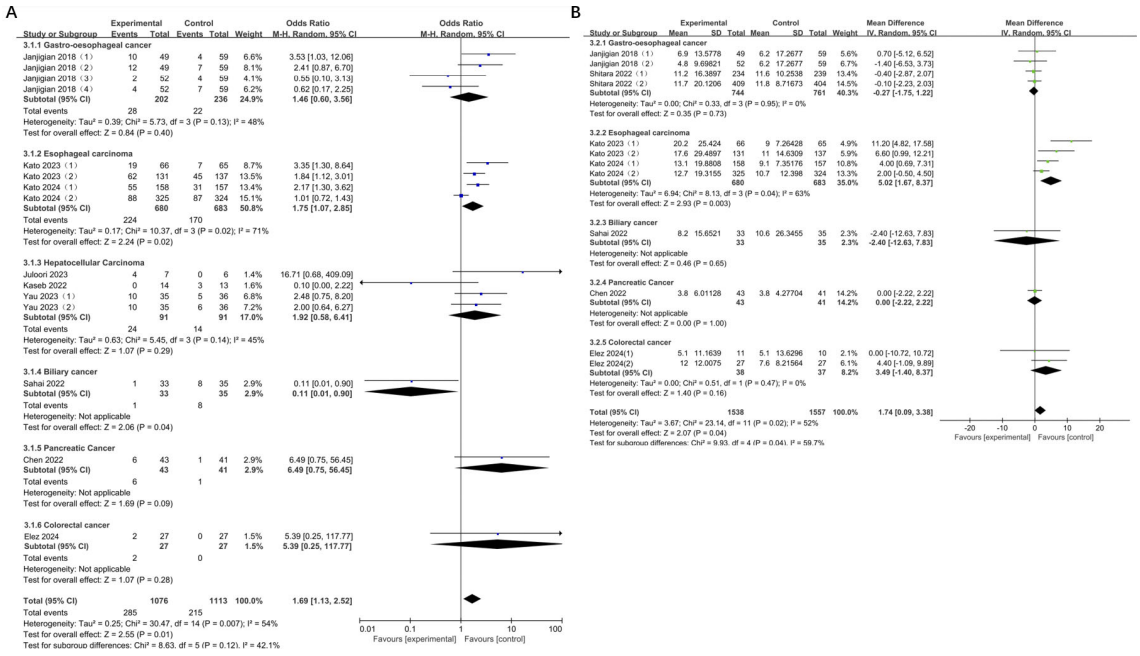

FIGURE 7
(A) Forest plot for subgroup analysis of ORR; **(B)** Forest plot for subgroup analysis of mOS.

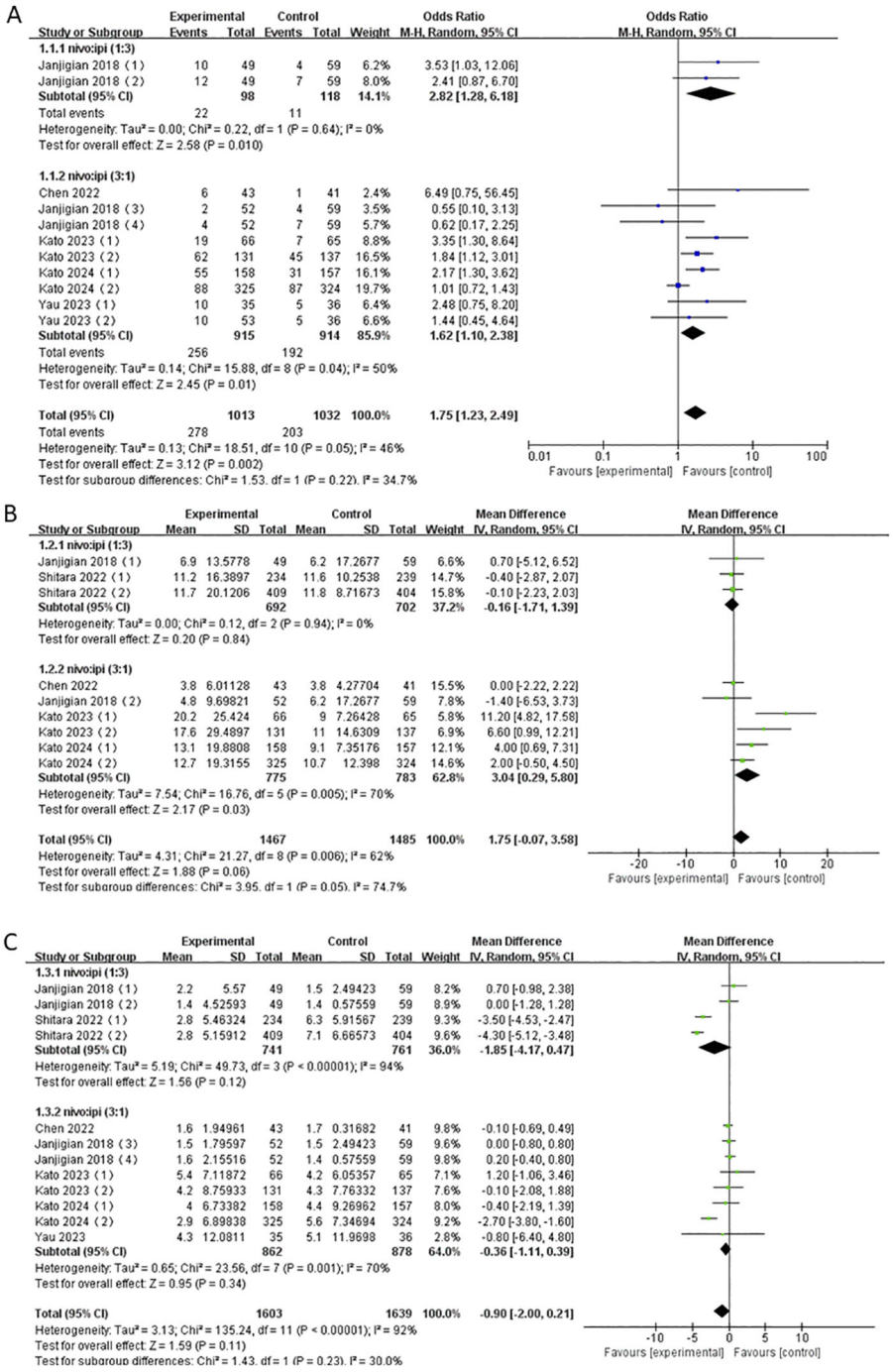

FIGURE 8
(A) Forest plot for subgroup analysis of ORR based on different doses. **(B)** Forest plot for subgroup analysis of mOS based on different doses. **(C)** Forest plot for subgroup analysis of mPFS based on different doses.

result, some patients may experience transient disease progression before their immune system is fully activated, leading to PFS inadequately capturing the treatment's efficacy promptly.

The results of a significant prolongation of ORR, mOS, and mDOR indicate that, although PFS was not significantly prolonged in some patients, the long-term effect may be more substantial and long-lasting once a response to immunotherapy is achieved. This may be attributed to the capacity of immunotherapy to enhance the activation of the patient's anti-tumor immune system, establish long-term immune memory, and prevent rapid tumor recurrence. These findings have significant clinical implications, particularly for patients with early-stage disease who initially exhibit slow progression but eventually achieve a sustained response. It is recommended that patients who respond to immunotherapy be monitored over an extended period in clinical practice and that immunotherapy be considered as part of a long-term treatment

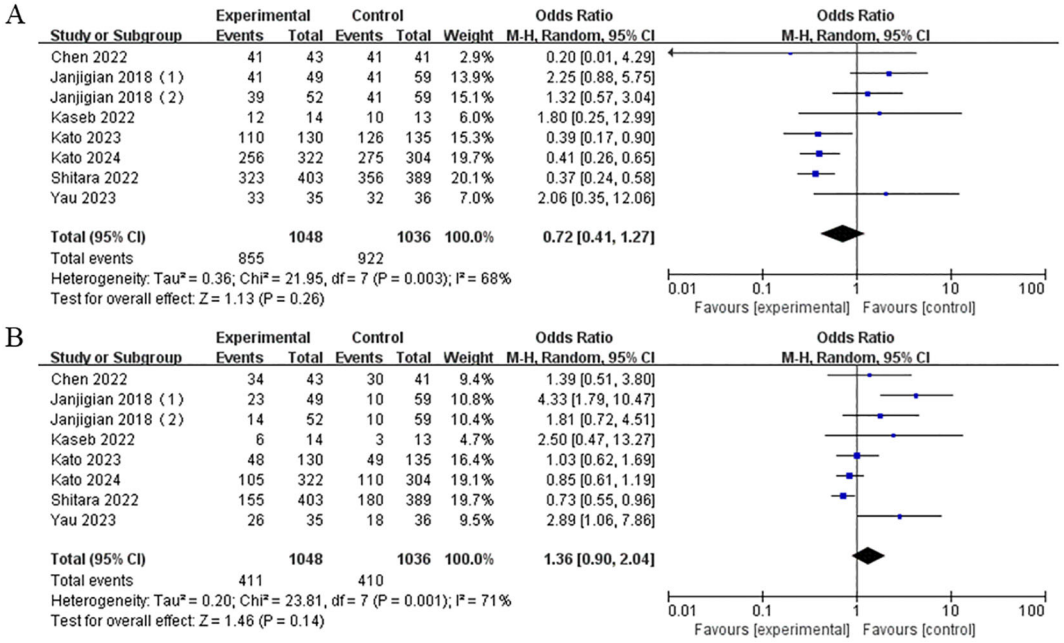

FIGURE 9
(A) Forest plot of any grade TRAEs in the combination of nivolumab and ipilimumab compared to the control group. **(B)** Forest plot of grade 3-4 TRAEs in the combination of nivolumab and ipilimumab compared to the control group.

plan, even in combination with other therapies to consolidate the treatment effect. Conversely, the heterogeneity of the ORR and mOS of this combination remains unresolved through subgroup analysis. Consequently, its clinical application should be exercised with caution.

The role of the tumor microenvironment in immunotherapy is of paramount importance. The TME of different types of GI cancers is highly heterogeneous, which has the potential to affect the efficacy of nivolumab and ipilimumab. In esophageal cancer, higher expression of PD-L1 and PD-L2 and greater T-cell infiltration have been observed to enhance tumor sensitivity to immunotherapy (39). In contrast, an immunosuppressive microenvironment (e.g. tumor-associated macrophages and tumor-infiltrating lymphocytes) has also been found to affect the prognosis of biliary tract cancer (40). Furthermore, the significant differences in the characteristic molecular targets of various GI cancers may also contribute to the observed heterogeneity in the efficacy of immune checkpoint inhibitors. The distinctive molecular characteristics of hepatocellular carcinoma are relatively concentrated and involve specific mutations or signaling pathways. These features include potential biomarkers such as interferon alpha (IFNα), alpha-fetoprotein (AFP), and transforming growth factor-beta (TGF-β), as well as the vascular endothelial growth factor (VEGF) pathway, mammalian target of rapamycin (mTOR) pathway, insulin-like growth factor 1 (IGF1) pathway and epidermal growth factor receptor (EGFR) pathway (41–43). Furthermore, numerous studies have demonstrated that multi-target tyrosine kinase inhibitors (TKIs)—such as sorafenib—can improve the survival rate of patients with advanced liver cancer to some extent (41, 44, 45). However, cholangiocarcinoma displays significant heterogeneity, with different biliary tract segments (including intrahepatic cholangiocarcinoma, extrahepatic cholangiocarcinoma, and gallbladder cancer) exhibiting distinct patterns of genetic mutations. For example, molecular abnormalities such as IDH1/2 mutations, FGFR2 fusions, and HER-2 overexpression are more common in some types of biliary tract cancer. However, these targets are only present in some patients, and the effect of targeted therapy is relatively limited. The use of anti-PD-1 or anti-CTLA-4 inhibitors in biliary tract cancer is uncommon and demonstrates limited efficacy (46). The disparate characteristics of TME and molecular targets are responsible for the varying responses observed in patients with GI cancers to the combination therapy of nivolumab and ipilimumab. Furthermore, a notable discrepancy was observed in the efficacy of nivolumab in combination with ipilimumab among patients with disparate PD-L1 expression levels within the same tumor. However, the literature included in the study provides only a limited range of efficacy data stratified by PD-L1 expression levels. This lack of data may contribute to the observed heterogeneity.

The combination of nivolumab and ipilimumab may represent a promising first-line treatment option for patients with GI cancers, particularly those with esophageal cancer. Nevertheless, for patients with biliary cancer, future clinical trials should investigate the potential of combining with other targeted or immune-enhancing therapies, given the likelihood of a poor response to immunotherapy. Furthermore, the findings of the study indicated that there was no notable enhancement in mPFS, thereby underscoring the necessity for greater emphasis on biomarker testing and dynamic efficacy assessment in clinical practice.

It is important to note that this study has limitations. Firstly, due to the paucity of data on TRAEs provided in the literature, our

analysis yielded no statistically significant results compared to the control group. It is widely accepted that this combination regimen has the potential to induce adverse reactions. Consequently, further research is required to investigate the effects of this regimen on specific TRAEs, such as decreased appetite and fatigue. Secondly, although this study provided a comprehensive analysis of the combination of nivolumab and ipilimumab, the small sample size, particularly in subgroups such as biliary cancer, may have an impact on the reliability of the results. Furthermore, larger, multicenter randomized controlled trials are required to corroborate the findings of this study, particularly for tumor types exhibiting suboptimal efficacy.

5 Conclusion

In conclusion, this meta-analysis offers a comprehensive evaluation of the efficacy and safety of nivolumab combined with ipilimumab in patients with GI cancers, based on all available randomized controlled trials. The findings suggest that this combination therapy represents a promising and effective option for managing GI cancers. However, caution is warranted in interpreting these results due to significant variability arising from the molecular heterogeneity of different GI cancer types.

Author contributions

BD: Conceptualization, Data curation, Methodology, Project administration, Software, Supervision, Visualization, Writing – original draft, Writing – review & editing. JJ: Conceptualization, Investigation, Project administration, Software, Writing – review & editing. XY: Data curation, Resources, Supervision, Validation, Writing – review & editing. HZ: Data curation, Project administration, Resources, Writing – review & editing. ZH: Conceptualization, Funding acquisition, Investigation, Methodology, Resources, Supervision, Writing – review & editing.

Funding

The author(s) declare that no financial support was received for the research, authorship, and/or publication of this article.

Acknowledgments

We would like to thank the corresponding author, ZH from the Department of Gastrointestinal Surgery at the Affiliated Hospital of Southwest Medical University, for his great support and help with this work.

Conflict of interest

The authors declare that the research was conducted in the absence of any commercial or financial relationships that could be construed as a potential conflict of interest.

Generative AI statement

The author(s) declare that no Generative AI was used in the creation of this manuscript.

Publisher's note

References

1. Torre LA, Siegel RL, Ward EM, Jemal A. Global cancer incidence and mortality rates and trends–an update. *Cancer Epidemiol Biomarkers Prevention: Publ Am Assoc Cancer Res Cosponsored By Am Soc Prev Oncol*. (2016) 25:16–27. doi: 10.1158/1055-9965.Epi-15-0578

2. Arnold M, Abnet CC, Neale RE, Vignat J, Giovannucci EL, McGlynn KA, et al. Global burden of 5 major types of gastrointestinal cancer. *Gastroenterology*. (2020) 159:335–49.e15. doi: 10.1053/j.gastro.2020.02.068

3. Bando H, Tsukada Y, Inamori K, Togashi Y, Koyama S, Kotani D, et al. Preoperative chemoradiotherapy plus nivolumab before surgery in patients with microsatellite stable and microsatellite instability-high locally advanced rectal cancer. *Clin Cancer Res: An Off J Am Assoc Cancer Res*. (2022) 28:1136–46. doi: 10.1158/1078-0432.Ccr-21-3213

4. Llovet JM, Castet F, Heikenwalder M, Maini MK, Mazzaferro V, Pinato DJ, et al. Immunotherapies for hepatocellular carcinoma. *Nat Rev Clin Oncol*. (2022) 19:151–72. doi: 10.1038/s41571-021-00573-2

5. Mou P, Ge QH, Sheng R, Zhu TF, Liu Y, Ding K. Research progress on the immune microenvironment and immunotherapy in gastric cancer. *Front Immunol*. (2023) 14:1291117. doi: 10.3389/fimmu.2023.1291117

6. Tang T, Huang X, Zhang G, Hong Z, Bai X, Liang T. Advantages of targeting the tumor immune microenvironment over blocking immune checkpoint in cancer immunotherapy. *Signal Transduct Target Ther*. (2021) 6:72. doi: 10.1038/s41392-020-00449-4

7. Gu L, Khadaroo PA, Su H, Kong L, Chen L, Wang X, et al. The safety and tolerability of combined immune checkpoint inhibitors (Anti-pd-1/pd-L1 plus anti-ctla-4): A systematic review and meta-analysis. *BMC Cancer*. (2019) 19:559. doi: 10.1186/s12885-019-5785-z

8. Ajani JA, D'Amico TA, Bentrem DJ, Chao J, Corvera C, Das P, et al. Esophageal and esophagogastric junction cancers, version 2.2019, nccn clinical practice guidelines in oncology. *J Natl Compr Cancer Network: JNCCN*. (2019) 17:855–83. doi: 10.6004/jnccn.2019.0033

9. Janjigian YY, Shitara K, Moehler M, Garrido M, Salman P, Shen L, et al. First-line nivolumab plus chemotherapy versus chemotherapy alone for advanced gastric, gastro-oesophageal junction, and oesophageal adenocarcinoma (Checkmate 649): A randomised, open-label, phase 3 trial. *Lancet*. (2021) 398:27–40. doi: 10.1016/s0140-6736(21)00797-2

10. Kato K, Doki Y, Ogata T, Motoyama S, Kawakami H, Ueno M, et al. First-line nivolumab plus ipilimumab or chemotherapy versus chemotherapy alone in advanced esophageal squamous cell carcinoma: A Japanese subgroup analysis of open-label, phase 3 trial (Checkmate 648/ono-4538-50). *Esophagus: Off J Japan Esophageal Soc*. (2023) 20:291–301. doi: 10.1007/s10388-022-00970-1

11. Pardoll DM. The blockade of immune checkpoints in cancer immunotherapy. *Nat Rev Cancer*. (2012) 12:252–64. doi: 10.1038/nrc3239

12. Simpson TR, Li F, Montalvo-Ortiz W, Sepulveda MA, Bergerhoff K, Arce F, et al. Fc-dependent depletion of tumor-infiltrating regulatory T cells co-defines the efficacy of anti-ctla-4 therapy against melanoma. *J Exp Med*. (2013) 210:1695–710. doi: 10.1084/jem.20130579

13. Latchman Y, Wood CR, Chernova T, Chaudhary D, Borde M, Chernova I, et al. Pd-L2 is a second ligand for pd-1 and inhibits T cell activation. *Nat Immunol*. (2001) 2:261–8. doi: 10.1038/85330

14. Freeman GJ, Long AJ, Iwai Y, Bourque K, Chernova T, Nishimura H, et al. Engagement of the pd-1 immunoinhibitory receptor by a novel B7 family member leads to negative regulation of lymphocyte activation. *J Exp Med*. (2000) 192:1027–34. doi: 10.1084/jem.192.7.1027

15. Wang J, Yuan R, Song W, Sun J, Liu D, Li Z. Pd-1, pd-L1 (B7-H1) and tumor-site immune modulation therapy: the historical perspective. *J Hematol Oncol*. (2017) 10:34. doi: 10.1186/s13045-017-0403-5

16. Topalian SL, Hodi FS, Brahmer JR, Gettinger SN, Smith DC, McDermott DF, et al. Safety, activity, and immune correlates of anti-pd-1 antibody in cancer. *New Engl J Med*. (2012) 366:2443–54. doi: 10.1056/NEJMoa1200690

17. Brahmer JR, Tykodi SS, Chow LQ, Hwu WJ, Topalian SL, Hwu P, et al. Safety and activity of anti-pd-L1 antibody in patients with advanced cancer. *New Engl J Med*. (2012) 366:2455–65. doi: 10.1056/NEJMoa1200694

18. Chen K, Wang X, Yang L, Chen Z. The anti-pd-1/pd-L1 immunotherapy for gastric esophageal cancer: A systematic review and meta-analysis and literature review. *Cancer Control: J Moffitt Cancer Center*. (2021) 28:1073274821997430. doi: 10.1177/1073274821997430

19. Wen W, Zhang Y, Zhang H, Chen Y. Clinical outcomes of pd-1/pd-L1 inhibitors in patients with advanced hepatocellular carcinoma: A systematic review and meta-analysis. *J Cancer Res Clin Oncol*. (2023) 149:969–78. doi: 10.1007/s00432-022-04057-3

20. Cheng W, Kang K, Zhao A, Wu Y. Dual blockade immunotherapy targeting pd-1/pd-L1 and ctla-4 in lung cancer. *J Hematol Oncol*. (2024) 17:54. doi: 10.1186/s13045-024-01581-2

21. Das R, Verma R, Sznol M, Boddupalli CS, Gettinger SN, Kluger H, et al. Combination therapy with anti-ctla-4 and anti-pd-1 leads to distinct immunologic changes *in vivo*. *J Immunol (Baltimore Md: 1950)*. (2015) 194:950–9. doi: 10.4049/jimmunol.1401686

22. Wei SC, Duffy CR, Allison JP. Fundamental mechanisms of immune checkpoint blockade therapy. *Cancer Discovery*. (2018) 8:1069–86. doi: 10.1158/2159-8290.Cd-18-0367

23. Gourd E. Nivolumab plus ipilimumab in metastatic colorectal cancer. *Lancet Oncol*. (2018) 19:e139. doi: 10.1016/s1470-2045(18)30067-6

24. Yau T, Kang YK, Kim TY, El-Khoueiry AB, Santoro A, Sangro B, et al. Efficacy and safety of nivolumab plus ipilimumab in patients with advanced hepatocellular carcinoma previously treated with sorafenib: the checkmate 040 randomized clinical trial. *JAMA Oncol*. (2020) 6:e204564. doi: 10.1001/jamaoncol.2020.4564

25. Chen IM, Johansen JS, Theile S, Hjaltelin JX, Novitski SI, Brunak S, et al. Randomized phase ii study of nivolumab with or without ipilimumab combined with stereotactic body radiotherapy for refractory metastatic pancreatic cancer (Checkpac). *J Clin Oncol: Off J Am Soc Clin Oncol*. (2022) 40:3180–9. doi: 10.1200/jco.21.02511

26. Kaseb AO, Hasanov E, Cao HST, Xiao L, Vauthey JN, Lee SS, et al. Perioperative nivolumab monotherapy versus nivolumab plus ipilimumab in resectable hepatocellular carcinoma: A randomised, open-label, phase 2 trial. *Lancet Gastroenterol Hepatol*. (2022) 7:208–18. doi: 10.1016/s2468-1253(21)00427-1

27. Yau T, Zagonel V, Santoro A, Acosta-Rivera M, Choo SP, Matilla A, et al. Nivolumab plus cabozantinib with or without ipilimumab for advanced hepatocellular carcinoma: results from cohort 6 of the checkmate 040 trial. *J Clin Oncol: Off J Am Soc Clin Oncol*. (2023) 41:1747–57. doi: 10.1200/jco.22.00972

28. Juloori A, Katipally RR, Lemons JM, Singh AK, Iyer R, Robbins JR, et al. Phase 1 randomized trial of stereotactic body radiation therapy followed by nivolumab plus ipilimumab or nivolumab alone in advanced/unresectable hepatocellular carcinoma. *Int J Radiat Oncol Biol Phys*. (2023) 115:202–13. doi: 10.1016/j.ijrobp.2022.09.052

29. Sahai V, Griffith KA, Beg MS, Shaib WL, Mahalingam D, Zhen DB, et al. A randomized phase 2 trial of nivolumab, gemcitabine, and cisplatin or nivolumab and ipilimumab in previously untreated advanced biliary cancer: bilt-01. *Cancer*. (2022) 128:3523–30. doi: 10.1002/cncr.34394

30. Parikh ND, Marshall A, Betts KA, Song J, Zhao J, Yuan M, et al. Network meta-analysis of nivolumab plus ipilimumab in the second-line setting for advanced hepatocellular carcinoma. *J Comp Effectiveness Res*. (2021) 10:343–52. doi: 10.2217/cer-2020-0236

31. Park S, Nam CM, Kim SG, Mun JE, Rha SY, Chung HC. Comparative efficacy and tolerability of third-line treatments for advanced gastric cancer: A systematic review with bayesian network meta-analysis. *Eur J Cancer (Oxford England: 1990)*. (2021) 144:49–60. doi: 10.1016/j.ejca.2020.10.030

32. Nejadghaderi SA, Balibegloo M, Rezaei N. The cochrane risk of bias assessment tool 2 (Rob 2) versus the original rob: A perspective on the pros and cons. *Health Sci Rep*. (2024) 7:e2165. doi: 10.1002/hsr2.2165

33. Higgins JP, Thompson SG, Deeks JJ, Altman DG. Measuring inconsistency in meta-analyses. *BMJ (Clin Res ed)*. (2003) 327:557–60. doi: 10.1136/bmj.327.7414.557

34. Shitara K, Ajani JA, Moehler M, Garrido M, Gallardo C, Shen L, et al. Nivolumab plus chemotherapy or ipilimumab in gastro-oesophageal cancer. *Nature*. (2022) 603:942–8. doi: 10.1038/s41586-022-04508-4

35. Kato K, Doki Y, Chau I, Xu J, Wyrwicz L, Motoyama S, et al. Nivolumab plus chemotherapy or ipilimumab versus chemotherapy in patients with advanced esophageal squamous cell carcinoma (Checkmate 648): 29-month follow-up from a randomized, open-label, phase iii trial. *Cancer Med*. (2024) 13:e7235. doi: 10.1002/cam4.7235

36. Janjigian YY, Bendell J, Calvo E, Kim JW, Ascierto PA, Sharma P, et al. Checkmate-032 study: efficacy and safety of nivolumab and nivolumab plus ipilimumab in patients with metastatic esophagogastric cancer. *J Clin Oncol: Off J Am Soc Clin Oncol*. (2018) 36:2836–44. doi: 10.1200/jco.2017.76.6212

37. Elez E, Cubillo A, Alfonso PG, Middleton MR, Chau I, Alkuzweny B, et al. Binimetinib in combination with nivolumab or nivolumab and ipilimumab in patients with previously treated microsatellite-stable metastatic colorectal cancer with ras mutations in an open-label phase 1b/2 study. *BMC Cancer*. (2024) 24:446. doi: 10.1186/s12885-024-12153-5

38. Huynh JC, Schwab E, Ji J, Kim E, Joseph A, Hendifar A, et al. Recent advances in targeted therapies for advanced gastrointestinal Malignancies. *Cancers (Basel)*. (2020) 12:11–2. doi: 10.3390/cancers12051168

39. Lin EW, Karakasheva TA, Hicks PD, Bass AJ, Rustgi AK. The tumor microenvironment in esophageal cancer. *Oncogene*. (2016) 35:5337–49. doi: 10.1038/onc.2016.34

40. Tanaka R, Eguchi S, Kimura K, Ohira G, Tanaka S, Amano R, et al. Tumor-infiltrating lymphocytes and macrophages as a significant prognostic factor in biliary tract cancer. *PloS One*. (2023) 18:e0280348. doi: 10.1371/journal.pone.0280348

41. Qin R, Jin T, Xu F. Biomarkers predicting the efficacy of immune checkpoint inhibitors in hepatocellular carcinoma. *Front Immunol*. (2023) 14:1326097. doi: 10.3389/fimmu.2023.1326097

42. Donne R, Lujambio A. The liver cancer immune microenvironment: therapeutic implications for hepatocellular carcinoma. *Hepatology*. (2023) 77:1773–96. doi: 10.1002/hep.32740

43. Ji S, Feng L, Fu Z, Wu G, Wu Y, Lin Y, et al. Pharmaco-proteogenomic characterization of liver cancer organoids for precision oncology. *Sci Trans Med*. (2023) 15:eadg3358. doi: 10.1126/scitranslmed.adg3358

44. Llovet JM, Ricci S, Mazzaferro V, Hilgard P, Gane E, Blanc JF, et al. Sorafenib in advanced hepatocellular carcinoma. *New Engl J Med*. (2008) 359:378–90. doi: 10.1056/NEJMoa0708857

45. Pinyol R, Montal R, Bassaganyas L, Sia D, Takayama T, Chau GY, et al. Molecular predictors of prevention of recurrence in hcc with sorafenib as adjuvant treatment and prognostic factors in the phase 3 storm trial. *Gut*. (2019) 68:1065–75. doi: 10.1136/gutjnl-2018-316408

46. Ros-Buxó M, Mauro E, Sauri T, Iserte G, Fuster-Anglada C, Díaz A, et al. Integrating molecular insights into biliary tract cancer management: A review of personalized therapeutic strategies. *Curr Oncol (Toronto Ont)*. (2024) 31:3615–29. doi: 10.3390/curroncol31070266

frontiers | Frontiers in Oncology

TYPE Case Report
PUBLISHED 26 February 2025
DOI 10.3389/fonc.2025.1507281

OPEN ACCESS

EDITED BY
Giovanna Damia,
Mario Negri Institute for Pharmacological Research (IRCCS), Italy

REVIEWED BY
Hesong Wang,
Fourth Hospital of Hebei Medical University, China
Somnath Roy,
Tata Medical Centre, India

*CORRESPONDENCE
Yuanhua Zhao
15107168769@163.com
Bo Luo
79019884@qq.com

RECEIVED 07 October 2024
ACCEPTED 07 February 2025
PUBLISHED 26 February 2025

CITATION
Liang G, Zhang Q, Luo Y, Zhao Y and Luo B (2025) Efficacy of anlotinib and chemotherapy combination as neoadjuvant therapy in the treatment of pulmonary artery intimal sarcoma: a case report.
Front. Oncol. 15:1507281.
doi: 10.3389/fonc.2025.1507281

Efficacy of anlotinib and chemotherapy combination as neoadjuvant therapy in the treatment of pulmonary artery intimal sarcoma: a case report

Gai Liang, Qu Zhang, Yan Luo, Yuanhua Zhao* and Bo Luo*

Department of Radiation Oncology, Hubei Cancer Hospital, TongJi Medical College, Huazhong University of Science and Technology, Wuhan, China

Pulmonary arterial intimal sarcoma (PAIS) is a rare malignant mesenchymal tumor often associated with an unfavorable prognosis and lacks a standardized treatment approach to date. This report presents a notable case of PAIS treated with neoadjuvant therapy involving anlotinib concomitantly administered with chemotherapy of ifosfamide and pirarubicin, which resulted in a favorable outcome. A 38-year-old man was admitted to our hospital with chest tightness, cough, and dyspnea, all of which had persisted for more than a week. Initial evaluation via chest computed tomography (CT) revealed a sizable posterior mediastinal tumor measuring 11.9 × 7.6 cm. A CT-guided biopsy was performed, and pathological findings confirmed the diagnosis of PAIS. Efficacy evaluation showed slow progress after one cycle of chemotherapy with ifosfamide and pirarubicin. To enhance treatment outcomes, we incorporated anlotinib as a neoadjuvant therapy alongside ifosfamide and pirarubicin. Subsequent CT imaging demonstrated a significant reduction in tumor size, and the patient experienced notable alleviation of symptoms. The patient then underwent surgery, radiation, and subsequently, maintenance treatment with anlotinib for one year. No severe drug-related side effects were observed. The patient achieved progression-free survival of 25 months following administration of anlotinib. Thus, the combination of anlotinib with ifosfamide and pirarubicin demonstrated significant efficacy and safety. This approach holds promise as an effective therapeutic strategy for managing unresectable, locally advanced, or advanced PAIS. However, further clinical studies are necessary to validate these findings.

KEYWORDS

pulmonary artery intimal sarcoma, anlotinib, neoadjuvant treatment, chemotherapy, case report

Introduction

Pulmonary arterial intimal sarcoma (PAIS) is a rare malignant mesenchymal tumor that occurs in large blood vessels of the pulmonary circulation (1). PAIS can originate from the left and right pulmonary arteries, as well as the intimal layer of the pulmonary arteries, forming a tumor that either grows in a nodular cavity or spreads along the intimal surface (2). The prognosis of PAIS is poor, and currently, there is no established standard treatment strategy (3). Surgical resection is presently the primary choice of treatment for PAIS, and the role of postoperative radiotherapy and chemotherapy remains controversial (4). However, there have been no reports on the treatment of PAIS using a neoadjuvant regimen with anlotinib. In this study, we present a noteworthy case of a patient with PAIS who underwent neoadjuvant treatment using the anlotinib and ifosfamide and pirarubicin regimen, resulting in a successful outcome. The combination therapy for neoadjuvant treatment may lead to a better PAIS prognosis.

Case/case series presentation

In June 2022, a 38-year-old man was admitted to our hospital with chest tightness, cough, and dyspnea, all of which had persisted for more than a week. Physical examination of the patient revealed a body temperature of 36.6°C, blood pressure of 95/78 mmHg, tachycardia characterized by a heart rate of 120 bpm, and tachypnea with a respiratory rate of 24 bpm. The oxygen saturation (SpO_2) in room air was recorded at only 98%. Liver function tests, renal function tests, and complete blood count showed normal results. He had no medical, family, psychosocial, or genetic history. Upon assessment, the Eastern Cooperative Oncology Group (ECOG) performance status score was determined to be 2. On July 4, 2022, an initial chest computed tomography (CT) evaluation revealed a sizable posterior mediastinal tumor measuring 11.9 × 7.6 cm. This tumor not only involved the right pulmonary arteries but also led to pericardial effusion, accompanied by a minor pleural effusion on both sides (Figure 1A). Further positron emission tomography-computed tomography (PET-CT) investigations revealed a large soft-tissue mass with increased metabolic activity (SUV_{max}: 26.3) within the posterior mediastinum. Notably, this mass involved the right pulmonary artery trunk and its associated arteries, prompting considerations of a potential malignant tumor (Figure 1B).

After discussions with specialists in thoracic surgery, medical oncology, radiation oncology, and radiology during a multidisciplinary treatment (MDT) consultation, we concluded that complete tumor resection was not feasible in this case. Therefore, a CT-guided biopsy was performed on July 18, 2022. Pathological findings revealed spindle or epithelioid shapes in the

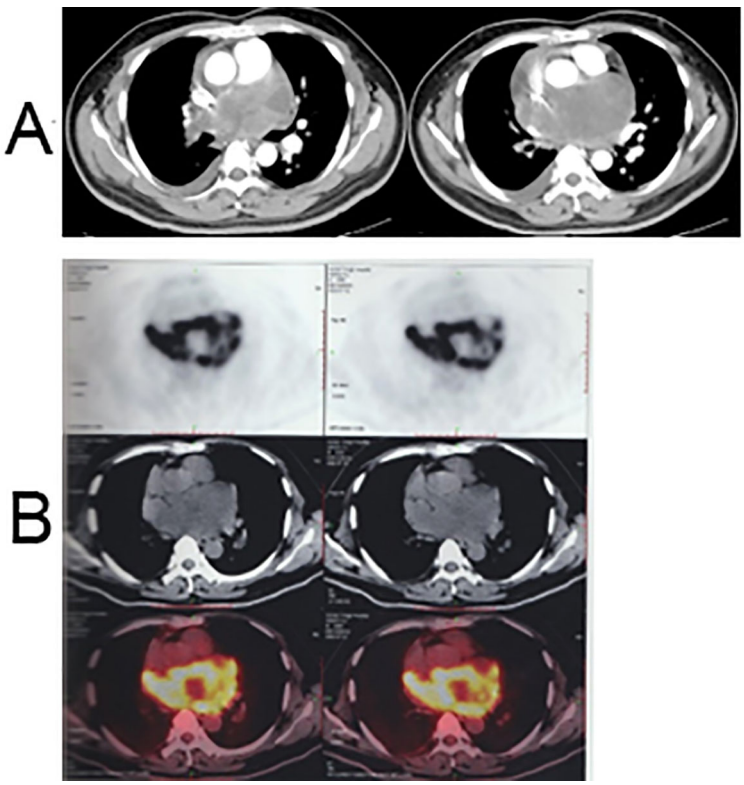

FIGURE 1
Chest CT and PET-CT scan before treatment. **(A)** Enhanced chest CT scan images: a posterior mediastinal tumor measuring 11.9 × 7.6 cm with involvement of the right pulmonary arteries, accompanied by pericardial effusion and minor pleural effusion on both sides; **(B)** PET-CT scan image: a large soft tissue mass in the posterior mediastinum with increased metabolism (SUV_{max}: 26.3), involving the right pulmonary artery trunk and associated arteries.

tumor cells, characterized by abundant cytoplasm and large nuclei with rough chromatin. Positive immunohistochemical staining for SATB2 and MDM2 was observed, along with a high proliferative index (Ki67). Amplification of MDM2 was confirmed through fluorescence *in situ* hybridization detection (Figures 2A–E). Combining the medical history, clinical imaging, immunohistochemistry, and molecular test analyses, we established a diagnosis of PAIS with the clinical stage T3N0M0 (IIIB) according to the eighth edition of the AJCC cancer staging.

According to pathological findings, the patient underwent one cycle of chemotherapy using the ifosfamide and pirarubicin (ifosfamide, 2 g/m^2, days 1-5; pirarubicin, 40 mg/m^2, day 1) on July 22, 2022. Three weeks later, despite the treatment, the patient's chest pain and cough persisted. A follow-up CT scan indicated that the tumor had not diminished significantly and measured 14.0 × 7.5 cm. The efficacy evaluation progressed slowly but did not reach PD (Figure 3A). As the effect of chemotherapy alone proved unsatisfactory, and based on insights from prior clinical studies suggesting improved efficacy with antiangiogenic agents, the decision was made to incorporate anlotinib into the treatment plan. Anlotinib, which is known to improve the survival rates of patients with advanced soft tissue sarcomas (5), was prescribed at a dosage of 12 mg once daily for 2 weeks, followed by a 1-week break, in combination with ifosfamide and pirarubicin. After two cycles of administration, a subsequent CT scan revealed a significant reduction in tumor size, measuring approximately 10.1 × 6.3 cm (Figure 3B). Encouraged by the positive response, the patient continued treatment with a combination of anlotinib and chemotherapy with ifosfamide and pirarubicin for five cycles. The final CT scan at the end of the last cycle showed a substantial reduction in tumor size, measuring 6.8 × 3.7 cm. Clinically, the evaluation was a partial response (Figure 3C), and the patient experienced gradual relief from chest tightness, dyspnea, and cough. Throughout the treatment process, the patient experienced some adverse effects, including grade 1 nausea and vomiting, grade 1 hypertension, grade 3 leukopenia, and grade 1 rash.

Subsequently, the tumor stabilized at a size of 6.8 × 3.7 cm. Following a second MDT discussion, the patient was advised to undergo surgery for palliative tumor reduction. He consented to this treatment approach and underwent the resection of the remaining tumor on January 11, 2023.

Postoperative pathology revealed the following findings: a treatment-induced tumor reaction marked by the degeneration and necrosis of tumor cells, proliferation of stromal fibrous tissue, and infiltration of foam cells and mixed inflammatory cells. The remaining limited tumor cells still expressed MDM2 but exhibited a low Ki67 (Figures 2F–H).

One month post-surgery, the CT scan indicated normal postoperative changes, and the tumor size had decreased from 6.8 × 3.7 cm to 3.5 × 2.7 cm (Figure 4A). The patient then underwent intensity-modulated radiotherapy at a total dose of 66 Gy in 33 fractions. The planning target volume included the residual tumor and tumor bed. Throughout the radiotherapy sessions, the patient concurrently received maintenance treatment with anlotinib. After the completion of radiotherapy, the patient continued consolidation therapy with anlotinib for one year.

Clinical evaluation at the 8-month post-surgery mark revealed stable disease with a tumor size of 3.1 × 1.5 cm (Figure 4B). No

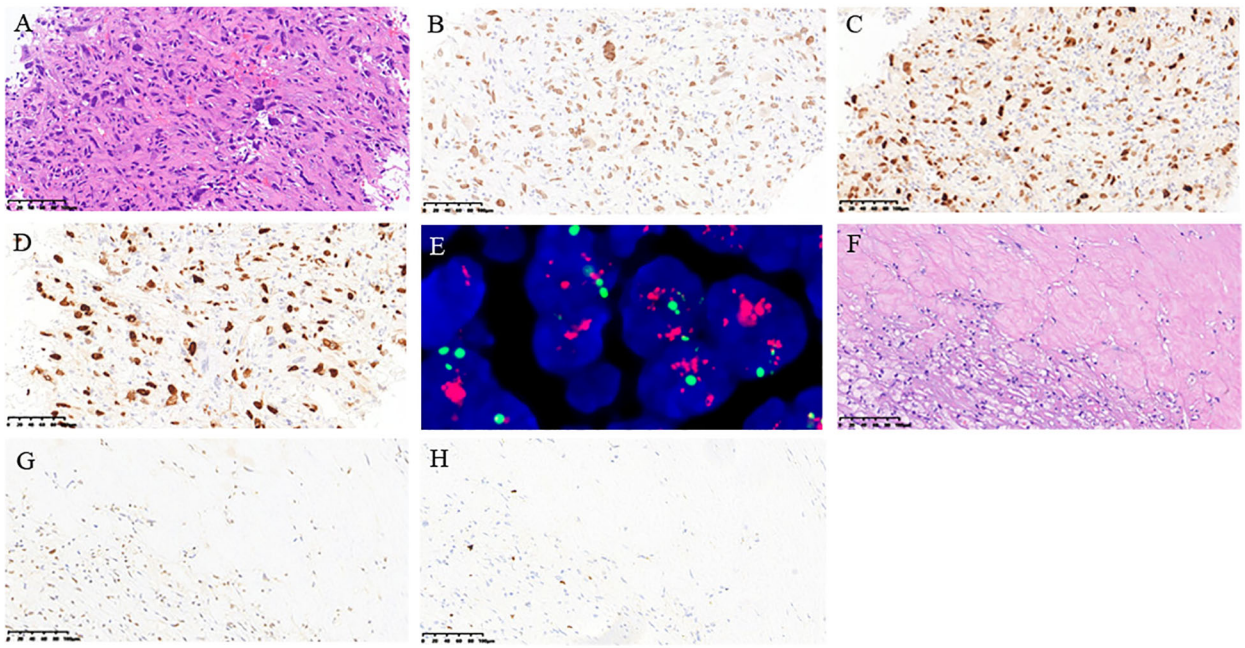

FIGURE 2
Pathological findings of the histology of posterior mediastinal biopsy tissue. **(A)** H&E staining; **(B)** immunohistochemical staining of SATB2; **(C)** immunohistochemical staining of MDM2; **(D)** immunohistochemical staining of Ki67 index; **(E)** fluorescence *in situ* hybridization detection of MDM2; **(F)** H&E staining; **(G)** immunohistochemical staining of MDM2; **(H)** immunohistochemical staining of Ki67. (**A-E**: From the biopsy sample before treatment, **F-H**: from the surgical sample after treatment).

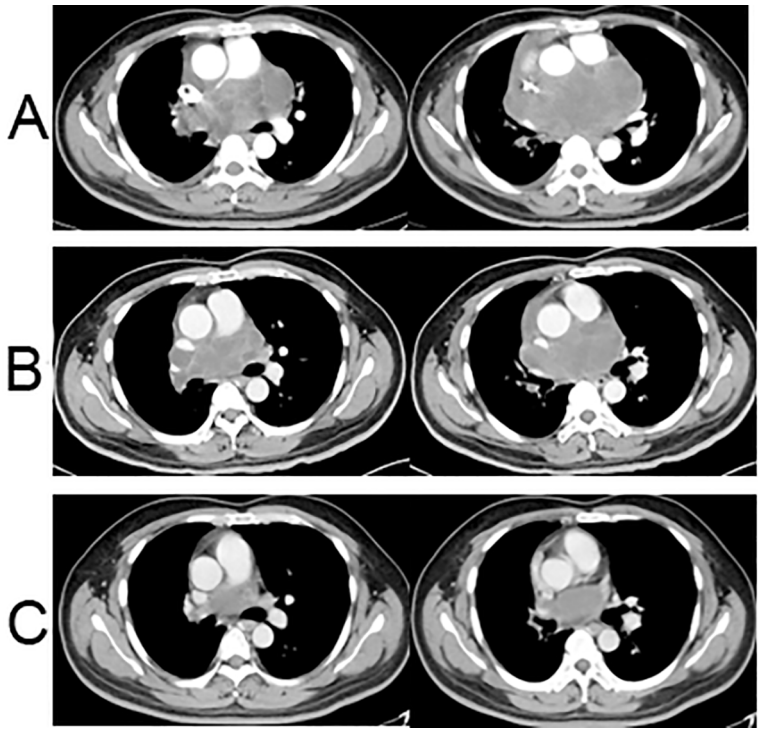

FIGURE 3
Chest CT scans after neoadjuvant treatment. **(A)** Chest CT enhanced scan after one cycle of chemotherapy: the tumor had increased in size, measuring 14.0 × 7.5 cm; **(B)** Chest CT enhanced scan after two cycles of chemotherapy + anlotinib: the tumor had significantly shrunk with a size of approximately 10.1 × 6.3 cm; **(C)** Enhanced chest CT scan after five cycles of chemotherapy + anlotinib: the tumor had significantly shrunk at the end of the fifth cycle of chemotherapy + anlotinib, measuring 6.8 × 3.7 cm.

severe drug-related side effects were observed. The timeline of changes in tumor size and treatments administered are shown in Figure 5. The patient achieved a progression-free survival (PFS) of 25 months as of September 27, 2024, and regular follow-up is being conducted.

Discussion

PAIS is an extremely rare malignant mesenchymal tumor. As of 2023, approximately 400 cases of PAIS have been reported in the literature (3), most of which have been published as case reports.

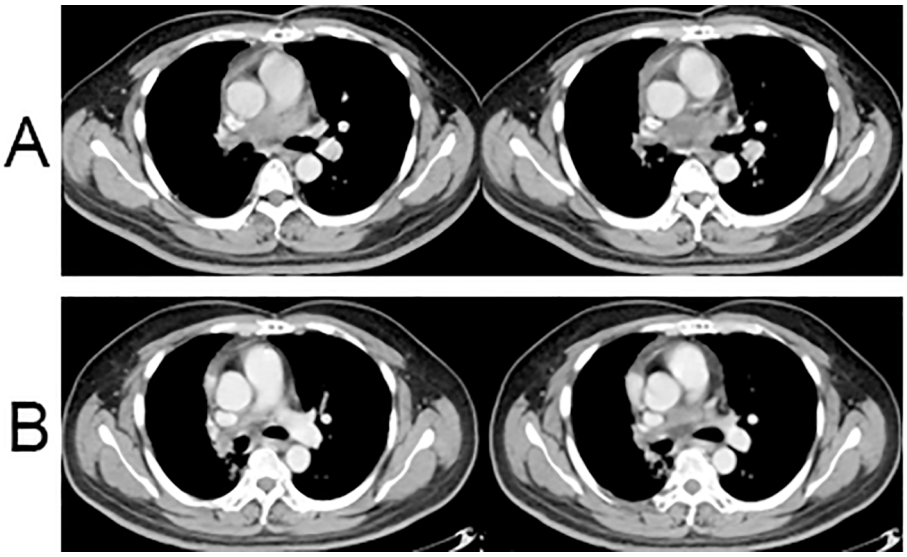

FIGURE 4
Postoperative chest CT results. **(A)** Enhanced chest CT scan at 1 month after surgery; **(B)** Enhanced chest CT scan at 6 months after surgery.

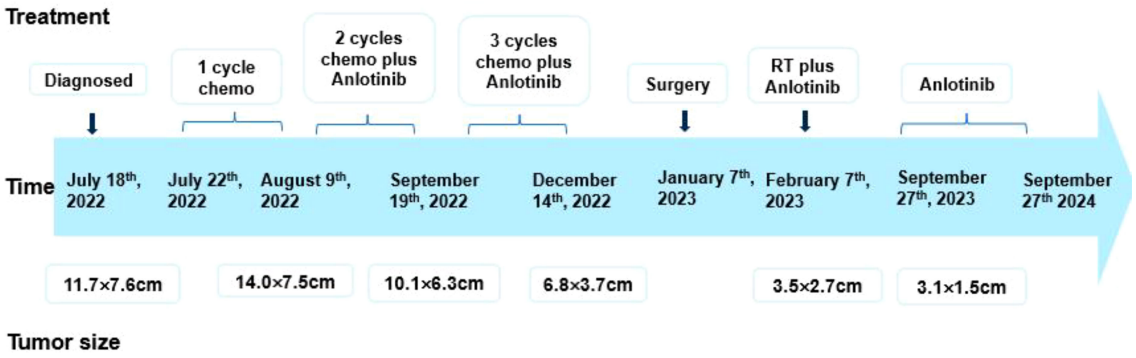

FIGURE 5
Timeline of tumor size and treatment of the patient. Chemo, ifosfamide and pirarubicin; RT, radiation therapy.

Despite this, the pathogenesis of the disease remains unclear. Common symptoms of PAIS include dyspnea, cough, chest tightness, and hemoptysis, often attributed to chronic right heart failure or associated malignant tumors (6). In the present case, the patient presented with difficulty in breathing, cough, and chest tightness associated with a malignant tumor.

The pathological characteristics of PAIS include predominantly spindle-shaped cells under light microscopy, along with scattered multinucleated giant cells and epithelioid cells. Immunohistochemistry lacks specificity, with most cases showing diffuse positivity for vimentin, along with partial expression of SMA and CD34 (7). Literature reports indicate frequent detections of PAIS based on gene amplifications, including MDM2 (65%), cyclin-dependent kinase 4, platelet-derived growth factor receptor α (81%), and EGFR (76%) (8). In the present case, MDM2 gene amplification was positive, aligning with findings in previous studies (3, 7).

Currently, no standardized treatment strategy exists for PAIS, particularly for cases that are unresectable or locally recurrent. Surgery remains the cornerstone of treatment for this condition, which may include pulmonary endarterectomy, lobectomy, or pneumonectomy. The role of adjuvant therapy is not well-defined; however, there are case reports indicating improved outcomes with the use of chemotherapy and/or radiation therapy (RT) (9). A review from the MD Anderson Cancer Center revealed a median survival of 25 months for patients receiving multimodal therapy, compared to just 8 months for those undergoing single-modality treatment (10). Most adjuvant chemotherapy regimens included anthracyclines, such as doxorubicin, as well as ifosfamide. Additionally, a limited number of studies have reported the use of gemcitabine and paclitaxel, although their efficacy appears to be suboptimal.

Neoadjuvant therapy involves the use of systemic treatments before surgery. Initially employed to treat inoperable locally advanced breast cancer (11), neoadjuvant therapy has proven effective in increasing the likelihood of breast-conserving surgery and thus established itself as a viable option for patients with operable disease (12, 13). Studies have shown that patients who achieved a pathologic complete response after neoadjuvant treatment had a significantly better prognosis than those with residual disease (14–16). For unresectable or recurrent focal sarcomas, common neoadjuvant therapies involve chemotherapy with doxorubicin and cyclophosphamide, either alone or in combination with radiotherapy (17, 18). However, there have been no studies on neoadjuvant chemotherapy with antiangiogenic drugs for PAIS.

Anlotinib is a multi-target tyrosine kinase inhibitor with dual effects: inhibiting angiogenesis and directly impeding tumor growth. The functional targets of anlotinib encompass vascular endothelial growth factor receptors 1/2/3, platelet-derived growth factor receptor, fibroblast growth factor receptor, and c-Kit (19). Anlotinib's mechanism of action includes inhibition of tumor vascular survival, normalization of tumor tissue blood vessels, improvement in tumor hypoxia, increase in chemotherapy distribution in tumor tissue, and further enhancement of anti-tumor effects. Therefore, the combination of anlotinib and chemotherapy can have a synergistic effect (20). Research has shown that in second-line advanced soft tissue sarcoma, anlotinib has an efficacy rate of 12.7%, with a PFS rate of 86.4% at 12 weeks. Results from the Phase IIB Alter0203 study reveal that, compared to a placebo, anlotinib significantly prolongs the time without disease progression and reduces the risk of progression in patients (6.27 months vs 1.47 months, HR=0.33) (5, 21). Notably, pathological types in this study mainly included leiomyosarcoma, synovial sarcoma, acinar soft tissue sarcoma, clear cell sarcoma, epithelioid sarcoma, undifferentiated pleomorphic sarcoma, liposarcoma, and fibrosarcoma and did not include PAIS. In the present case, clinical evaluation progressed slowly after one cycle of chemotherapy with ifosfamide and pirarubicin. The patient was dissatisfied with the efficacy of chemotherapy alone and continued to experience symptoms of cough and chest tightness. Following extensive communication with the patient, we decided to administer anlotinib in combination with ifosfamide and pirarubicin. After two treatment cycles, we observed a significant improvement in the patient's symptoms of cough and chest tightness, reflected in the clinical evaluation as a partial response. Consequently, the patient continued this combined regimen for three cycles. The tumor size was effectively reduced with the combination treatment, leading to an improvement in the patient's overall condition.

After the final chemotherapy session, a follow-up CT scan revealed a residual tumor in the right pulmonary artery, and the patient was intolerant to further chemotherapy. Following an MDT discussion, we recommended local surgery and radiotherapy. Postoperative pathology closely resembled complete remission. To minimize local recurrence and distant metastases, radiation therapy was administered for residual lesions after surgery concurrently with anlotinib therapy. As demonstrated in a clinical trial investigating the safety and efficacy of anlotinib, the most common adverse drug reactions (ADRs) associated with anlotinib include hypertension, hand-foot syndrome, and hyperlipidemia, among others (5). The patient exhibited good tolerance with no serious adverse effects.

The prognosis for patients with PAIS is generally poor, with untreated patients having an overall survival of approximately 1.5 to 3 months (4). The median survival after complete surgical resection can extend to 36.5 ± 20.2 months, whereas after incomplete surgical resection, it can reach 11.3 months (10). Funatsu (22) reported a partial response of PAIS to pazopanib as second-line treatment in a case with PFS of 4 months, and the patient required cessation of pazopanib because of severe hand-foot syndrome. Kollár's study showed that pazopanib had promising activity as a second-line treatment in angiosarcoma with PFS of 3 months and OS of 9.9 months (23). Therapeutic interventions aimed at MDM2-amplified sarcoma are presently being evaluated in clinical trials. Takafumi noted that milademetan, an MDM2 inhibitor, showed effectiveness in patients with MDM2-amplified intimal sarcoma. This suggests it could be a viable treatment option for intimal sarcoma, as indicated by a Phase Ib/II study that reported PFS of 4.7 months, which merits further investigation (24).

In this case, the patient achieved a PFS of 25 months after treatment with anlotinib and maintained a good condition during follow-up. Such kind of multimodal therapy for PAIS may be a viable strategy. However, these data from the case report are still very limited, and further research is needed to elucidate the value of neoadjuvant chemotherapy with anlotinib for PAIS to improve the prognosis of patients.

Conclusion

In summary, neoadjuvant treatment using the combination of anlotinib and chemotherapy with ifosfamide and pirarubicin successfully reduced the tumor size in a patient with PAIS, demonstrating favorable efficacy and safety. The combination of anlotinib and chemotherapy as a neoadjuvant therapy could be an effective strategy for unresectable locally advanced or advanced PAIS. However, further clinical studies are necessary to validate these findings.

Data availability statement

The raw data supporting the conclusions of this article will be made available by the authors, without undue reservation.

Ethics statement

The studies involving humans were approved by Ethics Committee of Hubei Cancer Hospital. The studies were conducted in accordance with the local legislation and institutional requirements. The participants provided their written informed consent to participate in this study. Written informed consent was obtained from the individual(s) for the publication of any potentially identifiable images or data included in this article.

Author contributions

GL: Conceptualization, Data curation, Investigation, Methodology, Writing – original draft. QZ: Formal analysis, Funding acquisition, Project administration, Resources, Validation, Visualization, Writing – original draft. YL: Data curation, Methodology, Supervision, Writing – original draft. YZ: Visualization, Writing – review & editing. BL: Validation, Visualization, Writing – review & editing.

Funding

The author(s) declare that no financial support was received for the research, authorship, and/or publication of this article.

Acknowledgments

We would like to thank Professor Guo Fang from the Department of Pathology at our hospital for revising the manuscript. Additionally, we would like to thank Editage (www.editage.cn) for English language editing.

Conflict of interest

The authors declare that the research was conducted in the absence of any commercial or financial relationships that could be construed as a potential conflict of interest.

Generative AI statement

The author(s) declare that no Generative AI was used in the creation of this manuscript.

Publisher's note

References

1. WHO Classification of Tumours Editorial Board. *WHO classification of tumours, Thoracic tumours. 5th ed*. Lyon: IARC Press (2021).

2. Bai X, Ruan L. A case report of primary pulmonary artery intimal sarcoma. *Eur J Med Res*. (2021) 26:89. doi: 10.1186/s40001-021-00568-w

3. Shao N, Deng C. Pulmonary thromboembolic disease or pulmonary artery intimal sarcoma: Case report and literature review. *Oncol Lett*. (2022) 24:350. doi: 10.3892/ol.2022.13470

4. Li X, Hong L, Huo XY. Undifferentiated intimal sarcoma of the pulmonary artery: A case report. *World J Clin cases*. (2021) 9:3960–5. doi: 10.12998/wjcc.v9.i16.3960

5. Chi Y, Yao Y, Wang S, Cai Q, Shang S, Wang G, et al. Anlotinib for metastasis soft tissue sarcoma: a randomized, double-blind, placebo-controlled and multi-centered clinical trial. *J Clin Oncol*. (2018) 36:11503. doi: 10.1200/JCO.2018.36.15_suppl.11503

6. Li YC, Li LY, Tong HC, Xu HT, Ma S, Yang LH, et al. Pulmonary artery intimal sarcoma mimicking pulmonary thromboembolism: A case report. *Med (Baltimore)*. (2021) 100:e24699. doi: 10.1097/MD.0000000000024699

7. Wang B, Zhang T, Liu HY. Clinicopathological characteristics of pulmonary artery intimal sarcoma. *Chin J Pathol*. (2021) 50:38. doi: 10.3760/cma.j.cn112151-20200413-00313

8. Van Dievel J, Sciot R, Delcroix M, Vandeweyer RO, Debiec-Rychter M, Dewaele B, et al. Single-center experience with intimal sarcoma, an ultra-orphan, commonly fatal mesenchymal Malignancy. *Oncol Res Treat*. (2017) 40:353–9. doi: 10.1159/000476036

9. Atahan C, Güral Z, Yücel S, Ağaoğlu F. Pulmonary artery intimal sarcoma: Case report of a patient managed with multimodality treatment and a comprehensive literature review. *Strahlenther Onkol*. (2024) 200:725–9. doi: 10.1007/s00066-024-02250-6

10. Blackmon SH, Rice DC, Correa AM, Mehran R, Putnam JB, Smythe WR, et al. Management of primary pulmonary artery sarcomas. *Ann Thorac Surg*. (2009) 87:977–84. doi: 10.1016/j.athoracsur.2008.08.018

11. Korde LA, Somerfield MR, Carey LA, Crews JR, Denduluri N, Hwang ES, et al. Neoadjuvant chemotherapy, endocrine therapy, and targeted therapy for breast cancer: ASCO guideline. *J Clin Oncol*. (2021) 39:1485. doi: 10.1200/JCO.20.03399

12. Bear HD, Anderson S, Brown A, Smith R, Mamounas EP, Fisher B, et al. The effect on tumor response of adding sequential preoperative docetaxel to preoperative doxorubicin and cyclophosphamide: preliminary results from National Surgical Adjuvant Breast and Bowel Project Protocol B-27. *J Clin Oncol*. (2003) 21:4165–74. doi: 10.1200/JCO.2003.12.005

13. Golshan M, Loibl S, Wong SM, Houber JB, O'Shaughnessy J, Rugo HS, et al. Breast conservation after neoadjuvant chemotherapy for triple-Negative breast cancer: surgical results from the brighTNess randomized clinical trial. *JAMA Surg*. (2020) 155:e195410. doi: 10.1001/jamasurg.2019.5410

14. Rastogi P, Anderson SJ, Bear HD, Geyer CE, Kahlenberg MS, Robidoux A, et al. Preoperative chemotherapy: updates of National Surgical Adjuvant Breast and Bowel Project Protocols B-18 and B-27. *J Clin Oncol*. (2008) 26:778–85. doi: 10.1200/JCO.2007.15.0235

15. Cortazar P, Zhang L, Untch M, Mehta K, Costantino JP, Wolmark N, et al. Pathological complete response and long-term clinical benefit in breast cancer: the CTNeoBC pooled analysis. *Lancet*. (2014) 384:164–72. doi: 10.1016/S0140-6736(13)62422-8

16. Spring LM, Fell G, Arfe A, Sharma C, Greenup R, Reynolds KL, et al. Pathologic complete response after neoadjuvant chemotherapy and impact on breast cancer recurrence and survival: A comprehensive meta-analysis. *Clin Cancer Res*. (2020) 26:2838–48. doi: 10.1158/1078-0432.CCR-19-3492

17. Goerlich CE, Zehr K, Aziz H, Kilic A, et al. Repeat resection for recurrence of pulmonary artery intimal sarcoma. *J Card Surg*. (2021) 36:3889–91. doi: 10.1111/jocs.v36.10

18. Allen A, Smith SC, Pillappa R, Boikos S, Medalion B, Grizzard J, et al. Intimal sarcoma of the pulmonary artery treated with neoadjuvant radiation prior to pulmonary artery resection and reconstruction. *Respir Med Case Rep*. (2021) 33:101414. doi: 10.1016/j.rmcr.2021.101414

19. Li S, Wang H. Research progress on mechanism and management of adverse drug reactions of anlotinib. *Drug Des Devel. Ther*. (2023) 17:3429–37. doi: 10.2147/DDDT.S426898

20. Su Y, Luo B, Lu Y, Wang D, Yan J, Zheng J, et al. Anlotinib induces a T cell-Inflamed tumor microenvironment by facilitating vessel normalization and enhances the efficacy of PD-1 checkpoint blockade in neuroblastoma. *Clin Cancer Res*. (2022) 28:793–809. doi: 10.1158/1078-0432.CCR-21-2241

21. Zhang RS, Liu J, Deng YT, Wu X, Jiang Y, et al. The real-world clinical outcomes and treatment patterns of patients with unresectable locally advanced or metastatic soft tissue sarcoma treated with anlotinib in the post-ALTER0203 trial era. *Cancer Med*. (2022) 11:2271–83. doi: 10.1002/cam4.v11.11

22. Funatsu Y, Hirayama M, Shiraishi J, Asakura T, Wakaki M, Yamada E, et al. Intimal sarcoma of the pulmonary artery treated with pazopanib. *Intern Med*. (2016) 55:2197–202. doi: 10.2169/internalmedicine.55.6199

23. Kollár A, Jones RL, Stacchiotti S, Gelderblom H, Guida M, Grignani G, et al. Pazopanib in advanced vascular sarcomas: an EORTC Soft Tissue and Bone Sarcoma Group (STBSG) retrospective analysis. *Acta Oncol*. (2017) 56:88–92. doi: 10.1080/0284186X.2016.1234068

24. Koyama T, Shimizu T, Kojima Y, Sudo K, Okuma HS, Shimoi T, et al. Clinical activity and exploratory resistance mechanism of milademetan, an MDM2 inhibitor, in intimal sarcoma with MDM2 amplification: an open-label phase ib/II study. *Cancer Discovery*. (2023) 13:1814–25. doi: 10.1158/2159-8290.CD-23-0419

frontiers | Frontiers in Oncology

TYPE Original Research
PUBLISHED 16 May 2025
DOI 10.3389/fonc.2025.1533059

OPEN ACCESS

EDITED BY
Giovanna Damia,
Mario Negri Institute for Pharmacological Research (IRCCS), Italy

REVIEWED BY
Haiwei Du,
Chinese Academy of Medical Sciences and Peking Union Medical College, China
Nimish Gera,
Mythic Therapeutics, United States

*CORRESPONDENCE
Mark L. Chiu
Mark.Chiu@tavotek.com

RECEIVED 23 November 2024
ACCEPTED 23 April 2025
PUBLISHED 16 May 2025

CITATION
Jin Y, Sun P, Chen P, Xu Y, Mu G, Zha Z, Wu S, Fu M, Jiang H, Huang S, Zhou F, Han C and Chiu ML (2025) A trispecific antibody targeting EGFR/cMET/VEGF-A demonstrates multiple mechanisms of action to inhibit wild-type and mutant NSCLC animal models. *Front. Oncol.* 15:1533059. doi: 10.3389/fonc.2025.1533059

A trispecific antibody targeting EGFR/cMET/VEGF-A demonstrates multiple mechanisms of action to inhibit wild-type and mutant NSCLC animal models

Ying Jin[1], Ping Sun[1], Peng Chen[1], Yuqiang Xu[1], Guangmao Mu[1], Zhengxia Zha[1], Simin Wu[1], Meixia Fu[1], Hao Jiang[1], Sheng Huang[1], Fulai Zhou[1], Chao Han[1,2] and Mark L. Chiu[1,2]*

[1]Research & Development Department, Tavotek Biotherapeutics, Suzhou, Jiangsu, China, [2]Research & Development, Tavotek Biotherapeutics, Spring House, PA, United States

Introduction: Non-small cell lung cancer (NSCLC) patients who do not respond to standard of care treatment can have activating mutations in the epidermal growth factor receptor (EGFR) and mesenchymal epithelial transition factor (cMET) signaling pathways, as well as having enhanced levels of vascular endothelial growth factor (VEGF). To combat such resistance mechanisms, TAVO412, was engineered to control aberrant cMET, VEGF-A, and EGFR activities.

Methods: *In vitro* assays assessed TAVO412's cell binding, ligand blockade, phosphorylation inhibition, and Fc effector functions. In vivo efficacy was evaluated in NSCLC xenograft models, with subsequent tumor resection for ex vivo quantification of EGFR and cMET levels.

Results: TAVO412 robustly suppressed ligand-induced phosphorylation of EGFR and cMET in NSCLC cell lines. TAVO412 demonstrated more potent antitumor activity than amivantamab and cetuximab in NSCLC xenograft models using cell lines with varying levels of mutant and wild-type *EGFR* and *cMET*. In addition, TAVO412 had both EGFR/ cMET receptor degradation and enhanced Fc effector functions for tumor cell cytotoxicity. Moreover, TAVO412 in combination with osimertinib, lazertinib, docetaxel, and radiotherapy, resulted in complete and durable regression of NSCLC xenograft tumors.

Discussion: These findings highlight TAVO412 as a promising therapeutic agent with multiple mechanisms of action and strong potential for synergistic combinations in NSCLC treatment.

KEYWORDS

trispecific antibodies, NSCLC, EGFR cancer cells +, cmet, VEGF

Introduction

Non-small cell lung cancer (NSCLC) is the most common type of lung cancer with a poor prognosis and low 5-year overall survival (OS) (1). Prognosis and treatment approaches are primarily influenced by histology, stage at diagnosis, and molecular abnormalities. Since standards of care therapies such as surgery, chemotherapy, and radiotherapy do not fully meet the medical needs, there are ongoing discovery of better targeted therapies to provide greater efficacy and safety especially for patients with specific genomic alterations (2). Epidermal growth factor receptor (*EGFR*) gene dysregulation accounts for 23 - 30% of the NSCLC activating mutations (3–5). About 90% of the dominant *EGFR* mutations are short, in-frame deletions of exon 19 (Ex19Del) and mutations at position 858 in exon 21 (L858R missense replacements); and 4-10% being *EGFR* exon 20 insertions (*EGFR* Ex20ins) (5, 6).

The first-line standards of care for *EGFR* mutation-positive NSCLC patients include tyrosine kinase inhibitors (TKIs) that have considerable higher efficacy than standard chemotherapy (7). However with the emerging NSCLC resistance arising from different mutations, subsequent generations of small molecule EGFR TKIs have been developed (8). Unfortunately, small-molecule kinase inhibitors are constrained because of their intrinsically limited molecular surface area for binding that can be rendered ineffective by receptor mutations; sometimes just a single amino acid change (9, 10). One approach to target a broader pool of mutant EGFR is to employ anti-EGFR antibodies that provide therapeutic benefits in NSCLC, but still fall short with ensuing development of resistance (5). The mesenchymal-epithelial transition factor (*cMET*) amplification has a role in the resistance mechanism in patients that are no longer responsive to EGFR-TKIs and anti-EGFR antibodies (11, 12). Thus, amivantamab, designed for dual inhibition of EGFR and cMET, was developed and demonstrated promising tumor inhibition activities in preclinical and clinical studies (13–15). Amivantamab, a fully human bispecific antibody (BsAb) that targets both EGFR and cMET, received FDA approval in May 2021 for the treatment of advanced or metastatic NSCLC with *EGFR* Ex20ins mutations (5, 16, 17). However, some patients treated with amivantamab experience limited progression-free survival (PFS) and eventual disease progression, while a subgroup of patients do not respond to the treatment (18). Thus, there remains a need for drugs that could help patients with innate and acquired resistance to these standard-of-care therapies.

TKI resistant NSCLC patients exhibit aberrant EGFR and cMET signaling as well as elevated vascular endothelial growth factor (VEGF) receptor pathway activity which is a critical driver of solid tumor angiogenesis (19). EGFR and the receptor for VEGF, VEGF receptor 2 (VEGFR-2), share common downstream pathways such that inhibition of one pathway can be compensated by the upregulation of the other. In addition, *EGFR*-mutant tumors are more dependent on VEGF-A signaling compared to *EGFR* wild-type tumors (20). VEGF-A has a dual role of promoting tumor cell proliferation through autocrine signaling and stimulating angiogenesis via paracrine mechanisms (21). In line with this mechanism, two anti-angiogenic agents were approved by the FDA for the treatment of advanced NSCLC: bevacizumab [an anti-VEGF-A monoclonal antibody (mAb)] and ramucirumab (an anti-VEGFR-2 mAb) (22, 23). To control EGFR and VEGF signal pathways, the dual-targeted approach combining erlotinib (EGFR TKI) with bevacizumab demonstrated superior antitumor activity compared to monotherapy in clinical practice, leading to its approval as a first-line treatment option for EGFR-mutant NSCLC (19, 24). In addition, dual inhibition of cMET and VEGFR-2 has shown strong inhibition of tumor growth and angiogenesis in xenograft models (25, 26). However, since these strategies still have a narrow therapeutic index, a more comprehensive treatment is required.

Considering the extensive crosstalk among the three pathways, the combined inhibition of the EGFR, cMET, and VEGF pathways could overcome resistance and could be an effective treatment approach for NSCLC patients. The aim of the current study was to demonstrate how TAVO412, a trispecific antibody targeting EGFR, cMET, and VEGF, controlled dysfunctional NSCLC tumor growth activities. TAVO412 was engineered to have differentiated mechanisms of action (MOA) that included ligand blocking, EGFR/cMET receptor phosphorylation inhibition, EGFR/c-MET receptor degradation, shutdown of angiogenesis, and enhanced Fc effector functions. These MOAs manifested in *in vivo* antitumor activities of TAVO412 in a diverse panel of NSCLC tumor models with varying *EGFR* mutations, a broad range of EGFR and cMET receptor densities, and VEGF secretion levels. In addition, TAVO412 was shown to have stronger anti-tumor activities in combination with other standards of care treatments that included radiotherapy, chemotherapy, and 3rd generation EGFR TKIs.

Results

TAVO412 bound and inhibited ligand binding to NSCLC cell lines

TAVO412 was produced in CHO cells and purified to high monomeric purity (>98%), as confirmed by SEC-HPLC and further validated by SDS-PAGE (Supplementary Figures S1A, B). The antibody demonstrated excellent thermal stability, with a melting temperature (Tm) of 65.2 ± 0.3°C (Tm1) and 74.6 ± 0.4°C (Tm2) determined by differential scanning fluorometry (DSF). TAVO412, the comparator amivantamab analogue, and a null control antibody binding to NSCLC cell lines were assessed by flow cytometry. The NSCLC cell lines (NCI-H292, HCC827, NCI-H1975, NCI-H460, NCI-H1299, NCI-H358, and NCI-H596) spanned different *EGFR* mutation profiles, a range of EGFR/cMET receptor densities, and varying levels of VEGF secretion (Supplementary Table S1). TAVO412 had high avidity binding with EC_{50} values that were similar to those of the amivantamab analogue (NCI-H292: 0.399 nM versus 1.150 nM; HCC827: 1.037 nM versus 1.885 nM; NCI-H1975: 1.358 nM versus 0.626 nM, for TAVO412 versus amivantamab analogue respectively) (Figures 1A–C; Supplementary Figures S2A-D; Supplementary Table S2). The levels of TAVO412 binding correlated with the EGFR receptor densities that were in higher levels than cMET receptor densities (data not shown).

The ability of TAVO412 to block EGF and HGF binding to their respective receptors was assessed using a cell-based flow cytometry assay in HCC827 cells(EGFR: cMET receptor density ratio = 14.5, Supplementary Table S1). TAVO412 effectively blocked EGF binding in comparison to the amivantamab analogue (IC_{50} of 4.013 nM versus 11.86 nM) and HGF binding (IC_{50} of 0.282 nM versus 0.689 nM) (Figures 1D, E; Supplementary Table S3). The non-binding (null) control antibody showed no inhibitory effects. The potency of TAVO412 in blocking VEGF-A binding to VEGFR2 was tested and has been reported elsewhere (manuscript submitted).

TAVO412 inhibited ligand-induced receptor phosphorylation

Patients with hyperactivation of the EGFR and cMET signaling pathways often have higher levels of respective ligand expression (25, 27). Thus, TAVO412 was engineered to inhibit EGF binding to EGFR and HGF binding to cMET; thereby antagonizing paracrine ligand-based EGFR and cMET activations. Using TR-FRET-based assays, TAVO412 was shown to inhibit EGF-induced phosphorylation of EGFR and HGF-induced phosphorylation of c-MET in NCI-H292 cells, whereas wild type *EGFR* and *c-MET* showed minimal baseline EGFR and cMET phosphorylation in the absence of growth factor stimulation (13) (Figures 2A, B; Supplementary Table S4). TAVO412 inhibited EGF-induced phosphorylation (IC50 of 0.941 nM) with a 3-fold greater potency than that of the amivantamab analogue (IC50 of 2.796 nM). In addition, the amivantamab analogue showed marginally enhanced inhibition of HGF-induced phosphorylation (IC50 of 0.430 nM) when compared to TAVO412 (IC50 of 0.568 nM). (Figures 2A, B; Supplementary Table S4). The null control antibody did not inhibit receptor phosphorylation. The stronger effect on EGF-induced phosphorylation resulted from blockade of ligand binding and receptor dimerization by the dual epitope EGFR arm as anticipated, while the avidity effect maintained a strong HGF blockade in the tumor cells.

Since HCC827 cells (wild type cMET, and the Ex19Del EGFR mutation which conferred a high baseline level of EGFR phosphorylation) had constitutively activated EGFR, EGF addition did not significantly increase the amount of phospho-EGFR over the high baseline level. Therefore, phospho-EGFR levels remained unchanged by the addition of TAVO412 or amivantamab (Figure 2C; Supplementary Table S4). Consistent with observations in H292 cells, TAVO412 inhibited HGF-induced cMET phosphorylation in HCC827 (Figure 2D; Supplementary Table S4).

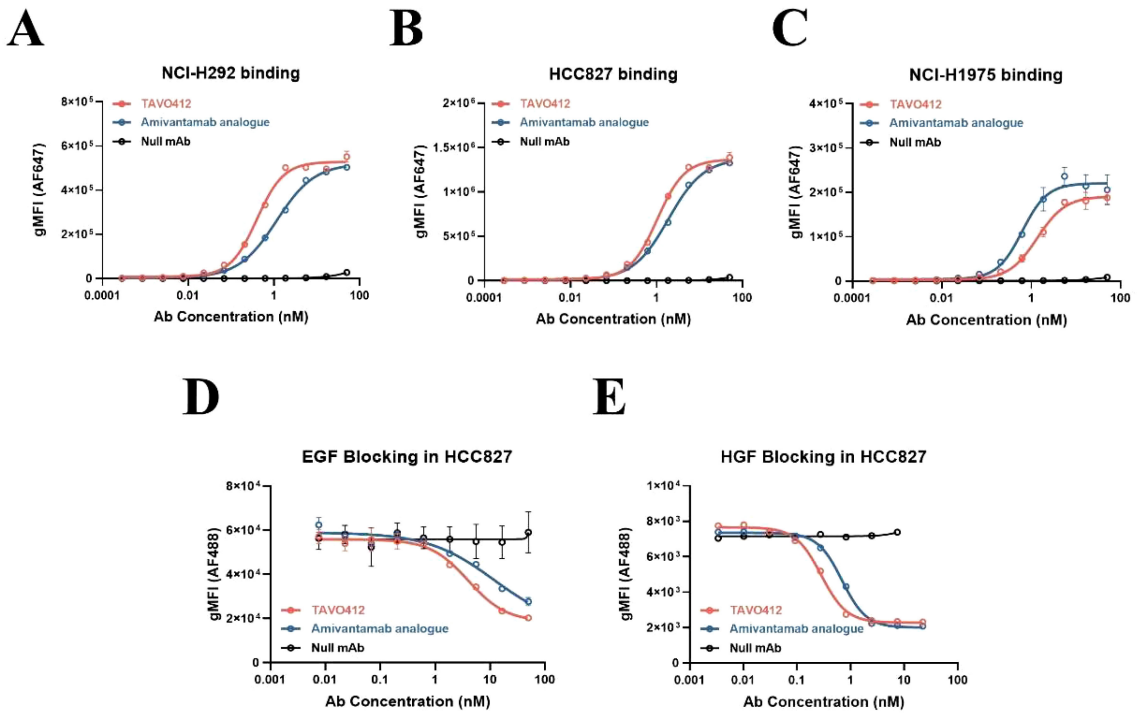

FIGURE 1
TAVO412 bound to NSCLC cell lines and blocked binding of EGF and HGF. The binding of TAVO412 (red open circle), Amivantamab analogue (blue open circle) and null mAb (black open circle) to **(A)** NCI-H292; **(B)** HCC827; and **(C)** NCI-H1975 NSCLC cell lines as analyzed by flow cytometry. See Supplementary Table S2 for corresponding EC_{50}, 95% CI for EC_{50}, and efficacy (span in y axis). Blocking of **(D)** EGF and **(E)** HGF from binding to HCC827 cells was assessed by flow cytometry with TAVO412 (red open circle), Amivantamab analogue (blue open circle) and null mAb (black open circle). See Supplementary Table S3 for corresponding IC_{50}, 95% CI for IC_{50}, and efficacy (span in Y-axis). The data from three independent experiments were expressed as the mean ± SEM of duplicate treatments. The amivantamab analogue served as a positive control molecule while the null mAb served as a negative control. The abbreviations were: gMFI, geometric mean fluorescent intensity; AF647, Alexa Fluor 647 dye; AF488, Alexa Fluor 488 dye; Ab, antibody; nM, nanomolar; EGF, epidermal growth factor; HGF, hepatocyte growth factor; SEM, standard error of the mean.

TAVO412 had enhanced Fc effector function

Fc effector functions play crucial roles in the efficacy of therapeutic antibodies (28). TAVO412 had enhanced Fc effector functions by incorporating clinically-verified point mutations in the Fc domain (F243L/R292P/Y300L/V305I/P396L) (29). TAVO412 and amivantamab analogue had comparable binding affinities for CD16a, CD32a, and CD64 (manuscript submitted). However, TAVO412 bound to C1q, while the amivantamab analogue and control IgG1 antibodies did not bind to C1q.

TAVO412's Fc effector functions were demonstrated in assays that monitored antibody-dependent cellular cytotoxicity (ADCC), antibody-dependent cellular phagocytosis (ADCP), and complement-dependent cytotoxicity (CDC) in NCI-H292, HCC827, and NCI-H1975 cell lines. Although TAVO412 and the amivantamab analogue exhibited comparable binding activity to Fc gamma receptors (FcγR), TAVO412 demonstrated a stronger ADCC response than the amivantamab analogue (NCI-H292: EC_{50} of 0.051 nM versus 0.114 nM; HCC827: 0.066 nM versus 0.483 nM; NCI-H1975: 0.003 nM versus 0.005 nM, for TAVO412 versus amivantamab analogue respectively) (Figures 3A–C; Supplementary Table S5). Both TAVO412 and amivantamab analogue had similar ADCP responses in the three NSCLC cell lines (NCI-H292: EC_{50} of 0.009 nM versus 0.012 nM; HCC827: 0.112 nM versus 0.126 nM; NCI-H1975: 0.163 nM versus 0.125 nM, for TAVO412 versus amivantamab analogue respectively) (Figures 3D–F; Supplementary Table S5). Consistent with the ELISA binding to C1q, TAVO412 exhibited CDC killing of NCI-H292 (EC_{50} of 0.297 nM) and HCC827 (3.139 nM), whereas the amivantamab analogue showed only minimal CDC killing (Figures 3G, H). With an approximately 10% maximum lysis, H1975 cells were resistant to CDC killing as reported earlier (Figure 3I) (30).

To confirm that TAVO412 has enhanced Fc effector functions, TAVO412-A (a TAVO412 isoform without the VEGF binding domain) was compared to TAVO412-A_NF (a TAVO412-A isotype with wild type Fc) and TAVO412-A_SF (a TAVO412-A isoform with a silenced Fc) in the ADCC and ADCP reporter assays, and in CDC induced killing assays using the NCI-H292 cell line. TAVO412-A

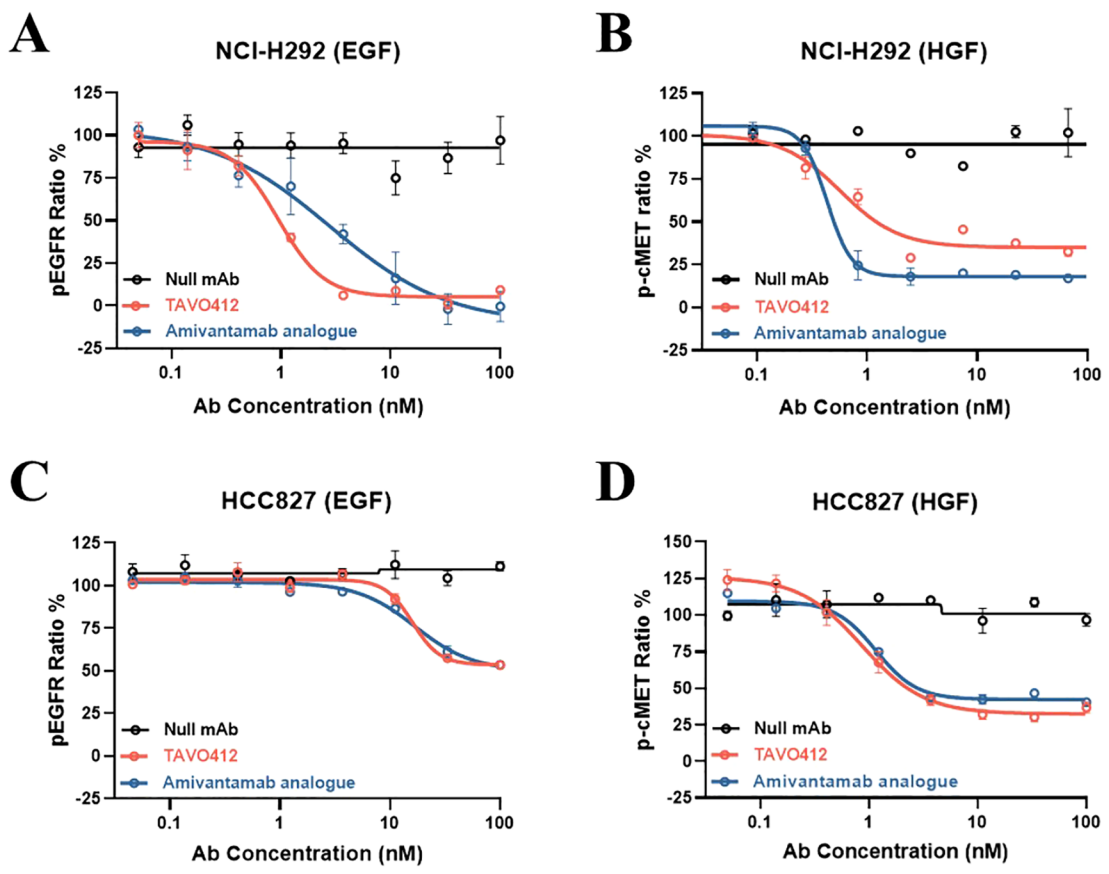

FIGURE 2
TR-FRET assay demonstration of TAVO412 inhibition of ligand-induced EGFR and cMET phosphorylation in NSCLC cell lines. Inhibition of **(A)** EGF ligand-induced phosphorylation of EGFR and **(B)** HGF ligand-induced phosphorylation of cMET in NCI-H292 cell line. Inhibition of **(C)** EGF ligand-induced phosphorylation of EGFR and **(D)** HGF ligand-induced phosphorylation of cMET in HCC827 cell line. TAVO412 (red open circle), amivantamab analogue (blue open circle) or null mAb (black open circle) were tested. The data from three independent experiments were expressed as the mean ± SEM of duplicate treatments. The amivantamab analogue served as a positive control molecule while the null mAb served as a negative control. The corresponding IC_{50}, 95% CI for IC_{50} values and efficacy (span in Y-axis) were reported in Supplementary Table S4. The abbreviations were: pEGFR ratio%, phosphorylation rate of EGFR; p-cMET ratio%, phosphorylation rate of cMET; Ab, antibody; nM, nanomolar; EGF, epidermal growth factor; HGF, hepatocyte growth factor; SEM, standard error of the mean.

indeed induced dramatically enhanced ADCC, ADCP and CDC both in terms of potency and efficacy compared to TAVO412-A_NF. The role of the Fc mutations was further confirmed as TAVO412-A_SF had no Fc effector functions (Supplementary Figures S3A–D).

Amivantamab Fc effector functions were dependent on cell binding by its anti-EGFR arm (14). To investigate whether TAVO412 had similar EGFR binding-driven Fc effector function, TAVO412-A's activity was compared to its isoforms with an inert arm in the cMET arm position (EGFR x Inert) or the EGFR arm position (cMET x Inert). In the NCI-H292 cells, EGFR x Inert had comparable Fc effector activities compared to TAVO412-A, while the cMET x Inert did not induce significant responses (Supplementary Figures S3E–H). Thus, we demonstrated that TAVO412's Fc effector functions are also dependent on its binding to EGFR. The EGFR-driven Fc-effector functions were also observed in other cancer cell lines (data not shown).

TAVO412 suppressed tumor growth in xenograft models with EGFR and cMET degradation

The antitumor activities of TAVO412 were assessed in six NSCLC xenograft models that spanned different *EGFR* and *cMET* genotypes, receptor densities, and VEGF-A secretion levels (Supplementary Table 1). Monotherapy with TAVO412 at doses of 1 (low), 3 (medium), and 10 (high) mg/kg inhibited tumor growth in both HCC827 and NCI-H1975 xenograft models in a dose-dependent

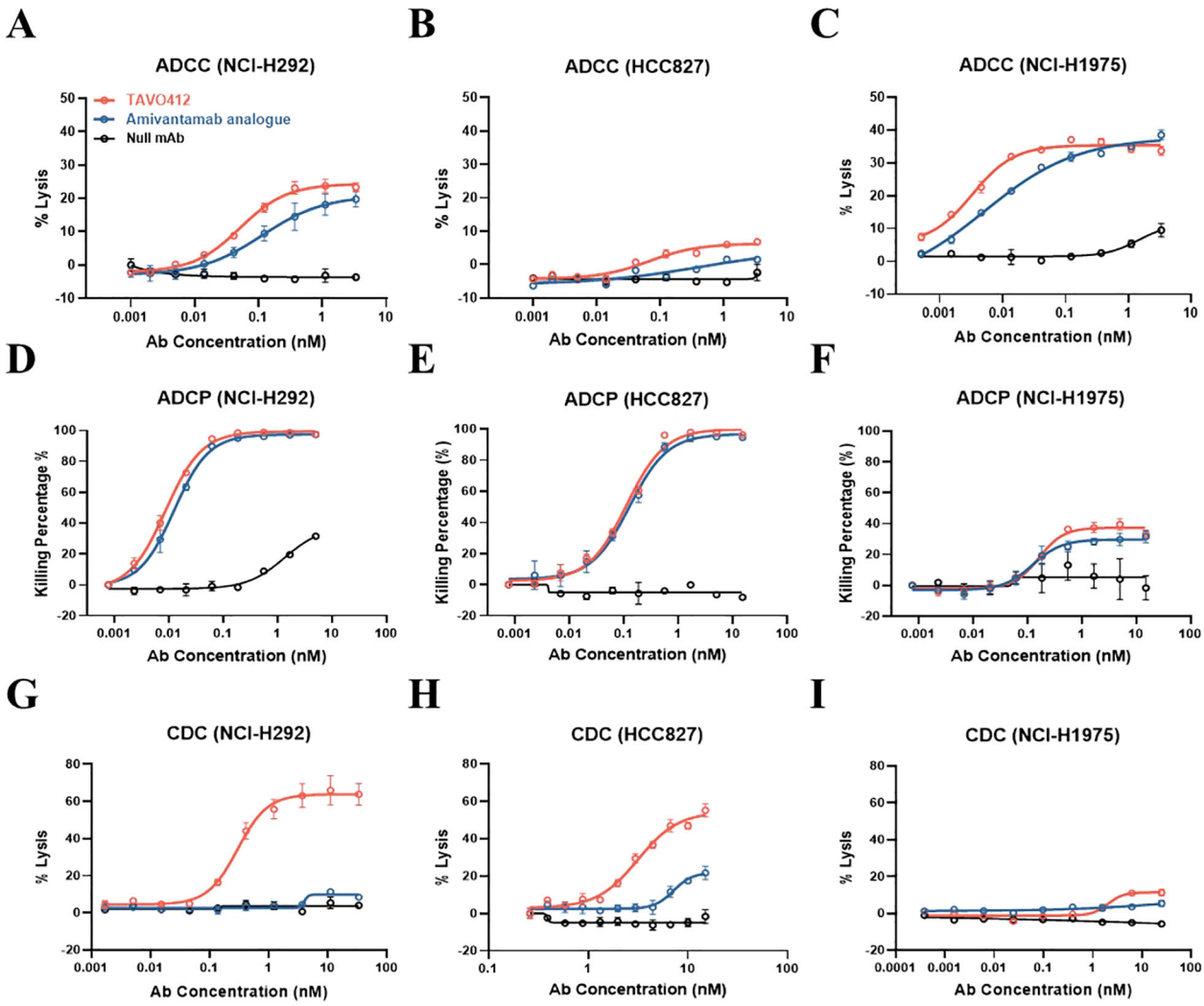

FIGURE 3
TAVO412 mediated Fc effector functions in NSCLC cell lines. TAVO412 Fc effector function showing ADCC for **(A)** NCI-H292, **(B)** HCC827 and **(C)** NCI-H1975 cells, respectively; TAVO412 Fc effector function showing ADCP for **(D)** NCI-H292, **(E)** HCC827 and **(F)** NCI-H1975 cells, respectively; TAVO412 Fc effector function showing CDC for **(G)** NCI-H292, **(H)** HCC827 and **(I)** NCI-H1975 cells, respectively. TAVO412 (red open circle), Amivantamab analogue (blue open circle) or null mAb (black open circle) were tested. The data from three independent experiments were expressed as the mean ± SEM of duplicate treatments. The amivantamab analogue served as a positive control molecule while the null mAb served as a negative control. The EC_{50}, 95% CI for EC_{50} values and efficacy (span in Y-axis) were reported in Supplementary Table S5. The abbreviations were: Ab, antibody; nM, nanomolar; ADCC, antibody-dependent cellular cytotoxicity; ADCP, antibody-dependent cellular phagocytosis; CDC, complement-dependent cytotoxicity; SEM, standard error of the mean.

manner (Figures 4A, B). The amivantamab analogue administered at 3 mg/kg showed comparable antitumor activities as TAVO412 at similar dosing level (Figures 4A, B). Tumor weights and photos taken on the last day of each experiment were consistent with the tumor volume data (Figures 4C–F). TAVO412 treatment was well-tolerated without compromising the mice body weight (Figures 4G, H). TAVO412 at 10 mg/kg had excellent anti-tumor activity in the other four xenograft models (Supplementary Figures S4A–H).

TAVO412 also demonstrated EGFR and cMET receptor degradation *in vivo*. Mice bearing HCC827 or NCI-H1975 tumors were treated with TAVO412 twice. The tumors were collected 24 h after the second dose. The Western blots indicated that the average total protein levels of EGFR and cMET were significantly decreased in both models after TAVO412 treatment; thereby demonstrating receptor degradation (Supplementary Figures S5A–F).

To quantify the drug exposure in the animal models, the pharmacokinetics (PK) profile of TAVO412 was studied in the same stain of mice without tumor bearing. Following a single intraperitoneal injection, TAVO412 exhibited linear PK in the dose range from 1 to 3 mg/kg. The half-life was estimated to be 4.6 to 4.8 days (Supplementary Figure S6).

The combination of EGFR TKIs and TAVO412 had stronger anti-tumor efficacy in xenograft models

Amivantamab and lazertinib combination therapy has enhanced antitumor activity in NSCLC patients in clinical trials (31). In light of this, we combined TAVO412 with lazertinib in the HCC827 xenograft model and with osimertinib in the NCI-H1975 xenograft model. Tumor-bearing mice were treated when the average tumor volume reached 200 mm^3 in the HCC827 model (Figures 5A, B). While tumors were effectively inhibited by either single agent or the combination up to day 32, tumor relapses were observed in all the mice treated with lazertinib shortly after the treatment was stopped. TAVO412-treated tumors showed a longer lasting inhibition compared to lazertinib, but tumor regrowth still occurred by the end of the study with only one mouse having partial regression (day 92). The combination of TAVO412 and lazertinib induced complete tumor regression (CR) and partial regression (PR) in 2/5 and 3/5 mice, respectively, until the last observation day (Figure 5A). Similarly in NCI-H1975, the combination of TAVO412 with osimertinib showed a significant additive effect: the combination group having a significantly smaller tumor burden compared to each monotherapy group and the control (Figures 5C, E). NCI-H1975 tumors treated with TAVO412 appeared paler compared to tumors in other treatment groups (Figure 5E), which indicated reduced vasculature due to VEGF-A neutralization by TAVO412. This phenomenon was also observed in other xenograft models with different tumor cell types (data not shown). Treatments of TAVO412 were well tolerated with no body weight loss (Figures 5B, D). These findings showed that the combination of TAVO412 with either lazertinib or osimertinib had stronger tumor growth inhibition compared to the monotherapies and prevented relapse in the mouse models of HCC827 and NCI-H1975. We used 2 mg/kg TAVO412 (suboptimal dose) in NCI-H1975 models to assess combination potential, and 10 mg/kg (optimal dose) in HCC827 models to demonstrate complete tumor control. This dual approach allowed evaluation of both combination effects and maximal efficacy.

EGFR TKIs enhanced the efficacy of TAVO412 by stabilizing EGFR receptor on cell surface or enhancing ADCC

The basis for the EGFR-TKI enhancement of TAVO412 was further probed by conducting cell-based assays. H1975 cells were treated with varying concentrations of osimertinib for 48h at 37°C and then stained with either anti-EGFR or anti-cMET detection antibodies to assess receptor density via flow cytometry analysis. When compared to the absence of osimertinib treatment, the incubation of H1975 with osimertinib at 0.1, 1, and 20 nM resulted in 1.1-, 1.5-, and 2.6-fold MFI increase in EGFR binding but did not affect cMET binding levels (Supplementary Figures S7A, B). The binding of TAVO412 to osimertinib-treated H1975 cells was then evaluated at both 1h and 24h at 37°C. The level of TAVO412 binding (at 16 nM TAVO412 for all the following comparisons) after 24h was 80% lower than the binding after 1h (Figures 6A, B). The longer incubation time for binding could manifest in higher levels of internalization and degradation of the receptors. At 1 h, the MFI ratios of TAVO412 binding to H1975 cells treated with osimertinib at 1 nM, 20 nM, or 125 nM to that without osimertinib treatment were 1.3, 1.3, and 1.2, respectively. After 24h, these MFI ratios were 1.1, 1.7, and 2.6, respectively, indicating that there was an osimertinib dose-dependent increase in TAVO412 binding. However, the TAVO412 increase in cell binding did not further increase the ADCC effect *in vitro* (Figure 6E).

Since lazertinib showed synergy with TAVO412 *in vivo* in the HCC827 model, we assessed the impact of lazertinib on receptor densities, TAVO412 binding, and ADCC effects on HCC827 cells. In comparison to the absence of lazertinib treatment, culturing HCC827 cells with lazertinib at 0.3, 3, and 100 nM at 37°C after 48 h led to 10, 60 and 70% reductions in cMET receptor density, respectively. Surprisingly, the EGFR density levels were unaffected (Supplementary Figures S7C, D). As with H1975 cells, TAVO412 alone demonstrated decreased binding to HCC827 cells (by 60%, at 16 nM TAVO412 for all the following comparisons) after 24 h versus 1 h at 37°C (Figures 6C, D). Upon addition of 0.3, 3, and 100 nM lazertinib, TAVO412 binding was decreased by 0, 70, and 70% at 1 h, respectively. After 24 h, the TAVO412 binding to HCC827 was decreased by 20, 30 and 60%, respectively (Figures 6C, D). This reduction in TAVO412 binding could be associated with the decreased cMET receptor density upon lazertinib treatment. HCC827 cells exhibited a 14-fold higher TAVO412 binding (at 16 nM) than on H1975 after 24 h (Figures 6B, D), which corresponded to the relative receptor densities of EGFR and cMET (Supplementary Table S1). There was still a 2.5-fold higher binding of TAVO412 to HCC827 cells compared to H1975 cells with EGFR-TKI supplemented (100 nM lazertinib versus 125 nM osimertinib; Figures 6B, D). Despite a reduced binding of TAVO412, the vitro

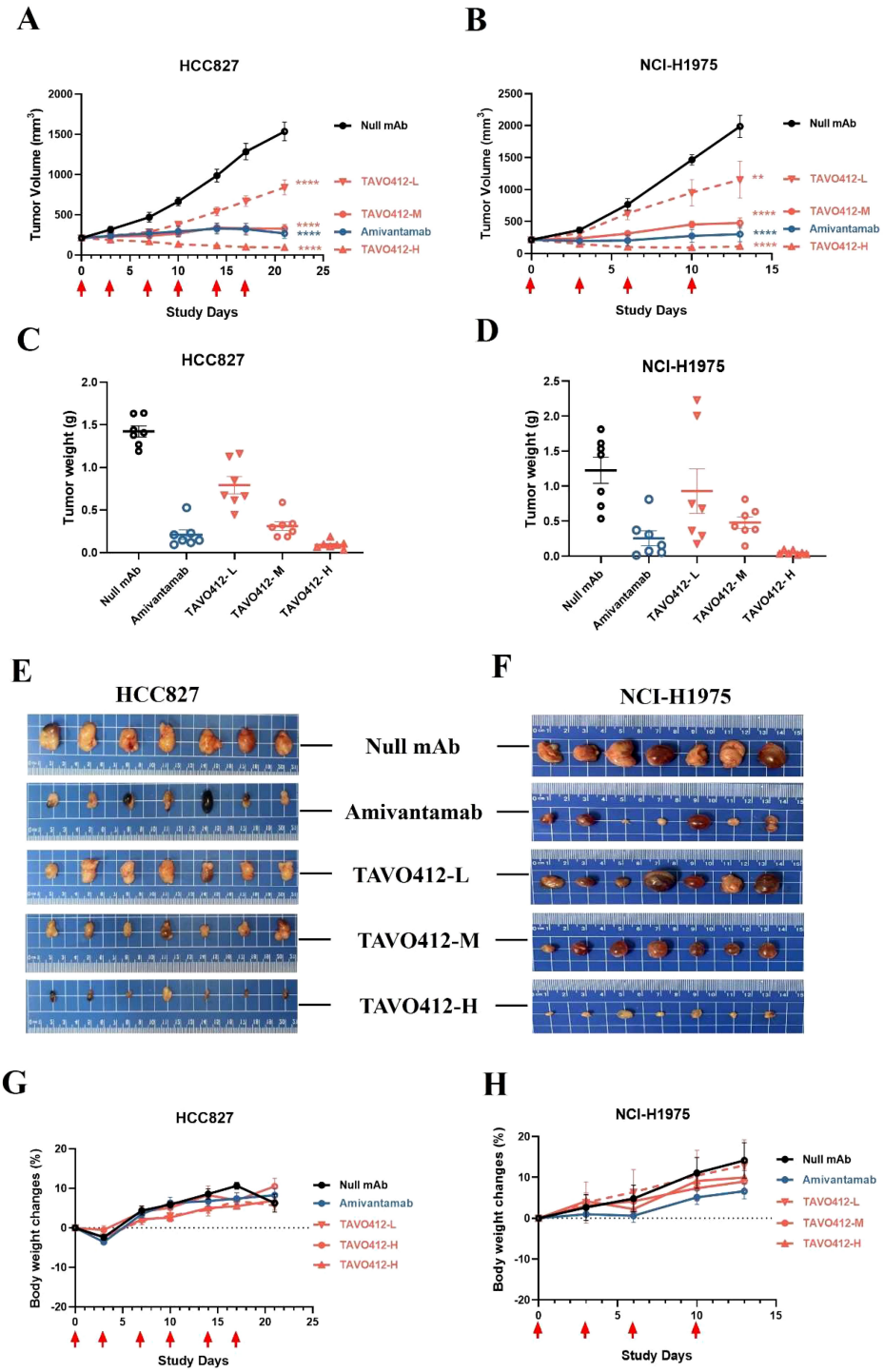

FIGURE 4
TAVO412 antitumor activity in NSCLC xenograft models. Female Balb/c nude mice bearing NSCLC xenograft tumors were given intraperitoneal injections twice per week of TAVO412 (1, 3, 10 mg/kg), amivantamab analogue (3 mg/kg), or null mAb (10 mg/kg). Tumor growth was monitored twice weekly. The mean tumor growth curves for mice treated with indicated antibodies in **(A)** HCC827 for a total of 6 doses and **(B)** NCI-H1975 for a total of 4 doses were shown. Tumors were collected and tumor weight measured for **(C)** HCC827 at the end of the 21-day observation period and **(D)** NCI-H1975 at the end of the 13-day observation period. Photographs of the resected tumor xenograft specimens at the end of the study were recorded for **(E)** HCC827 tumors and **(F)** NCI-H1975 tumors. The body weight of the tumor-bearing mice treated with indicated antibodies were measured twice weekly until the end of study for **(G)** HCC827 and **(H)** NCI-H1975. The antibodies were labeled: TAVO412 – L for 1 mg/kg dosing (red open down triangle); TAVO412 – M for 3 mg/kg dosing (red open circle); TAVO412 – H for 10 mg/kg dosing (red open up triangle); amivantamab for amivantamab analogue (blue open circle); Null mAb for control (black open circle). The data represented the mean values ± SEM (n = 7/group). The red arrows indicated the specific dosing days. **P < 0.01; ****P < 0.0001; ns: not significant compared to control group. Statistical significance was determined using one-way ANOVA, followed by Tukey's multiple comparisons test to compare each treatment group with the null mAb group.

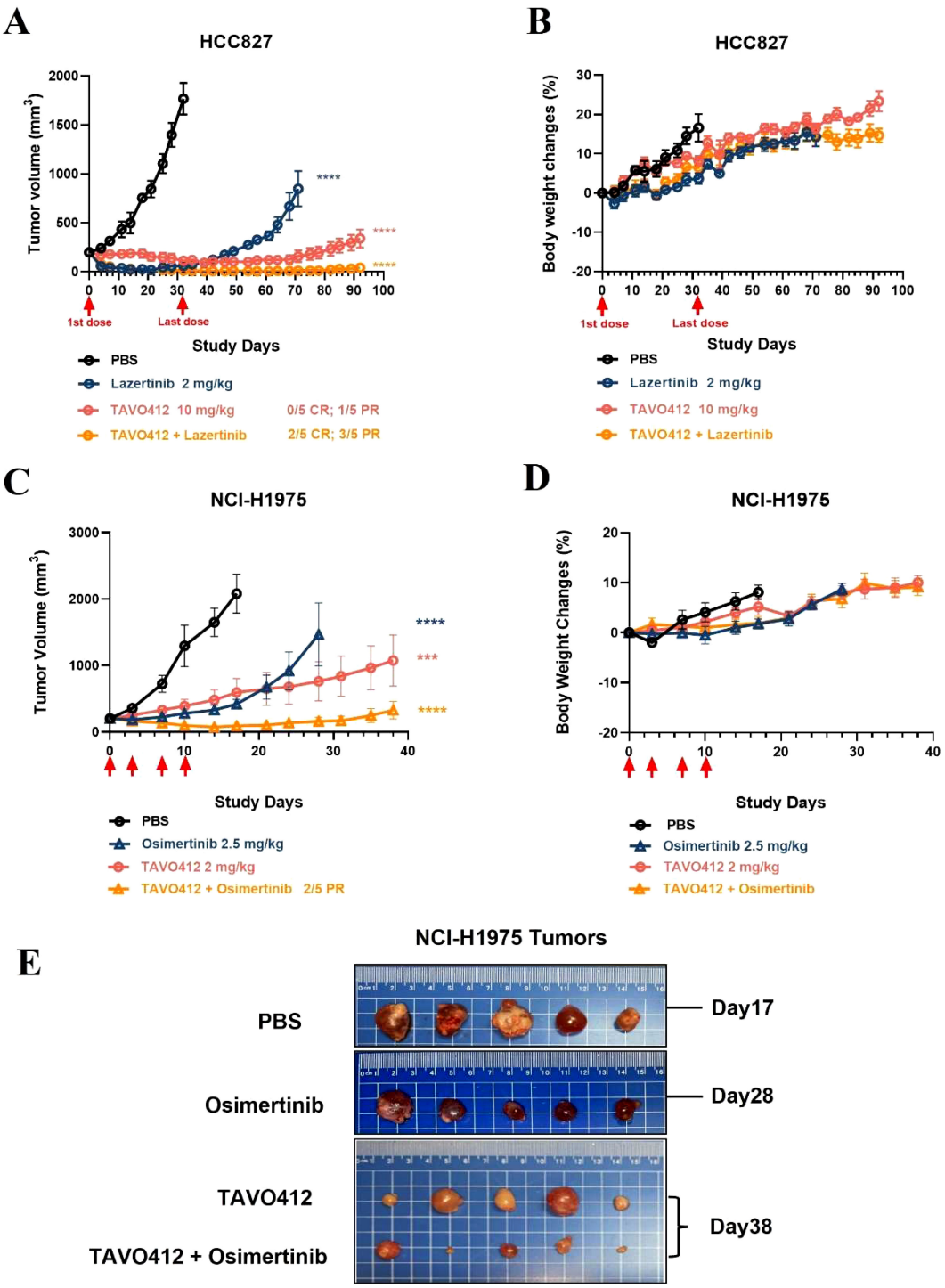

FIGURE 5
Combination of TAVO412 with Lazertinib and osimertinib in NSCLC xenograft models. Mice bearing HCC827 tumors were treated with TAVO412 (red open circle), Lazertinib (navy open circle), the combination of TAVO412 and Lazertinib (orange open circle) and PBS control (black open circle). TAVO412 was dosed at 10 mg/kg twice per week for a total of 10 intraperitoneal injections (the red arrows indicated the first and last dose). Lazertinib was dosed at 2 mg/kg daily orally for 21 days (day 0 – day 20). **(A)** The HCC827 tumor growth profiles and **(B)** corresponding body weight changes were monitored twice weekly. Mice bearing NCI-H1975 tumors were treated with TAVO412 (red open circle), osimertinib (navy open up triangle), the combination of TAVO412 and Osimertinib (orange open up triangle), and PBS control (black open circle). TAVO412 was dosed at 2 mg/kg twice per week for a total of 4 intraperitoneal injections (the red arrow indicated the specific dosing for TAVO412). Osimertinib was dosed at 2.5 mg/kg daily orally for 14 days (day 0 – day 13). **(C)** The NCI-H1975 tumor growth and **(D)** body weight changes were monitored twice weekly. **(E)** Photographs of the resected tumor xenograft specimens at the end of the study were recorded for NCI-H1975. The treatments were indicated on the left, and the termination day was specified on the right of the photographs. The data represented the mean values ± SEM (n = 5/group). Statistical significance was calculated at day 32 and day 17 for HCC827 and NCI-H1975, respectively by one-way ANOVA followed by Tukey's multiple comparisons test to compare each treatment group with the null mAb group. ***P < 0.001; ****P < 0.0001. The abbreviations were: ns: not significant compared to control group. CR and PR indicated complete response and partial response; PBS represented phosphate buffered saline; SEM, standard error of the mean.

ADCC assay showed an enhancement of the killing effect by addition of lazertinib at 100 nM concentration (Figure 6F).

Combination of TAVO412 with conventional chemotherapy and radiotherapy induced complete regression of tumors *in vivo*

We examined whether combining TAVO412 with either taxane chemotherapy or radiotherapy would yield a more effective anti-cancer treatment. Chemotherapy and radiotherapy are extensively used in the clinic to treat NSCLC patients. Docetaxel was selected to combine with TAVO412 to investigate their combination effect on NCI-H1975 tumor growth in xenograft mouse models (Figures 7A, B). Both TAVO412 and docetaxel were dosed twice a week for 4 weeks, via intraperitoneal injection. Initially, docetaxel as a single agent showed minimal tumor control effect. However, all tumors in this group reached their peak volume and began to regress at day 14. The maximal tumor control effect was observed at day 38 (14 days after the end of treatment), and then 3 out of 5 tumors began to regrow and 2 out of 5 tumors remained stable with a volume of less than 20 mm^3 by the end of the study (day 87) (Figure 7A). TAVO412 exhibited a strong tumor growth inhibition effect in this model as a monotherapy, with 4 out of 5 mice achieving partial regression by the end of the treatment period (day 28). After cessation of treatment, 3 out of 5 tumors gradually regrew, while 2 out of 5 tumors remained stable by the end of the study. The combination of TAVO412 with docetaxel demonstrated superior antitumor activity compared to each single agent, with 2 out of 5 mice achieved complete regression, and 3 out of 5 mice achieved partial regression with a tumor volume measured less than 10 mm^3 at the end of the study.

The NCI-H292 xenograft model was used to examine the effect of TAVO412 and X-ray irradiation combination therapy based on published evidence demonstrating that the anti-EGFR antibody nimotuzumab potentiates radiation sensitivity more effectively in this cell line than in NCI-H1975 (32). NCI-H292 tumor cells were implanted in immune-compromised mice and the treatments were started when the tumor volume reached ~200 mm^3. TAVO412 was dosed twice a week for 4 weeks by intraperitoneal injection, irradiation (4 Gy per fraction) was performed on the first two days each week for 4 weeks in total, while the combination group followed the same regimen with each monotherapy (Figures 7C–E). The irradiation therapy alone only produced modest antitumor activity; all the tumors continued to grow, albeit at a slower rate compared to null control-treated tumors. TAVO412 alone showed a more potent tumor control effect with NCI-H292 tumors: all the tumors regressed to a tumor volume below the starting size, and 2/5 mice achieved partial regression by day 28. However, all the tumors gradually regrew when the treatment stopped. In contrast, the combination treatment induced a remarkable decrease of tumor burden: all the tumors regressed quickly starting from the beginning of treatment (the tumor size regressed to less than 10 mm^3 by day 21), and the effect persisted in all treated animals until the end of the study (Figure 7C). Figure 7E showed photographs of resected xenograft tumors taken at the endpoint of each group and the specimen sizes were consistent with the tumor volume data (Figure 7C). As anticipated, both Docetaxel and X-ray irradiation resulted in weight loss in mice. Notably, mice in the TAVO412 combination group did not experience weight loss. Instead, they showed a consistent increase in body weight throughout the entire study period (Figures 7B, D).

Discussion

Although the overall mortality rate of NSCLC has decreased due to the identification of disease-specific oncogenes coupled with personalized, genotype-directed therapies, the 5-year survival rate remains poor at 17.4%. In relapsed patients, drug resistance develops through emergence of secondary mutations, activation of by-pass signaling pathways, or phenotypic transformation. The development of novel therapies that can overcome such diverse resistance mechanisms remains a substantial clinical need. EGFR, cMET, and VEGF play critical and complementary roles in NSCLC cell survival, proliferation, and resistance to conventional therapies (33). Hence, we developed TAVO412, a single trispecific antibody-based molecule that inhibited EGFR, cMET, and VEGF-A. The molecular construct of TAVO412 was designed with a dual epitope variable heavy-chain only (VHO) EGFR binding arm on the N-terminal and an anti-VEGF-A ScFv domain on the C-terminal of one heavy chain, and an anti-cMET Fab arm on the other chain. Utilizing Knob-in-Hole mutations, TAVO412 was expressed in a single CHO cell line. Its developability characteristics and downstream processing were comparable to monoclonal antibodies in general, with high-yield production (2.5 g/L in CHO cells), stable monomeric purity (>97%), high thermal stability (Tm > 65°C), and no post-translational modification mutation hotspots in the CDR region. TAVO412 binds human targets at high affinities; it is fully cross reactive with the monkey targets, but not those of the mouse (data not shown, is published elsewhere). We demonstrated how TAVO412 manifested multiple mechanisms of action, including ligand blocking (Figures 1D, E), receptor phosphorylation inhibition (Figure 2), Fc effector functions including ADCC, ADCP, and CDC (Figure 3) and EGFR/cMET receptor degradation (Supplementary Figure S5). All of these mechanisms of action translated into excellent tumor growth inhibition effects *in vivo*, as observed in a panel of NSCLC xenograft models with diverse receptor density and EGFR and kRAS mutation status (Figure 4; Supplementary Table 1; Supplementary Figure S4).

Receptor degradation was observed in tumor samples for both EGFR and cMET 24 h after two doses of TAVO412, as compared to control tumors (Supplementary Figure S5). Such a mechanism could remove dysfunctional autocrine signaling of EGFR and cMET. The effect of receptor degradation by TAVO412 could be linked to immune effector-based mechanisms, such as trogocytosis (antibody-dependent cellular trogocytosis, ADCT), which had been identified as a dominant mechanism of antibody-directed receptor downregulation and tumor cell killing *in vivo* for amivantamab (34). However, further studies are needed to confirm this hypothesis.

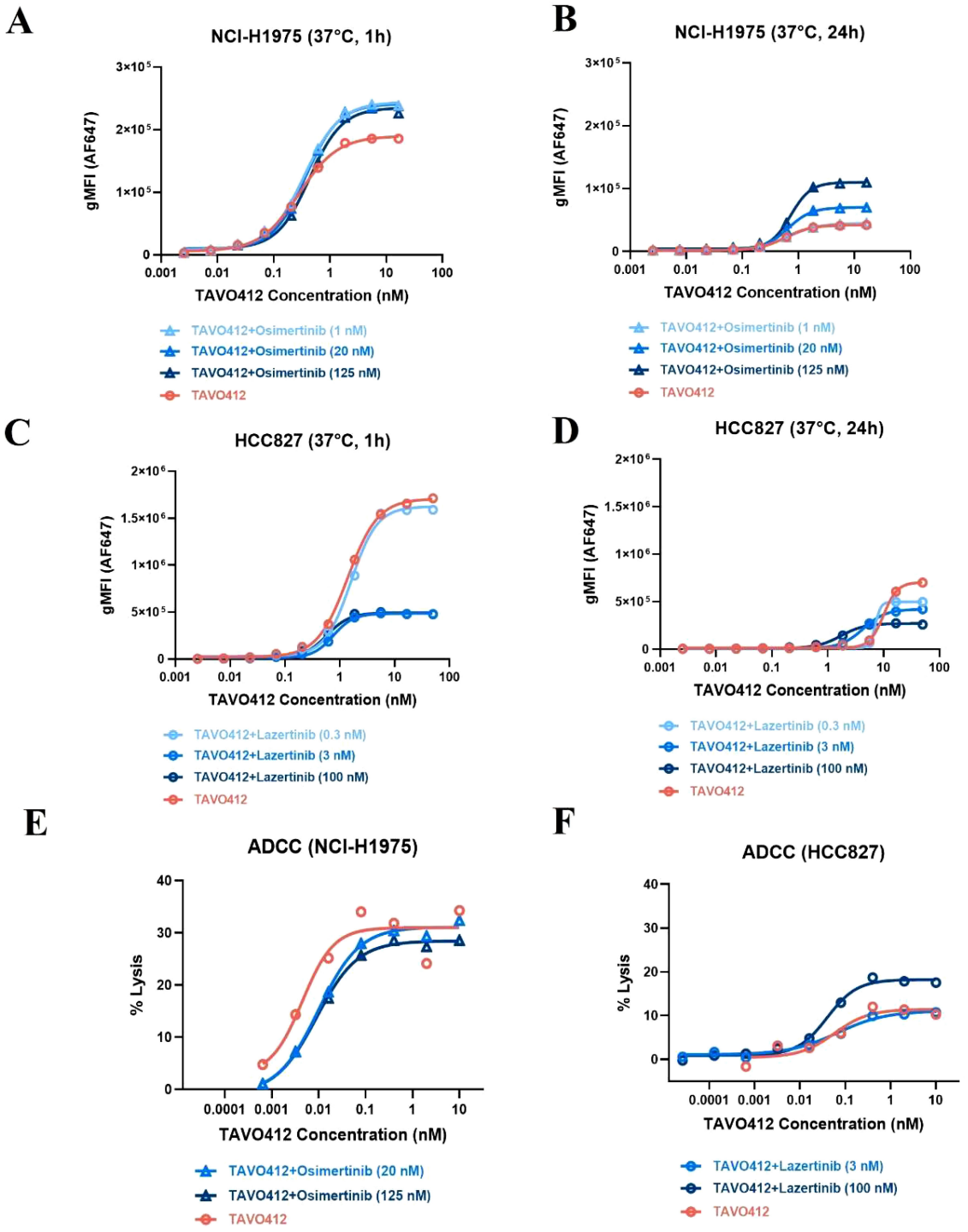

FIGURE 6
EGFR-TKI affected the cell binding and TAVO412 ADCC effector function. **(A, B)** NCI-H1975 and **(C, D)** HCC827 cells were pre-treated with osimertinib and lazertinib, respectively, for 48 h at specified concentrations. Then TAVO412 was added to the cells in a serial dilution and incubated for 1 h **(A, C)** or 24 h **(B, D)** at 37°C. The binding of TAVO412 in both cell lines were measured by flow cytometry. The EC_{50}, 95% CI for EC_{50} values and efficacy (span in y axis) were reported in Supplementary Table S6. **(E)** NCI-H1975 and **(F)** HCC827 cells were pre-treated with Osimertinib and Lazertinib, respectively, for 48 h at specified concentrations and then ADCC-induced killing was assessed. The treatments were labeled: TAVO412 alone: red open circle; TAVO412 + osimertinib: light, medium and dark blue open up triangle for addition of 1, 20 and 125 nM of osimertinib, respectively; TAVO412 + lazertinib: light, medium and dark blue open circle for addition of 0.3, 3 and 100 nM of lazertinib, respectively; Representative data from 2 to 3 independent experiments are shown. The EC_{50}, 95% CI for EC_{50} values and efficacy (span in y axis) were reported in Supplementary Table S7. The abbreviations were: gMFI, geometric mean fluorescent intensity; h, hour; nM, nanomolar; ADCC, antibody-dependent cellular cytotoxicity; SEM, standard error of the mean.

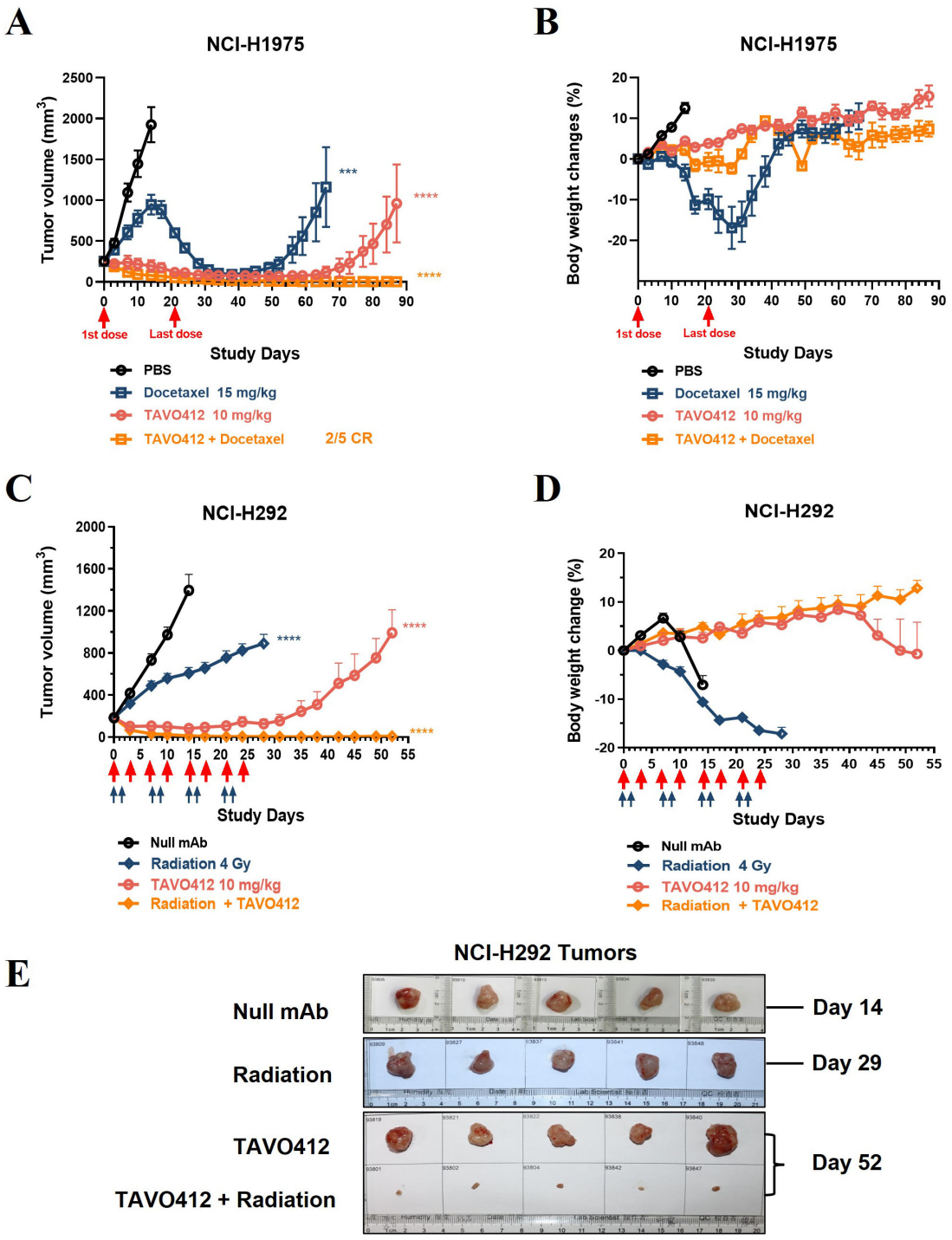

FIGURE 7
Treatment with TAVO412 in combination with docetaxel or radiation induced tumor regression in NSCLC xenograft models. **(A, B)** Mice bearing NCI-H1975 tumors were given intraperitoneal injections twice per week with: TAVO412 (10 mg/kg, red open circle), Docetaxel (15 mg/kg, navy open square), the combination of TAVO412 and Docetaxel (orange open square), or PBS vehicle control (black open circle). The red arrows mark the first and last dosing with a total of 8 intraperitoneal injections administered over this period. The mice were monitored 2X/week for **(A)** tumor growth and **(B)** body weight changes. **(C-E)** Mice bearing NCI-H292 tumors were treated with: TAVO412 (10 mg/kg, right open circle), x-ray radiation (4 Gy per fraction, navy open diamond), the combination of TAVO412 and irradiation (orange open diamond), or null mAb (10 mg/kg, black open circle). The red arrows marked the dosing days for TAVO412 and the light blue arrows marked the irradiation treatment days. The mice were monitored twice weekly for **(C)** tumor growth and **(D)** body weight changes. **(E)** Photographs of resected NCI-292 xenograft tumors collected on the termination days indicated to the right of figure. The treatments listed on the left. The data represent the mean values ± SEM (n = 5/group). Statistical significance was calculated at day 14 for both models by one-way ANOVA followed by Tukey's multiple comparisons test to compare each treatment group with the null mAb group. ***P < 0.001; ****P<0.0001. The abbreviations were: ns, not significant compared to control group; Gy, gray; CR indicates complete response.

TAVO412 was capable of mediating ADCC, ADCP, and CDC-induced killing effects, while amivantamab only showed ADCC and ADCP effects, and not CDC (14, 34). An earlier published study (35) showed that zanidatamab, an anti-HER2 biparatopic antibody, could enhance CDC by enhancing receptor clustering, and the effects were correlated with the receptor densities. We obtained similar experimental results showing that the dual epitope EGFR VHO promotes antibody clustering on the cell surface more effectively than any of the monovalent or bivalent parental antibodies (manuscript already submitted). TAVO412 was designed with dual epitope EGFR plus cMET bindings to enhance its cell surface presentation and clustering in addition to its enhanced Fc functions, which resulted in much stronger effector functions.

We used Balb/c Nude mice for *in vivo* xenograft model to test the anti-tumor effects of TAVO412 and comparator molecules. These mice are characterized by a mutation in the Foxn1 gene, leading to an absent or underdeveloped thymus and, consequently, a deficiency in T-cell production. However, the nude mice maintain an active macrophage system and exhibit high levels of NK cell reactivity (36).Therefore, the ADCC and ADCP effects can be tested with mouse NK cells (37).

The HCC827 cell line, with the *EGFR* Ex19Del mutation that accounts for ~ 60% of *EGFR* mutations in lung cancer, is highly responsive to first-generation EGFR TKIs, such as erlotinib. The NCI-H1975 cell line harbors both the L858R and the T790M mutations that confer resistance to first- and second-generation TKIs; but retains sensitivity to third - generation TKIs such as osimertinib. The remaining four cell lines (NCI-H460, NCI-H1299, NCI-H358 and NCI-H596) have wild-type *EGFR* and *cMET* genotypes at different receptor density levels. The NSCLC model NCI-H1975 (L858R/T790M) and HCC827 (Ex19Del) are sensitive to TKIs and amivantamab. In both models, TAVO412 exhibited potent and comparable antitumor activity to the amivantamab analogue (Figure 4). TAVO412 demonstrated anti-tumor activities against four NSCLC xenograft models with low, moderate, and high levels of wild-type genotype *EGFR* expression. (Supplementary Table S1; Supplementary Figure S4). TAVO412 and the amivantamab analogue were equally potent in inhibiting the growth of NCI-H358 and NCI-H596 xenografts, while only TAVO412 produced moderate antitumor activity in NCI-H460 and NCI-H1299 xenografts. Amivantamab showed no antitumor activity in these two models. The difference in response to TAVO412 could be explained by the different levels of EGFR receptor expression in these cell lines, considering the fact that Fc-dependent activity plays a critical role in tumor inhibition efficacy *in vivo* while the effector functions were driven by the anti-EGFR arm of TAVO412. Indeed, the two models with moderate responses had low EGFR and cMET expression levels (Supplementary Table S1). The fact that the antigen density on tumor cells must exceed a threshold for even high-affinity IgG antibodies to mediate ADCC could explain why both the amivantamab analogue in our study and cetuximab in another study did not show any antitumor activity in NCI-H460 xenografts (38, 39). Nonetheless, TAVO412 was more efficacious than the amivantamab analogue and cetuximab in these two low EGFR/cMET density models. TAVO412 had stronger tumor growth inhibition than amivantamab and cetuximab, since the design had more engineered MOA that included: angiogenesis control by the anti-VEGF arm; enhanced ADCC, ADCP, and CDC mediated by the unique dual-epitope EGFR and cMET binding epitopes. These results suggested that TAVO412 could be an effective treatment option for a broad range of NSCLC patients, regardless of the EGFR or KRAS mutational status.

Considering that many patients could have been treated with standard of care treatments, we explored the potential role for TAVO412 as a combination partner. Here, we demonstrated how TAVO412 showed substantially greater antitumor activity when combined with either third-generation TKIs or conventional chemoradiotherapy, compared to single-agent treatments, and prevented the emergence of resistance.

We observed enhanced TAVO412 anti-tumor effects when tumors were treated in combination with EGFR-TKIs in several *in vivo* models. To explore possible underlying mechanisms, we conducted a series of *in vitro* cell-based assays that showed how osimertinib increased EGFR receptor density on NCI-H1975 cell surface, resulting in an enhanced TAVO412 cell binding (Supplementary Figures S7A, B; Figures 6A, B). Similarly, erlotinib induced higher levels of cetuximab binding to EGFR on NSCLC tumor cells, which translated to enhanced cytotoxicity and a stronger *in vivo* anti-cancer effect (40). We corroborated their conclusions by demonstrating that osimertinib, a third-generation EGFR-TKI, exerted similar EGFR receptor stabilizing effects in NCI-H1975 cell line (with *EGFR* mutations) and led to enhanced TAVO412 cell binding. Other reports showed that while EGFR-TKIs were capable of decreasing EGF-induced internalization and could promote EGFR dimerization in a ligand-independent manner (41–44). While the osimertinib-enhanced TAVO412 binding on the cell surface did not translate into enhanced ADCC activity, the induction of stronger tumor growth inhibition could be linked to other mechanisms involving stronger blockade of signal transduction, enhanced ADCP, and CDC.

Amivantamab in combination with lazertinib in the CHRYSALIS-2 (NCT04077463) clinical trial has demonstrated a clinical benefit rate (CBR) of 57% in patients with common *EGFR* exon 19 deletion or L858R mutations who had previously progressed on osimertinib and platinum-based chemotherapy (31). Likewise, we confirmed that TAVO412 with lazertinib demonstrated enhanced tumor growth inhibition effects *in vivo*. However, the combination of TAVO412 with lazertinib in treating HCC827 cells showed more interesting mechanistic aspects. Lazertinib treatment reduced the cMET receptor density in a dose-dependent manner without an apparent impact on the EGFR density. Perhaps some crosstalk between the two receptors and signal pathways could be associated with the reduced levels of TAVO412 binding at physiological conditions (Supplementary Figures S7C-D; Figures 6C, D). Nonetheless, lazertinib showed a trend of enhancing the ADCC killing effect of TAVO412 (Figure 6F).

The correlations of cell surface drug presentation with effector functions could involve a dynamic balance among extracellular EGFR

and cMET receptor densities, receptor internalization/degradation rates, and recycling. Our *in vitro* results only provided a glimpse of the complexities. Moreover, drug presentation was only one of several factors that could influence effector functions. An example from our study highlighted that despite HCC827 having significantly higher TAVO412 presentation than H1975, it exhibited a weaker ADCC effect (Figures 3B, C, 7E, F). The balance amongst the activating and inhibitory signaling pathway ultimately determines effector cell responses. For instance, the density of ULBP1 ligands on NSCLC tumor cells could affect NKG2D regulation of NK cell induced-killing (45).

Chemotherapy and radiotherapy are the cornerstone of combined-modality therapy used to cure early and locally advanced NSCLC patients (46). The activation of EGFR, cMET, and VEGF signaling pathways has been linked to chemotherapy and radiotherapy resistance (25, 47). Blocking these pathways has been shown to enhance the effectiveness of chemotherapy and radiotherapy in preclinical studies (38, 48–50). However, in clinical trials, the combination of chemoradiotherapies (CRT) with anti-EGFR or anti-VEGF agents has often been disappointing because of the lack of significant improvement in survival. Additionally, there is a risk of excessive toxicity when combining CRT with targeted agents (9, 47, 51). Our studies provided proof of concept demonstration of the anti-tumor response of chemo- or radio-therapy when combined with TAVO412. In these models, the mice that received either docetaxel or radiation alone experienced a body weight loss of approximately 20%, while mice that received combination treatments maintained their normal growths. (Figures 7B, D). Thus, TAVO412 could have a protective effect against radiation and docetaxel treatment in animal models. Notwithstanding, careful study design and proper patient selection are necessary for further clinical studies to ensure both safety and efficacy when combining TAVO412 with CRT.

Besides the NSCLC tumor models, TAVO412 was also tested in several other tumor models including triple negative breast, gastric, esophageal, head and neck cancers, and pancreatic ductal adenocarcinoma. Manuscripts reporting the results have been prepared and will be published elsewhere separately (37). Although we did not conduct a standalone study to assess the individual contributions of the EGFR, cMET, and VEGFA arms in one NSCLC xenograft model using inert arm comparator molecules, we performed such study in a triple-negative breast cancer (TNBC) model. The results showed that, while TAVO412 has a monovalent anti-soluble VEGF-A arm with a slightly weaker binding affinity than bevacizumab, it demonstrated significantly stronger tumor growth inhibition in the model compared to bevacizumab or bevacizumab plus amivantamab at comparable dose levels (data submitted in another manuscript on TNBC). The anti-VEGF effect driven by EGFR/cMET targeting exhibited stronger and more promising anti-tumor results. We also anticipate that TAVO412 will have fewer anti-VEGF-related toxicity issues compared to molecules lacking homing mechanisms. In conclusion, TAVO412, which targeted EGFR, cMET, and VEGF, was demonstrated to have multiple mechanisms of antitumor activity in multiple preclinical models with varying levels of EGFR, cMET, and VEGF. TAVO412 showed potential as a valuable agent for combination therapy with standard-of-care treatments. This combination approach could potentially delay or prevent the development of drug resistance, providing valuable therapeutic options for lung cancer patients. While preparing this manuscript, TAVO412 has been tested in a Phase 1a clinical trial (NCT06761651) and has demonstrated reasonable safety, tolerability, and preliminary positive efficacy signals in NSCLC and other tumor types.

Materials and methods

Test antibodies and reagents

TAVO412 was a trispecific antibody with F243L/R292P/Y300L/V305I/P396L and Knob-in-Hole mutations. The molecular construct was designed with dual EGFR binding domains on the N-terminal and anti-VEGFA ScFv on the C-terminal of one heavy chain, and an anti-cMET Fab arm on the other chain. TAVO412 was expressed from a single stably-transfected CHO cell line, purified using Protein A and ion exchange chromatography, and characterized by SEC-HPLC and SDS-PAGE. Thermal stability was evaluated by differential scanning fluorometry (DSF) with a 1°C/min ramp (20–100°C). The amivantamab analogue (sequences referred to World Health Organization Proposed INN List 121) was generated in-house (52). Anti-gp120 hIgG1 was produced in-house to serve as a negative control antibody (null mAb) in cell-based experiments. HIgG1 (HAOKESAIYE, Beijing) served as an isotype control antibody (null mAb) in the animal studies. Lazertinib (Selleck #S8724), osimertinib (MCE LLC #HY-15772A), and docetaxel (injection from the Yangtze River Pharmaceutical Group, Jiangsu, China) were used in the combination experiments.

Tumor cell lines

NCI-H460, NCI-H1299, NCI-H358 and NCI-H596 cell lines (ATCC); and NCI-H1975, HCC827 and NCI-H292 cell lines (National Collection of Authenticated Cell cultures, Shanghai, China) were authenticated using short tandem repeat profiling and screened for mycoplasma contamination using the Myco-Lumi™ Luminescent Mycoplasma Detection Kit (Beyotime, #C0297M). Cells were cultured following ATCC cell line-specific recommendations. Frozen human peripheral blood mononuclear cells (PBMCs) were purchased from ALLCELLS and SAILYBIO.

Binding to EGFR and cMET expressing NSCLC cells

The NSCLC cells were seeded at a density of 50,000 cells per well in 96-well plates and treated with the test articles. After 1 h incubation at 4°C, the cells underwent three washes with fluorescence activated cell sorting (FACS) buffer (PBS supplemented with 2% (v/v) fetal

bovine serum). The cells were then incubated with AF647 goat anti-human IgG1 Fc (Jackson ImmunoResearch, 109-605-190) in the dark for 30 min at 4°C, washed three times with FACS buffer, and resuspended in FACS buffer for flow cytometry (Beckman CytoFLEX) experiments. The cells were gated initially based on forward and side scatter (FSC vs SSC) to eliminate debris and to define a population gate (P1). P1 was then analyzed on forward scatter height (FSC-H) versus forward scatter area (FSC-A) to isolate single cells (P2). The geometric mean fluorescence intensity (gMFI) of P2 cells was calculated with the CytExpert 2.4 software (Beckman Coulter). The gMFI values on the y axis was plotted against the antibody concentration on the x axis using a four-parameter logistic (4PL) model. EC_{50} values, efficacy (Y-axis span), and 95% confidence intervals (CI) were calculated in GraphPad Prism 9.3.1(GraphPad Software, Inc.).

To assess the effect of EGFR-TKIs to TAVO412 binding to tumor cells, NCI-H1975 and HCC827 cells were pre-treated with osimertinib or lazertinib for 48 h at 37°C. The cells were then cocultured with TAVO412 for 1 h and 24 h respectively at 37°C, and the gMFI level of AF647 goat anti-human IgG1 Fc was measured by flow cytometry as stated above.

Competitive ligand binding in HCC827 cells

Upon plating 50,000 HCC827 cells per well in 96-well plates, TAVO412, amivantamab analogue, or Null mAb were added in FACS buffer. After incubation 1 h at 4°C, the cell-antibody mixtures were washed three times with the FACS buffer. Either 50 µL of 1 µg/mL EGF or 50 µL of 0.2 µg/mL Biotin-HGF were added; incubated in the dark at 4°C for 1 h; and then followed by three FACS buffer washes. Rabbit anti-human EGF antibody (Sino Biological, #10605-T16) and Alexa Fluor 488 (AF488)-labeled anti-rabbit IgG1 (Jackson ImmunoResearch, #111-545-144) were added to test for EGF binding, while AF488 streptavidin (Invitrogen, #S11223) was added to test HGF binding. After 0.5 h incubation at 4°C, the cells were washed three times and resuspended in FACS buffer for flow cytometry analysis (Beckman CytoFLEX) with the FACS gating strategy as described above. The AF488 fluorescence signals of the P2-gated cells were captured and the gMFI was calculated with CytExpert 2.4 software (Beckman Coulter). The gMFI of the cells was plotted on the y axis against the antibody concentration on the x axis using a four-parameter logistic (4PL) model. IC_{50} values, efficacy (y-axis span) and 95% CI for IC_{50} were calculated in GraphPad Prism 9.3.1(GraphPad Software, Inc.).

Inhibition of ligand-induced receptor phosphorylation

Time-Resolved Fluorescence and Resonance Energy Transfer (TR-FRET) assay was used to measure the phosphorylation of EGFR and cMET receptors in NSCLC cells. Forty thousand cells were seeded in RPMI 1640 medium per well in 96-well plates overnight and starved for 24 h, before being treated with test articles for 1 h at 37°C. After stimulation with 22 nM EGF or 10 nM HGF at 37°C for 5 and 15 min respectively, the cells were lysed, and the levels of receptor phosphorylation were monitored using TR-FRET kits (Bioauxilium, KIT-EGFRP-5000 or KIT-METP-5000). The phosphorylation rate (%) on the y axis was plotted against the antibody concentration on the x axis using a four-parameter logistic (4PL) model. The IC_{50}, efficacy (y-axis span), and 95% CI for IC_{50} values were calculated in GraphPad Prism 9.3.1 (GraphPad Software, Inc.). The phosphorylation rate (%) was determined by calculating $[(\text{Signal}_{\text{Test article}}\text{-Signal}_{\text{detection buffer control}})/(\text{Signal}_{\text{None treated}}\text{- Signal}_{\text{detection buffer control}})] \times 100\%$.

ADCC assays

Primary ADCC killing assays assessed *in vitro* killing of NSCLC cells. Ten thousand tumor cells were plated per well in RPMI1640. Antibodies were added to the wells and incubated at 37°C for 15 min. Upon thawing, 500,000 PBMCs in RPMI1640 were added to each well and incubated at 37°C for 4 h. The release of lactate dehydrogenase (LDH) was measured using a Roche Cytotoxicity Detection Kit. Controls included untreated effector and target cells, target cells only, and target cells plus 0.2% (w/v) Triton X-100. The lysis ratio on the y axis was plotted against the antibody concentration on the x axis using a four-parameter logistic (4PL) model. EC_{50} values, efficacy (y-axis span) and 95% CI for EC_{50} were calculated in GraphPad Prism 9.3.1(GraphPad Software, Inc.). Lysis ratio (%) was determined by the following equation with OD values (492 nm - 650 nm):

$$\%\ \text{Lysis} = [(\text{Signal}_{\text{Test article}} - \text{Signal}_{\text{untreated effector target cell control}}/(\text{Signal}_{\text{target cell maximum control}} - \text{Signal}_{\text{target cells spontaneous control}})] \times 100.$$

To evaluate the effect of EGFR-TKIs on the TAVO412-mediated ADCC killing, NCI-H1975 and HCC827 cells were pre-treated with osimertinib or lazertinib for 48 h at 37°C before undergoing the ADCC assay as described above.

ADCP assays

Phagocytosis was evaluated with human peripheral blood monocyte–derived macrophages as effector cells. Monocytes were isolated from previously frozen human PBMCs using EasySep™ Human Monocyte Enrichment Kit (StemCell) and were induced to differentiate into macrophages with macrophage colony stimulating factor (M-CSF) (StemCell) and interferon gamma (IFNγ) (StemCell) according to the manufacturer's instructions. NSCLC target cells were labeled with Carboxy Fluorescein Succinimidyl Ester (CFSE) using the CFSE-Cell Labeling KIT (Abcam). Fifty thousand cancer cells per well were cocultured with 100,000 macrophages per well with the test articles for 24 h at 37°C. Next, Alexa-647-labeled anti-CD14 and anti-CD11b antibodies (R&D) were added to the culture and then

incubated for 30-min at 4°C to label the macrophages. Flow cytometry (Beckman CytoFLEX) detected CSFE (FITC-A channel) positive cells and Alexa 647 (APC-A channel) positive cells. The cells initially were gated based on FSC vs SSC to eliminate debris and define a population gate (P1). P1 was then analyzed on FSC-H vs. FSC-A to isolate single cells (P2). A quadrant gate divided the P2 cells into four sub-populations with FITC-A vs APC-A ($FITC^+$ APC^+; $FITC^-$ APC^+; $FITC^+$ APC^-; $FITC^-$ APC^-) and the percentage of Q3 ($FITC^+$ APC^-) was calculated. CytExpert 2.4 software (Beckman Coulter) was used to calculate the killing percentage (%) as plotted on the y axis against the antibody concentration on the x axis using a four-parameter logistic (4PL) model. EC_{50} values, efficacy (y-axis span) and 95% CI for EC_{50} were calculated in GraphPad Prism 9.3.1 (GraphPad Software, Inc.). Killing percentage (%) is determined by the following equation (14): % Killing = 100 x {(average % $FITC^+APC\text{-}A^-$ of [lowest mAb] for each antibody -%$FITC^+$ $APC\text{-}A^-$ sample)/(average %$FITC^+$ $APC\text{-}A^-$ of [lowest mAb] for each antibody)}.

CDC assays

Twenty thousand tumor cells in RPMI 1640 medium were plated per well in 96-well plates. Upon the addition of test articles, the cells were incubated for 1 h at room temperature. After a 2-fold diluted Baby Rabbit Complement (Cedarlane) was added, the wells were incubated at 37°C for 1 h. The release of lactate dehydrogenase (LDH) in the supernatants was measured with the Roche Cytotoxicity Detection Kit. Control wells included: the target cells and complement at the lowest concentration of test antibody (TC spontaneous release); target cells only (T spontaneous release); and target cells plus 0.2% (w/v) Triton X-100 (maximum release). The lysis ratio on the y axis was plotted against the antibody concentration on the x axis using a four-parameter logistic (4PL) model. EC_{50} values, efficacy (y-axis span) and 95% CI for EC_{50} were calculated in GraphPad Prism 9.3.1(GraphPad Software, Inc.). The lysis ratio (%) was determined by the following equation with OD values (492 nm - 650 nm):

$$\%\ \text{Lysis} = [(\text{Experimental} - \text{TC spontaneous})/(\text{Maximum release} - \text{T spontaneous})] \times 100\,\%.$$

In vivo efficacy studies in mice

All procedures related to animal care, handling, and treatment were carried out in accordance with the guidelines of GenePharma's Institutional Animal Care and Use Committee (IACUC).

Tumor cells were injected subcutaneously into female Balb/c Nude mice (n = 5 or 7 per group; 6–10 weeks old; Nanjing GemPharmatech Co., Ltd.) at the right flank ($5x10^6$ cells in 50% Matrigel admixed with 50% PBS for HCC827; $5x10^6$ NCI-H1975 in PBS; $1x10^7$ NCI-H292 in PBS). Therapeutic treatments began when the mean tumor volume reached approximately 200 mm^3 and the first day of dosing was denoted as day 0. The detailed treatment regimens were described in each figure legend. In certain studies, at the end of the research, tumors were collected, weighed, and/or photographed. The average tumor volume in each group was calculated as length x $width^2$ x 0.5 with units of mm^3. Tumor volumes and body weights were recorded twice weekly, and the tumor growth curves of each treatment group were plotted as mean ± SEM. Tumor regression was defined as partial regression (PR) if the tumor volume decreased to 50% of the tumor volume at the start of treatment and as complete regression (CR) if the tumor volume too small to be recorded (tumor volume ~ 0 mm^3).

Statistical analysis of *in vivo* results

Statistical analysis was performed using GraphPad Prism software version 9.3.1 (GraphPad Software, Inc.). A comparison between two groups was performed using the Student's T-test. Multiple group comparisons used a parametric one-way ANOVA followed by *post hoc* test (Tukey's test). P values less than 0.05 were considered statistically significant.

Data availability statement

The original contributions presented in the study are included in the article/Supplementary Material. Further inquiries can be directed to the corresponding author.

Ethics statement

The animal study was approved by GenePharma's Institutional Animal Care and Use Committee (IACUC). The study was conducted in accordance with the local legislation and institutional requirements.

Author contributions

YJ: Conceptualization, Formal Analysis, Investigation, Project administration, Resources, Supervision, Writing – original draft, Writing – review & editing. PS: Data curation, Formal Analysis, Investigation, Methodology, Resources, Validation, Visualization, Writing – original draft. PC: Data curation, Formal Analysis, Investigation, Methodology, Resources, Software, Supervision, Visualization, Writing – original draft. YX: Conceptualization, Data curation, Formal Analysis, Investigation, Methodology, Resources, Software, Supervision, Validation, Visualization, Writing – original draft. GM: Data curation, Investigation, Methodology, Resources, Software, Visualization, Writing – original draft. ZZ: Data curation, Formal Analysis, Investigation, Methodology, Resources, Software, Validation, Visualization, Writing – original draft. SW: Data curation, Formal Analysis,

Investigation, Methodology, Resources, Software, Validation, Visualization, Writing – original draft. MF: Data curation, Formal Analysis, Investigation, Methodology, Resources, Validation, Visualization, Writing – original draft. HJ: Data curation, Formal Analysis, Investigation, Methodology, Resources, Software, Validation, Visualization, Writing – original draft. SH: Data curation, Formal Analysis, Methodology, Resources, Visualization, Writing – original draft. FZ: Data curation, Formal Analysis, Investigation, Methodology, Supervision, Writing – original draft. CH: Conceptualization, Formal Analysis, Investigation, Visualization, Writing – original draft. MC: Conceptualization, Funding acquisition, Investigation, Resources, Supervision, Writing – review & editing.

Funding

The author(s) declare that no financial support was received for the research and/or publication of this article.

Acknowledgments

We thank Songling Zhang, Pu Pu, and Maria P. MacWilliams for the technical support and review of this manuscript. We thank Mann Fung for advice on research design.

Conflict of interest

All authors are employees of Tavotek Biotherapeutics, Inc.

Generative AI statement

The author(s) declare that no Generative AI was used in the creation of this manuscript.

Publisher's note

Supplementary material

The Supplementary Material for this article can be found online at: https://www.frontiersin.org/articles/10.3389/fonc.2025.1533059/full#supplementary-material

References

1. Araghi M, Mannani R, Heidarnejad maleki A, Hamidi A, Rostami S, Safa SH, et al. Recent advances in non-small cell lung cancer targeted therapy; an update review. *Cancer Cell Int*. (2023) 23. doi: 10.1186/s12935-023-02990-y

2. Majeed U, Manochakian R, Zhao Y, Lou Y. Targeted therapy in advanced non-small cell lung cancer: current advances and future trends. *J Hematol Oncol*. (2021) 14. doi: 10.1186/s13045-021-01121-2

3. Sholl LM, Aisner DL, Varella-Garcia M, Berry LD, Dias-Santagata D, Wistuba II, et al. Multi-institutional oncogenic driver mutation analysis in lung adenocarcinoma: the lung cancer mutation consortium experience. *J Thoracic Oncology*. (2015) 10:768–77. doi: 10.1097/jto.0000000000000516

4. Zhang Y-L, Yuan J-Q, Wang K-F, Fu X-H, Han X-R, Threapleton D, et al. The prevalence of EGFR mutation in patients with non-small cell lung cancer: a systematic review and meta-analysis. *Oncotarget*. (2016) 7(48):78985–93. doi: 10.18632/oncotarget.12587

5. Cho BC, Simi A, Sabari J, Vijayaraghavan S, Moores S, Spira A. Amivantamab, an epidermal growth factor receptor (EGFR) and mesenchymal-epithelial transition factor (MET) bispecific antibody, designed to enable multiple mechanisms of action and broad clinical applications. *Clin Lung Cancer*. (2023) 24:89–97. doi: 10.1016/j.cllc.2022.11.004

6. Li AR, Chitale D, Riely GJ, Pao W, Miller VA, Zakowski MF, et al. EGFR mutations in lung adenocarcinomas. *J Mol Diagnostics*. (2008) 10:242–8. doi: 10.2353/jmoldx.2008.070178

7. Passaro A, Mok T, Peters S, Popat S, Ahn M-J, de Marinis F. Recent advances on the role of EGFR tyrosine kinase inhibitors in the management of NSCLC with uncommon, non exon 20 insertions, EGFR mutations. *J Thoracic Oncology*. (2021) 16:764–73. doi: 10.1016/j.jtho.2020.12.002

8. Nan X, Xie C, Yu X, Liu J. EGFR TKI as first-line treatment for patients with advanced EGFR mutation-positive non-small-cell lung cancer. *Oncotarget*. (2017) 8:75712–26. doi: 10.18632/oncotarget.20095

9. Johnson M, Garassino MC, Mok T, Mitsudomi T. Treatment strategies and outcomes for patients with EGFR-mutant non-small cell lung cancer resistant to EGFR tyrosine kinase inhibitors: Focus on novel therapies. *Lung Cancer*. (2022) 170:41–51. doi: 10.1016/j.lungcan.2022.05.011

10. He J, Huang Z, Han L, Gong Y, Xie C. Mechanisms and management of 3rd –generation EGFR–TKI resistance in advanced non–small cell lung cancer (Review). *Int J Oncol*. (2021) 59:90. doi: 10.3892/ijo.2021.5270

11. Piper-Vallillo AJ, Sequist LV, Piotrowska Z. Emerging treatment paradigms for EGFR-mutant lung cancers progressing on osimertinib: A review. *J Clin Oncology*. (2020) 38:2926–36. doi: 10.1200/jco.19.03123

12. Krumbach R, Schüler J, Hofmann M, Giesemann T, Fiebig H-H, Beckers T. Primary resistance to cetuximab in a panel of patient-derived tumor xenograft models: Activation of MET as one mechanism for drug resistance. *Eur J Cancer*. (2011) 47:1231–43. doi: 10.1016/j.ejca.2010.12.019

13. Moores SL, Chiu ML, Bushey BS, Chevalier K, Luistro L, Dorn K, et al. A Novel Bispecific Antibody Targeting EGFR and cMet Is Effective against EGFR Inhibitor–Resistant Lung Tumors. *Cancer Res*. (2016) 76:3942–53. doi: 10.1158/0008-5472.Can-15-2833

14. Grugan KD, Dorn K, Jarantow SW, Bushey BS, Pardinas JR, Laquerre S, et al. Fc-mediated activity of EGFR x c-Met bispecific antibody JNJ-61186372 enhanced killing of lung cancer cells. *mAbs*. (2016) 9:114–26. doi: 10.1080/19420862.2016.1249079

15. Park K, Haura EB, Leighl NB, Mitchell P, Shu CA, Girard N, et al. Amivantamab in EGFR exon 20 insertion–mutated non–small-cell lung cancer progressing on platinum chemotherapy: initial results from the CHRYSALIS phase I study. *J Clin Oncology*. (2021) 39:3391–402. doi: 10.1200/jco.21.00662

16. Guo MZ, Marrone KA, Spira A, Freeman K, Scott SC. Amivantamab: a potent novel EGFR/c-MET bispecific antibody therapy for EGFR-mutated non-small cell lung cancer. *touchREVIEWS in Oncol & Haematol*. (2021) 17(1):42–7. doi: 10.17925/OHR.2021.17.1.42

17. Vyse S, Huang PH. Amivantamab for the treatment ofEGFRexon 20 insertion mutant non-small cell lung cancer. *Expert Rev Anticancer Ther*. (2021) 22:3–16. doi: 10.1080/14737140.2022.2016397

18. Pacheco JM. Mobocertinib: A potential treatment for NSCLC with EGFR exon 20 insertions. *Cancer Discovery*. (2021) 11:1617–9. doi: 10.1158/2159-8290.Cd-21-0379

19. Le X, Nilsson M, Goldman J, Reck M, Nakagawa K, Kato T, et al. Dual EGFR-VEGF pathway inhibition: A promising strategy for patients with EGFR-mutant NSCLC. *J Thoracic Oncology*. (2021) 16:205–15. doi: 10.1016/j.jtho.2020.10.006

20. Nilsson MB, Robichaux J, Herynk MH, Cascone T, Le X, Elamin Y, et al. Altered regulation of HIF-1α in naive- and drug-resistant EGFR-mutant NSCLC: implications for a vascular endothelial growth factor-dependent phenotype. *J Thoracic Oncology*. (2021) 16:439–51. doi: 10.1016/j.jtho.2020.11.022

21. Lichtenberger BM, Tan PK, Niederleithner H, Ferrara N, Petzelbauer P, Sibilia M. Autocrine VEGF signaling synergizes with EGFR in tumor cells to promote epithelial cancer development. *Cell*. (2010) 140:268–79. doi: 10.1016/j.cell.2009.12.046

22. Cohen MH, Gootenberg J, Keegan P, Pazdur R. FDA drug approval summary: bevacizumab (Avastin®) plus carboplatin and paclitaxel as first-line treatment of advanced/metastatic recurrent nonsquamous non-small cell lung cancer. *Oncologist*. (2007) 12:713–8. doi: 10.1634/theoncologist.12-6-713

23. Larkins E, Scepura B, Blumenthal GM, Bloomquist E, Tang S, Biable M, et al. Food and drug administration approval summary: ramucirumab for the treatment of metastatic non-small cell lung cancer following disease progression on or after platinum-based chemotherapy. *Oncologist*. (2015) 20:1320–5. doi: 10.1634/theoncologist.2015-0221

24. Masuda C, Yanagisawa M, Yorozu K, Kurasawa M, Furugaki K, Ishikura N, et al. Bevacizumab counteracts VEGF-dependent resistance to erlotinib in an EGFR-mutated NSCLC xenograft model. *Int J Oncology*. (2017) 51:425–34. doi: 10.3892/ijo.2017.4036

25. Raghav KP, Gonzalez-Angulo AM, Blumenschein GRJr. Role of HGF/MET axis in resistance of lung cancer to contemporary management. *Transl Lung Cancer Res*. (2012) 1:179–93. doi: 10.3978/j.issn.2218-6751.2012.09.04

26. Takeuchi S, Wang W, Li Q, Yamada T, Kita K, Donev IS, et al. Dual inhibition of met kinase and angiogenesis to overcome HGF-induced EGFR-TKI resistance in EGFR mutant lung cancer. *Am J Pathology*. (2012) 181:1034–43. doi: 10.1016/j.ajpath.2012.05.023

27. Rivera-Soto R, Henley B, Pulgar MA, Lehman SL, Gupta H, Perez-Vale KZ, et al. Amivantamab efficacy in wild-type EGFR NSCLC tumors correlates with levels of ligand expression. *NPJ Precis Oncol*. (2024) 8:192. doi: 10.1038/s41698-024-00682-y

28. Liu R, Oldham R, Teal E, Beers S, Cragg M. Fc-engineering for modulated effector functions—Improving antibodies for cancer treatment. *Antibodies*. (2020) 9. doi: 10.3390/antib9040064

29. Stavenhagen JB, Gorlatov S, Tuaillon N, Rankin CT, Li H, Burke S, et al. Fc Optimization of Therapeutic Antibodies Enhances Their Ability to Kill Tumor Cells*In vitro*and Controls Tumor Expansion*In vivo*via Low-Affinity Activating Fcγ Receptors. *Cancer Res*. (2007) 67:8882–90. doi: 10.1158/0008-5472.Can-07-0696

30. Varsano S, Rashkovsky L, Shapiro H, Ophir D, Mark-Bentankur T. Human lung cancer cell lines express cell membrane complement inhibitory proteins and are extremely resistant to complement-mediated lysis; a comparison with normal human respiratory epithelium *in vitro*, and an insight into mechanism(s) of resistance. *Clin Exp Immunol*. (1998) 113:173–82. doi: 10.1046/j.1365-2249.1998.00581.x

31. Shu CA, Goto K, Ohe Y, Besse B, Lee S-H, Wang Y, et al. Amivantamab and lazertinib in patients with EGFR-mutant non–small cell lung (NSCLC) after progression on osimertinib and platinum-based chemotherapy: Updated results from CHRYSALIS-2. *J Clin Oncol*. (2022) 40:9006–6. doi: 10.1200/JCO.2022.40.16_suppl.9006

32. Teng K, Zhang Y, Hu X, Ding Y, Gong R, Liu L. Nimotuzumab enhances radiation sensitivity of NSCLC H292 cells *in vitro* by blocking epidermal growth factor receptor nuclear translocation and inhibiting radiation-induced DNA damage repair. *Onco Targets Ther*. (2015) 8:809–18. doi: 10.2147/ott.S77283

33. Nakade J, Takeuchi S, Nakagawa T, Ishikawa D, Sano T, Nanjo S, et al. Triple inhibition of EGFR, met, and VEGF suppresses regrowth of HGF-triggered, erlotinib-resistant lung cancer harboring an EGFR mutation. *J Thoracic Oncology*. (2014) 9:775–83. doi: 10.1097/jto.0000000000000170

34. Vijayaraghavan S, Lipfert L, Chevalier K, Bushey BS, Henley B, Lenhart R, et al. Amivantamab (JNJ-61186372), an fc enhanced EGFR/cMet bispecific antibody, induces receptor downmodulation and antitumor activity by monocyte/macrophage trogocytosis. *Mol Cancer Ther*. (2020) 19:2044–56. doi: 10.1158/1535-7163.Mct-20-0071

35. Weisser NE, Sanches M, Escobar-Cabrera E, O'Toole J, Whalen E, Chan PWY, et al. An anti-HER2 biparatopic antibody that induces unique HER2 clustering and complement-dependent cytotoxicity. *Nat Commun*. (2023) 14:1394. doi: 10.1038/s41467-023-37029-3

36. Chen J, Liao S, Xiao Z, Pan Q, Wang X, Shen K, et al. The development and improvement of immunodeficient mice and humanized immune system mouse models. *Front Immunol*. (2022) 13:1007579. doi: 10.3389/fimmu.2022.1007579

37. Jin Y, Chen P, Zhou H, Mu G, Wu S, Zha Z, et al. Developing transcriptomic biomarkers for TAVO412 utilizing next generation sequencing analyses of preclinical tumor models [Original Research. *Front Immunol*. (2025) 16:1505868. doi: 10.3389/fimmu.2025.1505868

38. Steiner P, Joynes C, Bassi R, Wang S, Tonra JR, Hadari YR, et al. Tumor growth inhibition with cetuximab and chemotherapy in non–small cell lung cancer xenografts expressing wild-type and mutated epidermal growth factor receptor. *Clin Cancer Res*. (2007) 13:1540–51. doi: 10.1158/1078-0432.Ccr-06-1887

39. Tang Y, Lou J, Alpaugh RK, Robinson MK, Marks JD, Weiner LM. Regulation of antibody-dependent cellular cytotoxicity by igG intrinsic and apparent affinity for target antigen. *J Immunol*. (2007) 179:2815–23. doi: 10.4049/jimmunol.179.5.2815

40. Cavazzoni A, Alfieri RR, Cretella D, Saccani F, Ampollini L, Galetti M, et al. Combined use of anti-ErbB monoclonal antibodies and erlotinib enhances antibody-dependent cellular cytotoxicity of wild-type erlotinib-sensitive NSCLC cell lines. *Mol Cancer*. (2012) 11:91. doi: 10.1186/1476-4598-11-91

41. BjÖRkelund H, Gedda L, Malmqvist M, Andersson K. Resolving the EGF-EGFR interaction characteristics through a multiple-temperature, multiple-inhibitor, real-time interaction analysis approach. *Mol Clin Oncology*. (2013) 1:343–52. doi: 10.3892/mco.2012.37

42. Buday L, Björkelund H, Gedda L, Barta P, Malmqvist M, Andersson K. Gefitinib induces epidermal growth factor receptor dimers which alters the interaction characteristics with 125I-EGF. *PloS One*. (2011) 6. doi: 10.1371/journal.pone.0024739

43. Arteaga CL, Ramsey TT, Shawver LK, Guyer CA. Unliganded epidermal growth factor receptor dimerization induced by direct interaction of quinazolines with the ATP binding site. *J Biol Chem*. (1997) 272:23247–54. doi: 10.1074/jbc.272.37.23247

44. Gan HK, Walker F, Burgess AW, Rigopoulos A, Scott AM, Johns TG. The epidermal growth factor receptor (EGFR) tyrosine kinase inhibitor AG1478 increases the formation of inactive untethered EGFR dimers. *J Biol Chem*. (2007) 282:2840–50. doi: 10.1074/jbc.M605136200

45. Kim H, Kim SH, Kim MJ, Kim SJ, Park SJ, Chung JS, et al. EGFR inhibitors enhanced the susceptibility to NK cell-mediated lysis of lung cancer cells. *J Immunother*. (2011) 34:372–81. doi: 10.1097/CJI.0b013e31821b724a

46. Upadhya A, Yadav KS, Misra A. Targeted drug therapy in non-small cell lung cancer: Clinical significance and possible solutions-Part I. *Expert Opin Drug Deliv*. (2021) 18:73–102. doi: 10.1080/17425247.2021.1825377

47. Wrona A, Dziadziuszko R, Jassem J. Combining radiotherapy with targeted therapies in non-small cell lung cancer: focus on anti-EGFR, anti-ALK and anti-angiogenic agents. *Trans Lung Cancer Res*. (2021) 10:2032–47. doi: 10.21037/tlcr-20-552

48. Raben D, Helfrich B, Chan DC, Ciardiello F, Zhao L, Franklin W, et al. The effects of cetuximab alone and in combination with radiation and/or chemotherapy in lung cancer. *Clin Cancer Res*. (2005) 11:795–805. doi: 10.1158/1078-0432.795.11.2

49. De Bacco F, Luraghi P, Medico E, Reato G, Girolami F, Perera T, et al. Induction of MET by ionizing radiation and its role in radioresistance and invasive growth of cancer. *JNCI: J Natl Cancer Institute*. (2011) 103:645–61. doi: 10.1093/jnci/djr093

50. Gao H, Xue J, Zhou L, Lan J, He J, Na F, et al. Bevacizumab radiosensitizes non-small cell lung cancer xenografts by inhibiting DNA double-strand break repair in endothelial cells. *Cancer Letters*. (2015) 365:79–88. doi: 10.1016/j.canlet.2015.05.011

51. Yang Z, Tam KY. Combination strategies using EGFR-TKi in NSCLC therapy: learning from the gap between pre-clinical results and clinical outcomes. *Int J Biol Sci*. (2018) 14:204–16. doi: 10.7150/ijbs.22955

52. Labrijn AF, Meesters JI, Priem P, de Jong RN, van den Bremer ETJ, van Kampen MD, et al. Controlled Fab-arm exchange for the generation of stable bispecific IgG1. *Nat Protoc*. (2014) 9:2450–63. doi: 10.1038/nprot.2014.169

Glossary

ADCC	Antibody-Dependent Cellular Cytotoxicity
ADCP	Antibody-Dependent Cellular Phagocytosis
ADCT	Antibody-Dependent Cellular Trogocytosis
CDC	Complement-Dependent Cytotoxicity
CFSE	Carboxyfluorescein succinimidyl ester
cMET	Mesenchymal Epithelial Transition Factor
CI	Confidence Interval
CRT	Chemoradiotherapy
EGF	Epidermal Growth Factor
EGFR	Epidermal Growth Factor Receptor
ELISA	Enzyme-Linked Immunosorbent Assay
FACS	Fluorescence-Activated Cell Sorting
FcγR	Fc gamma Receptor
GADPH	GlycerAldehyde-3-Phosphate Dehydrogenase
GM-CSF	Granulocyte-Macrophage Colony-Stimulating Factor
HGF	Hepatocyte Growth Factor
HRP	Horseradish Peroxidase
IgG	Immunoglobulin G
LDH	Lactate Dehydrogenase
NSCLC	Non-Small Cell Lung Cancer
OS	Overall Survival
PBMC	Peripheral Blood Mononuclear Cell
PBS	Phosphate Buffer Saline
PFS	Progression-Free Survival
RPMI	Roswell Park Memorial Institute
SDS-PAGE	Sodium Dodecyl Sulfate–Polyacrylamide Gel Electrophoresis
SEC	Size Exclusion Chromatography
SEM	Standard Error of the Mean
SOC	Standard of Care
TKI	Tyrosine Kinase Inhibitor
TR-FRET	Time Resolved-Fluorescence Resonance Energy Transfer
VEGF	Vascular Endothelial Growth Factor
VEGFR2	Vascular Endothelial Growth Factor Receptor 2
PK	Pharmacokinetics
DSF	Differential Scanning Fluorometry
Tm	melting temperature

frontiers | Frontiers in Oncology

TYPE Original Research
PUBLISHED 04 June 2025
DOI 10.3389/fonc.2025.1595812

OPEN ACCESS

EDITED BY
Massimo Broggini,
Mario Negri Institute for Pharmacological Research (IRCCS), Italy

REVIEWED BY
Jing Wang,
Mass General Brigham, United States
Claudia Scimone,
University of Naples Federico II, Italy

*CORRESPONDENCE
Diansheng Zhong
dzhong@tmu.edu.cn
Fanlu Meng
mengfanlu1101@163.com

†These authors have contributed equally to this work

RECEIVED 18 March 2025
ACCEPTED 16 May 2025
PUBLISHED 04 June 2025

CITATION
Kong L, Peng L, Yang X, Ma Q, Zhang L, Liu X, Zhong D and Meng F (2025) Aumolertinib plus bevacizumab for untreated advanced NSCLC with EGFR sensitive mutation. *Front. Oncol.* 15:1595812. doi: 10.3389/fonc.2025.1595812

Aumolertinib plus bevacizumab for untreated advanced NSCLC with EGFR sensitive mutation

Lingping Kong†, Lina Peng†, Xue Yang, Qing Ma, Linlin Zhang, Xia Liu, Diansheng Zhong* and Fanlu Meng*

Department of Medical Oncology, Tianjin Medical University General Hospital, Tianjin, China

Background: Aumolertinib is a novel third-generation epidermal growth factor receptor tyrosine kinase inhibitor (EGFR-TKI) with proven efficacy and safety for untreated non-small-cell lung cancer (NSCLC) patients with EGFR sensitizing mutations (EGFRm) in China. The progression-free survival (PFS) improvement of the combination of first-generation EGFR-TKIs and bevacizumab was confirmed by CTONG1509, JO25567, and NEJ026 studies, however, the effect of third-generation EGFR-TKIs plus bevacizumab remains under debate. This study aimed to investigate the efficacy and safety of aumolertinib plus bevacizumab in untreated EGFRm advanced NSCLC.

Methods: We conducted a phase II single-arm prospective clinical trial for advanced EGFRm NSCLC treated with aumolertinib combined with bevacizumab. Treatment continued until disease progression, occurrence of unacceptable toxicities, or the patient withdrew consent. The study was stratified according to sex, smoking history, stage, EGFR mutation status, and central nervous system (CNS) metastasis. The primary endpoint was the 12–month progression-free survival rate (PFS%), and secondary endpoints included the objective response rate (ORR), overall survival (OS), and progression-free survival (PFS).

Results: Between September 16, 2020, and November 11, 2021, a total of 21 patients were enrolled in the study. The median follow-up was 36.8 months (ranging from 33.2 to 40.4 months), and all 21 patients were included in the evaluation. The PFS% at 12-month was 81% (95% confidence interval (CI): 64.1–97.9%), the median PFS was 26 months (95% CI: 16.5-35.5) and the ORR reached 85.7%, with an average reduction of the target lesions of 48.2%. Among patients with CNS metastasis, the ORR was 92.9% (13/14), and for TP53 co-mutation patients, the ORR was 86.6% (12/14). Grade 3 adverse events were observed in 4 patients (19.2%), and no grade 4 or 5 adverse events reported.

Conclusion: The combination of aumolertinib and bevacizumab in patients with advanced EGFRm NSCLC achieved the study's primary endpoint. This study indeed extended PFS compared with previous literature, and it was deemed safe and tolerable.

KEYWORDS

aumolertinib, bevacizumab, EGFR-TKI, non-small cell lung cancer, progression-free survival

Introduction

Approximately 20-40% of non-small-cell lung cancer (NSCLC) patients harbor epidermal growth factor receptor mutations (EGFRm), primarily consisting of exon 19 deletions and exon 21 p.L858R (L858R) mutations (1). Epidermal growth factor receptor tyrosine kinase inhibitors (EGFR-TKIs), including gefitinib, erlotinib, and osimertinib, are the preferred first-line treatment for patients with EGFR mutations (2–4). Notably, when employed as the initial treatment for EGFRm NSCLC patients, osimertinib has demonstrated prolonged progression-free survival (PFS) and overall survival (OS) compared to erlotinib and gefitinib (2, 5). Furthermore, studies have indicated its superior brain permeability compared to first- and second-generation treatments (6, 7). Nevertheless, despite these advancements, disease progression and acquired resistance remain inevitable.

To address this challenge, integrated treatment strategies have been proposed. Bevacizumab, a recombinant anti-vascular endothelial growth factor (VEGF) monoclonal antibody, functions by inhibiting angiogenesis and impeding tumor growth (8). In numerous clinical phase 2/3 trials, the combination of EGFR-TKIs and bevacizumab has consistently shown a significant enhancement in progression-free survival (PFS) compared to EGFR-TKIs monotherapy when used as the primary treatment for patients with EGFRm NSCLC (9–11). Various phase 3 studies, such as FLAURA2 and AENEAS, which compare third-generation TKIs with first-generation TKIs as the initial therapy for patients with advanced EGFRm NSCLC, have reported the superior PFS associated with third-generation agents. Consequently, the exploration of combining third-generation EGFR-TKIs with bevacizumab in the first-line treatment of EGFRm NSCLC represents a current focal point of research.

Aumolertinib (formerly known as almonertinib; HS-10296) is an oral, third-generation EGFR-TKI designed to selectively target mutant EGFR rather than wild-type EGFR. It has been specifically formulated for the treatment of advanced EGFRm NSCLC. The APPOLO study demonstrated the remarkable efficacy and safety profile of aumolertinib in patients with EGFR T790M-positive NSCLC, showcasing its effectiveness, particularly in brain metastases (BM) (13). In the AENEAS trial, a phase 3 study conducted among Chinese patients, aumolertinib, as a first-line treatment, significantly extended progression-free survival (PFS) and duration of response (DOR) when compared to gefitinib in patients with advanced EGFRm NSCLC. However, the overall survival (OS) data from this study are currently immature (12).

A phase 1/2 single-arm study evaluating the initial treatment of osimertinib plus bevacizumab for advanced EGFRm NSCLC patients successfully achieved its primary endpoint, which was the 12-month progression-free survival rate (PFS%) (14). Building upon this foundation, we propose an investigation into the combination of aumolertinib and bevacizumab as a first-line therapy for advanced EGFRm NSCLC. Our objective is to explore the efficacy and safety of aumolertinib plus bevacizumab in untreated EGFRm advanced NSCLC.

Methods

Patient selection

Patients were enrolled between September 2020 to November 2021, and followed up until August 2024. The eligibility criteria were as follows: (1) individuals aged 18 years or older, (2) NSCLC confirmed histologically/cytologically or diagnosed clinically as advanced peripheral lung cancer, (3) EGFR-sensitizing mutation identified through next-generation sequencing (NGS) analysis, (4) clinical stage IIIB, IIIC, or IV disease not suitable for radical radiation therapy (based on the eighth edition of lung cancer TNM staging system), (5) presence of measurable lesion according to the Response Evaluation Criteria in Solid Tumors (RECIST) version 1.1; (6) adequate hematologic and organ function; (7) Eastern Coop-erative Oncology Group performance status 0 or 1, (8) signed informed consent form.

The exclusion criteria were: (1) previous exposure to EGFR inhibitors or VEGF receptor inhibitors, (2) coexistence or history of interstitial lung disease, (3) a high susceptibility to bleeding or embolism, (4) unmanaged hypertension, (5) Patients who received radiotherapy to the brain can participate, but are required to have an interval ≥14 days between the last days of radiotherapy and study treatment.

Treatment

The patients received oral aumolertinib (110 mg) once daily and bevacizumab (Avastin, 7.5 mg/kg) on day 1 intravenously every 3 weeks. Treatment persisted until disease progression, occurrence of unacceptable toxicities, or withdrawal of patient consent.

Evaluation of efficacy and safety

Eight weeks following the initiation of aumolertinib and bevacizumab, routine chest/abdominal computed tomography and brain magnetic resonance imaging (MRI) were conducted, with subsequent assessments every 2-4 months. Tumor lesion response was evaluated based on the Response Evaluation Criteria in Solid Tumors (RECIST) version 1.1. The Objective Response Rate (ORR) was defined as the proportion of patients achieving complete response and partial response (CR+PR). The Disease Control Rate (DCR) was calculated as the proportion of patients demonstrating objective response or stable disease for a minimum of four weeks. PFS was delineated as the duration from the initiation of the first medication to disease progression or death. The primary endpoint focused on 12-month PFS%, while secondary endpoints encompassed ORR, PFS, and safety parameters.

Adverse events (AEs) were systematically evaluated throughout the study, graded in accordance with the National Cancer Institute Common Terminology Criteria for Adverse Events version 5.0.

Sample size calculation

To consider combined aumolertinib and bevacizumab a promising treatment strategy, we aimed for an improvement in 12-month PFS rates from a historical 60% to 80%, which would require a sample size of 24 patients to provide 80% power while controlling the type 1 error at 10%. Ultimately, we achieved 80% of our projected enrollments.

Statistical analysis

Survival analyses were performed according to the Kaplan-Meier method, and confidence intervals (CIs) were calculated at a 95% confidence level. All analyses were performed using IBM SPSS software, version 24.0.

Ethics

This study adhered to the rules and regulations of clinical studies with respect to human subject protection, and it was approved by the Tianjin Medical University of General Hospital of Ethics Committee and conducted in accordance with the principles of the Declaration of Helsinki. Informed consent was obtained from all enrolled patients.

Results

Patient characteristics

A total of 21 patients, comprising four men and fifteen women, were included in this study conducted between September 16, 2020, and November 11, 2021. The detailed characteristics of these enrolled patients are presented in Table 1. The median age of the participants was 62 years, with an age range spanning from 41 to 89 years. The majority of patients presented with adenocarcinoma (85.7%), while one had squamous cell carcinoma, another had NSCLC (undetermined pathological subtype), and one patient clinically manifested advanced peripheral lung cancer. All patients were diagnosed at clinical stage IV and received primary treatment. The EGFR mutations at diagnosis were located in exons 19 deletion (42.9%) and 21 L858R (57.1%). TP53 mutation and primary T790M occurred in 71.4% and 19.0% of cases, respectively. 14 patients had concomitant CNS involvement, with 21.4% (3/14) presenting symptomatic brain metastases at enrollment. Brain radiotherapy was administered to two patients, one undergoing whole-brain radiotherapy (WBRT), and the other receiving gamma knife radiosurgery.

TABLE 1 Patient characteristics.

Characteristics	Variables	N
Total case		21
Age	Median(range), y	62 (41-89)
Sex	Male	4 (19%)
	Female	17 (81%)
Smoking	Yes	5 (23.8%)
	No	16 (76.2%)
Histology	Adenocarcinoma	18 (85.7%)
	Squamous cell carcinoma	1 (4.8%)
	NSCLC, unspecified type	1 (4.8%)
	Peripheral lung cancer	1 (4.8%)
Clinical stage	IV	21 (100.0%)
EGFR mutation	Exon 19 del	9 (42.9%)
	Exon 20 L858R	12 (57.1%)
T790M mutation	Yes	4 (19.0%)
	No	17 (81.0%)
TP53 mutation	Yes	15 (71.4%)
	No	6 (28.6%)
CNS	Yes	14 (66.7%)
	No	7 (33.3%)
Neurological symptoms	Yes	3 (21.4%)
	No	11 (78.6%)
Brain radiotherapy	Yes	2 (14.3%)
	No	12 (85.7%)
CEA	Abnormal	18 (85.7%)
	Normal	3 (14.3%)

CNS, central nervous system; EGFR, epidermal growth factor receptor; CEA, carcino-embryonic antigen.

Clinical responses

All 21 patients were ultimately evaluated. The primary endpoint, the 12-month PFS%, reached 81% (95% CI: 64.1–97.9%). The patients exhibited a median PFS of 26 months (95% CI: 16.5-35.5) (Figure 1A), with a median follow-up for PFS of 36.8 months (33.2m- 40.4m). The median OS was 32.8 months (95% CI: 26.1-39.5) (Figure 1B).

Within this cohort, seventeen patients experienced disease progression, whereas two withdrew from treatment without progression. Two patients continue to receive ongoing treatment (Figure 2A). Notably, 95.2% (20/21) of patients demonstrated a clinical response, marked by an average reduction of 48.2% in target lesions (Figure 2B).

Subgroup analysis further explored various parameters. The median PFS for patients with CNS metastases (n=14) or without (n=7) were 21 (95% CI: 13.7-28.3) and 31 months (95% CI: 0–64.4), respectively, with a Hazard Ratio (HR) of 1.77(95% CI: 0.62–5.08)

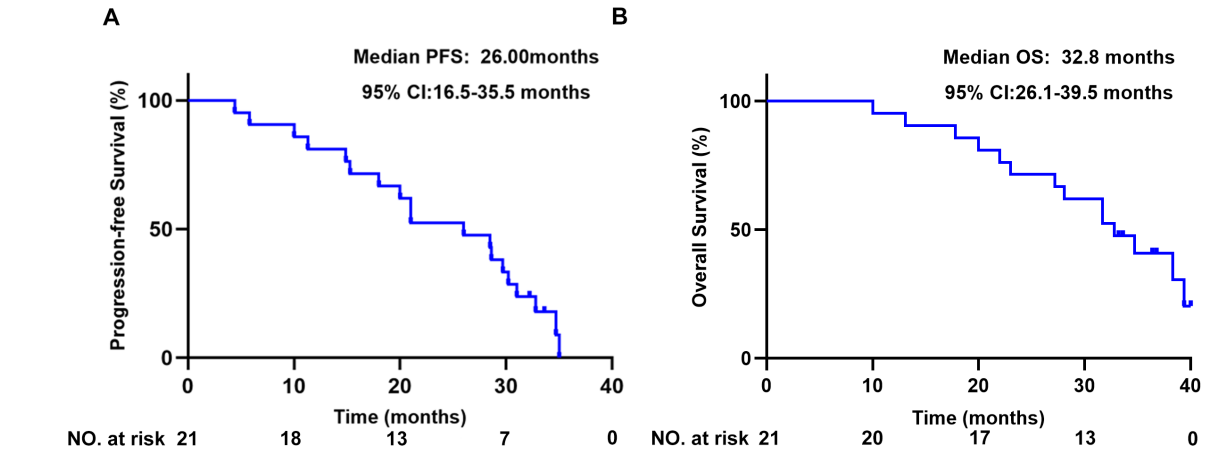

FIGURE 1
Kaplan-Meier estimates of **(A)** PFS, and **(B)** OS.

(Figure 3A). For patients with exon 19 deletion (n=9) or exon 21 p.L858 (n=12), the median PFS was 26 (95% CI: 11.4-40.6) and 20 months (95% CI: 2.2-37.8), respectively, with an HR of 0.57 (95% CI: 0.21–1.56) (Figure 3B). In patients with (n=15) and without (n=6) TP53 mutation, the median PFS was 21 months (95% CI: 4.34–37.67) and 26 months (95% CI: 15.68–36.32), respectively, with an HR of 0.86 (95% CI: 0.32–2.35) (Figure 3C). For patients with (n=4) and without (n=17) T790M mutation, the median PFS was 26 months (95% CI: 9.05–42.95) and 21 months (95% CI: 9.57–32.43), respectively, with an HR of 0.71 (95% CI: 0.20–2.48) (Figure 3D).

The ORR was 85.7% (18/21) (Table 2). Noteworthy ORRs were observed in patients with CNS metastasis (92.9%), intracranial lesions (90%), EGFR 19del (100.0%), EGFR L858R (75%), TP53 comutation (86.6%), and primary T790M comutation (100.0%) (Table 2).

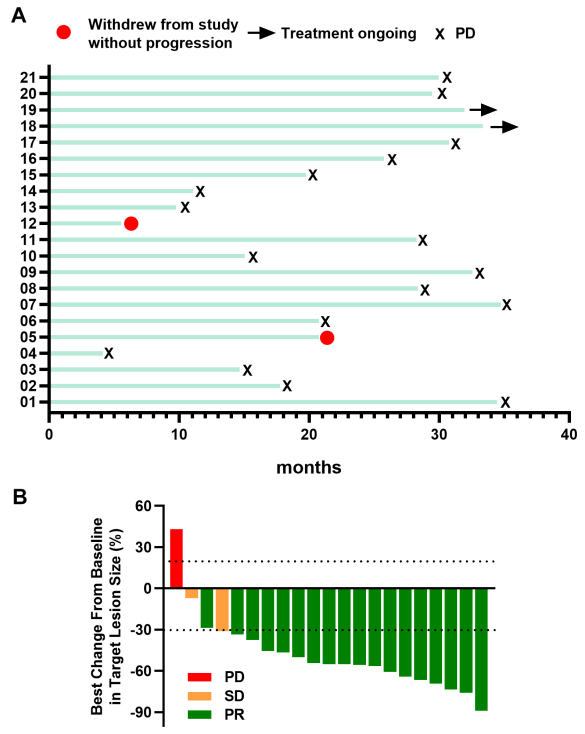

FIGURE 2
(A) Swimming plot of patients. **(B)** Best percentage change from baseline in target lesion size Responders were confirmed by Response Evaluation Criteria in Solid Tumors guidelines. PR, partial response; SD, stable disease; PD, progressive disease.

Safety

The AEs encountered by patients during treatment with aumolertinib and bevacizumab are delineated in Table 3. The predominant AEs included increased creatine phosphokinase (28.6%), proteinuria (19.0%), elevated AST/ALT levels (19.0%), and weakness (14.3%). AEs of grade 3 or higher severity were noted in four patients (19%), with no occurrences of grade 4 or 5 events. Bevacizumab discontinuation was necessitated in four patients (23.5%) due to bleeding risk or creatine phosphokinase elevation accompanied by chest pain and arrhythmia.

Discussion

This phase 2 trial investigated the combined administration of aumolertinib and bevacizumab in previously untreated stage IV EGFRm NSCLC patients. This prospective Phase II clinical trial met the primary study endpoint. Moreover, in comparison with previously published literature, it demonstrated favorable treatment efficacy and exhibited good safety and tolerability. The adverse events align with the known characteristics of each agent.

The study design is rooted in prior trials showing improved efficacy and safety when combining first-generation EGFR-TKIs with VEGF inhibitors for EGFRm NSCLC patients (9–11, 16, 17). Previous trials revealed the significant improvement in PFS with third-generation TKIs as first-line treatment (2) (Table 4). Our

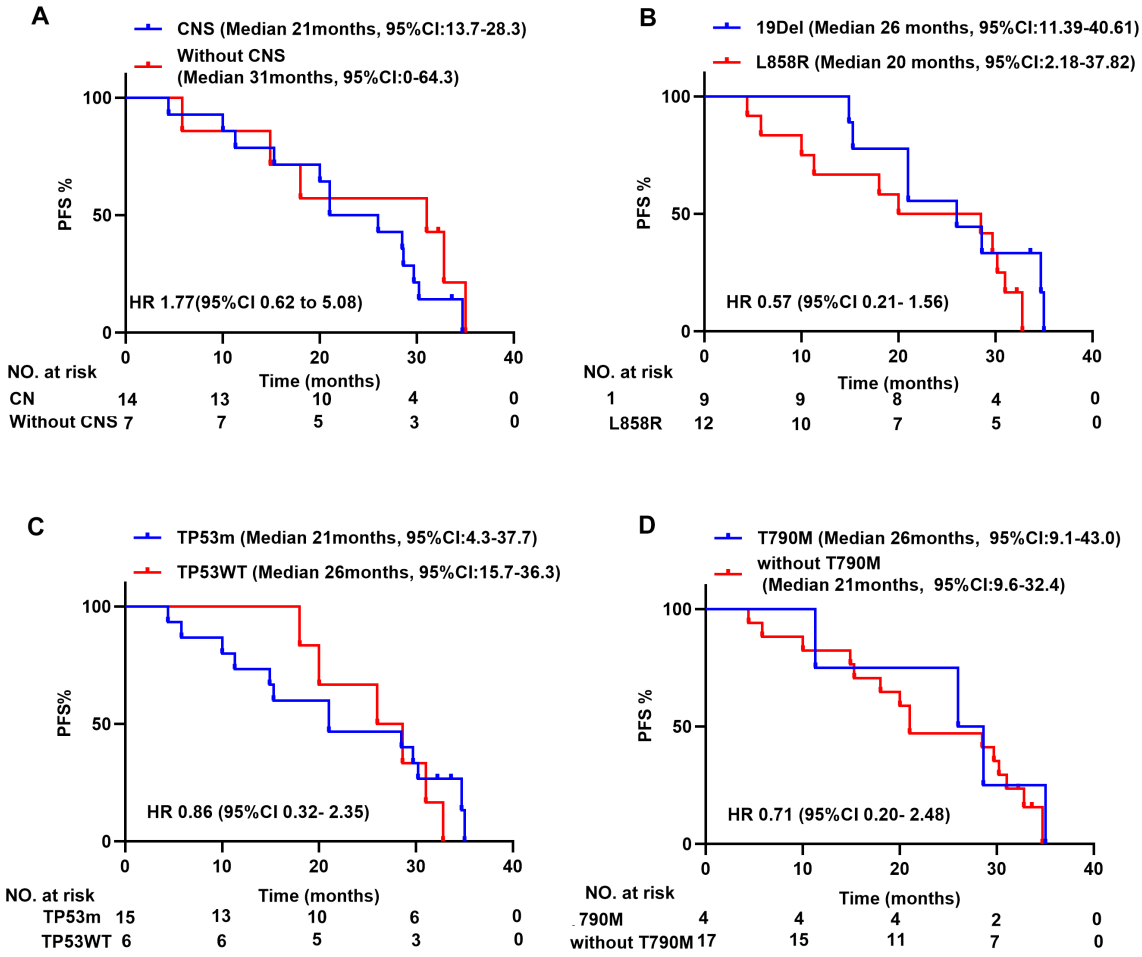

FIGURE 3
Subgroup analysis of PFS. **(A)**: 19Del and L858R. **(B)**: With or without CNS. **(C)**: with or without TP53 mutant. **(D)**: with or without T790M mutant. PFS, progression-free survival; 19 Del, EGFR 19 Del; L858R, EGFR 21 Exon L858R; CNS, central nervous system; TP53m, with TP53 mutant; TP53WT, without TP53 mutant; NE, not estimable; CI, confidence interval; HR, hazard ratio.

study, notably, emulated the structure of a phase 1/2 trial investigating osimertinib and bevacizumab. The results showcased a 12-month PFS of 81%, surpassing the outcomes observed with aumolertinib alone and the osimertinib-bevacizumab combination. Compared with aumolertinib alone in AENEAS (19.3 months), the median PFS (26 months) in this study seemed to be more beneficial (12). During the period of our study, data from phase 3 studies of third-generation EGFR-TKIs and studies investigating osimertinib in combination with bevacizumab have been published and are summarized in Table 4 (12, 14, 18–20). The WJOG9717L study,

TABLE 2 The response to aumolertinib and bevacizumab in subgroup analysis.

Response	Total N=21	CNS1 N=14	CNS2* N=10	19Del N=9	L858R N=12	TP53 N=15	T790M N=4
PR	18	13	9	9	9	13	4
SD	2	0	1	0	2	1	0
PD	1	1	0	0	1	1	0
ORR	18/21 (85.7%)	13/14 (92.9%)	9/10 (90%)	9/9 (100.0%)	9/12 (75%)	12/14 (86.6%)	3/3 (100.0%)
DCR	20/21 (95.2%)	13/14 (92.9%)	10/10 (100%)	9/9 (100.0%)	11/12 (91.7%)	14/15 (93.3%)	3/3 (100.0%)

* Eight patients have measureable intracranial lesions.
PR, partial response; SD, stable disease; PD, progressed disease; ORR, objective response rate; DCR, disease control rate; CNS, central nervous system.

TABLE 3 Adverse events (AEs) graded according to the common toxicity criteria for adverse events (CTCAE).

AEs	All	Grade 1-2 (%)	Grade 3 (%)	Grade 4 (%)
Hematological				
Leucopenia	1 (4.8)	1 (4.8)	0 (0)	0 (0)
Nonhematological				
Rash	5 (23.8)	5 (23.8)	0 (0)	0 (0)
Pruritus	1 (4.8)	1 (4.8)	0 (0)	0 (0)
Anorexia	1 (4.8)	1 (4.8)	0 (0)	0 (0)
Constipation	1 (4.8)	1 (4.8)	0 (0)	0 (0)
Fatigue	3 (14.3)	3 (14.3)	0 (0)	0 (0)
Proteinuria	4 (19.0)	4 (19.0)	0 (0)	0 (0)
Oral mucositis	1 (4.8)	1 (4.8)	0 (0)	0 (0)
Toothache	1 (4.8)	1 (4.8)	0 (0)	0 (0)
Oral bleeding	2 (9.5)	2 (9.5)	0 (0)	0 (0)
Epistaxis	2 (9.5)	2 (9.5)	0 (0)	0 (0)
Hypertension	2 (9.5)	2 (9.5)	0 (0)	0 (0)
Chest pain	1 (4.8)	0 (0)	1 (4.8)	0 (0)
Myalgia	1 (4.8)	0 (0)	1 (4.8)	0 (0)
ALT/ AST elevation	4 (19.0)	4 (19.0)	0 (0)	0 (0)
CPK elevation	6 (28.6)	4 (19.0)	2 (9.6)	0 (0)

ALT, alanine aminotransferase; AST, aspartate aminotransferase; CPK, Creatinine phosphokinase.

however, indicated no improvement in PFS with osimertinib-bevacizumab as first-line treatment (15). The mPFS and 1-year PFS rate in our study are higher than those in these studies, heralding the potential for the combination treatment regimen in this study to become a frontline therapeutic approach. It may require more refined stratification to identify specific populations that may precisely benefit from the combination therapy.

Our study's patient characteristics differed, notably with a higher percentage of patients having preexisting CNS metastases (66.7%, Table 4) (2, 12, 18–20). CNS metastases associated with a more aggressive disease phenotype and significantly shorter TKI treatment-related PFS compared to those without CNS metastases (21). The established vascular normalization effect of antiangiogenic drugs in the central nervous system has therapeutic implications. The BRAIN study demonstrated that bevacizumab could delay brain metastases, showcasing its potential value (22). A retrospective study on EGFRm NSCLC patients with brain metastases revealed a 100% ORR and a 2-year survival rate of 62.5%, suggesting the efficacy of first-generation EGFR-TKI combined with bevacizumab as first-line therapy (23). Presently, third-generation EGFR-TKIs like osimertinib exhibit superior CNS efficacy in patients with EGFR-mutant brain metastases (24, 25). Our study aligns with the AENEAS analysis at ASCO 2022 (NO.9096), indicating that combining aumolertinib and bevacizumab may be effective and protective against CNS progression, as suggested by a 92.9% ORR in our study.

In subgroup analysis, patients with EGFR exon 19 deletions exhibited better PFS trends, contrasting with worse trends in those with EGFR L858R. This is consistent with the trend of subgroup analysis in the WJOG9717L study (15). The relationship between TP53 mutation and EGFR-TKI efficacy remains debated, our data

TABLE 4 Literature review of third-generation EGFR-TKIs for EGFRm NSCLC.

Trial	Treatment	N	CNS (%)	ORR (%)	PFS% (12mo)	mPFS (mo)
AENEAS (12)	Aumolertinib vs Gefitinib	214 215	26.2 27.4	73.8 72.1	66.2 37.9	19.3 9.9
FLAURA (2)	Osimertinib vs Gefitinib or Erlotinib	279 277	19.0 22.7	80 76	70 47	18.9 10.2
FULONG (18)	Furmonertinib vs Gefitinib	178 179	35 32	NA NA	NA NA	20.8 11.1
NCT03861156 (19)	Befotertinib vs Icotinib	182 180	32.4 31.7	75.8 78.3	NA NA	22.1 13.8
LASER301 (20)	Lazertinib vs Gefitinib	196 197	26 24	76 94	NA NA	20.6 9.7
NCT02803203 (14)	Osimertinib + Bevacizumab	49	31	80	76	19
WJOG9717L (15)	Osimertinib ± Bevacizumab	61 61	37.7 29.5	86 82	63.7 73.8	17.1 24.3

15, 21 were osimertinib plus bevacizumab as first-line treatment.
mPFS, median progression-free survival; PFS%, progress free survival rate; ORR, objective response rate; mo, months; N, patient numbers; CNS, central nervous system.

indicate better PFS trends in patients without TP53 mutation. Additionally, previous studies indicated that the occurrence of a primary T790M mutation was associated with worse response and poor prognosis in patients with advanced EGFR-m NSCLC treated with first-generation (26–29), and second-generation (30, 31) EGFR-TKIs. In recent studies, primary T790M mutation showed some sensitivity towards osimertinib with the ORR fluctuating between 10% and 72.2% (32–37). In our study, four patients who had concurrent EGFR T790M at baseline benefited from the treatment strategy combining bevacizumab with aumolertinib. The best therapeutic outcome was PR, and the ORR reached 100%. This suggests that in cases of primary resistance to first-generation EGFR TKIs mediated by the primary EGFR T790M mutation, the treatment strategy adopted in this study is capable of enhancing the clinical efficacy.

Despite these therapeutic implications, our study has limitations. A small sample size from a single institution may impact result conclusiveness. Being a single-arm study lacks a control group, and future studies should expand the sample size and consider randomized controlled trials.

In conclusion, our study suggests potential benefits of aumolertinib and bevacizumab combination treatment for EGFRm advanced NSCLC compared to aumolertinib monotherapy. Nonetheless, it cannot be concluded arbitrarily that aumolertinib combined with bevacizumab is the first-line treatment of EGFRm NSCLC. Next, we should focus on subgroup analysis to select the population more suitable for the combination of aumolertinib and bevacizumab, further expand the sample size, and conduct randomized controlled studies. In the future, whether aumolertinib combined with bevacizumab can significantly improve PFS as a first-line treatment strategy may be answered.

Data availability statement

The raw data supporting the conclusions of this article will be made available by the authors, without undue reservation.

Ethics statement

The studies involving humans were approved by Tianjin Medical University of General Hospital of Ethics Committee. The studies were conducted in accordance with the local legislation and institutional requirements. The participants provided their written informed consent to participate in this study. Written informed consent was obtained from the individual(s) for the publication of any potentially identifiable images or data included in this article.

Author contributions

LK: Data curation, Formal Analysis, Writing – original draft, Funding acquisition, Writing – review & editing. LP: Data curation, Writing – original draft. XY: Data curation, Software, Writing – original draft. QM: Data curation, Investigation, Methodology, Resources, Writing – original draft. LZ: Data curation, Formal Analysis, Investigation, Writing – original draft. XL: Project administration, Software, Visualization, Writing – original draft. DZ: Conceptualization, Supervision, Funding acquisition, Writing – review & editing. FM: Conceptualization, Data curation, Supervision, Writing – review & editing.

Funding

The author(s) declare that financial support was received for the research and/or publication of this article. This study was funded by grants from the National Natural Science Foundation of China (grant number:81702678, 82272672), and the China Postdoctoral Science Foundation (Certificate Number:2023M742622).

Acknowledgments

We thank the study participants for their invaluable cooperation.

Conflict of interest

The authors declare that the research was conducted in the absence of any commercial or financial relationships that could be construed as a potential conflict of interest.

Generative AI statement

The author(s) declare that no Generative AI was used in the creation of this manuscript.

Publisher's note

References

1. Liu L, Liu J, Shao D, Deng Q, Tang H, Liu Z, et al. Comprehensive genomic profiling of lung cancer using a validated panel to explore therapeutic targets in East Asian patients. *Cancer Sci.* (2017) 108:2487–94. doi: 10.1111/cas.2017.108.issue-12

2. Soria JC, Ohe Y, Vansteenkiste J, Reungwetwattana T, Chewaskulyong B, Lee KH, et al. Osimertinib in untreated EGFR-mutated advanced non-small-cell lung cancer. *N Engl J Med.* (2018) 378:113–25. doi: 10.1056/NEJMoa1713137

3. Rosell R, Carcereny E, Gervais R, Vergnenegre A, Massuti B, Felip E, et al. Erlotinib versus standard chemotherapy as first-line treatment for European patients with advanced EGFR mutation-positive non-small-cell lung cancer (EURTAC): a multicentre, open-label, randomised phase 3 trial. *Lancet Oncol*. (2012) 13:239–46. doi: 10.1016/S1470-2045(11)70393-X

4. Maemondo M, Inoue A, Kobayashi K, Sugawara S, Oizumi S, Isobe H, et al. Gefitinib or chemotherapy for non-small-cell lung cancer with mutated EGFR. *N Engl J Med*. (2010) 362:2380–8. doi: 10.1056/NEJMoa0909530

5. Ramalingam SS, Vansteenkiste J, Planchard D, Cho BC, Gray JE, Ohe Y, et al. Overall survival with osimertinib in untreated, EGFR-mutated advanced NSCLC. *N Engl J Med*. (2020) 382:41–50. doi: 10.1056/NEJMoa1913662

6. Ballard P, Yates JW, Yang Z, Kim DW, Yang JC, Cantarini M, et al. Preclinical comparison of osimertinib with other EGFR-TKIs in EGFR-mutant NSCLC brain metastases models, and early evidence of clinical brain metastases activity. *Clin Cancer Res*. (2016) 22:5130–40. doi: 10.1158/1078-0432.CCR-16-0399

7. Ahn MJ, Chiu CH, Cheng Y, Han JY, Goldberg SB, Greystoke A, et al. Osimertinib for patients with leptomeningeal metastases associated with EGFR T790M-positive advanced NSCLC: the AURA leptomeningeal metastases analysis. *J Thorac Oncol*. (2020) 15:637–48. doi: 10.1016/j.jtho.2019.12.113

8. Sandler A, Gray R, Perry MC, Brahmer J, Schiller JH, Dowlati A, et al. Paclitaxel-carboplatin alone or with bevacizumab for non-small-cell lung cancer. *N Engl J Med*. (2006) 355:2542–50. doi: 10.1056/NEJMoa061884

9. Seto T, Kato T, Nishio M, Goto K, Atagi S, Hosomi Y, et al. Erlotinib alone or with bevacizumab as first-line therapy in patients with advanced non-squamous non-small-cell lung cancer harbouring EGFR mutations (JO25567): an open-label, randomised, multicentre, phase 2 study. *Lancet Oncol*. (2014) 15:1236–44. doi: 10.1016/S1470-2045(14)70381-X

10. Saito H, Fukuhara T, Furuya N, Watanabe K, Sugawara S, Iwasawa S, et al. Erlotinib plus bevacizumab versus erlotinib alone in patients with EGFR-positive advanced non-squamous non-small-cell lung cancer (NEJ026): interim analysis of an open-label, randomised, multicentre, phase 3 trial. *Lancet Oncol*. (2019) 20:625–35. doi: 10.1016/S1470-2045(19)30035-X

11. Zhou Q, Xu CR, Cheng Y, Liu YP, Chen GY, Cui JW, et al. Bevacizumab plus erlotinib in Chinese patients with untreated, EGFR-mutated, advanced NSCLC (ARTEMIS-CTONG1509): A multicenter phase 3 study. *Cancer Cell*. (2021) 39:1279–1291.e1273. doi: 10.1016/j.ccell.2021.07.005

12. Lu S, Dong X, Jian H, Chen J, Chen G, Sun Y, et al. AENEAS: A randomized phase III trial of aumolertinib versus gefitinib as first-line therapy for locally advanced or metastaticNon-small-cell lung cancer with EGFR exon 19 deletion or L858R mutations. *J Clin Oncol*. (2022) 40:3162–71. doi: 10.1200/JCO.21.02641

13. Lu S, Wang Q, Zhang G, Dong X, Yang CT, Song Y, et al. Efficacy of aumolertinib (HS-10296) in patients with advanced EGFR T790M+ NSCLC: updated post-national medical products administration approval results from the APOLLO registrational trial. *J Thorac Oncol*. (2022) 17:411–22. doi: 10.1016/j.jtho.2021.10.024

14. Yu HA, Schoenfeld AJ, Makhnin A, Kim R, Rizvi H, Tsui D, et al. Effect of osimertinib and bevacizumab on progression-free survival for patients with metastatic EGFR-mutant lung cancers: A phase 1/2 single-group open-label trial. *JAMA Oncol*. (2020) 6:1048–54. doi: 10.1001/jamaoncol.2020.1260

15. Kenmotsu H, Wakuda K, Mori K, Kato T, Sugawara S, Kirita K, et al. Randomized phase 2 study of osimertinib plus bevacizumab versus osimertinib for untreated patients with nonsquamous NSCLC harboring EGFR mutations: WJOG9717L study. *J Thorac Oncol*. (2022) 17:1098–108. doi: 10.1016/j.jtho.2022.05.006

16. Ichihara E, Hotta K, Nogami N, Kuyama S, Kishino D, Fujii M, et al. Phase II trial of gefitinib in combination with bevacizumab as first-line therapy for advanced non-small cell lung cancer with activating EGFR gene mutations: the Okayama Lung Cancer Study Group Trial 1001. *J Thorac Oncol*. (2015) 10:486–91. doi: 10.1097/JTO.0000000000000434

17. Nakagawa K, Garon EB, Seto T, Nishio M, Ponce Aix S, Paz-Ares L, et al. Ramucirumab plus erlotinib in patients with untreated, EGFR-mutated, advanced non-small-cell lung cancer (RELAY): a randomised, double-blind, placebo-controlled, phase 3 trial. *Lancet Oncol*. (2019) 20:1655–69. doi: 10.1016/S1470-2045(19)30634-5

18. Shi Y, Chen G, Wang X, Liu Y, Wu L, Hao Y, et al. Furmonertinib (AST2818) versus gefitinib as first-line therapy for Chinese patients with locally advanced or metastatic EGFR mutation-positive non-small-cell lung cancer (FURLONG): a multicentre, double-blind, randomised phase 3 study. *Lancet Respir Med*. (2022) 10:1019–28. doi: 10.1016/S2213-2600(22)00168-0

19. Shun Lu JZ, Jian H, Wu L, Chen Y, Fan Y, Fang J, et al. Befotertinib (D-0316) versus icotinib as first-line therapy for patients with EGFR-mutated locally advanced or metastatic non-small cell lung cancer: A multicentre, open-label, randomized phase III study. *ESMO ASIA*. (2022) 11:905-15.

20. Cho BC, Ahn MJ, Kang JH, Soo RA, Reungwetwattana T, Yang JC, et al. A randomized, double-blind, multinational phase III study to assess the efficacy and safety of lazertinib versus gefitinib in the first-line treatment of patients with EGFR mutation (EGFRm), advanced NSCLC. *ESMO ASIA*. (2022) 20:4208-17. doi: 10.1200/JCO.23.00515

21. Schuler M, Wu YL, Hirsh V, O'Byrne K, Yamamoto N, Mok T, et al. First-line afatinib versus chemotherapy in patients with non-small cell lung cancer and common epidermal growth factor receptor gene mutations and brain metastases. *J Thorac Oncol*. (2016) 11:380–90. doi: 10.1016/j.jtho.2015.11.014

22. Besse B, Le Moulec S, Mazieres J, Senellart H, Barlesi F, Chouaid C, et al. Bevacizumab in patients with nonsquamous non-small cell lung cancer and asymptomatic, untreated brain metastases (BRAIN): A nonrandomized, phase II study. *Clin Cancer Res*. (2015) 21:1896–903. doi: 10.1158/1078-0432.CCR-14-2082

23. Chikaishi Y, Kanayama M, Taira A, Nabe Y, Shinohara S, Kuwata T, et al. Effect of erlotinib plus bevacizumab on brain metastases in patients with non-small cell lung cancer. *Ann Transl Med*. (2018) 6:401. doi: 10.21037/atm.2018.09.33

24. Reungwetwattana T, Nakagawa K, Cho BC, Cobo M, Cho EK, Bertolini A, et al. CNS response to osimertinib versus standard epidermal growth factor receptor tyrosine kinase inhibitors in patients with untreated EGFR-mutated advanced non-small-cell lung cancer. *J Clin Oncol*. (2018) 36:JCO2018783118. doi: 10.1200/JCO.2018.78.3118

25. Wu YL, Ahn MJ, Garassino MC, Han JY, Katakami N, Kim HR, et al. CNS efficacy of osimertinib in patients with T790M-positive advanced non-small-cell lung cancer: data from a randomized phase III trial (AURA3). *J Clin Oncol*. (2018) 36:2702–9. doi: 10.1200/JCO.2018.77.9363

26. Yu HA, Arcila ME, Hellmann MD, Kris MG, Ladanyi M, Riely GJ. Poor response to erlotinib in patients with tumors containing baseline EGFR T790M mutations found by routine clinical molecular testing. *Ann Oncol*. (2014) 25:423–8. doi: 10.1093/annonc/mdt573

27. Ding D, Yu Y, Li Z, Niu X, Lu S. The predictive role of pretreatment epidermal growth factor receptor T790M mutation on the progression-free survival of tyrosine-kinase inhibitor-treated non-small cell lung cancer patients: a meta-analysis. *Onco Targets Ther*. (2014) 7:387–93. doi: 10.2147/OTT.S58870

28. Liu Y, Sun L, Xiong ZC, Sun X, Zhang SL, Ma JT, et al. Meta-analysis of the impact of *de novo* and acquired EGFR T790M mutations on the prognosis of patients with non-small cell lung cancer receiving EGFR-TKIs. *Onco Targets Ther*. (2017) 10:2267–79. doi: 10.2147/OTT.S133082

29. Costa C, Molina MA, Drozdowskyj A, Gimenez-Capitan A, Bertran-Alamillo J, Karachaliou N, et al. The impact of EGFR T790M mutations and BIM mRNA expression on outcome in patients with EGFR-mutant NSCLC treated with erlotinib or chemotherapy in the randomized phase III EURTAC trial. *Clin Cancer Res*. (2014) 20:2001–10. doi: 10.1158/1078-0432.CCR-13-2233

30. Yang JC, Schuler M, Popat S, Miura S, Heeke S, Park K, et al. Afatinib for the treatment of NSCLC harboring uncommon EGFR mutations: A database of 693 cases. *J Thorac Oncol*. (2020) 15:803–15. doi: 10.1016/j.jtho.2019.12.126

31. Yang JC, Schuler M, Popat S, Miura S, Park K, Passaro A, et al. Afatinib for the treatment of non-small cell lung cancer harboring uncommon EGFR mutations: an updated database of 1023 cases brief report. *Front Oncol*. (2022) 12:834704. doi: 10.3389/fonc.2022.834704

32. Wang S, Yan B, Zhang Y, Xu J, Qiao R, Dong Y, et al. Different characteristics and survival in non-small cell lung cancer patients with primary and acquired EGFR T790M mutation. *Int J Cancer*. (2019) 144:2880–6. doi: 10.1002/ijc.v144.11

33. Zhang B, Xu J, Zhang X, Gu P, Wang H, Wang S, et al. Coexistence of sensitive and resistant epidermal growth factor receptor (EGFR) mutations in pretreatment non-small cell lung cancer (NSCLC) patients: First or third generation tyrosine kinase inhibitors (TKIs)? *Lung Cancer*. (2018) 117:27–31. doi: 10.1016/j.lungcan.2018.01.006

34. Si J, Gu X, Wang W, Ying S, Song Z. Clinical outcomes of lung adenocarcinoma patients harboring uncommon epidermal growth factor receptor (EGFR) mutations treated with EGFR-tyrosine kinase inhibitors (TKIs). *Ann Palliat Med*. (2022) 11:1624–34. doi: 10.21037/apm-21-2828

35. Zeng Y, Guo T, Zhou Y, Zhao Y, Chu L, Chu X, et al. Clinical outcomes of advanced non-small cell lung cancer patients harboring distinct subtypes of EGFR mutations and receiving first-line tyrosine kinase inhibitors: brain metastasis and. *novo T790M matters. BMC Cancer*. (2022) 22:198. doi: 10.1186/s12885-022-09245-5

36. Chang JW, Huang CY, Fang YF, Chang CF, Yang CT, Kuo CS, et al. Epidermal growth factor receptor tyrosine kinase inhibitors for *de novo* T790M mutation: A retrospective study of 44 patients. *Thorac Cancer*. (2022) 13:1888–97. doi: 10.1111/1759-7714.14272

37. Panda GS, Noronha V, Shah D, John G, Chougule A, Patil V, et al. Treatment pattern and outcomes in *de novo* T790M-mutated non-small cell lung cancer. *Ecancermedicalscience*. (2022) 16:1385. doi: 10.3332/ecancer.2022.1385

frontiers | Frontiers in Oncology

TYPE Review
PUBLISHED 22 July 2025
DOI 10.3389/fonc.2025.1582738

OPEN ACCESS

EDITED BY
Shiv K. Gupta,
Mayo Clinic, United States

REVIEWED BY
Sonia Jain,
Mayo Clinic, United States
Sara Small,
Fox Chase Cancer Center, United States

*CORRESPONDENCE
Li Zhuang
zl777120191118@163.com

†These authors share first authorship

RECEIVED 24 February 2025
ACCEPTED 07 July 2025
PUBLISHED 22 July 2025

CITATION
Zhou K, Li Y, Wang W, Chen Y, Qian B, Liang Y, Li H, Xu R and Zhuang L (2025) SLFN11: a pan-cancer biomarker for DNA-targeted drugs sensitivity and therapeutic strategy guidance.
Front. Oncol. 15:1582738.
doi: 10.3389/fonc.2025.1582738

SLFN11: a pan-cancer biomarker for DNA-targeted drugs sensitivity and therapeutic strategy guidance

Kunzhong Zhou†, Yuewen Li†, Weifang Wang, Yilin Chen, Bingyan Qian, Yiteng Liang, Hongmei Li, Ruiting Xu and Li Zhuang*

Department of Rehabilitation and Palliative Medicine, The Third Affiliated Hospital of Kunming Medical University, Kunming, China

Therapeutic responses to identical chemotherapy regimens often vary significantly among patients with the same type of cancer, underscoring the need for additional biomarkers to identify individuals most likely to benefit from specific treatments. The expression of SLFN11 (Schlafen11) has been identified as a potential biomarker for predicting patient responses to DNA-damaging agents and PARP inhibitors, as it irreversibly blocks DNA replication under replication stress, thereby increasing the sensitivity of cancer cells to various DNA-damaging agents and PARP inhibitors. Preclinical and clinical trial data suggest that SLFN11 can predict therapeutic responses to multiple DNA- targeted drugs, including platinum-based agents, topoisomerase I/II inhibitors, DNA synthesis inhibitors, and PARP inhibitors. Leveraging the expression status of SLFN11 or modulating its expression offers exciting possibilities for clinical applications. In this review, we summarize the structure and function of SLFN11, as well as its progress as a biomarker across various cancer types. We also review the regulation of SLFN11 expression, its dynamic expression patterns, and potential strategies for combination therapies to enhance efficacy based on SLFN11 status. Furthermore, we discuss the potential of SLFN11 expression status in overcoming resistance to DNA-damaging drugs, optimizing treatment strategies, and advancing precision cancer therapy.

KEYWORDS

Schlafen11 (SLFN11), DNA damaging agents, PARP inhibitors, pan-cancer, DNA damage repair mechanisms, epigenetics, biomarkers

1 Introduction

Cancer continues to face challenges such as recurrence, drug side effects, drug resistance, and individual variations in treatment efficacy (1). The economic burden of 29 types of cancer across 204 countries and regions is projected to reach $25.2 trillion from 2020 to 2050 (2). The six hallmarks of cancer include sustaining proliferative signaling,

evading growth suppressors, resisting cell death, enabling replicative immortality, inducing angiogenesis, and activating invasion and metastasis, all of which are underpinned by genomic instability (3). For decades, chemotherapy and radiation therapy have been the cornerstones of cancer treatment, but sensitivities vary in unselected patients. Recently, more and more studies have found that the expression status of SLFN11 is associated with the chemotherapy sensitivity of tumor patients. These therapeutic drugs include platinum, topoisomerase I/II inhibitors, DNA damaging agents, and PARP inhibitors, which we collectively refer to as DNA-targeted drugs in this article. Small molecule inhibitors targeting the DNA damage response (DDR) have garnered significant interest. A prime example is PARP inhibitors, particularly in ovarian cancer with BRCA1/2 mutations, which are the most common cause of homologous recombination repair deficiency (HRD). Since these cells rely on PARP1/2 for single-strand repair, the use of PARPi leads to a "synthetic lethality" effect. In addition to BRCA gene mutations predicting the efficacy of PARP inhibitors, SLFN11 can also predict the therapeutic sensitivity of PARP inhibitors. SLFN11 has been recognized as a biomarker predictive of response to various DNA-damaging agents and PARPi across multiple cancer types, including gastric cancer (4), esophageal cancer (5), small cell lung cancer (6–9), breast cancer (10), ovarian cancer (11, 12), prostate cancer (13), Ewing sarcoma (14), glioblastoma (15), head and neck cancer (16), colorectal cancer (17, 18), clear cell renal cell carcinoma (19) and hepatocellular carcinoma (20). These findings provide a foundation for the clinical application of SLFN11 as a biomarker. In this article, we review the structure and function of SLFN11. We also review the progress in research on SLFN11 as a biomarker in various cancers, with a focus on SCLC. Additionally, we review the regulation and dynamic changes of SLFN11 expression and potential strategies for combination therapy based on its expression status. Finally, we discuss the potential of SLFN11 in overcoming drug resistance, optimizing treatment strategies, and advancing precision cancer therapy.

2 The structure and function of SLFN11

The SLFN gene family was first described in 1998 as a growth-regulating gene family influencing thymocyte development (21). The murine SLFN family comprises 10 members (SLFN1, 1L, 2, 3, 4, 5, 8, 9, 10, and 14), while the human SLFN family consists of 6 members (SLFN5, 11, 12, 12L, 13, and 14) (22). All human SLFN genes contain an SLFN box, a domain not found in other proteins, whose specific function remains to be elucidated. Except for the lack of a helicase domain in SLFN12, the remaining human SLFN proteins contain a helicase domain at the C - terminus (11).

Over the past decade, SLFN11 has been extensively studied for its relevance to cancer therapy. The SLFN11 gene is located on human chromosome 17 and encodes a protein consisting of 901 amino acid residues containing three major domains (11, 23): an N-terminal endonuclease domain (residues 1–353), an intermediate linker domain (residues 354–576), and a C-terminal domain (residues 577–901). The N-terminal domain is the critical domain of SLFN11, possessing endoribonuclease activity (22). Under DNA damage induction, SLFN11 mediates the cleavage of type II tRNAs (notably tRNA-Leu-TAA) through its N-terminal endoribonuclease activity, targeting their long variable loops. This degradation selectively disrupts the translation of DNA damage response and repair genes such as ATR and ATM, whose transcripts are enriched in TTA codons (Leu) that depend on the low-abundance tRNA-Leu-TAA for efficient protein synthesis (24). ATR (Ataxia Telangiectasia and Rad3-related) and ATM (Ataxia Telangiectasia Mutated) protein kinases are members of the phosphatidylinositol 3-kinase (PI3K)-related kinase (PIKK) protein family and play a key role in DNA damage response (25). ATR is mainly involved in the response to replication stress and maintaining replication fork stability. ATM is mainly involved in DNA double-strand break repair, regulating cell cycle checkpoints, and promoting homologous recombination (HR) repair. In response to DNA damage, it inhibits protein translation by degrading specific tRNAs, promoting the sensitivity of cancer cells to DNA-damaging agents (22). Studies have shown that mouse Slfn8 and Slfn9 may partially compensate for the function of human SLFN11 (26), but phylogenetic and sequence alignment analysis showed that mouse SLFN8/9/10 are orthologous genes of human SLFN13 rather than SLFN11 (27). Studies have determined the crystal structure and function of the Sus scrofa (wild boar) SLFN11 N-terminal domain (NTD). sSLFN11-NTD is a clamp molecule and an efficient RNase that cleaves type I and II tRNA and rRNA, and preferentially cleaves type II tRNA (27). Cryo-EM structures reveal that SLFN11 interacts with tRNA through the positively charged groove formed by the N-terminal nuclease domain of its dimer. The structure captured the binding state of SLFN11 with tRNA-Leu (type II) and tRNA-Met (type I) and confirmed that both tRNAs were cleaved at specific sites 10 nucleotides away from the 3' end (positions 76–77 for tRNA-Leu, positions 65–66 for tRNA-Met) (28). The phosphorylation sites S219 and T230 located in the N-terminal nuclease domain regulate tRNA recognition and ribonuclease activity. After phosphorylation, the negative charge repels the tRNA phosphate backbone, weakening the tRNA binding ability and resulting in a significant reduction in nuclease activity (28). The intermediate connecting domain of SLFN11 contains a conserved SWAVDL sequence, which is present in all SLFN family members (22). The C-terminal domain is homologous to superfamily I RNA/DNA helicases and contains a conserved Walker A/B motif (ATPase active site). Structural simulations show similarity to Dna2 helicase, suggesting involvement in chromatin remodeling (23, 29). Helicase activity is required for SLFN11-mediated chemosensitivity to DNA-damaging agents and replication fork degradation (30). The phosphorylation site S753 located in the C-terminal helicase domain acts as a conformational switch to regulate SLFN11 dimerization and nucleic acid binding ability. SLFN11 switches between monomer and dimer conformations through the phosphorylation state of S753. S753 phosphorylation induces a 140° rotation of the C-terminal helicase domain, destroying the ID helix and hydrophobic interactions to form a

monomer conformation. S753 dephosphorylation is a key trigger for dimerization. Protein phosphatase 1 catalytic subunit γ (PPP1CC)-mediated S753 dephosphorylation relieves conformational inhibition and promotes dimer formation. The monomeric SLFN11 has the following characteristics: no DNA binding, weakened nuclease activity, binding to ATP but no hydrolysis, and maintaining a "closed" state. The dimeric SLFN11 has the following characteristics: binding to ssDNA/tRNA, high cleavage activity, and performing replication fork arrest and translation regulation (28). S753 phosphorylation acts as a "safety lock" to inhibit SLFN11 activity under non-stress conditions, preventing abnormal replication fork blockage or excessive tRNA cleavage. When DNA is damaged, PPP1CC-mediated S753 dephosphorylation can activate SLFN11 dimerization, enabling it to coordinate the execution of replication fork blockage and tRNA cleavage functions. Dimerization underlies SLFN11-dependent chemosensitivity. In addition, studies have found that the single-stranded DNA (ssDNA) binding site K652 in the SLFN11 protein is a direct binding site for ssDNA (31). K652 (lysine) is positively charged and can form electrostatic interactions with negatively charged ssDNA. When K652 mutates to negatively charged glutamic acid (K652E) or aspartic acid (K652D), SLFN11 loses its ssDNA binding ability and cannot be recruited to chromatin, losing its replication blocking function and completely losing its drug sensitivity. S753 dephosphorylation may change the protein conformation, expose the K652 site or optimize its interaction with ssDNA.

SLFN11 is recruited to DNA damage sites through direct binding with RPA, promoting the destabilization of the RPA-ssDNA complex, thereby inhibiting checkpoint maintenance and homologous recombination repair (23, 32). SLFN11 promotes the degradation of CDT1 in response to CPT by binding to DDB1 of $CUL4^{CDT2}$ E3 ubiquitin ligase associated with replication forks, which irreversibly blocks replication and induces cell death (33). The SLFN11 protein enhances chromatin accessibility across the genome, particularly in response to replication stress induced by DNA-targeting drugs, with this increase being most pronounced in active gene promoter regions (34). Additionally, it responds to replication stress by regulating immediate early genes (such as JUN, FOS) and cell cycle arrest genes (such as CDKN1A), with this function of SLFN11 dependent on its ATPase and C-terminal helicase activities. In response to replication stress induced by camptothecin or the CHK1 inhibitor Prexasertib, SLFN11 is recruited to stressed replication forks, blocking replication by altering chromatin structure (30). In immune responses, the expression of SLFN11 enhances the effect of the IFNγ signaling pathway, making tumor cells more sensitive to cytotoxic T cells (35).

3 The significance of SLFN11 in various cancers

SLFN11 is a very important and widely recognized biomarker for predicting sensitivity to multiple DNA-targeted drugs. People have made great progress in this area. In this review, we summarized the role, mechanism and clinical significance of SLFN11 in gastric cancer, esophageal cancer, small cell lung cancer, breast cancer, ovarian cancer, prostate cancer, Ewing's sarcoma, glioblastoma, head and neck cancer, colorectal cancer, renal cancer, hepatocellular carcinoma and other cancers (Tables 1, 2).

3.1 Gastric cancer

SLFN11 plays a complex role in gastric cancer. Its expression is epigenetically regulated (promoter region methylation), and high expression (especially protein level) is associated with better survival prognosis and is a powerful biomarker for predicting sensitivity to platinum-based chemotherapy. SLFN11 inhibits tumor growth and significantly enhances the efficacy of platinum drugs by promoting S phase arrest and apoptosis. At the same time, SLFN11 is deeply involved in the regulation of the tumor immune microenvironment and is positively correlated with the infiltration of multiple immune cells and the expression of immune checkpoint molecules, suggesting its potential immune regulatory function.

The TCGA database showed that the mRNA expression of SLFN11 in gastric cancer (STAD) was significantly higher than that in normal tissues. Analysis of the UALCAN database showed the mRNA level of SLFN11 was significantly positively correlated with lymph node metastasis, tumor stage and grade (43). The Kaplan-Meier Plotter showed that high expression of SLFN11 was not significantly correlated with patients' overall survival (OS), and could not be used as a prognostic marker alone (unlike SLFN5/SLFN13) (43). However, a retrospective study evaluated the expression of SLFN11 in tumor cells using immunohistochemistry, and when >30% of tumor cells were stained, it was considered SLFN11 immunostaining positive. They used the median to divide patients into high SLFN11 group and low SLFN11 group. Kaplan-Meier analysis showed that the 5-year overall survival rates of 169 gastric cancer patients were 63% and 40% in the high SLFN11 group and the low SLFN11 group, respectively. The overall survival rate of the high SLFN11 group was significantly higher than that of the low SLFN11 group (HR, 0.5; 95% CI, 0.32-0.77; P = 0.0017). This difference was even more pronounced when analyzing patients who received either oxaliplatin or cisplatin(HR, 0.2; 95% CI, 0.06–0.51; $P = 0.0009$) (44). High expression of SLFN11 can be used as a predictive biomarker for gastric cancer patients receiving platinum-based chemotherapy (44).

GSEA functional enrichment analysis showed that SLFN11 was mainly involved in adaptive immune response and immune regulation (43). KEGG pathway analysis showed that SLFN11 was associated with inflammatory diseases (such as hepatitis, Epstein-Barr virus infection) and NF-κB signaling pathway (43). TIMER/TCGA database analysis showed that SLFN11 expression was positively correlated with the infiltration level of multiple immune cells, including $CD8^+$ T cells, $CD4^+$ T cells, macrophages (main associated cells), dendritic cells (DCs) (main associated cells), and neutrophils (43). TISIDB database shows that SLFN11 is positively correlated with NK cell, Th17 cell, and

TABLE 1 Studies that evaluated SLFN11 as a prognostic or predictive biomarker in cancer patients.

Evidence level	Type of cancer	n of patients	Drugs	Conclusions	Ref.
Retrospective study	Esophageal Squamous Cell Carcinoma	73	low-dose nedaplatin + 5-fluorouracil with concurrent radiation	Tumors with high SLFN11 H-score(≥ 51) were associated with longer PFI (p = 0.013).	(36)
Prospective Phase II study	Recurrent small cell lung cancer	104	Temozolomide +veliparib or placebo	Temozolomide + veliparib elicited longer PFS (5.7 v 3.6 months; p = 0.009) and OS (12.2 v 7.5 months; p = 0.014) in patients with SLFN11+ tumors vs. SLFN11- tumors(H score cutoff ≥1 defined SLFN11 positive).	(37)
Prospective I/ II-phase study	Recurrent small cell lung cancer	21	valemetostat (DS-3201b) combination with irinotecan	Combination EZH1/2 inhibitor valemetostat and irinotecan was not tolerated but demonstrated efficacy in recurrent SCLC	(38)
Prospective Phase II study	SLFN11-positive ES-SCLC	106	atezolizumab (A) versus atezolizumab plus talazoparib (AT)	PFS was improved with AT versus A (2.9 v 2.4 months; p = 0.019); OS was not different between groups (p = 0.47).	(39)
Observational study	Non-small cell lung cancer	22	Platinum-based chemotherapy	SLFN11 promoter methylation was associated with poor PFS (p = 0.031).	(6)
Observational study	Breast Cancer	32	chemotherapy (Not specified)	High SLFN11 mRNA levels were associated with better OS (p = 0.017).	(10)
Retrospective study	high-grade serous ovarian cancer	27	platinum-based chemotherapy	Tumors with high SLFN11 H-score("high" if H-score > 60) were associated with longer PFI (p = 0.004).	(12)
Retrospective study	Ovarian Cancer	110	Cisplatin-based chemotherapy	High SLFN11 mRNA levels were associated with better OS (p = 0.016).	(40)
Observational study	Ovarian Cancer	41	Cisplatin or carboplatin	SLFN11 promoter rmethylation was associated with shorter (OS) (p = 0.006) and PFS (p = 0.003).	(6)
Retrospective study	Castration-Resistant Prostate Cancer	20	platinum-based chemotherapy	Longer rPFS was associated with SLFN11+ CTCs compared to those without (6.0 versus 2.2 months, p=0.002)	(41)
Retrospective study	Ewing Sarcoma	44	Not specified	Tumors with high SLFN11 mRNA levels were associated with longer RFS (p = 0.0046).	(14)
Retrospective study	Head and Neck Squamous Cell Carcinoma	161	Platinum (cisplatin or carboplatin)-based chemoradiotherapy	Tumors with SLFN11-positive(SLFN11 positive staining was defined as ≥15% staining of the tumor nuclei) were associated with longer PFS p < 0.001).	(16)
Retrospective study	Colorectal Cancer	128	Not specified	SLFN11 promoter methylation was prognostic of poor 5-year OS and 5-year RFS (p<0.05).	(40)
Retrospective study	Colorectal Cancer with KRAS exon 2 wild type	153	Adjuvant oxaliplatin-based chemotherapy	Tumors with high SLFN11 expression score(>4.5) were associated with longer OS (p = 0.048).	(18)
Retrospective study	Hepatocellular Carcinoma	182	Underwent curative hepatectomy	Tumors with high SLFN11(moderate or strong H-score) were associated with longer OS andRFS (p < 0.001).	(20)
Retrospective study	Bladder Cancer	50	Platinum-based chemotherapy	Tumors with SLFN11-positive (SLFN11 was considered positive when at least 5% of the tumor cells were stained)were associated with longer OS p < 0.012).	(42)

Treg cell infiltration (43). SLFN11 expression was significantly positively correlated with multiple immune checkpoint molecules, including CD160, CD244, CD247, CTLA4, LAG3, PDCD1, PDCD1LG2, TIGIT, and HAVCR2 (43).

At the epigenetic level, SLFN11 is frequently methylated in gastric cancer and its expression is regulated by promoter region methylation (4). Compared to normal gastric mucosal tissues, SLFN11 gene methylation is more prevalent in gastric cancer tissues, and the methylation rate of SLFN11 was significantly higher in tumors with a diameter ≥5 cm than in tumors with a diameter <5 cm. The use of the demethylating agent 5-AZA can restore SLFN11 expression (4). Restoring SLFN11 expression significantly inhibits the proliferative capacity of gastric cancer cells (such as SNU16 and MGC803). Studies using a mouse xenograft model have shown that the re-expression of SLFN11 significantly reduces tumor weight and volume. SLFN11 can enhance the sensitivity of gastric cancer cells to cisplatin by promoting cisplatin-induced S-phase arrest and apoptosis (4).

10.3389/fonc.2025.1582738

TABLE 2 Summary of the roles, mechanisms and the clinical significance of SLFN11 in different cancer types.

Cancer types	Expression characteristics of SLFN11	Functional mechanism	Clinical significance
Gastric cancer	High expression in tumor tissues	Promote cisplatin-induced S-phase arrest and apoptosis. The expression of SLFN11 is regulated by the methylation of the promoter region.	High expression is associated with the improvement of PFS. Methylation silencing leads to chemotherapy resistance.
Esophageal squamous cell carcinoma	Patients with high expression who receive chemotherapy/radiotherapy have a better prognosis(regulated by promoter methylation)	Inhibition of the ATM pathway enhances sensitivity to radiotherapy/chemotherapy. Methylation silencing is associated with poor tumor differentiation.	High expression is associated with the improvement of OS. Patients with SLFN11 deletion may be sensitive to ATM inhibitors (AZD0156).
Small cell lung cancer	High expression is associated with sensitivity to PARP inhibitors.	EZH2-mediated H3K27me3 deposition leads to downregulation of expression.	High expression is associated with the improvement of PFS/OS. Patients with SLFN11 positivity are sensitive to PARP inhibitors. EZH2 inhibitors can restore expression and overcome chemotherapy resistance.
Breast cancer	Patients with high expression who receive chemotherapy have a better prognosis.	–	High expression is associated with the improvement of OS. ATR inhibitors can reverse the drug resistance caused by low SLFN11 expression.
Ovarian cancer	Patients with high expression who receive chemotherapy have a better prognosis	–	High expression is associated with the improvement of OS. The expression status of SLFN11 can predict the efficacy of platinum-based drugs and PARP inhibitors.
Castration-resistant Prostate cancer	Patients with high expression levels have a better response to platinum-based chemotherapy.	–	High expression is associated with the improvement of radiographic progression-free survival (rPFS). The expression status of SLFN11 can predict the efficacy of platinum-based drugs.
Ewing Sarcoma	EWS-FLI1 transcriptional target genes, High expression in tumor cell	Impede replication repair and enhance the sensitivity to DNA - damaging drugs. Activate the AP-1 pathway to inhibit the oncogene c - Myc.	High expression is associated with the improvement of RFS, Patients with high expression of SLFN11 respond better to the combination of PARP inhibitors and topoisomerase inhibitors (such as SN - 38).
Glioblastoma	High expression promotes tumor progression.	Negatively regulate the NF-κB pathway and inhibit the expression of p21.	High expression is associated with the improvement of OS. SLFN11 deficiency inhibits tumor growth.
Head and Neck Squamous Cell Carcinoma	High expression of SLFN11 is associated with a longer PFS.	–	Patients with high expression of SLFN11 respond better to cisplatin-based chemoradiotherapy (CRT).
Clear Cell Renal Cell Carcinoma	High expression is associated with poor OS.	SLFN11 promotes the phosphorylation of the PI3K/AKT signaling pathway. SLFN11 is highly expressed in ccRCC tissues and cell lines, and is associated with a decreased methylation level.	Overexpression of SLFN11 is an independent prognostic factor for clear cell renal cell carcinoma.
Colorectal cancer	In patients receiving oxaliplatin adjuvant chemotherapy, high expression of SLFN11 is associated with a favorable prognosis in patients with wild - type KRAS exon 2.	Methylation leads to low expression. May interact with the KRAS mutation status.	Patients with high expression of SLFN11 and wild-type KRAS have a better prognosis after adjuvant oxaliplatin chemotherapy.
Hepatocellular carcinoma	Low expression is associated with poor prognosis.	Inhibiting the mTOR pathway through RPS4X. Regulating the TRIM21-RBM10 axis to enhance the response to immune checkpoint inhibitors (ICI)	Combination of CCL2/CCR2 inhibitors and PD - 1 inhibitors can improve the therapeutic efficacy in patients with low SLFN11 expression.
Leukemic cell lines	–	SLFN11 expression is regulated via the JAK, AKT and ERK, and ETS axis	–
Mesothelioma cell lines	–	–	The response of mesothelioma cells to PARP inhibitors is associated with high SLFN11 expression. When used in combination with temozolomide, it can increase the sensitivity of cells with low or no MGMT expression.

3.2 Esophageal cancer

SLFN11 is a key biomarker for the efficacy of chemoradiotherapy in ESCC. Its high expression improves platinum and radiotherapy sensitivity by regulating the DNA damage repair pathway (inhibiting ATM and activating ATR/NHEJ), and is dynamically regulated by epigenetic methylation. Targeting the ATM pathway in SLFN11-deficient tumors (such as AZD0156) has therapeutic potential.

In ESCC patients with definitive chemoradiotherapy (dCRT), those with high expression of SLFN11(H-score ≥ 51 was defined as high SLFN11 expression) exhibited significantly better prognosis ($p = 0.013$), particularly notable in stage II and III patients ($p = 0.004$) (36). This prognostic improvement is primarily attributed to the heightened sensitivity of SLFN11-high tumors to nedaplatin and radiotherapy, rather than to 5-fluorouracil (36). Using a low-dose cisplatin-induced DNA damage model, we found that SLFN11 was able to activate non-homologous end joining and ATR/CHK1 signaling pathways, while inhibiting the ATM/CHK2 signaling pathway (5). Loss of SLFN11 promotes tumor cell proliferation by restoring ATM expression (5). Studies have shown that SLFN11-deficient ESCC cells are highly sensitive to the ATM inhibitor AZD0156.

At the epigenetic level, the expression of SLFN11 is regulated by promoter methylation, which is significantly associated with tumor differentiation and tumor size (5). There was a negative correlation between SLFN11 mRNA levels and methylation of CpG sites around the transcription start site (cg13341380, cg18108623, cg05224998, cg18608369, cg01348733, cg14380270, cg26573518, and cg05504685, all $P < 0.05$) (5). Cell experiments showed that high expression of SLFN11 can enhance the sensitivity of ESCC cells to cisplatin (5). In KYSE30 and KYSE450 cell lines, after restoring SLFN11 expression, the expression of ATM was significantly inhibited.

3.3 Small cell lung cancer

Small cell lung cancer (SCLC) is a highly aggressive malignancy characterized by rapid progression and early metastasis. Although initial responses to platinum-based chemotherapy combined with etoposide are often favorable, the majority of patients relapse due to the rapid development of drug resistance, highlighting an urgent need for predictive biomarkers and more effective targeted therapies.

Recent molecular profiling has stratified SCLC into four distinct subtypes—SCLC-A, SCLC-N, SCLC-P, and SCLC-I—based on the expression of lineage-defining transcription factors ASCL1, NEUROD1, and POU2F3 (45). While SCLC-A and SCLC-N exhibit neuroendocrine features, SCLC-P and SCLC-I display non-neuroendocrine characteristics. Importantly, each subtype exhibits differential therapeutic responses: SCLC-I responds well to immunotherapy (particularly when combined with chemotherapy) due to its high expression of inflammation-related and immune checkpoint genes; SCLC-P shows particular sensitivity to PARP inhibitors; SCLC-N demonstrates good response to Aurora kinase inhibitors; and SCLC-A exhibits sensitivity to BCL-2 inhibitors. Notably, high expression of SLFN11 in the SCLC-A subtype is associated with sensitivity to PARP inhibitors, while the SCLC-P subtype remains sensitive to PARP inhibitors even in the absence of high SLFN11 expression or low ATM expression. POU2F3 expression, similar to SLFN11 expression, may serve as a predictive biomarker for PARP inhibitor sensitivity (45, 46). In SCLC-A (ASCL1-driven) cell lines, SLFN11 expression showed a bimodal distribution (45): (1) high peak population: SLFN11 was highly expressed and sensitive to cisplatin/PARPi. (2) low peak population: SLFN11 was low expressed and significantly resistant.

SLFN11 has emerged as a pivotal biomarker of response to DNA-damaging agents, particularly PARP inhibitors and platinum compounds. High SLFN11 expression correlates with enhanced drug sensitivity, while low expression confers resistance. This has been consistently validated in: SCLC cell lines, where SLFN11 expression negatively correlates with talazoparib IC50 values (7). PDX models, where SLFN11-high tumors show better responses to talazoparib (8). SCLC xenograft models, showing stronger effects of PARP inhibitors combined with temozolomide in SLFN11-positive tumors (7, 8). Mechanistically, Murai et al. proposed that SLFN11 enhances the activity of PARP inhibitors by inhibiting DNA replication (7), while others suggested that SLFN11 creates a "BRCAness" state by inhibiting homologous recombination repair (RPA-dependent mechanism), making cancer cells sensitive to PARP inhibitors (8, 32). High levels of SLFN11 (protein/mRNA) are the strongest predictors of SCLC sensitivity to PARP inhibitors (e.g., talazoparib, olaparib) and cisplatin, a finding that was validated in PDX models and 51 SCLC cell lines. Notably, SLFN11 protein expression was significantly downregulated in SCLC cells treated with cisplatin or PARP inhibitors (confirmed by western blotting) (9). The combined expression of SLFN11, low ATM expression, and epithelial phenotype (high E-cadherin expression/low EMT score) can optimize the prediction of SCLC treatment response (9). In summary, SLFN11 is a key dynamic regulator of SCLC sensitivity to DNA-damaging drugs, and PARP1 and ETS family transcription factor EHF regulate SLFN11 expression: PARP1 knockdown reduces SLFN11, while EHF is positively correlated with SLFN11 in SCLC and regulates its expression (knockdown of EHF reduces SLFN11). Promoter methylation is also involved in regulation, but demethylation treatment failed to effectively upregulate SLFN11 (9).

Further studies have expanded the potential of SLFN11 in combination therapy. Studies have shown that the downregulation of SLFN11 observed in chemoresistant SCLC patient-derived xenograft (PDX) models can be reversed by targeted epigenetic intervention (47, 48). Mechanism 1: EZH2-mediated trimethylation of histone H3 at lysine 27 (H3K27me3): EZH2, the catalytic subunit of the PRC2 complex, inhibits SLFN11 expression by depositing the repressive histone mark H3K27me3 specifically on the SLFN11 gene body. EZH2 inhibitors effectively reverse this silencing by reducing H3K27me3 levels and restoring SLFN11 expression, thereby resensitizing resistant SCLC models to chemotherapeutic drugs (48). Mechanism 2: Promoter methylation and histone deacetylation: In small cell lung cancer (SCLC) cell lines, SLFN11 expression is often silenced by promoter hypermethylation, which is significantly

negatively correlated with SLFN11 expression (49). The histone deacetylase inhibitor (HDACi) FK228 reactivates SLFN11 expression primarily by increasing activating histone acetylation marks (H3K9Ac, H3K27Ac) at the promoter (47). Notably, this reactivation is associated with a decrease in promoter DNA methylation (47), suggesting that there may be a crosstalk between histone modifications and DNA methylation, although HDACs themselves act on histones rather than directly on DNA. FK228-induced restoration of SLFN11 expression effectively enhances the anticancer efficacy of topotecan (47). The DNA-damaging agent lurbinectedin effectively inhibits the proliferation of human SCLC cell lines, particularly those with high SLFN11 expression, while the combination of ATR inhibitors with lurbinectedin exhibits synergistic effects in SCLC cell lines with low SLFN11 expression (50). The novel ATR inhibitor M1774 has been shown to reverse chemotherapy resistance in SLFN11-deficient cells (51). Clinical sample analysis revealed that the proportion of SLFN11-positive circulating tumor cells is lowest in SCLC patients undergoing platinum-based therapy (52). This implies that SLFN11 expression levels decrease during platinum-based treatment. Dynamic expression of SLFN11 in circulating tumor cells can be used as a liquid biomarker for small cell lung cancer, which can predict patient sensitivity to treatment (52).

Multiple clinical studies have explored the practical application of SLFN11 as a predictive biomarker. In patients with recurrent SCLC, SLFN11-positive tumors(H score cutoff ≥1 defined SLFN11 positive) exhibited better responses to the combination therapy of temozolomide and veliparib, with significantly prolonged PFS and OS (37). Furthermore, following first-line chemotherapy, the maintenance therapy with the PARP inhibitor talazoparib combined with the immune checkpoint inhibitor atezolizumab significantly improved PFS in SLFN11-positive patients, although it did not significantly extend OS (39). The EZH2-SLFN11 pathway is a potentially targetable driver of acquired chemotherapy resistance. A single-arm phase I/II clinical trial reported that the combination of the EZH1/2 inhibitor Valemetostat (DS-3201b) with irinotecan in patients with recurrent small cell lung cancer presented toxicity issues, but some patients showed clinical benefit. No significant correlation was observed between SLFN11/EZH2 expression and SCLC subtype with treatment response (38).

Research on SLFN11 has also extended to non-small cell lung cancer (NSCLC). *In vitro* silencing of SLFN11 gene expression increases resistance to cisplatin and carboplatin in lung cancer cell lines (6). Clinical sample analysis revealed that SLFN11 methylation is associated with shortened PFS and OS in lung adenocarcinoma patients receiving platinum-based chemotherapy (6). NSCLC circulating tumor cell-derived xenograft (CDX) models and cell lines with high SLFN11 protein expression were more sensitive to PARP inhibitors, and CDX models and cell lines with high SLFN11 protein expression exhibited stronger metastatic potential and potential SCLC histological transformation (53).NSCLC cell lines with low SLFN11 expression and high cMYC expression demonstrated higher sensitivity to combined AXL/ATR inhibition therapy (54).

3.4 Breast cancer

The expression status of SLFN11 provides dual value for the precision treatment of breast cancer: on the one hand, it is a powerful biomarker for predicting the patient's response and prognosis to DNA-damaging chemotherapy (including traditional chemotherapy, pyrrolobenzodiazepine (PBD)-conjugated antibody-drug conjugates (ADCs), PARP inhibitors, TOP1 inhibitors, etc.), and can be used to guide treatment selection and patient stratification; on the other hand, for the drug resistance caused by low SLFN11 expression, the combination treatment strategy targeting the DNA damage response pathway (such as ATR, CHK1, WEE1, EZH2) shows significant reversal potential, providing a new direction for overcoming drug resistance.

Survival analysis of clinical samples showed that breast cancer patients with high SLFN11 expression who received chemotherapy (unspecified drug) had a significant OS advantage (10). The expression of SLFN11 is strictly regulated in breast cancer, and its promoter methylation is an important mechanism leading to the downregulation of its mRNA and protein expression (55). In cell line models, upregulation of SLFN11 expression using IFN-γ, the demethylating agent DAC, or CRISPR-UNISAM significantly enhanced the sensitivity of cells to multiple DNA damaging agents, including cisplatin, epirubicin, and olaparib (55). This association was further supported at the patient level and in models: breast cancer patients with high SLFN11 protein expression responded significantly better to standard chemotherapy with DNA damaging agents (DDAs), such as gemcitabine and cisplatin (56). Conversely, knockdown of SLFN11 expression in the MDA-MB-361 cell line resulted in resistance or significant reduction in sensitivity to SG3199 (free pyrrolobenzodiazepine(PBD)) and PBD-antibody drug conjugates (e.g., MEDI0641, trastuzumab-SG3249) (57). Importantly, combination therapy strategies, such as PBD-ADC combined with ATR inhibitors (AZD6738) or EZH2 inhibitors, can effectively restore the sensitivity of SLFN11 low-expressing or null cells to these drugs (57). In a xenograft (PDX) model of triple-negative breast cancer (TNBC), the combination of irinotecan (TOP1 inhibitor) and ATR inhibitor VE-822 significantly improved tumor growth inhibition and inhibited CHK1 phosphorylation in SLFN11-negative tumors, overcoming the limitations of single-drug therapy (58). For breast cancer patients with low SLFN11 expression, preclinical evidence (56) suggests that the combination of DDA (such as gemcitabine) and ATR/WEE1/CHK1 inhibitors (such as AZD6738) may be an effective treatment strategy to overcome their potential drug resistance.

3.5 Ovarian cancer

SLFN11 is a powerful prognostic and predictive biomarker in ovarian cancer (especially high-grade serous ovarian cancer, HGSOC). Its expression level affects patient survival, response to platinum/PARPi, and is associated with the immune microenvironment. Its

mechanism of inhibiting DDR (especially the ATR pathway) provides a theoretical basis for the use of targeted drugs (such as ATR inhibitors) to treat tumors with low SLFN11 expression. Future studies should be committed to verifying the clinical application value of SLFN11 as a predictive marker to guide targeted therapies such as PARP inhibitors (especially in BRCA wild-type populations) and ATR inhibitors.

High expression (mRNA expression above the median) of SLFN11 is significantly associated with longer overall survival (OS) and better efficacy of platinum-based drugs in ovarian cancer patients receiving cisplatin chemotherapy (10, 11). In HGSOC, high SLFN11 expression ("high" if H-score > 60) is closely related to the efficacy of platinum-taxane regimens and can be used as an independent predictor of efficacy (12). SLFN11 promoter methylation leads to decreased expression, which is significantly associated with shortened progression-free survival (PFS) and overall survival (OS) in patients with serous ovarian cancer (6), further confirming the key role of SLFN11 expression level in prognosis. In HGSOC samples, the transcription level and protein level of SLFN11 were positively correlated, and high expression level was closely associated with better prognosis of patients (12). The mechanism of action of SLFN11 is related to its function in the DNA damage response (DDR). After DNA damage induction, SLFN11 selectively inhibits the translation of key DDR repair genes (such as ATR and ATM) by mediating tRNA downregulation, thereby impairing the repair capacity of tumor cells (24). In tumor-infiltrating lymphocytes (TILs), the expression level of SLFN11 in non-tumor cells is positively correlated with the number of TILs (12). Analysis of the TCGA HGSOC dataset confirmed that SLFN11 is expressed in macrophages, T cells, and B cell subsets, and is associated with a variety of immune features, including immunogenic cell death features and IFN-γ response features (12). This suggests that SLFN11 not only affects tumor cells themselves, but is also related to the shaping of the anti-tumor immune microenvironment. In a phase II randomized controlled clinical trial of olaparib maintenance therapy, high SLFN11 expression levels were associated with improved prognosis in patients treated with olaparib. Although this association was not completely independent of BRCA mutation status, it suggests that SLFN11 may serve as a supplementary predictive marker in the context of BRCA mutations or for stratification of BRCA wild-type patients, which is worth verifying in larger studies (59). Given that SLFN11 impairs DNA repair by inhibiting the translation of key DDR genes such as ATR, it is theoretically possible that tumor cells with low SLFN11 expression may be more dependent on residual ATR pathway activity for survival, making them particularly sensitive to ATR inhibitors. This theory has been initially supported by clinical studies: a phase II clinical trial (60) conducted in patients with platinum-resistant HGSOC showed that the ATR inhibitor berzosertib combined with gemcitabine significantly prolonged PFS compared with gemcitabine alone (22.9 weeks vs 14.7 weeks, p=0.044). Unfortunately, the study did not evaluate SLFN11 status. Future studies should focus on analyzing whether SLFN11 expression levels (especially low expression) can predict patients' sensitivity to combined treatment with ATR inhibitors, which will provide an important basis for precision treatment.

3.6 Prostate cancer

SLFN11 expression level is a promising predictive biomarker: it not only predicts the benefit of platinum-based chemotherapy in patients with metastatic castration-resistant prostate cancer (mCRPC), but also shows the potential to predict the sensitivity of specific subpopulations (such as RB1 WT AR+) to new targeted therapies such as B7H3-PBD-ADC, providing an important basis for personalized treatment strategies for advanced prostate cancer.

SLFN11 is overexpressed in a significant proportion of advanced prostate cancers, including approximately 45% of metastatic castration-resistant prostate cancer (mCRPC) and 25% of primary prostate cancer (41). Importantly, high SLFN11 expression (greater than the median value of SLFN11 expression is high) was a strong predictor of responsiveness to platinum-based chemotherapy in patients with mCRPC, associated with significantly improved efficacy and longer progression-free survival (PFS) (41). The study also found that SLFN11 expression levels were positively correlated with the efficacy of the antibody-drug conjugate B7H3-PBD-ADC in a metastatic prostate cancer model; in particular, high SLFN11 expression was identified as a key factor in sensitivity to the drug in RB1 wild-type (WT) androgen receptor-positive (AR+) patients (13). The expression of SLFN11 is highly clinically detectable and can be reliably assessed at the mRNA or protein level in tumor tissue or circulating tumor cells (CTCs), with high concordance between the two methods (41).

3.7 Ewing sarcoma

SLFN11 is a key molecule in Ewing sarcoma that is directly regulated by the oncogenic driver EWS-FLI1. Its high expression not only has diagnostic and prognostic value, but also is a core biomarker and potential hub for predicting tumor sensitivity to multiple targeted therapy strategies (especially DNA damage response targeted therapy).

In Ewing sarcoma (ES), SLFN11 was shown to be a direct transcriptional target of the core oncogenic driver EWS-FLI1, and its expression is positively regulated by EWS-FLI1 through promoter binding (14). Compared with other pediatric tumors (e.g., neuroblastoma, rhabdomyosarcoma), SLFN11 is significantly overexpressed in ES cell lines, laying the foundation for its use as an ES-specific molecular marker (61). The expression level of SLFN11 is a key determinant of ES sensitivity to a variety of DNA damaging agents. Its high expression is closely associated with tumor sensitivity to topoisomerase I inhibitors (such as SN-38/irinotecan and its nanoliposome form), PARP inhibitors, and trabectedin (14, 61–63). The core mechanism is that SLFN11 can hinder DNA replication fork repair and significantly enhance the replication stress effect induced by these drugs, thereby effectively promoting tumor cell death (61, 62, 64). This mechanism also explains why

high SLFN11 expression also predicts the sensitivity of ES to ribonucleotide reductase (RNR) inhibitors (64). Clinical studies have confirmed that ES patients with high SLFN11 expression have a better prognosis (14). Importantly, preclinical models (*in vitro* and *in vivo*) consistently demonstrated that combination therapy with PARP inhibitors and topoisomerase I inhibitors exhibited significant synergistic antitumor activity in ES with high SLFN11 expression (62). The expression level of SLFN11 directly affects the therapeutic effect. Its reduced expression leads to resistance to the above-mentioned DNA damaging agents (61, 63). Crucially, this drug resistance mediated by low SLFN11 expression can be partially reversed by co-application of ATR inhibitors (61, 63), further highlighting the hub status of SLFN11 in the DNA damage response pathway.

The function of SLFN11 is not limited to the DNA damage response. Its expression level was found to directly regulate the sensitivity of ES cells to eltrombopag, a drug that inhibits proliferation through an iron chelation mechanism. Overexpression of SLFN11 enhanced sensitivity, while knockdown of SLFN11 reduced sensitivity (65), demonstrating a role for SLFN11 in a broader therapeutic mechanism.

Notably, although high SLFN11 expression is a strong predictor of sensitivity to DNA damaging agents, some ES cells with high SLFN11 expression still show drug resistance (62). Further studies have shown that such drug resistance is usually not related to the function of SLFN11 itself, but is caused by the impairment of downstream effector pathways (such as apoptosis inhibition, such as BCL-xL overexpression (62). In addition to being a biomarker, AP-1 signaling pathway activated by SLFN11 has been shown to inhibit ES cell growth and downregulate the expression of the oncogene c-Myc (66), suggesting that SLFN11 or its regulatory pathway itself may also be a potential target for therapeutic intervention.

3.8 Glioblastoma

In glioblastoma (GBM), the SLFN11 gene is highly expressed, and it promotes GBM progression by negatively regulating the non-classical NFκB signaling pathway. The study used CRISPR/Cas9 technology to knock out SLFN11, and the results showed that knockout significantly inhibited the proliferation and neurosphere formation ability of GBM cells, accompanied by downregulation of the expression of precursor cell/stem cell marker genes (such as NES, SOX2, and CD44), indicating that SLFN11 deficiency weakened tumor stemness. Mechanistically, SLFN11 deficiency directly stimulated the expression of NFκB target genes, including the cell cycle inhibitory protein p21; since upregulation of p21 can block cell cycle progression, this explains the growth inhibition phenotype and confirms the negative regulatory effect of SLFN11 on the NFκB pathway (i.e., SLFN11 deficiency leads to pathway de-inhibition and activation). Furthermore, in a GBM mouse model, SLFN11 deficiency significantly inhibited tumor growth and prolonged survival (15).

3.9 Head and neck squamous cell carcinoma

Patients with head and neck squamous cell carcinoma (HNSCC) have significant differences in their responses to cisplatin-based chemoradiotherapy (CRT), and SLFN11 expression levels have been revealed as a key prognostic factor that can predict treatment benefit. Specifically, clinical studies have shown that SLFN11-positive group (SLFN11 positive staining was defined as ≥15% staining of the tumor nuclei) is closely associated with longer progression-free survival; *in vitro* experiments have further confirmed that high SLFN11 expression enhances the sensitivity of cells to platinum drugs (DNA damaging agents), highlighting its potential as a response biomarker (16). Mechanistically, SLFN11 deficiency specifically reduces the sensitivity of cells to DNA-damaging drugs, but has no effect on non-DNA-damaging drugs (such as docetaxel), which emphasizes the central role of SLFN11 in the DNA damage response pathway (16). Interestingly, SLFN11 also has a radiosensitizing effect, and the radiosensitization of DNA-dependent protein kinase (DNA-PK) inhibitors is associated with the expression of SLFN11 mRNA (67).

3.10 Colorectal cancer

SLFN11 profoundly affects the response of colorectal cancer (CRC) to DNA-damaging chemotherapy drugs, including irinotecan and platinum (oxaliplatin, cisplatin), by participating in the DNA damage response pathway. Its expression level, especially in the context of KRAS wild-type, has important prognostic value; and its frequent epigenetic silencing (methylation) is one of the key mechanisms leading to chemotherapy resistance and adverse clinical outcomes.

The expression level of SLFN11 is a key determinant regulating the sensitivity of colorectal cancer (CRC) cells to DNA-damaging chemotherapeutic drugs. *In vitro* studies have shown that high expression of SLFN11 can significantly enhance the sensitivity of CRC cells to irinotecan's active metabolite SN-38, manifested by strong anti-proliferative effects, cell apoptosis and cell cycle arrest, which directly confirms that SLFN11 plays an indispensable role in the DNA damage response pathway induced by irinotecan (17). This effect is also clinically significant in platinum drugs. In CRC patients receiving adjuvant chemotherapy with oxaliplatin, the study revealed an important stratification effect: in KRAS exon 2 wild-type patients, high SLFN11 expression (the final score (0–6) was calculated from the ratio and staining intensity, and a score >4.5 was defined as high expression) was closely associated with significantly prolonged overall survival (OS), indicating a good prognosis; however, in KRAS exon 2 mutant patients, SLFN11 expression levels were not significantly correlated with OS (18). This finding clearly establishes SLFN11 as a potential predictive biomarker for response to oxaliplatin in KRAS wild-type CRC patients. Notably, the expression of SLFN11 itself is significantly

affected by epigenetic regulation. About 55.47% of CRC samples have methylation in the promoter region of the SLFN11 gene. This epigenetic silencing event directly leads to a significant decrease in the expression level of SLFN11. Functionally, the loss of expression mediated by SLFN11 methylation weakens the sensitivity of CRC cells to another important platinum drug, cisplatin. More importantly, clinically, the methylation status of SLFN11 is an independent poor prognostic factor, which is clearly associated with patients' poor 5-year overall survival (OS) and significantly shortened recurrence-free survival (RFS) (68).

3.11 Clear cell renal cell carcinoma

SLFN11 is a key tumor promoter and poor prognostic marker for clear cell renal cell carcinoma (ccRCC). Its overexpression (Greater than the median value of SLFN11 expression is high) is an independent prognostic factor and is associated with T stage (T3-T4), distant metastasis (M1), high pathological stage, and death ($P < 0.01$) (69). SLFN11 is significantly overexpressed at both mRNA and protein levels in ccRCC tissues and cell lines (such as ACHN and 786-O), and promoter hypomethylation may be the reason for its upregulation (69). Functionally, knockdown of SLFN11 can effectively inhibit the proliferation, migration and invasion of ccRCC cells and promote cell apoptosis (19). One of its core cancer-promoting mechanisms is to activate the PI3K/AKT signaling pathway: SLFN11 knockdown inhibits the phosphorylation of this pathway, and this effect can be reversed by the PI3K activator 740Y-P (19).

More importantly, SLFN11 is closely associated with the shaping of the immunosuppressive tumor microenvironment (TME) in ccRCC, which constitutes another key mechanism for its cancer promotion (69). SLFN11 expression is positively correlated with the abundance of various tumor-infiltrating lymphocytes (TILs), including CD4+ T cells, $CD8^+$ T cells, macrophages, neutrophils, and dendritic cells. At the same time, it is significantly positively correlated with various immune checkpoint genes (such as CD86, CTLA4, CD244, CD48, CD27, CD40) and key chemokines (such as CXCL5, CXCL10, CXCL11, CXCL13) and their receptors (such as CXCR3, CXCR4, CXCR5, CXCR6, CCR5, CCR6). Functional enrichment analysis (GO/KEGG/GSEA) further confirmed that SLFN11 is involved in immune-related processes such as T cell activation, chemokine signaling pathways, and leukocyte migration. It is worth noting that studies have shown that in ccRCC, chemokines such as CXCL13 (whose receptor CXCR5 is strongly positively correlated with SLFN11) can promote tumor progression by binding to CXCR5 to activate the PI3K/AKT/mTOR pathway, and high expression of CXCR3/4/5/6 is associated with poor overall survival (OS) of patients (70, 71). Therefore, we speculate that SLFN11 may shape an immunosuppressive/pro-tumor TME through regulation (especially inducing specific chemokine networks and immune checkpoint expression), which synergizes with its directly activated PI3K/AKT signaling pathway to jointly drive the aggressive progression and poor prognosis of ccRCC. PPI network analysis: SLFN11 interacts with genes such as SAMHD1 and ETS1 (69). SAMHD1 has been found to play an important role in cell cycle, cancer and innate immunity (72, 73). These interactions may be involved in mediating its regulation of the immune microenvironment and deserve further study in the future.

The clinical significance of SLFN11 needs to be considered in conjunction with the current status of ccRCC treatment. Although the DNA repair-related function of SLFN11 gives it a "beneficial" predictive value in patients treated with DNA-damaging drugs (such as platinum and PARP inhibitors) (14, 18, 40, 41), the first-line treatment of ccRCC mainly relies on anti-angiogenic drugs and immune checkpoint inhibitors (ICIs). In this context, the immunosuppressive microenvironment driven by SLFN11 (manifested by high immune checkpoint expression and specific immune cell composition) may become a key factor affecting the efficacy of treatment. We believe that in ccRCC, this immunomodulatory effect of SLFN11 dominates the cancer-promoting mechanism and may mask the impact of its function in DNA damage response on current mainstream treatment options.

3.12 Hepatocellular carcinoma

Recent studies have strongly suggested that SLFN11 is a key regulator in the immune microenvironment of hepatocellular carcinoma (HCC) and shows great potential as a biomarker for predicting the efficacy of immune checkpoint inhibitors (ICI) treatment.

SLFN11 is often downregulated in HCC, and its low expression (Samples with a negative or weak H-score were determined to be the low protein expression group) is significantly associated with poor prognosis of patients (20). Functionally, SLFN11 has been shown to effectively inhibit the proliferation, migration, invasion and metastasis of HCC cells and promote apoptosis. Its molecular mechanism involves interaction with RPS4X, leading to weakened S6 and eIF4E phosphorylation in the ribosome complex, thereby inhibiting the cancer-promoting mTOR signaling pathway. More importantly, recent studies (2024) revealed the central role of SLFN11 in shaping the immune microenvironment of HCC (74). The study found that SLFN11 expression was significantly upregulated in tumor tissues of HCC patients who responded to ICI treatment. In contrast, SLFN11 deficiency promoted the infiltration of immunosuppressive macrophages and aggravated tumor progression. Mechanistic studies have shown that SLFN11 stabilizes RBM10 and promotes NUMB exon 9 skipping by inhibiting TRIM21-mediated RBM10 degradation, a process that is critical for regulating anti-tumor immune responses. It is worth noting that for patients with low SLFN11 expression, the study proposed a potential intervention strategy: blocking the CCL2/CCR2 signaling pathway can effectively enhance their sensitivity to ICI treatment, which provides a new idea for overcoming immunotherapy resistance in such patients (74).

3.13 Other

SLFN11 is a predictive biomarker for bladder cancer patients receiving platinum-based chemotherapy, and its expression level can specifically predict chemotherapy response and patient survival outcomes (42). This conclusion is based on a clinical study of 120 cases of bladder cancer: the patients were divided into two groups, the first group (50 cases) were patients with unresectable locally advanced or metastatic bladder cancer who received platinum-containing chemotherapy, and the second group (70 cases) were patients who received surgical resection without chemotherapy. The key findings showed that in the chemotherapy group, the overall survival rate of SLFN11-positive patients (SLFN11 was considered positive when at least 5% of the tumor cells were stained) was significantly better (P=0.012), and SLFN11 expression was positively correlated with the luminal subtype marker GATA3 (p=0.027). In contrast, in the non-chemotherapy group, the overall survival rate of SLFN11-positive patients was worse (P=0.034), which highlights the "predictive" nature of SLFN11-its benefits are only manifested in the context of chemotherapy, probably because high expression of SLFN11 marks the inherent sensitivity of the tumor to DNA damaging agents, but in the absence of chemotherapy, it is associated with an aggressive phenotype.

In vitro mechanistic experiments (42) further confirmed the causal role of SLFN11: in bladder cancer cell lines, SLFN11 gene knockout led to resistance to cisplatin, while epigenetic modification drugs (such as 5-azacytidine and entinostat) restored SLFN11 expression and resensitized SLFN11-negative cells to cisplatin and carboplatin. This provides a molecular basis for SLFN11 as a biomarker and suggests that epigenetic therapy can reverse resistance.

Notably, the predictive value of SLFN11 may extend to other cancers. For example, SLFN11 expression is elevated in acute myeloid leukemia (AML) and acute lymphoblastic leukemia (ALL) cells. High expression of SLFN11 is regulated by interferon-JAK signaling and ETS family transcription factors (such as ETS-1 and FLI1) (75); JAK, AKT, ERK, or ETS inhibitors can all downregulate SLFN11. Similarly, in mesothelioma cells, high SLFN11 expression correlated with response to PARP inhibitors, and combination with temozolomide enhanced the sensitivity of cells with low MGMT expression (76), further supporting the broad potential of SLFN11 as a biomarker of DNA damage response (76).

4 Potential treatment strategies based on the expression status of SLFN11

4.1 Epigenetic re-expression of SLFN11: a combined strategy to enhance chemotherapy efficacy

SLFN11 is an important DNA damage response factor. Its promoter hypermethylation leads to silencing expression, which is a key mechanism for various cancers (such as small cell lung cancer (SCLC)) to develop resistance to platinum and other DNA damaging agents (DDA), and is directly related to the poor prognosis of patients (6). Therefore, reversing SLFN11 silencing through epigenetic drugs and directly restoring its function is an effective way to overcome drug resistance.

DNA demethylating agents (such as decitabine) and histone deacetylase (HDAC) inhibitors (such as FK228) can effectively reverse the abnormal methylation status of the SLFN11 promoter, and FK228 has been shown to upregulate SLFN11 expression in a dose-dependent manner (47, 77, 78). Re-expression of SLFN11 can significantly restore cancer cell sensitivity to DDA: Decitabine significantly enhanced the efficacy of the TROP2-targeting antibody-drug conjugate sacituzumab govitecan by upregulating SLFN11 and TROP2 (a cell surface antigen highly expressed in various epithelial cancers) (78). The HDAC inhibitor FK228 restores sensitivity of SCLC cells to the topoisomerase I inhibitor topotecan (47). More extensive studies have shown that class I HDAC inhibitors can universally induce SLFN11 expression and effectively overcome multiple DDA resistance, but class II HDAC inhibitors have no such effect (77). The EZH1/2 inhibitor valemetostat combined with irinotecan showed efficacy in relapsed SCLC (38), further confirming the clinical translational potential of combining epigenetic drugs with chemotherapy to enhance the therapeutic effect by reactivating SLFN11.

4.2 Overcoming SLFN11 deficiency: targeting the DDR pathway to achieve synthetic lethality

SLFN11-deficient tumors rely on the S-G2/M checkpoint to repair DNA damage and survive, leading to DDA resistance (56). Targeting checkpoint kinases such as ATR/CHK1/WEE1 can abrogate this survival pathway.

Preclinical studies have demonstrated the efficacy of DDR inhibitors in overcoming SLFN11 deficiency-associated drug resistance: ATR/CHK1 inhibitors (such as M4344, M6620, and SRA737) have been reported in the clinic to resensitize SLFN11-deficient cells to topoisomerase inhibitors, PARP inhibitors, and cisplatin (33). *In vitro* experiments and PDX models showed that gemcitabine combined with other DDRi (such as ATR inhibitors, WEE1 inhibitors or CHK1 inhibitors) can overcome gemcitabine resistance in SLFN11-deficient cell lines or PDX models (56). Low-dose M1774 showed high synergy with a variety of clinical DDAs, including TOP1 and TOP2 inhibitors, cisplatin, RNA polymerase II inhibitors, and PARP inhibitors (51). M1774 reversed the chemotherapeutic resistance of cancer cells lacking SLFN11 expression to anticancer DDAs. In cell lines or PDX/xenograft models of breast cancer, colon cancer, and SCLC, ATR inhibitors or CHK1 inhibitors combined with chemotherapy regimens (such as TOP1 inhibitors exatecan, lurbinectedin, and PARP inhibitors) showed synergistic effects (50, 79, 80). Notably, ATR inhibition directly reverses SLFN11 deficiency-associated resistance to DNA-damaging agents, pyrrolobenzodiazepine dimer (57) and PARP inhibitors (7), by blocking the S phase checkpoint. This strategy has shown positive clinical translational signals: gemcitabine

combined with an ATR inhibitor showed efficacy in a phase II trial for high-grade serous ovarian cancer (60); an ATR inhibitor combined with a PARP inhibitor/lurbinectedin (an alkylating agent/DNA damaging agent) showed synergistic effects in SCLC cell lines (50, 79). Together, these results highlight targeting the DDR pathway as a powerful therapeutic prospect to overcome SLFN11 loss-associated drug resistance and achieve synthetic lethality.

5 Challenges and future prospects

Future research directions based on SLFN11 should focus on the selection of evaluation methods, dynamic monitoring technology, optimization of combination therapy, elucidation of molecular mechanisms, cross-cancer validation, and regulation of the immune microenvironment. By focusing these research directions, it not only addresses the limitations of existing treatments (such as drug resistance and heterogeneity),but also provides an actionable path for clinical translation. The following suggestions are directly related to the core functions of SLFN11 and the reported treatment strategies, which contribute to promoting its transition from a biomarker to a therapeutic target.

5.1 Detection methods for SLFN11

SLFN11 can predict the efficacy of DNA-targeted drugs in various tumors, and this effect has been confirmed by immunohistochemistry (IHC) in multiple previous studies (12, 20, 36, 37). Additionally, we analyzed two datasets, GSE37751 and GSE29013, from the Gene Expression Omnibus (GEO) database. When only analyzing breast cancer patients who received chemotherapy (n = 34), patients with high SLFN11 expression showed a significant benefit in overall survival (OS) ($p = 0.048$). Similarly, in a dataset of 110 ovarian cancer patients who received cisplatin chemotherapy, high SLFN11 expression showed a trend associated with longer OS ($p = 0.053$). However, some studies suggest that the expression level of SLFN11 obtained by tissue RNA-seq may be overestimated in certain tumor tissues. In addition to tumor cells, there are other non-tumor cells (such as immune cells) in tumor tissues, and SLFN11 is also expressed, or even strongly expressed, in these non-tumor cells (12, 81). The study compared the RNA-seq data of SLFN11 in the TCGA database with the IHC staining of clinicopathological tissue specimens, and emphasized the importance of using IHC rather than tissue RNA-seq to evaluate the expression of SLFN11 in patient samples (81). In a study on high - grade serous ovarian cancer, they separately investigated the IHC semi - quantitative H - scores of SLFN11 in tumor and non - tumor cells, emphasizing the hypothesis that cancer - expressed SLFN11 is directly related to the sensitivity of tumor cells to DNA - damaging agents such as platinum. Moreover, they believed that the overall SLFN11 H - score is a more powerful prognostic biomarker compared to the separately measured cancer or non - cancer SLFN11 (12). A study on the prognostic role of SLFN11 in bladder cancer only evaluated the expression score of SLFN11 in tumor cells and found that SLFN11 was associated with better overall survival (OS) in patients receiving platinum - based chemotherapy ($p = 0.012$) (42). In some tissues (such as breast and pancreatic tissues), there are significant differences in the distribution of TCGA and IHC between normal and tumor tissues (81). For different types of cancers, there are some differences in the selection of SLFN11 detection methods (IHC or RNA - seq) and evaluation regions (non - tumor cells, tumor cells, or overall). Further research is required in different cancers to screen and evaluate specific evaluation strategies.

5.2 Development and validation of a dynamic monitoring technology for SLFN11 expression

Research has shown that SLFN11 undergoes dynamic changes during the treatment process (52), and its expression status can affect the efficacy of DNA-targeted drugs. Therefore, dynamic detection of SLFN11 expression is particularly important for the precise treatment of cancer patients. Non-invasive detection methods based on liquid biopsy (such as circulating tumor cells) should be developed to monitor the dynamic changes in SLFN11 expression during the treatment in real time, especially the downward trend of SLFN11 expression after chemotherapy or treatment with PARP inhibitors. Dynamic monitoring data can be used to guide the timing of combination therapy with ATR inhibitors, ATM inhibitors, CHK1 inhibitors, WEE1 inhibitors or EZH2 inhibitors. For example, timely intervention when the expression of SLFN11 decreases can be carried out to overcome drug resistance. In addition, given the challenges in obtaining sufficient tumor tissues from non - small cell lung cancer, liquid biopsy should be regarded as an important tool in research and treatment. In several preclinical studies using cell lines and patient - derived xenograft models, the expression of SLFN11 strongly predicted the response to cisplatin and PARP inhibitors (8, 9). Therefore, the dynamic detection of SLFN11 in circulating tumor cells shows special potential. For example, screening out the SLCC population sensitive to cisplatin and PARP inhibitors through dynamic monitoring of liquid biopsy and timely intervention when SLFN11 expression decreases all require more prospective studies for verification.

5.3 Optimization of combination therapies based on SLFN11 status

High expression of SLFN11 is associated with the sensitivity of tumor cells to DNA-targeted drugs, while low expression of SLFN11 is associated with the resistance of tumor cells to DNA-targeted drugs. It is of potential value to explore combined treatment options based on the expression status of SLFN11 (Table 3). The combination of the PARP inhibitor talazoparib and the immune checkpoint inhibitor atezolizumab as maintenance therapy

TABLE 3 Potential treatment strategies based on the expression status of SLFN11.

Strategy classification	Specific methods	Applicable scenarios	Mechanism of action
Epigenetic regulation	HDAC inhibitors (FK228) or demethylation agents (5-AZA/DAC) induce SLFN11 expression	SLFN11 low expression tumor	Reverse promoter methylation or histone modification to restore the expression of SLFN11
Combination therapy (high expression of SLFN11)	1. Combination of PARP inhibitors and immune checkpoint inhibitors (small cell lung cancer, breast cancer); 2. Combination of PARP inhibitors and topoisomerase inhibitors (Ewing sarcoma)	1. SCLC, breast cancer 2. Ewing sarcoma	1. High expression of SLFN11 in tumors with enhanced immune response characteristics, Enhance DNA damage 2. Enhance DNA damage
Combination therapy (low expression of SLFN11)	1. ATR inhibitor + chemotherapy, 2. ATR inhibitor + PARP inhibitor, 3. EZH2 inhibitor + chemotherapy, 4. ATR inhibitor + lurbinectedin, 5. CCL2/CCR2 inhibitor + immune checkpoint inhibitor, 6. ATM inhibitors + chemotherapy	1. Breast cancer 2. SCLC 3. SCLC 4. SCLC 5. Hepatocellular carcinoma 6. Esophageal cancer	Inhibit the replication stress checkpoint to overcome the drug resistance caused by SLFN11 deficiency.
Targeting the functional module of SLFN11	Kinase inhibitors regulate the phosphorylation sites (such as S753) of SLFN11.	–	Regulate the conformation of SLFN11 and its binding ability to ssDNA.
Dynamic monitoring and precise intervention	Liquid biopsy (CTC/ctDNA) monitors the dynamic expression of SLFN11 to guide the timing of combination therapy with ATR/ATM/EZH2 inhibitors.	Tumors that progress after chemotherapy or treatment with PARP inhibitors	Adjust the treatment strategy in real - time to prevent drug resistance caused by the down - regulation of SLFN11.

significantly improved the progression-free survival (PFS) of patients with SLFN11-positive small cell lung cancer (SCLC) (39). In tumor-infiltrating lymphocytes (TILs), the expression level of SLFN11 in non-tumor cells was positively correlated with the number of TILs (12). Breast cancer samples with high SLFN11 expression were accompanied by enhanced immune response characteristics, including T cell infiltration and high expression of immune checkpoints (such as PD-L1) (56, 58, 82). The results of a phase II clinical study comparing the ATR inhibitor berzosertib in combination with gemcitabine versus gemcitabine alone for the treatment of platinum-resistant high-grade serous ovarian cancer showed that the combination therapy group significantly prolonged progression-free survival (PFS) (22.9 weeks vs 14.7 weeks, $p = 0.044$) (60). For tumors with high SLFN11 expression, exploring the synergistic effect and mechanism of action of immune checkpoint inhibitors combined with PARP inhibitors or chemotherapy has potential clinical significance. For tumors with low SLFN11 expression, systematically evaluate the efficacy of the combination regimens of ATR inhibitors, ATM inhibitors, CHK1 inhibitors, and WEE1 inhibitors with standard chemotherapy in different cancers.

Screen specific epigenetic drugs (such as HDAC inhibitors or low - toxicity demethylating agents) targeting SLFN11 promoter methylation or histone modification, and evaluate the differences in their efficacy among different cancer types. In tumors with low SLFN11 expression, such as ovarian cancer, breast cancer, colorectal cancer, small - cell lung cancer, and bladder cancer, combine chemotherapy with HDAC inhibitors or demethylating agents to verify whether they can enhance chemotherapy sensitivity by upregulating SLFN11.

5.4 In - depth analysis and targeted intervention of the molecular mechanism of SLFN11

Analyze the interaction mechanisms of SLFN11 with RPA1, ssDNA, DDB1 of $CUL4^{CDT2}$ E3 ubiquitin ligase, and develop small - molecule drugs to mimic or block its functions. Explore the regulatory network of SLFN11 phosphorylation sites (such as S753) and design kinase inhibitors to modulate its conformation and activity. In glioblastoma, target the interaction between SLFN11 and the NF - κB pathway and verify whether it can reverse the characteristics of tumor stem cells.

5.5 Cross-cancer clinical validation and biomarker stratification

Establish a multi - center cohort study and enroll patients with pan - cancer types (such as ovarian cancer, small - cell lung cancer (SCLC), and triple - negative breast cancer (TNBC)). Stratify patients based on the expression level of SLFN11 (using immunohistochemistry (IHC) or next - generation sequencing (NGS)) and evaluate its predictive value for different DNA - targeting drugs (such as PARP inhibitors, platinum - based drugs, and TOP inhibitors). In BRCA wild - type ovarian cancer, determine whether SLFN11 can serve as an independent predictive marker for the efficacy of olaparib to compensate for the limitations of homologous recombination deficiency (HRD) testing.

5.6 The interaction between SLFN11 and the tumor microenvironment

Investigate how SLFN11 affects the response to immunotherapy by regulating immune cell infiltration (such as T cells and macrophages) or cytokine secretion (such as the CCL2/CCR2 axis), especially in hepatocellular carcinoma (74) and ovarian cancer (12). In HCC with low SLFN11 expression, combine CCR2 inhibitors with PD - 1 inhibitors to verify whether it can reverse the immunosuppressive microenvironment (74).

6 Discussion

SLFN11 has emerged as a pivotal biomarker and potential therapeutic modulator in the era of precision oncology. This review consolidates compelling evidence demonstrating that SLFN11 expression strongly correlates with increased sensitivity to a wide array of DNA-damaging agents (DDAs), including platinum compounds, topoisomerase inhibitors, and PARP inhibitors across diverse cancer types (7, 8, 11). The mechanistic underpinnings of this sensitivity—ranging from replication fork arrest and tRNA cleavage to inhibition of homologous recombination via RPA1 destabilization—are unique and position SLFN11 as a functional gatekeeper of DNA damage response (DDR) (22, 32). Furthermore, the modulation of SLFN11 through epigenetic silencing, post-translational modifications, and transcriptional regulation provides clinically actionable targets for reversing drug resistance.

One of the most striking findings across cancer types is the context-dependent role of SLFN11 in influencing prognosis and therapy response. In cancers such as ovarian, breast, gastric, and small cell lung cancer (SCLC), high SLFN11 expression consistently predicts better outcomes in patients treated with DNA-targeting chemotherapy (10–12, 37, 44). In Ewing sarcoma, SLFN11 is transcriptionally activated by the EWS-FLI1 oncogene and is required for sensitivity to PARP and topoisomerase I inhibitors (14). These data support its role as a lineage-influenced, mechanistically relevant biomarker.

Despite its promise, the utility of SLFN11 as a universal biomarker faces several challenges. A key limitation is the dynamic and heterogeneous expression of SLFN11 both within and between tumors, which can fluctuate during treatment (9, 52). This necessitates the development of real-time, non-invasive monitoring technologies, such as liquid biopsy-based assays using circulating tumor cells (CTCs) (52). Moreover, there is no standardized detection method—while RNA-seq data provide transcriptional snapshots, protein-level evaluation via immunohistochemistry (IHC) may offer a more accurate reflection of functional SLFN11 expression, especially given its expression in immune and stromal cells (12, 81).

Therapeutically, SLFN11-deficient tumors often exhibit intrinsic resistance to DDAs. However, this resistance is not insurmountable. Multiple preclinical studies, including those in SCLC, breast, and colorectal cancers, demonstrate that SLFN11 loss can be overcome by targeting compensatory DDR pathways, particularly ATR, CHK1, and WEE1 (7, 56, 79, 80). This introduces a synthetic lethality-based rationale for combination regimens in SLFN11-low or silenced tumors. Epigenetic drugs, such as HDAC inhibitors and demethylating agents, have shown efficacy in reactivating SLFN11 expression, thereby restoring chemosensitivity (47, 77). These findings underscore the therapeutic flexibility of SLFN11 as both a predictive marker and a targetable resistance mechanism.

Additionally, SLFN11 has emerging significance in shaping the tumor immune microenvironment (TME). Its positive correlation with immune cell infiltration and immune checkpoint expression in several tumor types—most notably in gastric cancer, breast cancer, and hepatocellular carcinoma—suggests an immunomodulatory role that may synergize with immune checkpoint inhibitors (12, 43, 74). Early clinical evidence from SCLC patients receiving PARP inhibitors in combination with ICIs supports this hypothesis, although further prospective trials are needed to validate such approaches (39).

Moving forward, several research directions are warranted. First, pan-cancer prospective clinical trials should evaluate the predictive power of SLFN11-guided therapies, especially in patients without BRCA mutations or homologous recombination deficiency. Second, investigations into post-translational regulation (e.g., S753 phosphorylation) of SLFN11 activity may yield new therapeutic levers (28). Third, integrative studies that stratify patients based on SLFN11 expression alongside other biomarkers (e.g., ATM, EMT status, TIL density) may refine response prediction models (9, 12).

In conclusion, SLFN11 represents a paradigm-shifting biomarker at the intersection of DNA damage response, epigenetics, and immunology. Its integration into clinical oncology not only promises to optimize treatment efficacy and reduce unnecessary toxicity but also offers new avenues for therapeutic innovation, especially in drug-resistant and biomarker-poor cancers. With further validation and clinical translation, SLFN11 has the potential to evolve from a predictive biomarker into a central node of personalized cancer therapy.

Author contributions

KZ: Conceptualization, Data curation, Methodology, Writing – original draft, Writing – review & editing. YL: Writing – review & editing, Conceptualization, Formal analysis, Project administration, Software. WW: Data curation, Formal analysis, Methodology, Writing – original draft, Writing – review & editing. YC: Conceptualization, Data curation, Formal analysis, Writing – original draft, Writing – review & editing. BQ: Writing – review & editing, Data curation, Methodology, Validation, Resources. YL: Writing – review & editing, Validation. HL: Writing – review & editing, Validation. RX: Writing – review & editing, Validation. LZ: Conceptualization, Data curation, Methodology, Project administration, Software, Supervision, Writing – original draft, Writing – review & editing.

Funding

The author(s) declare that financial support was received for the research and/or publication of this article. This review was funded by the Translational Application Research Team Project of Precision Treatment and Diagnosis Strategies for Lung Cancer of Kunming Medical University (ZC2024XKTDPY08), the Special Project for Medical and Health Talents of the "Xingdian Talent Support Program" (CZ0096-901895), and the National Natural Science Foundation of China (8226110412, 82460540). The funders had no role in the study design, data collection, analysis, decision to publish, or preparation of the manuscript.

Acknowledgments

We would like to thank the corresponding author, LZ from the Department of Rehabilitation and Palliative Medicine at the Third Affiliated Hospital of Kunming Medical University, for her great support and help with this work.

Conflict of interest

The authors declare that the research was conducted in the absence of any commercial or financial relationships that could be construed as a potential conflict of interest.

Generative AI statement

The author(s) declare that no Generative AI was used in the creation of this manuscript.

Publisher's note

References

1. Barretina J, Caponigro G, Stransky N, Venkatesan K, Margolin AA, Kim S, et al. The cancer cell line encyclopedia enables predictive modelling of anticancer drug sensitivity. *Nature*. (2012) 483:603–7. doi: 10.1038/nature11003

2. Chen S, Cao Z, Prettner K, Kuhn M, Yang J, Jiao L, et al. Estimates and projections of the global economic cost of 29 cancers in 204 countries and territories from 2020 to 2050. *JAMA Oncol*. (2023) 9:465–72. doi: 10.1001/jamaoncol.2022.7826

3. Hanahan D, Weinberg RA. Hallmarks of cancer: the next generation. *Cell*. (2011) 144:646–74. doi: 10.1016/j.cell.2011.02.013

4. Peng Y, Wang L, Wu L, Zhang L, Nie G, Guo M. Methylation of slfn11 promotes gastric cancer growth and increases gastric cancer cell resistance to cisplatin. *J Cancer*. (2019) 10:6124–34. doi: 10.7150/jca.32511

5. Zhou J, Zhang MY, Gao AA, Zhu C, He T, Herman JG, et al. Epigenetic silencing schlafen-11 sensitizes esophageal cancer to atm inhibitor. *World J Gastrointestinal Oncol*. (2024) 16:2060–73. doi: 10.4251/wjgo.v16.i5.2060

6. Nogales V, Reinhold WC, Varma S, Martinez-Cardus A, Moutinho C, Moran S, et al. Epigenetic inactivation of the putative DNA/rna helicase slfn11 in human cancer confers resistance to platinum drugs. *Oncotarget*. (2016) 7:3084–97. doi: 10.18632/oncotarget.6413

7. Murai J, Feng Y, Yu GK, Ru Y, Tang SW, Shen Y, et al. Resistance to parp inhibitors by slfn11 inactivation can be overcome by atr inhibition. *Oncotarget*. (2016) 7:76534–50. doi: 10.18632/oncotarget.12266

8. Lok BH, Gardner EE, Schneeberger VE, Ni A, Desmeules P, Rekhtman N, et al. Parp inhibitor activity correlates with slfn11 expression and demonstrates synergy with temozolomide in small cell lung cancer. *Clin Cancer Res: Off J Am Assoc Cancer Res*. (2017) 23:523–35. doi: 10.1158/1078-0432.Ccr-16-1040

9. Allison Stewart C, Tong P, Cardnell RJ, Sen T, Li L, Gay CM, et al. Dynamic variations in epithelial-to-mesenchymal transition (Emt), atm, and slfn11 govern response to parp inhibitors and cisplatin in small cell lung cancer. *Oncotarget*. (2017) 8:28575–87. doi: 10.18632/oncotarget.15338

10. Shee K, Wells JD, Jiang A, Miller TW. Integrated pan-cancer gene expression and drug sensitivity analysis reveals slfn11 mrna as a solid tumor biomarker predictive of sensitivity to DNA-damaging chemotherapy. *PloS One*. (2019) 14:e0224267. doi: 10.1371/journal.pone.0224267

11. Murai J, Thomas A, Miettinen M, Pommier Y. Schlafen 11 (Slfn11), a restriction factor for replicative stress induced by DNA-targeting anti-cancer therapies. *Pharmacol Ther*. (2019) 201:94–102. doi: 10.1016/j.pharmthera.2019.05.009

12. Winkler C, King M, Berthe J, Ferraioli D, Garuti A, Grillo F, et al. Slfn11 captures cancer-immunity interactions associated with platinum sensitivity in high-grade serous ovarian cancer. *JCI Insight*. (2021) 6(18). doi: 10.1172/jci.insight.146098

13. Agarwal S, Fang L, McGowen K, Yin J, Bowman J, Ku AT, et al. Tumor-derived biomarkers predict efficacy of B7h3 antibody-drug conjugate treatment in metastatic prostate cancer models. *J Clin Invest*. (2023) 133(22). doi: 10.1172/jci162148

14. Tang SW, Bilke S, Cao L, Murai J, Sousa FG, Yamade M, et al. Slfn11 is a transcriptional target of ews-fli1 and a determinant of drug response in ewing sarcoma. *Clin Cancer Res: Off J Am Assoc Cancer Res*. (2015) 21:4184–93. doi: 10.1158/1078-0432.Ccr-14-2112

15. Fischietti M, Eckerdt F, Perez RE, Guillen Magaña JN, Mazewski C, Ho S, et al. Slfn11 negatively regulates non-canonical nfkb signaling to promote glioblastoma progression. *Cancer Res Commun*. (2022) 2:966–78. doi: 10.1158/2767-9764.crc-22-0192

16. Hamada S, Kano S, Murai J, Suzuki T, Tsushima N, Mizumachi T, et al. Schlafen family member 11 indicates favorable prognosis of patients with head and neck cancer following platinum-based chemoradiotherapy. *Front Oncol*. (2022) 12:978875. doi: 10.3389/fonc.2022.978875

17. Tian L, Song S, Liu X, Wang Y, Xu X, Hu Y, et al. Schlafen-11 sensitizes colorectal carcinoma cells to irinotecan. *Anti-cancer Drugs*. (2014) 25:1175–81. doi: 10.1097/cad.0000000000000151

18. Deng Y, Cai Y, Huang Y, Yang Z, Bai Y, Liu Y, et al. High slfn11 expression predicts better survival for patients with kras exon 2 wild type colorectal cancer after treated with adjuvant oxaliplatin-based treatment. *BMC Cancer*. (2015) 15:833. doi: 10.1186/s12885-015-1840-6

19. Wang HX, Zhao ZP, Du XY, Peng SL, Xu HY, Tang W, et al. Slfn11 promotes clear cell renal cell carcinoma progression via the pi3k/akt signaling pathway. *Med Oncol*. (2024) 41:54. doi: 10.1007/s12032-023-02262-9

20. Zhou C, Liu C, Liu W, Chen W, Yin Y, Li CW, et al. Slfn11 inhibits hepatocellular carcinoma tumorigenesis and metastasis by targeting rps4x via mtor pathway. *Theranostics*. (2020) 10:4627–43. doi: 10.7150/thno.42869

21. Schwarz DA, Katayama CD, Hedrick SM. Schlafen, a new family of growth regulatory genes that affect thymocyte development. *Immunity*. (1998) 9:657–68. doi: 10.1016/s1074-7613(00)80663-9

22. Jo U, Pommier Y. Structural, molecular, and functional insights into schlafen proteins. *Exp Mol Med*. (2022) 54:730–8. doi: 10.1038/s12276-022-00794-0

23. Metzner FJ, Wenzl SJ, Kugler M, Krebs S, Hopfner KP, Lammens K. Mechanistic understanding of human slfn11. *Nat Commun*. (2022) 13:5464. doi: 10.1038/s41467-022-33123-0

24. Li M, Kao E, Malone D, Gao X, Wang JYJ, David M. DNA damage-induced cell death relies on slfn11-dependent cleavage of distinct type ii trnas. *Nat Struct Mol Biol*. (2018) 25:1047–58. doi: 10.1038/s41594-018-0142-5

25. Blackford AN, Jackson SP. Atm, atr, and DNA-pk: the trinity at the heart of the DNA damage response. *Mol Cell*. (2017) 66:801–17. doi: 10.1016/j.molcel.2017.05.015

26. Alvi E, Mochizuki AL, Katsuki Y, Ogawa M, Qi F, Okamoto Y, et al. Mouse slfn8 and slfn9 genes complement human cells lacking slfn11 during the replication stress response. *Commun Biol*. (2023) 6:1038. doi: 10.1038/s42003-023-05406-9

27. Hou P, Hao W, Qin B, Li M, Zhao R, Cui S. Structural and biochemical characterization of schlafen11 N-terminal domain. *Nucleic Acids Res*. (2023) 51:7053–70. doi: 10.1093/nar/gkad509

28. Kugler M, Metzner FJ, Witte G, Hopfner KP, Lammens K. Phosphorylation-mediated conformational change regulates human slfn11. *Nat Commun*. (2024) 15:10500. doi: 10.1038/s41467-024-54833-7

29. Wiese C, Hinz JM, Tebbs RS, Nham PB, Urbin SS, Collins DW, et al. Disparate requirements for the walker a and B atpase motifs of human rad51d in homologous recombination. *Nucleic Acids Res*. (2006) 34:2833–43. doi: 10.1093/nar/gkl366

30. Murai J, Tang SW, Leo E, Baechler SA, Redon CE, Zhang H, et al. Slfn11 blocks stressed replication forks independently of atr. *Mol Cell*. (2018) 69:371–84.e6. doi: 10.1016/j.molcel.2018.01.012

31. Fujiwara K, Maekawa M, Iimori Y, Ogawa A, Urano T, Kono N, et al. The crucial role of single-stranded DNA binding in enhancing sensitivity to DNA-damaging agents for schlafen 11 and schlafen 13. *iScience*. (2023) 26:108529. doi: 10.1016/j.isci.2023.108529

32. Mu Y, Lou J, Srivastava M, Zhao B, Feng XH, Liu T, et al. Slfn11 inhibits checkpoint maintenance and homologous recombination repair. *EMBO Rep*. (2016) 17:94–109. doi: 10.15252/embr.201540964

33. Jo U, Murai Y, Chakka S, Chen L, Cheng K, Murai J, et al. Slfn11 promotes cdt1 degradation by cul4 in response to replicative DNA damage, while its absence leads to synthetic lethality with atr/chk1 inhibitors. *Proc Natl Acad Sci United States America*. (2021) 118(6). doi: 10.1073/pnas.2015654118

34. Murai J, Zhang H, Pongor L, Tang SW, Jo U, Moribe F, et al. Chromatin remodeling and immediate early gene activation by slfn11 in response to replication stress. *Cell Rep*. (2020) 30:4137–51.e6. doi: 10.1016/j.celrep.2020.02.117

35. Mezzadra R, de Bruijn M, Jae LT, Gomez-Eerland R, Duursma A, Scheeren FA, et al. Slfn11 can sensitize tumor cells towards ifn-Γ-mediated T cell killing. *PloS One*. (2019) 14:e0212053. doi: 10.1371/journal.pone.0212053

36. Kagami T, Yamade M, Suzuki T, Uotani T, Tani S, Hamaya Y, et al. The first evidence for slfn11 expression as an independent prognostic factor for patients with esophageal cancer after chemoradiotherapy. *BMC Cancer*. (2020) 20:1123. doi: 10.1186/s12885-020-07574-x

37. Pietanza MC, Waqar SN, Krug LM, Dowlati A, Hann CL, Chiappori A, et al. Randomized, double-blind, phase ii study of temozolomide in combination with either veliparib or placebo in patients with relapsed-sensitive or refractory small-cell lung cancer. *J Clin Oncol: Off J Am Soc Clin Oncol*. (2018) 36:2386–94. doi: 10.1200/jco.2018.77.7672

38. Choudhury NJ, Lai WV, Makhnin A, Heller G, Eng J, Li B, et al. A phase I/ii study of valemetostat (Ds-3201b), an ezh1/2 inhibitor, in combination with irinotecan in patients with recurrent small-cell lung cancer. *Clin Cancer Res: Off J Am Assoc Cancer Res*. (2024) 30:3697–703. doi: 10.1158/1078-0432.Ccr-23-3383

39. Karim NA, Miao J, Reckamp KL, Gay CM, Byers LA, Zhao YQ, et al. Phase ii randomized study of maintenance atezolizumab (a) versus atezolizumab + Talazoparib (at) in patients with slfn11 positive extensive stage small cell lung cancer. S1929. *J Thorac Oncol: Off Publ Int Assoc Study Lung Cancer*. (2025) 20(3):383–94. doi: 10.1016/j.jtho.2024.10.021

40. Zoppoli G, Regairaz M, Leo E, Reinhold WC, Varma S, Ballestrero A, et al. Putative DNA/rna helicase schlafen-11 (Slfn11) sensitizes cancer cells to DNA-damaging agents. *Proc Natl Acad Sci United States America*. (2012) 109:15030–5. doi: 10.1073/pnas.1205943109

41. Conteduca V, Ku SY, Puca L, Slade M, Fernandez L, Hess J, et al. Slfn11 expression in advanced prostate cancer and response to platinum-based chemotherapy. *Mol Cancer Ther*. (2020) 19:1157–64. doi: 10.1158/1535-7163.Mct-19-0926

42. Taniyama D, Sakamoto N, Takashima T, Takeda M, Pham QT, Ukai S, et al. Prognostic impact of schlafen 11 in bladder cancer patients treated with platinum-based chemotherapy. *Cancer Sci*. (2022) 113:784–95. doi: 10.1111/cas.15207

43. Xu J, Chen S, Liang J, Hao T, Wang H, Liu G, et al. Schlafen family is a prognostic biomarker and corresponds with immune infiltration in gastric cancer. *Front Immunol*. (2022) 13:922138. doi: 10.3389/fimmu.2022.922138

44. Takashima T, Taniyama D, Sakamoto N, Yasumoto M, Asai R, Hattori T, et al. Schlafen 11 predicts response to platinum-based chemotherapy in gastric cancers. *Br J Cancer*. (2021) 125:65–77. doi: 10.1038/s41416-021-01364-3

45. Gay CM, Stewart CA, Park EM, Diao L, Groves SM, Heeke S, et al. Patterns of transcription factor programs and immune pathway activation define four major subtypes of sclc with distinct therapeutic vulnerabilities. *Cancer Cell*. (2021) 39:346–60.e7. doi: 10.1016/j.ccell.2020.12.014

46. Gay C, Diao L, Stewart C, Xi Y, Cardnell R, Swisher S, et al. Abstract 3772: inter- and intra-tumoral variations in ascl1, neurod1, and pou2f3 transcriptional programs underlie three distinct molecular subtypes of small cell lung cancers. *Cancer Res*. (2019) 79:3772. doi: 10.1158/1538-7445.AM2019-3772

47. Yin YP, Ma LY, Cao GZ, Hua JH, Lv XT, Lin WC. Fk228 potentiates topotecan activity against small cell lung cancer cells via induction of slfn11. *Acta Pharmacol Sin*. (2022) 43:2119–27. doi: 10.1038/s41401-021-00817-y

48. Gardner EE, Lok BH, Schneeberger VE, Desmeules P, Miles LA, Arnold PK, et al. Chemosensitive relapse in small cell lung cancer proceeds through an ezh2-slfn11 axis. *Cancer Cell*. (2017) 31:286–99. doi: 10.1016/j.ccell.2017.01.006

49. Krushkal J, Silvers T, Reinhold WC, Sonkin D, Vural S, Connelly J, et al. Epigenome-wide DNA methylation analysis of small cell lung cancer cell lines suggests potential chemotherapy targets. *Clin Epigenet*. (2020) 12:93. doi: 10.1186/s13148-020-00876-8

50. Kundu K, Cardnell RJ, Zhang B, Shen L, Stewart CA, Ramkumar K, et al. Slfn11 biomarker status predicts response to lurbinectedin as a single agent and in combination with atr inhibition in small cell lung cancer. *Trans Lung Cancer Res*. (2021) 10:4095–105. doi: 10.21037/tlcr-21-437

51. Jo U, Arakawa Y, Zimmermann A, Taniyama D, Mizunuma M, Jenkins LM, et al. The novel atr inhibitor M1774 induces replication protein overexpression and broad synergy with DNA-targeted anticancer drugs. *Mol Cancer Ther*. (2024) 23(7):911–23. doi: 10.1158/1535-7163.c.7311489.v1

52. Zhang B, Stewart CA, Wang Q, Cardnell RJ, Rocha P, Fujimoto J, et al. Dynamic expression of schlafen 11 (Slfn11) in circulating tumour cells as a liquid biomarker in small cell lung cancer. *Br J Cancer*. (2022) 127:569–76. doi: 10.1038/s41416-022-01811-9

53. Tayoun T, Faugeroux V, Oulhen M, Déas O, Michels J, Brulle-Soumare L, et al. Targeting genome integrity dysfunctions impedes metastatic potency in non-small cell lung cancer circulating tumor cell-derived explants. *JCI Insight*. (2022) 7(11). doi: 10.1172/jci.insight.155804

54. Ramkumar K, Stewart CA, Cargill KR, Della Corte CM, Wang Q, Shen L, et al. Axl inhibition induces DNA damage and replication stress in non-small cell lung cancer cells and promotes sensitivity to atr inhibitors. *Mol Cancer Res: MCR*. (2021) 19:485–97. doi: 10.1158/1541-7786.Mcr-20-0414

55. Raynaud CM, Ahmed EI, Jabeen A, Sanchez A, Sherif S, Carneiro-Lobo TC, et al. Modulation of slfn11 induces changes in DNA damage response in breast cancer. *Cancer Cell Int*. (2023) 23:291. doi: 10.1186/s12935-023-03144-w

56. Winkler C, Armenia J, Jones GN, Tobalina L, Sale MJ, Petreus T, et al. Slfn11 informs on standard of care and novel treatments in a wide range of cancer models. *Br J Cancer*. (2021) 124:951–62. doi: 10.1038/s41416-020-01199-4

57. Mao S, Chaerkady R, Yu W, D'Angelo G, Garcia A, Chen H, et al. Resistance to pyrrolobenzodiazepine dimers is associated with slfn11 downregulation and can be reversed through inhibition of atr. *Mol Cancer Ther*. (2021) 20:541–52. doi: 10.1158/1535-7163.Mct-20-0351

58. Coussy F, El-Botty R, Château-Joubert S, Dahmani A, Montaudon E, Leboucher S, et al. Brcaness, slfn11, and rb1 loss predict response to topoisomerase I inhibitors in triple-negative breast cancers. *Sci Trans Med*. (2020) 12(531). doi: 10.1126/scitranslmed.aax2625

59. Willis SE, Winkler C, Roudier MP, Baird T, Marco-Casanova P, Jones EV, et al. Retrospective analysis of schlafen11 (Slfn11) to predict the outcomes to therapies affecting the DNA damage response. *Br J Cancer*. (2021) 125:1666–76. doi: 10.1038/s41416-021-01560-1

60. Konstantinopoulos PA, Cheng SC, Wahner Hendrickson AE, Penson RT, Schumer ST, Doyle LA, et al. Berzosertib plus gemcitabine versus gemcitabine alone in platinum-resistant high-grade serous ovarian cancer: A multicentre, open-label, randomised, phase 2 trial. *Lancet Oncol*. (2020) 21:957–68. doi: 10.1016/s1470-2045(20)30180-7

61. Kang MH, Wang J, Makena MR, Lee JS, Paz N, Hall CP, et al. Activity of mm-398, nanoliposomal irinotecan (Nal-iri), in ewing's family tumor xenografts is associated with high exposure of tumor to drug and high slfn11 expression. *Clin Cancer Res: Off J Am Assoc Cancer Res*. (2015) 21:1139–50. doi: 10.1158/1078-0432.Ccr-14-1882

62. Gartrell J, Mellado-Largarde M, Clay MR, Bahrami A, Sahr NA, Sykes A, et al. Slfn11 is widely expressed in pediatric sarcoma and induces variable sensitization to replicative stress caused by DNA-damaging agents. *Mol Cancer Ther*. (2021) 20:2151–65. doi: 10.1158/1535-7163.Mct-21-0089

63. Iwasaki J, Komori T, Nakagawa F, Nagase H, Uchida J, Matsuo K, et al. Schlafen11 expression is associated with the antitumor activity of trabectedin in human sarcoma cell lines. *Anticancer Res*. (2019) 39:3553–63. doi: 10.21873/anticanres.13501

64. Goss KL, Gordon DJ. Gene expression signature based screening identifies ribonucleotide reductase as a candidate therapeutic target in ewing sarcoma. *Oncotarget*. (2016) 7:63003–19. doi: 10.18632/oncotarget.11416

65. Waters T, Goss KL, Koppenhafer SL, Terry WW, Gordon DJ. Eltrombopag inhibits the proliferation of ewing sarcoma cells via iron chelation and impaired DNA replication. *BMC Cancer*. (2020) 20:1171. doi: 10.1186/s12885-020-07668-6

66. Croushore EE, Koppenhafer SL, Goss KL, Geary EL, Gordon DJ. Activator protein-1 (Ap-1) signaling inhibits the growth of ewing sarcoma cells in response to DNA replication stress. *Cancer Res Commun*. (2023) 3:1580–93. doi: 10.1158/2767-9764.Crc-23-0268

67. Lee TW, Wong WW, Dickson BD, Lipert B, Cheng GJ, Hunter FW, et al. Radiosensitization of head and neck squamous cell carcinoma lines by DNA-pk inhibitors is more effective than parp-1 inhibition and is enhanced by slfn11 and hypoxia. *Int J Radiat Biol*. (2019) 95:1597–612. doi: 10.1080/09553002.2019.1664787

68. He T, Zhang M, Zheng R, Zheng S, Linghu E, Herman JG, et al. Methylation of slfn11 is a marker of poor prognosis and cisplatin resistance in colorectal cancer. *Epigenomics*. (2017) 9:849–62. doi: 10.2217/epi-2017-0019

69. Liu Y, Zhang Z, Fu S, Wang S, Cheng X, Lei K, et al. Study of clinical predictive value and immune characterization of slfn11 in clear cell renal cell carcinoma. *Int J Gen Med*. (2021) 14:6741–54. doi: 10.2147/ijgm.S336823

70. Zheng Z, Cai Y, Chen H, Chen Z, Zhu D, Zhong Q, et al. Cxcl13/cxcr5 axis predicts poor prognosis and promotes progression through pi3k/akt/mtor pathway in

clear cell renal cell carcinoma. *Front Oncol*. (2018) 8:682. doi: 10.3389/fonc.2018.00682

71. Wu Z, Zhang Y, Chen X, Tan W, He L, Peng L. Characterization of the prognostic values of the cxcr1–7 in clear cell renal cell carcinoma (Ccrcc) microenvironment. *Front Mol Biosci*. (2020) 7:601206. doi: 10.3389/fmolb.2020.601206

72. Mauney CH, Hollis T. Samhd1: recurring roles in cell cycle, viral restriction, cancer, and innate immunity. *Autoimmunity*. (2018) 51:96–110. doi: 10.1080/08916934.2018.1454912

73. Zhang Z, Zheng L, Yu Y, Wu J, Yang F, Xu Y, et al. Involvement of samhd1 in dntp homeostasis and the maintenance of genomic integrity and oncotherapy (Review). *Int J Oncol*. (2020) 56:879–88. doi: 10.3892/ijo.2020.4988

74. Zhou C, Weng J, Liu C, Liu S, Hu Z, Xie X, et al. Disruption of slfn11 deficiency-induced ccl2 signaling and macrophage M2 polarization potentiates anti-pd-1 therapy efficacy in hepatocellular carcinoma. *Gastroenterology*. (2023) 164:1261–78. doi: 10.1053/j.gastro.2023.02.005

75. Murai Y, Jo U, Murai J, Fukuda S, Takebe N, Pommier Y. Schlafen 11 expression in human acute leukemia cells with gain-of-function mutations in the interferon-jak signaling pathway. *iScience*. (2021) 24:103173. doi: 10.1016/j.isci.2021.103173

76. Rathkey D, Khanal M, Murai J, Zhang J, Sengupta M, Jiang Q, et al. Sensitivity of mesothelioma cells to parp inhibitors is not dependent on bap1 but is enhanced by temozolomide in cells with high-schlafen 11 and low-O6-methylguanine-DNA methyltransferase expression. *J Thorac Oncol: Off Publ Int Assoc Study Lung Cancer*. (2020) 15:843–59. doi: 10.1016/j.jtho.2020.01.012

77. Tang SW, Thomas A, Murai J, Trepel JB, Bates SE, Rajapakse VN, et al. Overcoming resistance to DNA-targeted agents by epigenetic activation of schlafen 11 (Slfn11) expression with class I histone deacetylase inhibitors. *Clin Cancer Res: Off J Am Assoc Cancer Res*. (2018) 24:1944–53. doi: 10.1158/1078-0432.Ccr-17-0443

78. Zhao M, DiPeri TP, Raso MG, Zheng X, Rizvi YQ, Evans KW, et al. Epigenetically upregulating trop2 and slfn11 enhances therapeutic efficacy of trop2 antibody drug conjugate sacitizumab govitecan. *NPJ Breast Cancer*. (2023) 9:66. doi: 10.1038/s41523-023-00573-8

79. Knelson EH, Patel SA, Sands JM. Parp inhibitors in small-cell lung cancer: rational combinations to improve responses. *Cancers*. (2021) 13(4). doi: 10.3390/cancers13040727

80. Jo U, Murai Y, Agama KK, Sun Y, Saha LK, Yang X, et al. Top1-DNA trapping by exatecan and combination therapy with atr inhibitor. *Mol Cancer Ther*. (2022) 21:1090–102. doi: 10.1158/1535-7163.Mct-21-1000

81. Takashima T, Sakamoto N, Murai J, Taniyama D, Honma R, Ukai S, et al. Immunohistochemical analysis of slfn11 expression uncovers potential non-responders to DNA-damaging agents overlooked by tissue rna-seq. *Virchows Archiv: Int J Pathol*. (2021) 478:569–79. doi: 10.1007/s00428-020-02840-6

82. Isnaldi E, Ferraioli D, Ferrando L, Brohée S, Ferrando F, Fregatti P, et al. Schlafen-11 expression is associated with immune signatures and basal-like phenotype in breast cancer. *Breast Cancer Res Treat*. (2019) 177:335–43. doi: 10.1007/s10549-019-05313-w

frontiers | Frontiers in Oncology

TYPE Original Research
PUBLISHED 19 August 2025
DOI 10.3389/fonc.2025.1609735

OPEN ACCESS

EDITED BY
Giovanna Damia,
Mario Negri Institute for Pharmacological Research (IRCCS), Italy

REVIEWED BY
Er Yue,
City of Hope National Medical Center, United States
Fabiana Conciatori,
Hospital Physiotherapy Institutes (IRCCS), Italy

*CORRESPONDENCE
Ann Richmond
ann.richmond@vanderbilt.edu
Chi Yan
chi.yan@umanitoba.ca

†These authors have contributed equally to this work

RECEIVED 10 April 2025
ACCEPTED 16 July 2025
PUBLISHED 19 August 2025

CITATION
Yang J, Luo W, Ward P, Chen S-C, Zebala J, Maeda D, Yan C and Richmond A (2025) Combined treatment with CDK4/6, CDK2, and CXCR1/2 inhibitors effectively halts the growth of BRAF wild-type melanoma tumors. *Front. Oncol.* 15:1609735. doi: 10.3389/fonc.2025.1609735

Combined treatment with CDK4/6, CDK2, and CXCR1/2 inhibitors effectively halts the growth of BRAF wild-type melanoma tumors

Jinming Yang[1,2†], Weifeng Luo[1,2†], Patricia Ward[2], Sheau-Chiann Chen[3], John Zebala[4], Dean Maeda[4], Chi Yan[1,2,5,6*] and Ann Richmond[1,2*]

[1]Tennessee Valley Healthcare System (TVHS) Department of Veterans Affairs, Nashville, TN, United States, [2]Department of Pharmacology, Vanderbilt University, Nashville, TN, United States, [3]Department of Biostatistics, Vanderbilt University Medical Center, Nashville, TN, United States, [4]Syntrix Biosystems, Auburn, WA, United States, [5]Department of Immunology, Max Rady College of Medicine and Rady Faculty of Health Sciences, University of Manitoba, Winnipeg, MB, Canada, [6]Paul Albrechtsen Research Institute, CancerCare Manitoba, Winnipeg, MB, Canada

Introduction: Inhibitors of cyclin-dependent kinase 4 and 6 (CDK4/6) are approved for the treatment of locally advanced or metastatic breast cancer, but not for melanoma.

Methods: In this study, we evaluated the effectiveness of the CDK4/6 inhibitor, palbociclib, the CDK2 inhibitor, PF-07104091, the dual CXCR1 and CXCR2 (CXCR1/2) antagonist, SX-682, and the combination of these inhibitors for effective treatment of melanoma in preclinical models.

Results: Both palbociclib and SX-682 inhibited the growth of $BRAF^{WT}$/$NRAS^{WT}$ B16-F10 and $NRAS^{mut}$ 1014 melanoma tumors and in both models, SX-682 created a more anti-tumor immune microenvironment. The combination effect was additive in the B16F10 model, but not in the 1014 model. In the B16F10 model, the addition of the CDK2 inhibitor, PF-07104091, overcame B16F10 acquired resistance to CDK4/6 inhibitors by suppressing the induction of cyclin D1 and E1 expression by palbociclib. In the less responsive 1014 cells, cyclin D1 was reduced, but cyclin E1 was induced in response to PF-07104091. However, in both models, combined treatment with palbociclib and PF-07104091 markedly suppressed cyclin A2, cyclin D1, cyclin E1 and pRB-S807/S811. Combining CDK4/6 and CDK2 inhibitors with the CXCR1/2 antagonist, SX-682, halted B16F10 tumor growth by blocking tumor cell proliferation and increasing the anti-tumor immune response in the tumor microenvironment.

Conclusions: The combination of all three inhibitors resulted in a tumor microenvironment characterized by increased IFNγ-producing CD4+ T cells, decreased CD4+FOXP3+ T regulatory cells (Tregs), and decreased IL-10-producing CD4+ T cells. This combination also decreased the percentage of CD8+ T cells that expressed PD-1 or TIM-3 and increased the ratio of MHCII+F4/

80+ M1-like macrophages to CD206+F4/80+ M2-like macrophages. These data suggest that inhibiting CDK4/6 and CDK2, combined with antagonism of CXCR1/2, may be an effective treatment for BRAF wild-type melanoma tumors and NRAS mutant melanoma tumors that express Rb and are resistant to immune checkpoint inhibitors.

KEYWORDS

CDK inhibitors, CXCR2 antagonist, tumor immune microenvironment, tumor growth, melanoma

1 Introduction

Metastatic melanoma has the highest death rate in relation to incidence of any skin cancer (1). Recent advances in treatment have led to significant improvements in the outcomes for patients with melanoma. Immune checkpoint inhibitors (ICI) are the standard of care, with combined nivolumab and ipilimumab treatment yielding a median overall survival (OS) of 71.9 months in untreated advanced melanoma (2). Recently, a phase 2 trial involving 333 patients revealed that neo-adjuvant treatment of resectable stage III or stage IV melanoma with pembrolizumab significantly improved event-free survival (72%) compared to adjuvant-only treatment (49%) after 2 years (3). Despite the clinical success of ICI in advanced melanoma, outcomes remain sobering, with more than half of patients eventually progressing, after which median OS is only about 6 months (4, 5). The need for improved treatments thus remains high. It has been demonstrated that ICI is less effective for those melanoma tumors with an immunosuppressive tumor microenvironment (TME) (6). For metastatic melanoma patients who progress on ICI therapy, BRAF/MEK inhibitors offer an additional follow-up therapy option for patients with BRAF-mutant ($BRAF^{V600E}$) advanced melanoma. Adjuvant treatment of stage III resected melanoma with BRAF/MEK inhibitors provided a 71% OS at 8 years and a median progression-free survival (PFS) of 93.1 months. However, treatment with the BRAF inhibitor encorafenib plus the MEK inhibitor binimetinib provided only a seven-year 21.2% PFS and 27.4% OS in 192 patients with unresectable or metastatic BRAF-mutant melanoma who were treatment-naïve or had progressed on first-line immunotherapy (7). Another study of 589 stage III BRAF-mutant melanoma patients revealed that treatment with anti-PD1 monotherapy resulted in a similar OS compared to treatment with dabrafenib plus trametinib, and the median relapse-free survival was 51 months in the dabrafenib + trametinib treatment group compared to 44.8 months in the anti-PD-1 monotherapy group (8). However, based upon the results of the DREAMseq study, BRAF-mutant melanoma patients should first be treated with ICI, and if they progress, BRAF/MEK inhibitors can be highly successful (9).

In contrast, there are limited treatment choices for patients with NRAS-mutant or $BRAF^{WT}/NRAS^{WT}$ melanoma who progress after ICI therapy (i.e., *de novo* or acquired resistance). Based on the observation that the CDK4/6 pathway is frequently altered in melanoma, CDK4/6 inhibitors have emerged as potential agents for treating patients with NRAS-mutant and BRAF-wild-type tumors that have not lost the tumor suppressor retinoblastoma protein (pRb) (10, 11). Indeed, two ongoing clinical trials are evaluating the efficacy of CDK4/6 inhibitors, particularly when combined with a MEK inhibitor as part of a multidrug regime (NCT04720768 and NCT02645149) (12). CDK4/6 inhibitors have been reported to augment the anti-tumor memory T cell pool and improve the response to subsequent anti-PD-1 therapy, expanding the T effector population (13). However, sequential, rather than simultaneous, treatment of CDK4/6 inhibitors with anti-PD-1 or BRAF/MEK therapy is advised to optimize the positive and mitigate the adverse immunomodulatory effects of each treatment on the TME (14). Resistance mechanisms to CDK4/6 inhibition have been identified, which involve the induction of Cyclin D1, which sequesters p21 and p27, thereby leaving CDK2 uninhibited. Additionally, resistance to CDK4/6 inhibitors in breast cancer is acquired through CDK2-mediated phosphorylation of c-MYC, which enables cells to escape senescence. Thus, the synergistic antiproliferative effect of the combined inhibition of CDK2 and CDK4/6 in breast cancer can overcome acquired resistance to CDK4/6 inhibitors by enhancing senescence (15).

The gene encoding the cyclin-dependent kinase inhibitor 2A (CDKN2A) is frequently lost or mutated in 40-70% of sporadic melanoma tumors, and 20-40% of familial melanomas (10). It has been shown that melanoma tumors with loss of CDKN2A are often highly sensitive to CDK4/6 inhibition (16). We have previously demonstrated that combined treatment with a CDK4/6 inhibitor and an MDM2 inhibitor suppresses the growth of melanoma patient-derived xenografts and that knockdown of CDK2 overcomes resistance to CDK4/6 inhibition (17).

Melanoma tumors often exhibit an immune suppressive TME and secrete various cytokines and chemokines that are key signals involved in the recruitment of MDSCs. MDSCs express the CXC chemokine receptor 1 and 2 (CXCR1/2), and their ligands are produced by melanoma cells (18). Thus, CXCR1/2 not only regulates neutrophil trafficking from the bone marrow to peripheral circulation or inflammation sites (19) but also plays a

role in tumor progression by facilitating the migration of tumor-associated myeloid cells into the TME (20). Therefore, targeting CXCR1/2 should alter the accumulation of tumor-associated myeloid cells and MDSCs in the TME, favoring a less immune-suppressive TME (21, 22). We have previously demonstrated that the treatment of mice bearing genetically derived inducible melanoma tumors (BRAF/PTEN or NRAS/INK4a) with the CXCR1/2 antagonist (SX-682) inhibited tumor growth and increased activated CD8+ T cells, partly by reducing the intratumoral MDSCs (6). There are ongoing clinical trials combining SX-682 with anti-PD-1 to treat advanced metastatic melanoma (23). These compelling studies from solid tumors in either mice or humans prompted us to investigate the therapeutic potential of combining CDK inhibitors and SX-682 for treating $NRAS^{mut}$ and $BRAF^{WT}$ melanoma. Here, we initiate a preclinical study using murine $BRAF^{WT}$ murine B16-F10 melanoma and $NRAS^{mut}$ 1014 melanoma cells to examine the effectiveness of combining the CXCR1/2 antagonist, SX-682, with the CDK4/6 inhibitor, palbociclib. We also evaluate the addition of the CDK2 inhibitor, tagtociclib (PF-07104091) (24), to this treatment regimen and assess whether this triple- drug combination results in greater inhibition of tumor growth in the B16F10 mouse model of melanoma.

2 Materials and methods

2.1 Mouse melanoma tumor model

All mouse experiments were performed under a protocol approved by the Vanderbilt IACUC committee (#M2000008), and guidelines were strictly adhered to. C57/Bl6 female mice of 8-10 weeks old were purchased from Charles River (Wilmington, MA, RRID: IMSR_CRL:027). B16-F10 melanoma cells (ATCC, RRID : CVCL_0159) that carry amplifications of *Braf* and *Met* oncogenes and missense mutations of the tumor suppressor *Pten*, and loss of CDKNA (25) or 1014 $NRAS^{Q61K}/PTEN^{WT}/CDKN2A^{WT}$ expressing melanoma cells (the kind gift of Lionel Larue, Institut Curie, Centre Universitaire (26), were examined for mycoplasma contamination monthly and any contaminated cultures were discarded. Authentication of genotypes for these cell lines was determined by DNA sequence analysis. Tumor cells were implanted subcutaneously on both sides of the intrascapular region of the mouse (3 x 10^5 for B16F10 and 3 x10^5 for 1014 cells). When the tumor size reached approximately 125mm^3, mice were randomly assigned to two groups: half the tumor-bearing mice were fed regular chow, and the other half were fed chow containing SX-682 (1,428 mg/kg of chow), as previously described, but at a dose was twice that previously used (6). The toxicity and plasma levels of SX-682 administered PO *ad libitum* in chow have been previously described (6, 27, 28). We have previously compared the effects of SX-682 treatment to the targeted knock out of CXCR2 on myeloid cells or melanocytic cells, where treatment with SX-682 had similar effects on tumor growth as targeted knock out of CXCR2, indicating good drug delivery (6, 27). Half the mice in each chow-fed treatment group were randomly assigned to receive oral gavage containing either vehicle alone or palbociclib (100 mg/kg bodyweight) daily for 5 days per week. In some experiments, mice received both palbociclib (100 mg/kg) and the CDK2 inhibitor PF-07104091 (50 mg/kg) in two separate gavages with or without SX-682-containing chow. When two different vehicle controls were used, two separate vehicle gavages were administered. The body weight and tumor size of mice were measured twice a week. Tumor volume was determined as 0.5 x length x width x width. Power analysis indicated that an n of 5 mice per group provided sufficient power to detect differences with a p-value ≤ 0.05 approximately 80% of the time. Only female mice were used due to the issue of male mice fighting if not bred as siblings.

2.2 Reagents

Palbociclib-HCL (PD-0332991)(Cat# S1116, Selleckchem, 99.82% purity) was dissolved in water (50°C, 100 mg/10 ml). The CDK2 inhibitor, tagtociclib (PF-07104091) (Cat#CT-PF0710, Chemietek, >99% pure) was dissolved in DMSO (81 mg/ml) for *in vitro* experiments. For *in vivo* experiments, PF-07104091 was dissolved in 5% DMSO, 40% PEG 300, 5% Tween 80, and 50% water. In addition, chow containing SX-682 (1,428 mg/kg of chow, Syntrix Pharmaceuticals) or chow containing vehicle control was used as previously described (27). Monoclonal antibodies (mAb) to phospho-Rb (Ser807/811) (D20B12, XP® rabbit mAb Cat#8516, RRID: AB_11178658), Cyclin D1 (E3P5S, XP® rabbit mAb Cat#55506, RRID: AB_2827374), Cyclin A2 (E9Q5G, rabbit mAb Cat#81754), and Cyclin E1 (D7T3U, rabbit mAb #20808) were purchased from Cell Signaling Technology.

2.3 Flow cytometry analysis and antibodies

For flow cytometry, tissues were minced on a programmable gentleMACS dissociator (Miltenyi Biotec, USA) and digested with an enzyme solution of collagenase 1 (1,500 CDU, CAT#234153, Calbiochem), dispase II (1 mg/mL, CAT#13689500, Roche), and DNase I (0.1 mg/mL, CAT#260913, Calbiochem). Staining and analysis protocols were according to our previously published methodology (6). Cells were incubated with Ghost Dye TM Violet 510 (Tonbo Biosciences), an amine-reactive viability dye used to discriminate live/dead cells and then washed with fluorescence-activated cell sorting (FACS) buffer (PBS containing 2% v/v FBS). After blocking Fc receptors with anti-mouse CD16/CD32 (BioLegend) in FACS buffer for 15 minutes, cells were incubated with fluorescence-conjugated mAbs specific to mouse immune cell surface or intracellular markers (BD Cytofix/Cytoperm Plus Kit#554715), indicated below for an additional 30 minutes on ice. Cells were washed twice in FACS buffer (23), data were acquired with a FACSCanto II flow cytometer (Becton Dickinson), and data (FCS files) were analyzed using FlowJo software (Version 10.1, RRID: SCR_008520). For cell-surface markers, the following monoclonal antibodies (mAbs) from eBioscience were used:

CD11b-FITC (clone M1/70), CD3-FITC (clone 17A2), CD3-PECy5 (clone 17A2), CD103-Brilliant Violet 421 (clone 2E7), CD4-Pacific Blue (clone RM4–4), CD4-APC/Cy7 (clone RM4–4), CD8-PECy7 (clone 53–5.8), CD11c-APC (clone N418), CD19-PECy7 (clone N418), B220-APC (clone RA3–6B2), CD45-PerCp/Cy5.5 (clone 30-F11), CD45-APC/Cy7 (clone 30-F11), CD44-APC/Cy7 (clone IM7), NK1.1-APC/Cy7 (clone PK136), F4/80-Pacific Blue (clone BM8), CD69-APC (clone H1.2F3), CD107b-Alexa Fluor 647 (clone M3/84), CD62L-Alexa Fluor 647 (clone MEL-14), Ly6G-APC (clone 1A8), Ly6C-Alexa Fluor 647 (clone HK1.4), CD25-PerCp/Cy5.5 (clone 3C7), CD44-APC (clone IM7), MHC II-Alexa Fluor 647 (clone AF6–120.1), CD206-PE (clone C068C2), PD-1-APC/Cy7 (clone 29F.1A12), PD-L1-APC (clone 10F.9G2). For intracellular markers, monoclonal antibodies (mAbs) from BioLegend were used as follows: Foxp3-Alexa Fluor 647 (clone 150D), and Ki67-Pacific Blue (clone 16A8). We also used the following antibodies: IFNγ-Alexa Fluor 700 (clone XMG1.2, from BD Bioscience); Gost Dye violet 450, Gost Dye violet 510, and Gost Dye violet 780 (from Tonbo Biosciences).

2.4 Western blot analysis

After culturing 1014 or B16F10 melanoma cells in DMEM/F12 (1:1) with 10% FBS to 75% confluence, cells were treated with 20 μM Palbociclib and 20 μM PF-07104091 for 24 hours. Media was removed, and the cells were rinsed with cold PBS. The whole-cell lysates were prepared using RIPA buffer (Fisher Scientific, Cat. # PI89900) supplemented with a protease inhibitor cocktail (Roche, Cat. # 04693124001) and a phosphatase inhibitor cocktail (Roche, Cat. # 4906845001). The protein concentration was measured using Pierce™ BCA Protein Assay Kits (Thermo Scientific, Cat. # 23225). 40 μg of protein was separated on 4–20% Precast Midi Protein Gel (BioRad, Cat. # 5671094) and transferred to nitrocellulose membrane using Trans-Blot Turbo RTA Transfer Kit (Nitrocellulose, BioRad, Cat. # 1704272). Blots were blocked with Intercept Blocking Buffer (TBS) (LI-COR, Cat. # 927 60001) for 1 hour. Primary antibodies were diluted with Intercept Antibody Diluent (TBS) (LI-COR, Cat. # 927 65001). Blots were incubated with primary antibodies overnight at 4°C. These antibodies were purchased from Cell Signaling Technology: Cyclin A2 (Cat. # 81754), Cyclin D1 (Cat. # 55506), Cyclin E1 (Cat. # 20808), phospho-Rb S807/S811 (Cat. # 8516), and Caspase-3 (Cat. # 9662). Beta actin antibody was from Invitrogen (Cat. # MA5-15739). These secondary antibodies were used: IRDye® 800CW Goat anti-Rabbit IgG (H + L) (LI-COR, Cat. # 926-32211), IRDye® 680RD Goat anti-Mouse IgG (LI-COR, Cat. # 926-68070). Protein bands were visualized using the Odyssey CLx Imager (LI-COR). To detect cleaved caspase-3, the ECL Western blotting method was used. Blot was blocked with 5% non-fat milk in TBS buffer with 0.1% Tween-20 for 1 hour, then incubated with anti-cleaved caspase-3 (Cell Signaling Technology, Cat. # 9661) overnight at 4°C. After washing, the blot was incubated with the secondary antibody anti rabbit IgG-HRP (Cell Signaling Technology, Cat. # 7074P2) for 1 hour. After washing five times, the blot was incubated with SuperSignal™ West Pico PLUS Chemiluminescent Substrate for 5 minutes, and signals were captured using HyBlot CL® Autoradiography Film (Thomas Scientific). All western blot bands were quantified with Image Studio software, and data were statistically analyzed using One-way ANOVA and Tukey's test.

2.5 Cell cycle analysis

Cell cycle analysis by flow cytometry was based on measurement of DNA content by staining with propidium iodide (PI). Melanoma cells (B16-F10 and 1014) were plated in 6-well plates in DMEM/F-12 medium (Gibco, Cat. # 11330-032) + 10% FBS (Atlas Biologicals, Cat. # F-0500-A). When cell confluence reached approximately 80%, cells were treated with either 20 μM palbociclib alone, or 20 μM PF-07104091 alone, or 20 μM palbociclib plus 20 μM PF-07104091, or with vehicle control. After 24 hours of treatment, cells were trypsinized, and the cells in the media were also collected. After washing once with PBS, cells were fixed with 70% ethanol for 48 hours at -20°C. Cells were washed once, and the cells were counted for each sample. Cells were stained for 24 hours at 4°C at 1 x10^6/ml with PI stain solution [PBS buffer with 0.1% Triton-X100, 200 μg/ml RNase (Qiagen, Cat. #11330-032), and 20 μg/ml PI (Sigma-Aldrich, Cat. # P4864)]. PI fluorescence was collected using 5-laser BD LSRFortessa flow cytometer, and data were analyzed with BD FACSDiva 8.0.2.

2.6 Cell viability and apoptosis assay

B16F10 (from ATCC) and 1014 (the kind gift of Lionel LaRue, Pasteur Institute) melanoma cells were grown in DMEM/F-12 + 10% fetal bovine serum(FBS) in a 37°C, 5%CO2 humidified incubator (ThermoFisher Heracell Vios 160i) until cells were at approximately 80-90% confluent in T150 flask (Corning Cat. #431465). Cells were trypsinized with 0.05% trypsin, 0.53 mM EDTA 1X (Corning Cat. #25-052-CI) for 5 minutes in a humidified CO2 incubator and then checked under the microscope to ensure that all cells had been released from the flask.

Cells were collected from the flask and counted by using a cell counter (Gibco Cell Countess II). Cells were then plated at 10,000 cells/well in each 96-well plate (Genesee Scientific Cat. #25-109MP and Thermoscientific Cat. #165305 [optical bottom plate with black base]) in triplicate using FluoroBrite DMEM (Gibco Cat. #A18967-01)+ 10% FBS (100μL). Cells were allowed to attach to plates overnight, and treatments were initiated the next day. The zero (0) concentration was a DMSO control diluted in the same manner as the highest concentration of the PF inhibitor. The treatments were as follows: palbociclib (palbo) alone at final concentrations of 100nM, 500nM,1μM, and 10μM, PF-07104091 inhibitor (PF) alone at final concentrations of 50nM,100nM, 500nM,1μM, and 10μM, and for the four concentrations of Pablo each of the five concentrations of PF inhibitor were added (ex. 100nM palbociclib +50nM PF inhibitor, 100nM palbociclib + 100nM PF inhibitor, 100nM palbociclib + 500nM PF inhibitor, 100nM palbociclib + 1μM PF inhibitor, and 100nM palbociclib + 10μM PF inhibitor).

Treatment solutions were prepared at a 2X concentration of inhibitor in FluoroBrite DMEM media, with a final volume of 50µL. Removal of 50 µL of the original 100 µL of plated media was performed using a multichannel pipet and 50 µL of the treatments was added in triplicate wells following the template. Treatments were for 48, 72 or 144 hours. Cell viability was determined using the Cell Titer Blue assay (Promega, Cat. #G808A). Triplicate wells were set up with 100µL media containing no cells for background readings. The average of these three wells was subtracted from the reading of each treated well. The DMSO control wells were assigned a value of 100% viability, and a % viability was assigned to each treatment group and graphed based on this determination.

Apoptosis was determined by using the APO-One Homogeneous Caspase 3/7 assay (Promega, Cat. #G7791). Triplicate wells were set up with 100µL media with no cells for background readings. The average of these three wells were subtracted from the reading of each treated well. The amount of apoptosis is determined by the RFU reading from each well. These readings were averaged across the triplicate plates and graphed based on the RFU readings from each treatment ± standard deviation (SD). Statistical analysis was by ANOVA (Type III test). Additionally, we evaluated the RFU readings on a per cell basis to determine whether loss of cells contributed to reduction in the RFU readings per well.

2.7 Protein array

Mouse serum samples were prepared and examined in protein arrays using Mouse Antibody L308 Array Kit (308 proteins) (Cat. # AAM-BLG-1-4, RayBiotech), per the manufacturer's protocol. A serum sample was taken from two B16F10 tumor-bearing mice in each treatment group for analysis. The glass chip was scanned on the Cy3 channel of a GenoPix 4000B scanner (Genopix 6.1, Molecular Devices, Sunnyvale, CA). For each spot, the net density was determined by subtracting the background.

2.8 Statistical analysis

Statistical analyses were performed using Prism software version 8.3.0 (GraphPad Software, RRID : SCR_002798). Data were summarized in figures displaying the mean ± SD. Treatment effects in standard two-group experiments were compared using a two-way ANOVA with unequal variances or the Wilcoxon rank-sum test. For Western blot data, a one-way ANOVA was used with unequal variances and Tukey's multiple comparisons test. Where indicated, *$p < 0.05$; **$p < 0.01$; ***$p<0.001$; ****$p<0.0001$. For statistical analysis of the effects of targeted therapies on tumor volume, a mixed-effects model was used to account for the correlation among repeated measurements per mouse over time. Tumor volume was analyzed on a natural log scale to reduce heterogeneity. The mean tumor growth rates were estimated based on least-square means and compared using the Wald test. Pairwise comparisons were adjusted for p-values using the Holm correction.

A test for synergism between treatments was conducted, and a synergistic effect on tumor volume over time was defined as an effect from the drug combination (effect i) that exceeds the sum of the effects of each drug (effects a and b) (i.e., i>a+b). To evaluate this, a mixed-effects model including both individual and interaction effects was used to assess the impact of the drug combination on tumor volume over time. Model-based (least-squares) means were used to estimate average tumor growth for each treatment group. Synergism was evaluated using a multiple comparisons procedure within a generalized linear hypothesis testing framework, comparing the null hypothesis ($i \leq a + b$) against the alternative ($i > a + b$). Standard residual diagnostics were also performed to validate model assumptions.

3 Results

3.1 Cell cycle CDK4/6 and CDK2 inhibitors differentially affect the cell viability and apoptosis of melanoma cells

We first evaluated the effects of the CDK4/6 inhibitor palbociclib, the CDK2 inhibitor PF-07104091, or the combination of drugs on cell viability based on quantitation of cell titer blue staining. Cultured B16-F10 cells and 1014 cells were treated with palbociclib or PF-07104091 over a concentration range of 0 to 10 µM for 48, 72 or 144 hours. We observed a dose-dependent inhibition of cell viability in B16F10 (100 nM -10 µM) and 1014 (100 nM to 10 µM) in response to palbociclib over a 48, 72 and 144 hour time frame. However, the 1014 cells exhibited a greater reduction in viability at the 48- and 72-hour time points at a 10 µM concentration of palbociclib than the B16F10 cells (Figure 1A, Supplementary Figure S1). In contrast, at the 48-, 72- and 144-hour timepoints there was only a modest reduction in cell viability in response to PF-07104091 (50 nM to 10 µM) in both B16F10 and the 1014 cells showed a 60% inhibition in viability after 144 hours treatment with 10µM PF-07104091 (Figure 1B, Supplementary Figure S1). Interestingly, the addition of only 50 nM PF-07104091 to 1µM palbociclib significantly reduced the viability in B16F10 cells ($p<0.001$), while addition of 100 nM ($p<0.01$)or 1 µM ($p<0.001$) of PF-07104091 to 1 µM palbociclib significantly inhibited the viability of 1014 cells after 144 hours of treatment (Figure 1C, Supplementary Figure S1). To observe the induction of apoptosis of B16F10 and 1014 melanoma cells over time in response to palbociclib, we examined caspase 3/7 activity over 48 hours. Only modest induction of apoptosis occurred with 10 nM-1 µM concentrations of palbociclib in B16 melanoma cells, but 10 µM palbociclib induced a significant amount of apoptosis (Figure 1D). PF-07104091 did not significantly affect caspase 3/7 activity in B16F10 melanoma cells (Figure 1E). However, when combined with 1 µM palbociclib and increasing concentrations of PF-07104091, there was a significant increase in caspase 3/7 activity at the 10 µM concentration of PF-07104091 (Figure 1F). In contrast, 1014 cells exhibited highly variable levels of apoptosis which trended upward without showing a significant induction of

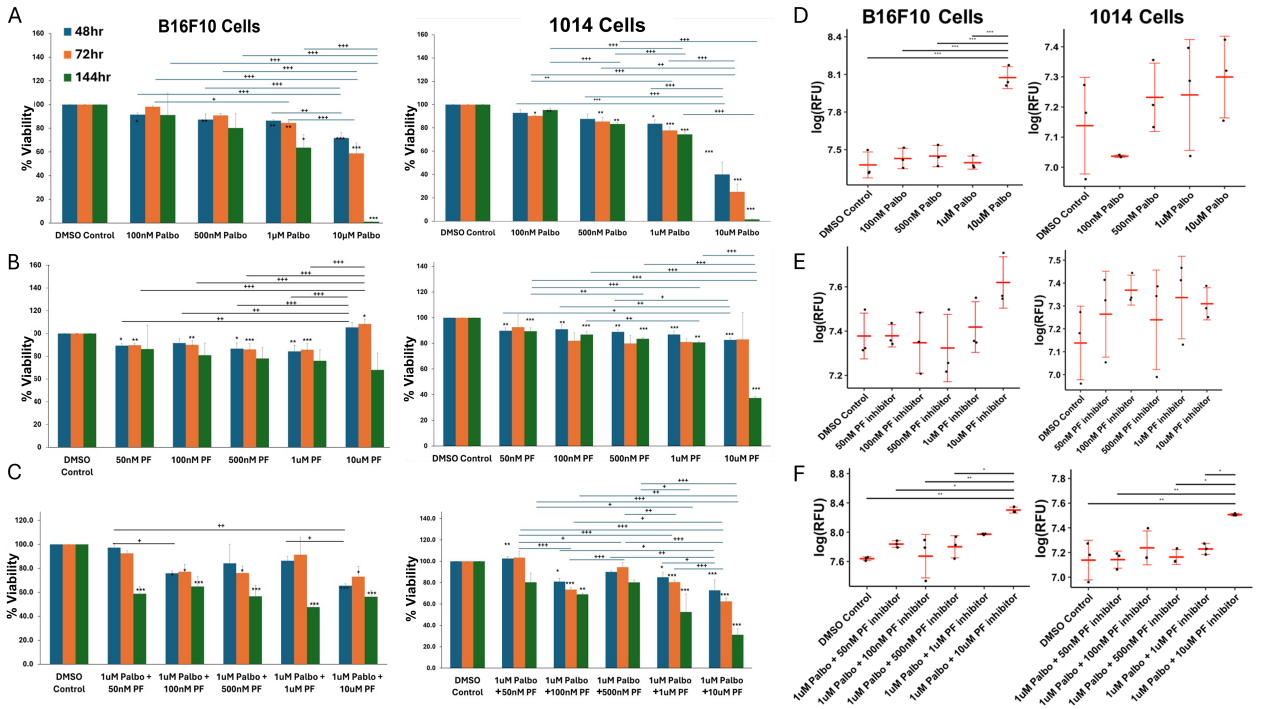

FIGURE 1
Cell cycle CDK4/6 and CDK2 inhibitors differentially affect melanoma cell viability and apoptosis. **(A)** effects of palbociclib or PF-07104091 on the *in vitro* viability/growth of B16-F10 melanoma cells over a concentration range of 100 nM to 10μM after 48h hour exposure; effect of PF-07104091 (PF-07104091 50 nM to 10 μM) on the viability/growth of B16F10 cells after 48h hour exposure; effect of 1μM palbociclib combined with concentrations of 50nM to 10μM of PF-07104091 on the viability/growth B16F10 melanoma cells after 48h hour exposure. **(B)** effects of palbociclib or PF-07104091 on the *in vitro* viability/growth of 1014 melanoma cells over a concentration range of 100 nM to 10 μM after 48h hour exposure; effect of PF-07104091 (PF-07104091 50nM to 10μM) on the viability/growth of 1014 cells after 48h hour exposure; effect of 1 μM palbociclib combined with concentrations of 50 nM to 10 μM of PF-07104091 on the viability/growth melanoma cells after 48 hour exposure. **(C)** palbociclib (5 or 10 μM) reduced the G1 to S-G2 transition of B16-F10 melanoma after a 24 hour exposure. **(D)** effects of palbociclib or PF-07104091 on the *in vitro* apoptosis of B16-F10 melanoma cells over a concentration range of 100nM to 10 μM after 48h hour exposure; effect of PF-07104091(50 nM to 10 μM) on the apoptosis of B16F10 cells after 48h hour exposure; effect of 1 μM palbociclib combined with concentrations of 50 nM to 10 μM of PF-07104091 on the viability/growth B16F10 melanoma cells after a 48 hour exposure. **(E)** effects of palbociclib or PF-07104091 on the *in vitro* apoptosis of 1014 melanoma cells over a concentration range of 100 nM to 10 μM after 48h hour exposure; effect of PF-07104091 (50 nM to 10 μM) on the viability/growth of 1014 cells after a 48h hour exposure **(F)**; effect of 1μM palbociclib combined with concentrations of 50 nM to 10 μM of PF-07104091 on the viability/growth melanoma cells after a 48 hour exposure. Data are shown as RFUs of caspase activity at each concentration of palbociclib. Adjusted p-values were analyzed using the Holm test to adjust for multiple comparisons. Adj. Sig. ***p<0.001, **p<0.01, and *p<0.05. The stars over the histogram indicate values that are significantly different from the DMSO control. The stars over the bars indicate the specific differences between treatment groups as indicated.

caspase activity at the 48-hour timepoint to palbociclib or PF-07104091 (Figures 1D, E), though the combination of 1 μM palbociclib and 1 μM PF-07104091 as well as 1 μM palbociclib and 10μM PF-07104091 significantly increased apoptosis (Figure 1F). It is unclear why we did not detect increases in caspase activity in 1014 cells in response to palbociclib at the 48-hour timepoint, although we did observe a reduction in viability at this time point. However, when we analyzed RFU/cell, we did detect significant induction of APO-One activity with the 10 μM concentration of palbociclib at the 48-hour timepoint in 1014 cells. We speculate that the early loss of dying cells floating in the media may have contributed to the inability to capture a significant difference in the total RFU for caspase activity in each well of cells. At the 72- and 144-hour time points there were greater increases in caspase 3/7 activity in response to single treatment and combination treatments (Supplementary Figure S1). Notably, the combination of 10 μM palbociclib and 10 μM PF-07104091 resulted in the elimination of melanoma cell viability after 48 hours of drug treatment (Supplementary Figure S1).

3.2 CDK4/6 and CDK2 inhibitors modulate cell cycle and cyclin levels and reduce the hyperphosphorylation of Rb

It is known that for cells to transit from the G1 to S phase in the cell cycle, the tumor suppressor pRb needs to become hyperphosphorylated (29). This hyperphosphorylation is catalyzed by the complex formed by CDK4/6 and the cyclin group of related D cyclins of which cyclin D1 is a member), as well as by the CDK2/Cyclin complex. Upon CDK4/6 phosphorylation of pRb, it becomes partially inactivated, releasing the E2F transcription factors, which activate the E2F transcriptional program, including cyclin E1. Cyclin E1 binds to CDK2 to form an

active complex that fully phosphorylates Rb, resulting in the full activation of the E2F transcriptional program and progression through the S-phase of the cell cycle. The transcription factor E2F is released, transcription of E2F regulated cell cycle genes, including Cyclin E1 ensues, and cells progress to S phase (30–32).

To evaluate the effects of CDK4/6 and CDK2 inhibitors on the cell cycle of B16F10 and 1014 melanoma cells, we chose a 24-hour treatment time to ensure capture of early and drug-specific effects. After examining a range of drug concentrations, we found that 20 µM concentrations of the drug, but not 10 µM concentrations, had significant effects on the cell cycle at the 24-hour time point. Therefore, subsequent experiments were performed with 20 µM concentrations of the drugs. We observed that 24-hour treatment of B16F10 cells with 20 µM palbociclib reduced the percentage of cells in S phase and had no significant effect on the percentage of cells in G1 or G2. At the same time, PF-07104091 increased the percentage of cells in S phase, decreased the percentage in G1 phase, and increased the percentage of cells in G2 and subG$_0$ (dying cells) compared to untreated control. The combination of palbociclib and PF-07109091 decreased the percentage of cells in G1, increased the percentage in S and G2 and markedly increased the dying cells in subG$_0$ compared to the untreated control (Figures 2A, B, upper panel). In 1014 cells the 24-hour, 20 µM treatment with palbociclib resulted in a decrease in sub-G$_0$, an increase in G1, but no change in S or G2 phases as compared to control. PF-07104091 (20 µM) decreased the percentage of cells in sub G$_0$ and G1 but increased the percentage of cells in S and G2 compared to control. The combination treatment decreased the percentage of cells in G1, had no effect on cells in S of sub G$_0$ phase, and increased the percentage of cells in G2 as compared to control (Figures 2A, B, lower panel). A diagram showing the expected effects of CDK4/6 and CDK2 inhibitors on cell cycle proteins is shown in Figure 2C.

To evaluate the effects of CDK4/6 and CDK2 inhibitors on cyclin and cleaved caspase 3 protein levels we again utilized a 24-hour time period and treated cells with high concentrations of inhibitors (20 µM) to effectively maximize the ability to capture inhibitor-induced changes in cell cycle proteins by Western blot analysis. In B16F10 melanoma cells, palbociclib decreased protein levels of cyclin A2 but increased cyclin D1 and cyclin E1 protein levels (Figure 2D). The CDK2 inhibitor decreased protein levels of cyclin A2 and cyclin D1 and had no significant effect on cyclin E1 protein levels. Combined treatment of B16-F10 cells with palbociclib (20µM) and the CDK2 inhibitor PF-07104091 (20µM) resulted in a reduction of both cyclin A2 and cyclin D1, reversed the

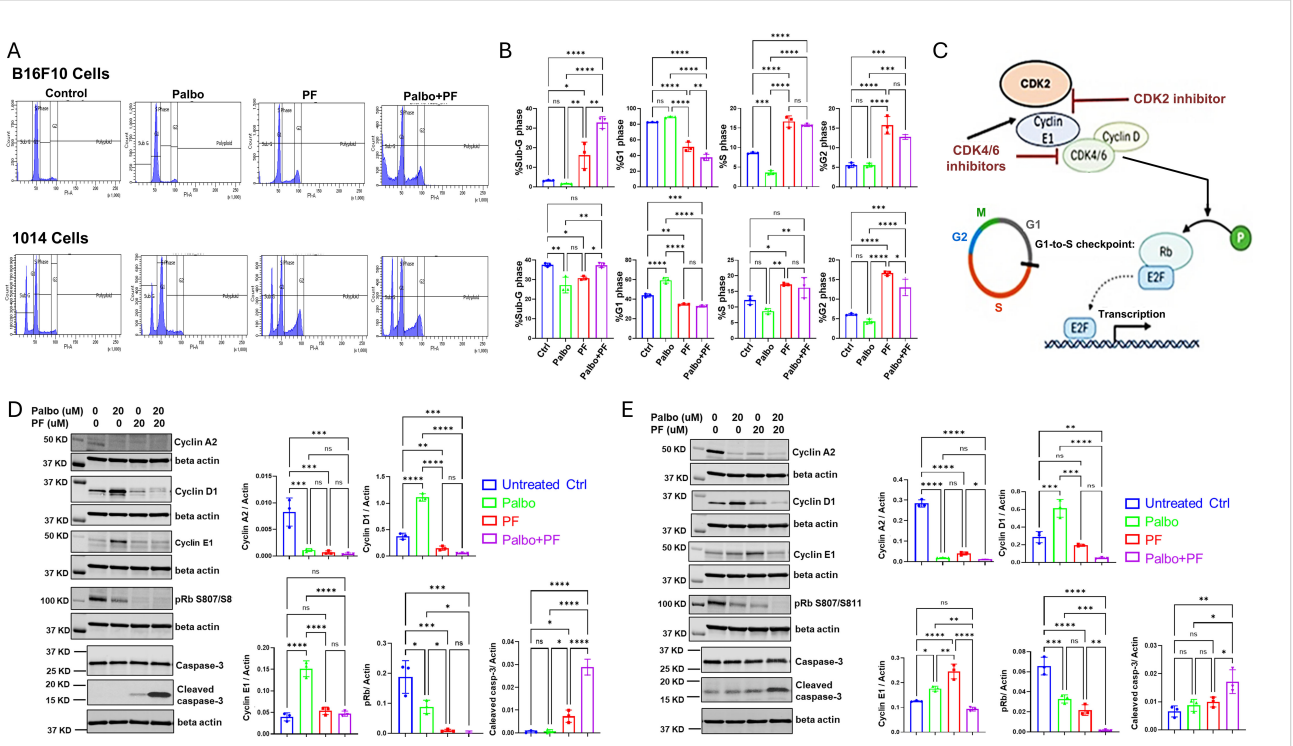

FIGURE 2
CDK4/6 and CDK2 inhibitors modulate cell cycle and cyclin levels and reduce the hyperphosphorylation of Rb in Braf-wild type melanoma. **(A)** representative flow cytometry cell cycle analysis for B16F10 and 1014 cells after treatment with control, palbociclib, PF-07104091, or the combination for 24 hours. **(B)** quantitation and statistical analysis of flow cytometry triplicate analysis of the effects of palbociclib, PF07104091, or their combination on cell cycle as compared to control. **(C)** diagram showing how the cascade of cyclin and pRb phosphorylation regulates the cell cycle and how cyclin E1 is up-regulated by palbociclib and down-regulated by the combined treatment of palbociclib and PF-07104091 in B16-F10 melanoma cells. **(D)** immunoblots and quantitative analysis of triplicate analysis of cell cycle proteins Cyclin A2, Cyclin D1, Cyclin E1, pRb, and cleaved caspase 3 in B16-F10 cells treated for 24 hours with either vehicle, palbociclib (20 µM), PF-07104091 (20 µM) or both inhibitors at 20 µM. **(E)** immunoblots and quantitative triplicate analysis of cell cycle proteins Cyclin A2, Cyclin D1, cyclin E1, pRB, and cleaved caspase 3 in 1014 cells treated with either vehicle, palbociclib (20 µM), PF-07104091 (20 µM) or both inhibitors at 20 µM. * p<0.05; ** p<0.01; *** p<0.001; **** p<0.0001; ns, non significant.

palbociclib induction of cyclin E1, and strongly induced cleaved caspase 3 levels (Figure 2D). Hyperphosphorylation of Rb(S807/811) was reduced by treatment with palbociclib (20μM) and was blocked entirely by PF-07104091 (20 μM), with the combination of palbociclib and PF-07104091 not having an effect greater than PF-07104091 alone (Figure 2D).

In 1014 cells, palbociclib (20μM) significantly reduced protein levels of cyclin A2, increased cyclin D1 levels and cyclin E1 levels, and reduced hyperphosphorylation of Rb (S807/S811). PF-07104091 (20μM) decreased cyclin A2 levels, had no significant effect on cyclin D1 levels, increased cyclin E1 levels and cleaved caspase 3 and reduced hyperphosphorylation of Rb (S807/S811). The combination treatment with palbociclib (20μM) and PF-07104091 (20μM) significantly reduced cyclin A2, reduced cyclin D1, and blocked phosphorylation of Rb (S807/S811). It reversed the elevations of cyclin E1 by each agent alone, restoring cyclin E1 levels to the control level (Figure 2E). The combination treatment also strongly induced cleavage of caspase 3 (Figure 2D).

The individual inhibitors and their combination resulted in a decrease in cyclin A2 levels (Figures 2D, E), which is similar to a previous report by Arora et al. in breast cancer cells. However, the concentration of the drug used here was higher (24). It is curious that, despite nearly complete inhibition of hyperphosphorylation of Rb S807/811 in response to 20 μM of PF-07104091 in B16F10 melanoma cells (Figure 2D), treatment with 10 μM of PF-07104091 for up to 48 hours had only a modest effect on cell viability (Figure 1A). In contrast, the 1014 cells were less sensitive to PF-07104091 regarding the reduction in Rb phosphorylation. However, the 24-hour treatment with a combination of palbociclib (20 μM) and PF-07104091 (20 μM) effectively blocked Rb807/811 phosphorylation and induced cleaved caspase 3 in both B16F10 and 1014 cells.

3.3 The CXCR1/2 antagonist, SX-682, affects the growth-inhibitory effect of palbociclib and anti-tumor immunity *in vivo*

To evaluate the hypothesis that the previously demonstrated anti-tumor effects of palbociclib on the memory CD8 T-cell pool (13) would be enhanced by co-treatment with SX-682, which has been shown to reduce the recruitment of myeloid-derived suppressor cells (MDSCs) into the TME, we compared the effects of palbociclib alone versus palbociclib in combination with the CXCR1/2 antagonist SX-682 on the tumor growth of B16-F10 melanoma in C57BL/6 mice. Tumor-bearing mice (5 mice/group) were treated with 100 mg/kg per day palbociclib HCL alone (5 days/week) or combined with chow containing SX-682. Because these tumors grow very rapidly, treatment was initiated when the tumor diameter was ~5mm yielding a tumor volume of ~125mm^3 to ensure that here was adequate time to monitor response to drug before control mice had to be euthanized due to tumor burden. Moreover, this ensures that at the end point, the tumors have not developed sufficient necrosis to limit the evaluation of the TME by flow cytometry. The anti-tumor effect of palbociclib was enhanced with the addition of SX-682 (Figure 3A), but synergism between the two treatments was not detected (Supplementary Figure S3A). All treatment groups tolerated the treatment for eleven days without significant loss of body weight (Figure 3B).

To examine the immune response to palbociclib and/or SX-682 treatment in the TME of tumors from Figure 3A, a single-cell tumor suspension was prepared, cells were stained with fluorescent conjugated antibodies and analyzed by flow cytometry. In comparison with vehicle controls, tumor-bearing mice fed with SX-682 chow showed an increase in the TME of CD45+ total tumor-infiltrated leukocytes (Figure 3C), including CD3+CD45+ T cells (Figure 3D) in the TME, an increase in CD8+ T cells (Figure 3E), an increase in CD69+ activated CD8+ T cells (Figure 3F), and an increase in the percentage of CD4+CD44+ T cells (Figure 3I). SX-682 also reduced the percentage of Ly6G+ CD11b+ and CD14+Ly6G myeloid cells (Figures 3J, K) in the TME. In contrast, palbociclib treatment reduced the percentage of CD3+CD45+ T cells (Figure 3D), decreased the CD4+CD3+ T cells (Figure 3G) in the TME as compared to control. The combination treatment (palbociclib + SX-682) compared to control exhibited a normalization of the effect of SX-682 on the percentage of CD3+ T cells in the tumor (Figure 3D). The combination treatment also increased the percentage of CD3+CD8+ T cells (Figure 3E), increased the percentage of CD44+CD4+ T cells (Figure 3H), increased the percentage of CD4+CD62L+ T cells (Figure 3I), and increased the percentage of CD11b+Ly6C+ monocytes (Figure 3L) compared to control. In some instances, the positive effects of the SX-682 chow on the anti-tumor immune environment were thus overridden by the addition of palbociclib (i.e., loss of reduction in Ly6GCD11b+ cells, loss of reduction in CD14+Ly6G+ cells, increase in Ly6C+CD11b+ cells, loss of increase in CD69+ CD8 + T cells, and reduction in total CD45+ cells and loss of increase in CD45+ CD3+ T cells compared to SX-682). However, the percentage of CD8+ T cells remained elevated in tumors treated with both SX-682 and palbociclib. The effects of combined therapies were additive, but not synergistic in B16-F10 melanoma tumors (Supplementary Figure S2A). Palbociclib appears to be exerting its major effect by slowing the movement of tumor cells through the cell cycle, thus slowing tumor growth. In contrast, SX-682 affects tumor growth (27) and produces a more anti-tumor immune environment characterized by increased CD8+ T cells and activated CD69+CD8+ T cells (Figures 3E, F).

3.4 SX-682 treatment tends to increase serum levels of cytokines involved in T cell response in B16-F10 tumor-bearing mice

A protein array was performed on the sera from B16F10 tumor-bearing C57Bl/6 mice at the endpoint of the tumor growth assay to define the values for 308 cytokines or receptors in each of the four treatment groups (Figure 4). Results showed that the mice in the

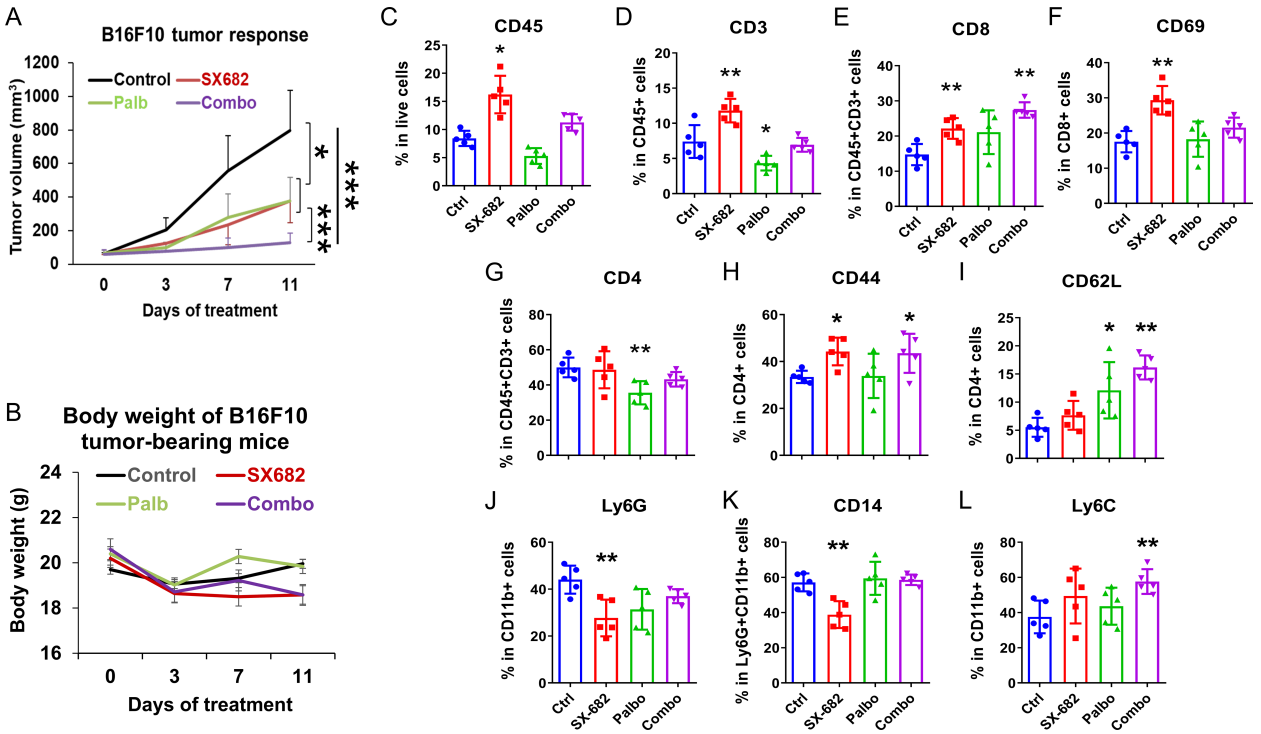

FIGURE 3
The CXCR1/2 antagonist, SX-682, affects the growth-inhibitory effect of palbociclib and increases anti-tumor immunity *in vivo*. **(A)** the effect of palbociclib dosing (100 mg/kg treatment), SX-682 chow, or the combination on body weight or **(B)** tumor growth of B16-F10 tumor-bearing C57Bl/6 mice. **(C–L)** the effect of palbociclib, SX-682, or the combination on various immune populations in the TME of B16-F10 tumor-bearing C57Bl/6 mice. *p<0.05, **p<0.01, ***p<0.001.

SX-682 treatment group exhibited trends toward increased levels of IP-10 (CXCL10), CTACK, CXCR4, CXCR6, Endocan, Endostatin, GDF-8, IFNγR1, IL-1α, IL-31, MCP-5 and TSLP compared to the control group. These cytokine array data demonstrate that treatment with the CXCR1/2 antagonist elevates factors associated with T cell activation and recruitment [IP-10 (CXCL10), CTAK, CXCR4, CXCR6, IFNγR1, IL-1α, TLSP] over that with the CDK4/6 inhibitor. Both SX-682 and palbociclib inhibitors suppressed amphiregulin. IL-1α, endostatin, GDF8, and IFNγR1 also trended upward in the serum of mice treated with the combination of SX-682 + palbociclib. Palbociclib did not increase the values of the cytokines assayed here over control, except GDF-8. Since the data represent duplicate values, statistically significant differences cannot be determined. Altogether, these data reinforce prior published data showing that SX-682 treatment increases the recruitment of T cells and activated T cells into the TME (27).

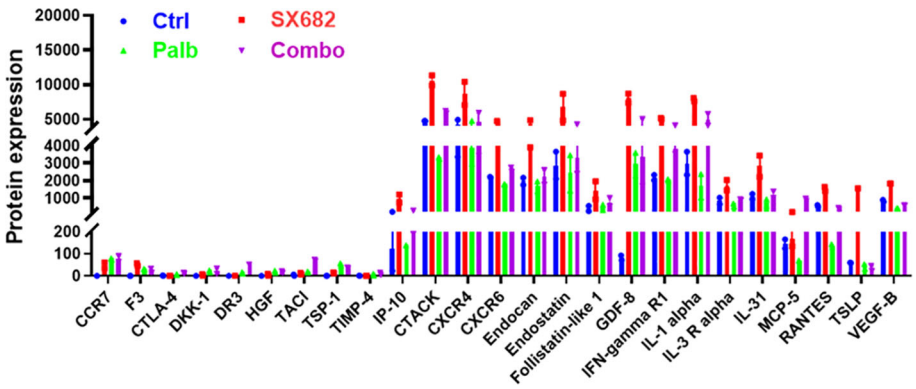

FIGURE 4
SX-682 treatment results in a trend toward increased serum levels of cytokines involved in T cell response in B16-F10 tumor-bearing mice. Comparison of protein levels in serum from B16F10 mice treated with SX-682, palbociclib, or the combination, normalized to mice in the vehicle control group.

3.5 Palbociclib, SX-682, and the combination of both drugs inhibit NRAS mutant 1014 melanoma tumor growth and result in a stronger anti-tumor immune microenvironment

Experiments evaluating the effect of SX-682, palbociclib, or the combination of inhibitors were also conducted in C57Bl/6 mice bearing 1014 NRAS mutant ($NRAS^{mut}$) melanoma xenografts over a treatment period of two weeks. Palbociclib significantly inhibited tumor growth ($p<0.01$), as did SX-682 ($p<0.05$). However, the effect of the combination treatment on inhibiting tumor growth was not greater than that of either treatment alone (Figure 5A). Individual therapies and the combination treatment did not result in a body weight reduction of greater than 10% over the treatment period (Figure 5B). Palbociclib reduced the percentage of CD45+ cells and CD3+CD45+ T cells in the tumors, but this effect was reversed by the combination with SX-682 treatment (Figures 5C, D). While neither treatment increased the percentage of CD3+ T cells that were CD8+ T cells, SX-682 chow increased the percentage of CD69+ activated CD8+ T cells (Figures 5E, F). Also, neither treatment affected the percentage of CD3 T cells that were CD4+. Both palbociclib and SX-682 increased the effector memory (CD44+) and naive (CD62L+) CD4+ T cells (Figures 5G–I), but the combination treatment was similar to the control treatment (Figure 5I). SX-682 chow, palbociclib alone, and the combination of both SX-682 and palbociclib reduced the percentage of CD11b cells (Figure 5J). The percentage of CD11b +Ly6G+ granulocytes, presumably granulocytic MDSCs (gMDSCs), was only reduced by SX-682 (Figure 5K). The lack of an additive effect of palbociclib and SX682 on the growth of the 1014 cells is consistent with the palbociclib- mediated reduction of immune cells in the TME. The palbociclib inhibition of Rb hyperphosphorylation was equivalent in both B16F10 and 1014 cells. These data suggest that the increased recruitment of CD8+ T and CD4+ T cells in palbociclib + SX-682-treated B16F10 tumors but not in 1014 tumors may be associated with the observation that the 1014 tumors are less growth-inhibited by palbociclib plus SX-682 than the B16F10 tumors. Alternatively, activation of the NRAS pathway in 1014 cells may result in production of factors that override the inhibition of CDK4/6 and CXCR2.

3.6 The addition of a CDK2 inhibitor (PF07104091) to the CDK4/6 inhibitor palbociclib and the CXCR2 inhibitor SX-682 improves the anti-tumor response in BRAF wild-type melanoma

When C57Bl/6 mice (10 mice/group) bearing B16-F10 tumors (~5mm diameter) were exposed to a daily dose of 100 mg/kg palbociclib, 50 mg/kg of the CDK2 inhibitor, PF-07104091, with control chow or SX-682 chow, the toxicity of palbociclib plus PF-07104091 or the triple therapy was acceptable and anti-tumor efficacy of the triple combination with SX-682 was increased relative CDK4/6 plus CDK2 inhibition or SX-682 alone (Figures 6A, B), resulting in a failure of tumors to grow. The effect of the triple combination treatment on tumor growth was additive, but not synergistic (Supplementary Figure S2B).

Analysis of the immune cells in the TME of B16-F10 (Figures 6C-O) melanoma tumors treated with SX-682 alone

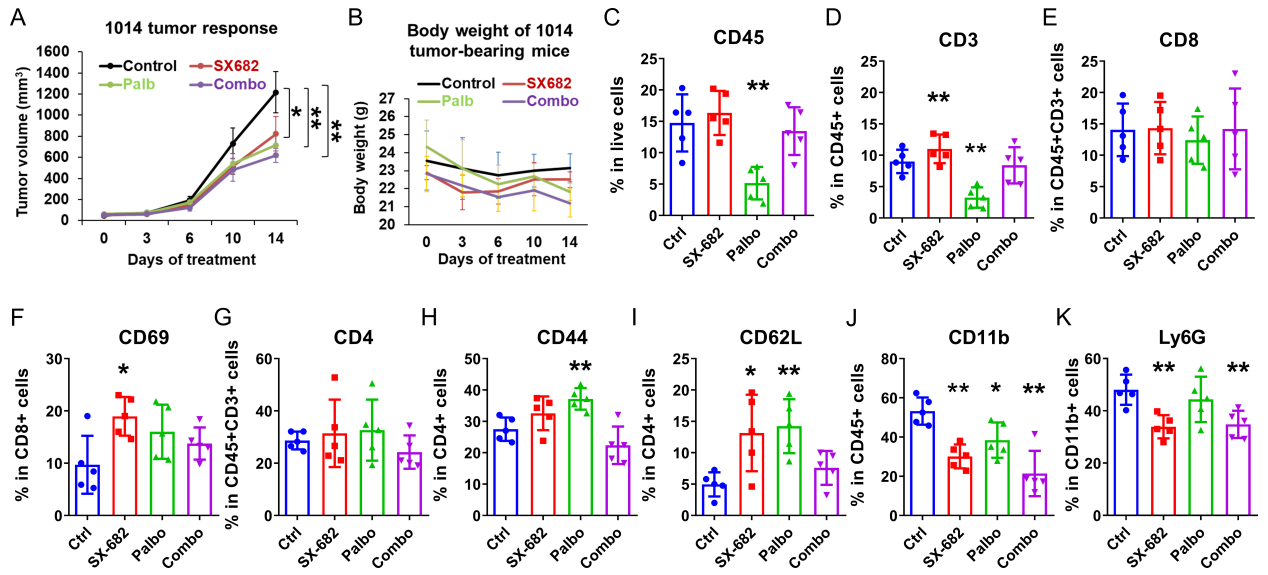

FIGURE 5
Palbociclib, SX-682, and the combination of both drugs inhibit Nras mutant 1014 melanoma tumor growth and result in a stronger anti-tumor immune microenvironment. The effect of palbociclib dosing (100 mg/kg treatment), SX-682 chow, or the combination on **(A)** tumor growth, or **(B)** body weight of C57Bl/6 mice bearing $NRAS^{mut}$ 1014 melanoma tumors. **(C–K)** profile of immune cell populations in the TME of $NRAS^{mut}$ 1014 tumor-bearing mice receiving treatment with palbociclib (100 mg/kg), SX-682 inhibitor containing chow, or the combination of treatments. *$p \leq 0.05$, **$p \leq 0.01$.

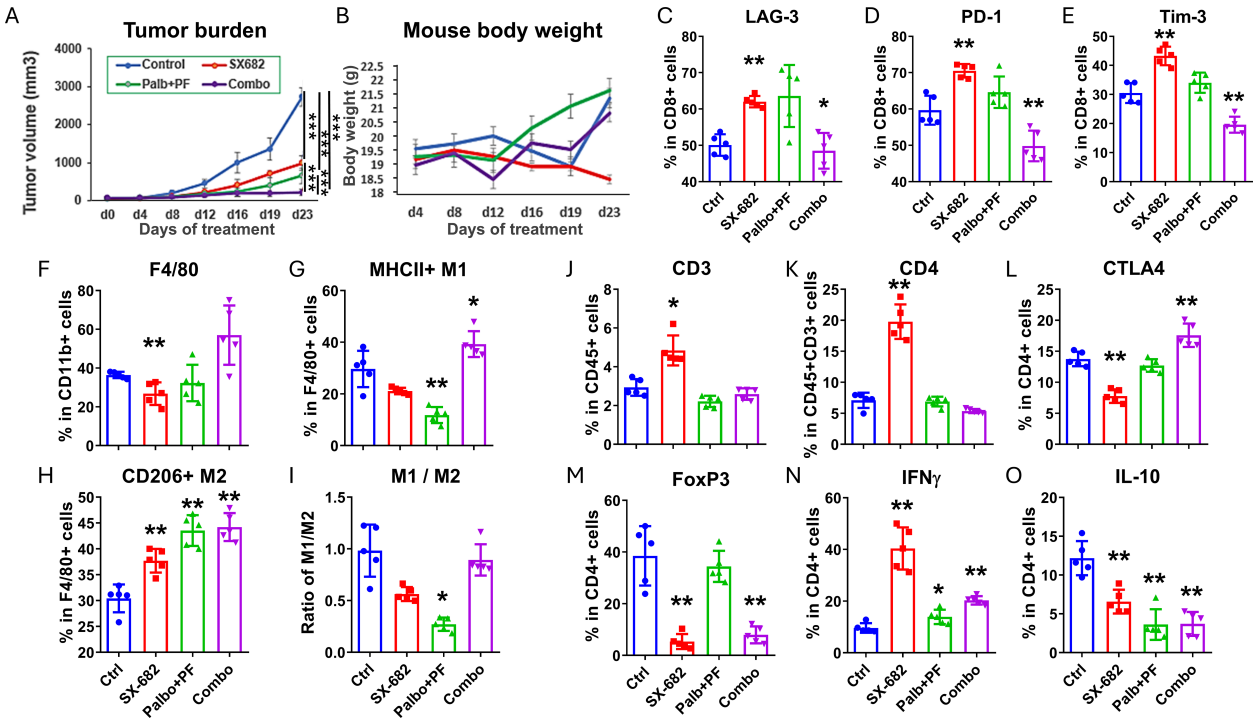

FIGURE 6
The addition of a CDK2 inhibitor (PF07104091) to the CDK4/6 inhibitor palbociclib and the CXCR2 inhibitor SX-682 improves the anti-tumor response in BRAF wild-type melanoma. **(A)** the effect of the following treatments on the tumor growth of B16F10 tumor xenografts growing in C57Bl/6 mice for four weeks: combination palbociclib (100 mg/kg) and PF 07104091 (50 mg/kg), SX-682 chow, or the combination of all three inhibitors. **(B)** the effect of the above treatments on B16F10 mouse weight in C57Bl/6 mice over 23 days. **(C–O)** the effect of palbociclib + PF07104091, SX-682, or the combination on various immune populations in the TME of C57Bl/6 mice bearing B16F10 tumors. *p ≤ 0.05, **p ≤ 0.01; ***p ≤ 0.001.

increased the CD3+ T cells. Palbociclib+ PF-07104091 reduced the CD3+ T cells, increased IFNγ+ CD4+ T cells, but reduced IL-10 + CD4+ T cells. This CDK inhibitor combination was associated with a decrease in F4/80+MHCII+ M1-like macrophages and an increase in CD206+F4/80+ M2-like macrophages. The triple combination of CDK4/6, CDK2, and CXCR1/2 antagonists revealed an increase in CD4+CTLA4+ T cells, an increase in IFNγ+ CD4+ T cells, but a reduction in Tregs (CD4+FOXp3+), CD8+PD-1+ T cells, CD8 +Tim-3+ T cells, and IL-10+ CD4+ T cells. These data indicate that there is a reduction in the exhaustion status of CD8+ T cells, an increase in CD4+ T cells, and a decrease in Tregs with the triple combination inhibitor treatment. Altogether, these data support combining inhibitors of CDK4/6, CDK2, and CXCR1,2 for the treatment of BRAF wild-type melanoma. The CDK inhibitors work together to inhibit Rb phosphorylation while the CXCR1,2 antagonist creates a more anti-tumor immune microenvironment.

We have previously demonstrated in preclinical models that CDK4/6 inhibitors, when combined with MDM2 inhibition, can effectively inhibit melanoma tumor growth, and that resistance to CDK4/6 inhibition can be overcome through the targeted deletion of CDK2 (17). However, MDM2 inhibitors are mostly effective only in $p53^{WT}$ tumors, and they have been shown to induce thrombocytopenia, neutropenia, and other toxicities, though several recent clinical trials continue to 'fine-tune' these inhibitors and combine them with other appropriate therapies for further clinical development (33–36). To determine how an MDM2 inhibitor might affect the response to SX-682 in melanoma, we performed experiments combining the MDM2 inhibitor, idasanutlin (50mg/kg), with SX-682 in B16F10 melanoma and we observed that idasanutlin reduced the effect of SX-682 on tumor growth inhibition (Figure 7A) and reversed the inhibitory effects of SX-682 on the Ly6G+CD11b+ granulocytic MDSCs (Figure 7B) and also increased the CD206+ M2 macrophages in the blood (Figure 7C). Thus, inclusion of an MDM2 inhibitor with treatment regimens that include the CXCR2 antagonist SX-682 is not advised. Our results show that optimal inhibition of tumor growth in the B16F10 melanoma model can be obtained with co-inhibition of CDK4/6 and CDK2 along with SX-682.

4 Discussion

Key to the process of cancer development is the failure to control cell proliferation, often resulting from an impaired regulation of proteins involved in cell cycle progression, particularly the constitutive activation of the cyclin-dependent kinases (CDKs) (37). Upon mitogenic stimulation, CDK4/6 hyperphosphorylates the tumor suppressor Rb, releasing the transcription factor E2F to drive expression of cyclin E, resulting in the elevation of this protein at the late restriction point of the G1

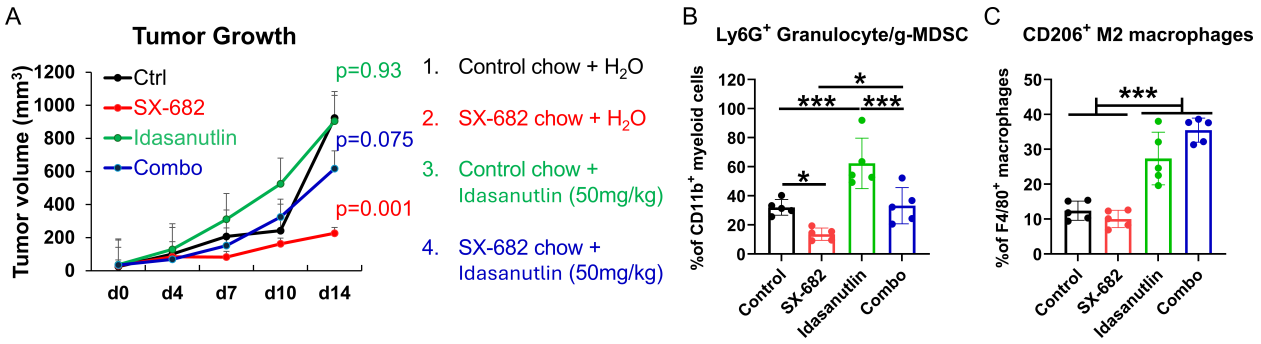

FIGURE 7
The MDM2 antagonist idasanutlin ablates the tumor growth inhibitory and anti-tumor immunity response to SX-682. **(A)** C57Bl/6 mice bearing B16F10 tumors were placed on chow containing SX-682 or control chow at the time tumors reached a diameter of 5mm. Mice were grouped into four groups: those that received control chow + vehicle, those that received SX-682 chow + vehicle, those receiving control chow and idasanutlin (50mg/kg), and those on SX-682 chow that also received idasanutlin (50mg/kg) by oral gavage. Treatments and measurements continued for fourteen days, after which time the mice were euthanized, and tumors **(B)** and blood **(C)** were collected for isolation and flow cytometry to characterize the immune cells. * p<0.05; *** p<0.001.

phase (38). When cyclin E binds to CDK2, and the active complex that also hyperphosphorylates Rb and numerous other substrates, controlling essential cellular processes, including the initiation of DNA replication and regulation of histone biosynthesis. Phosphorylated cyclin E protein is degraded by the SCF(Fbw7) ubiquitin ligase complex, thus eliminating cyclin E/CDK2 activity (39–41). A high level of cyclin E protein is associated with poor prognosis, reduced survival, and therapy resistance in cancer patients (40). Moreover, the overexpression of cyclin E has been proposed as a potential mechanism of resistance to CDK4/6 inhibitors (15, 42–44). Dysregulation of these kinases is a major contributor to endocrine therapy resistance in breast cancer (11).

CDK4/6 inhibitors induce cell cycle arrest in Rb protein (pRb)-competent cells by blocking the hyperphosphorylation of Rb by CDK4/6 (37, 45). Although early CDK4/6 inhibitors were quite toxic, the development of more selective CDK4/6 inhibitors, such as ribociclib, abemaciclib and palbociclib, has led to improved efficacy and reduced adverse events during the treatment of tumors that are driven by CDK4/6 pathway activation. Preliminary evidence showed promising activity in melanoma (17, 46) and improved progression-free survival with tolerable toxicity in patients with advanced-stage estrogen receptor (ER)-positive breast cancer, though resistance is an issue (42). Factors involved in acquired resistance to CDK4/6 inhibitors are being identified and new approaches to overcome this resistance are being developed. Biomarkers have been characterized that identify solid tumors that will not benefit from treatment with CDK4/6 inhibitors, such as loss of pRb (37).

The main objective of the study described in this report is to develop new approaches to improve the efficacy of CDK4/6 inhibitors for the treatment of melanoma. Our study design was informed by data comparing the clinical pharmacokinetics and pharmacodynamics of palbociclib (47–49). It is important to note that the GI50 concentrations of palbociclib (concentration of drug required to inhibit growth of 50% of the cells) required for the inhibition of melanoma cell growth here in B16F10 and 1014 cells is high (~10 μM) as compared to the reported GI50 of 100 nM to 1 μM for breast cancer cells. However, a wide range for the GI50 for melanoma cell lines has been observed previously by other groups, ranging from 30nM to 9 (16, 50, 51). The effective serum concentration of palbociclib delivered at a dose of 100 mg/kg body weight is between 3 and 5 μg/ml. Here we had a maximal response at 10 μM concentrations of palbociclib which is the equivalent of 4.473 μg/ml of palbociclib. There are many factors that affect the GI50, including genetic and phenotypic differences, culture conditions, time of exposure to the drug, cell density, genetic mutations and biomarkers, metabolic factors, prior drug treatment, and experimental techniques. Our data show the *in vitro* activity of palbociclib to be comparable to that reported by others for melanoma therapy.

The stability of cyclin D1 is regulated by Thr286 phosphorylation by GSK3β, and the stability of cyclin E1 is regulated by Thr380 phosphorylation of cyclin E1 by CDK2. These phosphorylation events allow cyclin ubiquitination by SCF(Fbx4/αB-crystallin) E3 ubiquitin ligase for cyclin D1 (52) and SCF(Fbw7) E3 for cyclin E1 (53), followed by degradation. We observed that palbociclib (20μM) alone induced cyclin D1 and cyclin E1 in B16F10 and 1014 cells, but in combination with the CDK2 inhibitor PF-07104091 (20 μM), this induction did not occur. The palbociclib increase in cyclin D1 levels in B16F10 and 1014 cells and the PF-07104091 increase in cyclin E1 in 1014 cells indicates that either the GSK2B and CDK2 phosphorylation may not be occurring, or the E3 ubiquitin ligase activity is deficient for these cyclins since the hyperphosphorylation of RB is inhibited by treatment with palbociclib and/or PF-07104091 with the combination treatment completely blocking phosphorylation of Rb on S807/S811. The increased cyclin E1 levels in 1014 cells in response to inhibition of CDK2 would be expected if CDK2 inhibition resulted in inability to phosphorylate cyclin E1 to target it for degradation. However, we did not observe a PF-07104091 elevation of cyclin E1 in B16F10 cells. In a separate study, low-dose CDK2 inhibition with PF-3600 resulted in a rebound phenotype that could be overcome with co-inhibition of both CDK4/6 and CDK2, or with high-dose PF-3600 (24). In 1014 melanoma cells, even with high-dose

CDK2 inhibition, addition of the CDK4/6 inhibitor was required to suppress cyclin E1 levels. Clearly, the response to these inhibitors varies among different cell lines depending on the activity of a spectrum of proteins involved in regulating the cell cycle.

The data from the analysis of the effects of palbociclib, PF-07104091, and the combination of drugs on the progression through cell cycle were surprising. While we expected that palbociclib would reduce the percentage of cells in S phase and that PF-07104091 alone would increase the S phase percentage (24), we did not expect to see an increase in cells in G2, or a reduction of cells in G1 in response to the CDK2 inhibitor. These data suggest that in melanoma cells, the CDK2 inhibitor may impinge on progression from G2 to M phase, and this has not been previously reported. The effects of PF-07104091 and the combination with palbociclib on increasing the percentage of cells in subG_0 could indicate that these drugs are inducing cell death in B16F10 cells, but not the more resistant 1014 cells. However, the combination of both inhibitors effectively induces apoptosis, reduces cell viability, and results in loss of hyperphosphorylation of Rb at S807/S811.

While CDK4/6 inhibitors have been effectively combined with ICI for the treatment of breast cancer, this combination with or without CDK2 inhibition has not yet been demonstrated to be clinically effective for metastatic melanoma. However, it has been demonstrated that CDK4/6 activity drives ICI resistance in RB competent immune cold melanoma tumor but when mouse models of these resistant melanoma tumors are treated first with ICI followed by CDK4/6 inhibition plus ICI, the resistance program is overcome and tumor growth is suppressed, demonstrating that order of delivery of the therapy is important.

In this study, we show that palbociclib is somewhat immune suppressive based upon its decrease in CD45+ cells, CD3+CD45+ T cells, CD4+CD3+ cells and CD11b+CD45+ cells, though it increased the CD44+CD4+ and CD62L+CD4+ T cells. In contrast, SX-682 blockade of CXCR1/2 in B16F10 tumors resulted in increased CD45+ immune cells, increased intratumoral CD8+T cells and CD69+CD8+ T cells, increased CD44+ CD4+ T cells and CD62L+ CD4+ T cells, and reduced CD11b+CD45+ cells, Ly6G+CD11b+ and CD14+Ly6G+ myeloid cells (Figure 3C). The combination of SX682 and palbociclib inhibited B16F10 melanoma tumor growth, increased the percentage of CD45+ cells, CD3+CD8+ T-cells, CD4+CD44+ T cells, and CD62L +CD4+ T cells. For myeloid cell effects, the combination decreased the percentage of CD11b+CD45+ cells and increased the Ly6c+CD11b+ cells. Analysis of data from a serum protein array indicated that mice fed SX-682 chow exhibited a trend toward higher levels of certain inflammatory cytokines involved in regulating T cells.

The effect of SX-682 or palbociclib individually on the growth of 1014 cells was equivocal to that for B16F10 melanoma cells (~50% inhibition). However, the effect if the combination therapy on the growth of 1014 $NRAS^{mut}$ melanoma xenografts was less than that observed with the B16F10 xenografts, though SX-682 increased the CD69+CD8+ activated T cells and decreased the CD11b+CD45+ myeloid cells, including Ly6G+CD11b+ granulocytes (and/or gMDSCs) in 1014 tumors similar to that observed in the B16F10 tumors. Palbociclib increased the $CD4+CD25^{high}$ T regulatory cells and the CD4+CD44+ effector memory T cells. Both palbociclib and SX-682 as single agents increased the CD4+CD62L+ central memory T cells, but the combination treatment eliminated this increase. This failure of the combined treatment with palbociclib and SX-682 to increase CD3+CD8+ T-cells, and CD62L+CD4+ T cells in 1014 tumors could explain in part the reduced response to SX-682 + palbociclib in 1014 tumors versus B16F10 tumors. As observed with SX-682 treatment, the combination treatment reduced the percentage of CD11b cells and the percentage of CD11b+ myeloid cells, including CD11b+Ly6G+ cells in both B16F10 and 1014 tumors, presumably gMDSCs.

In B16F10 tumors, addition of SX-682 containing chow to treatment with palbociclib + PF-07104091 blocked tumor growth and this was accompanied by reduced the percentage of CD8+ T cells, but also reduction in LAG-3+CD8+ T cells, TIM-3+ CD8+ T cells, PD-L1+ CD8+ T cells, Foxp3+CD4+ T cells, and IL-10+ CD4 + T cells in the TME, suggesting the CD8+ T cells were less exhausted compared to those in the control TME. In contrast, there was an increase in the CD4+ CTLA4+ T cells with the combined therapy. The combination treatment increased IFNγ+ CD4+ T cells, as well as M1-like and M2-like macrophages. Thus, addition of PF-07104091 to the SX-682 and palbociclib treatment was highly effective in inhibiting tumor growth and producing a more anti-tumor TME. Similar results would be expected for 1014 tumors, though the response would be expected to be somewhat reduced in comparison to B16F10 tumors, based on the more suppressive effect of palbociclib on the population of T cells in the TME.

A limitation of our study is that only two melanoma cell lines were evaluated in the study, $BRAF^{WT}$/$NRAS^{WT}$ B16F10 and $NRAS^{Q61R}$ mutant 1014 cells. We concentrated on melanoma lines that do not have a mutation in BRAF, since there are adequate second-line therapies available for BRAF mutant melanoma patients, but not for BRAF wild-type melanoma patients. One might argue that the B16F10 model may not fully represent the $BRAF/RAS^{WT}$ melanomas that usually harbor NF1 mutation or deletion, KIT mutation, or amplification of cyclin D. Certainly extension of the study to more representative murine models could provide additional information as to how various genetic modifications affect response to CDK4/6 and CDK2 inhibitors. On that note, we have previously examined the response of seven human melanoma cell lines and five melanoma patient-derived xenografts to treatment with a CDK4/6 inhibitor alone or in combination with an MDM2 inhibitor (17). We also demonstrated that blocking CDK2 activity enhanced the response to CDK4/6 inhibitors in these melanoma models. With SX-682 currently in clinical trials for the treatment of metastatic melanoma in combination with anti-PD1 in instances where there is resistance to ICI therapy, we propose that an alternative option may be to treat ICI-resistant BRAF wild-type melanoma with the combination of CDK4/6, CDK2, and CXCR2 antagonists.

5 Conclusions

Altogether, these data suggest that the addition of the CDK2 inhibitor to CDK4/6 and CXCR1/2 inhibitors not only reduces

melanoma tumor cell viability and tumor growth more effectively in $BRAF^{WT}NRAS^{WT}$ melanoma cells but also results in a less immunosuppressive tumor immune microenvironment. This study provides significant information for the design of future clinical trials for ICI-resistant melanomas without BRAF mutation.

Data availability statement

The original contributions presented in the study are included in the article/Supplementary Material. Further inquiries can be directed to the corresponding authors.

Ethics statement

The animal study was approved by Vanderbilt IACUC Committee, Vanderbilt University (M20000008-00, 01-14-2020). The study was conducted in accordance with the local legislation and institutional requirements.

Author contributions

JY: Data curation, Formal analysis, Investigation, Methodology, Validation, Writing – original draft, Writing – review & editing. CY: Project administration, Supervision, Validation, Writing – review & editing. WL: Data curation, Formal analysis, Investigation, Methodology, Validation, Visualization, Writing – review & editing. PW: Formal analysis, Investigation, Methodology, Validation, Writing – review & editing. S-CC: Data curation, Formal analysis, Validation, Writing – review & editing. JZ: Resources, Validation, Writing – review & editing. DM: Resources, Validation, Writing – review & editing. AR: Conceptualization, Data curation, Formal analysis, Funding acquisition, Project administration, Resources, Supervision, Validation, Writing – review & editing.

Funding

The author(s) declare financial support was received for the research and/or publication of this article. The work in this report was funded by the NCI, CA116021 (AR, CY), the Department of Veterans Affairs 5I01BX002301 (AR) and 5IK6BX005225 (AR). We utilized Flow Cytometry Core Facilities supported by P30-CA068485 and DK058404.

Acknowledgments

SX-682, a potent small molecule dual inhibitor of CXCR1/CXCR2, was kindly provided by Syntrix Pharmaceuticals.

Conflict of interest

Authors JZ and DM were employed by Syntrix Biosystems.

The remaining authors declare that the research was conducted in the absence of any commercial or financial relationships that could be construed as a potential conflict of interest.

The author(s) declared that they were an editorial board member of Frontiers, at the time of submission. This had no impact on the peer review process and the final decision.

Generative AI statement

The author(s) declare that no Generative AI was used in the creation of this manuscript.

Publisher's note

Supplementary material

The Supplementary Material for this article can be found online at: https://www.frontiersin.org/articles/10.3389/fonc.2025.1609735/full#supplementary-material

References

1. Pollack LA, Li J, Berkowitz Z, Weir HK, Wu XC, Ajani UA, et al. Melanoma survival in the United States, 1992 to 2005. *J Am Acad Dermatol.* (2011) 65:S78–86. doi: 10.1016/j.jaad.2011.05.030

2. Wolchok JD, Chiarion-Sileni V, Rutkowski P, Cowey CL, Schadendorf D, Wagstaff J, et al. Final, 10-year outcomes with nivolumab plus ipilimumab in advanced melanoma. *N Engl J Med.* (2024) 392:11–22. doi: 10.1056/NEJMoa2407417

3. Amir M, Khan ZA, Asad A, Shaikh TG. Role of neoadjuvant pembrolizumab in advanced melanoma. *Semin Oncol.* (2024) 51:161–2. doi: 10.1053/j.seminoncol.2024.09.001

4. Patrinely JR Jr., Baker LX, Davis EJ, Song H, Ye F, Johnson DB. Outcomes after progression of disease with anti-PD-1/PD-L1 therapy for patients with advanced melanoma. *Cancer.* (2020) 126:3448–55. doi: 10.1002/cncr.32984

5. Robert C, Ribas A, Schachter J, Arance A, Grob JJ, Mortier L, et al. Pembrolizumab versus ipilimumab in advanced melanoma (KEYNOTE-006): post-hoc 5-year results from an open-label, multicentre, randomised, controlled, phase 3 study. *Lancet Oncol.* (2019) 20:1239–51. doi: 10.1016/S1470-2045(19)30388-2

6. Yang J, Yan C, Vilgelm AE, Chen SC, Ayers GD, Johnson CA, et al. Targeted deletion of CXCR2 in myeloid cells alters the tumor immune environment to improve

antitumor immunity. *Cancer Immunol Res*. (2021) 9:200–13. doi: 10.1158/2326-6066.CIR-20-0312

7. Schadendorf D, Dummer R, Flaherty KT, Robert C, Arance A, de Groot JWB, et al. COLUMBUS 7-year update: A randomized, open-label, phase III trial of encorafenib plus binimetinib versus vemurafenib or encorafenib in patients with BRAF V600E/K-mutant melanoma. *Eur J Cancer*. (2024) 204:114073. doi: 10.1016/j.ejca.2024.114073

8. Bai X, Shaheen A, Grieco C, d'Arienzo PD, Mina F, Czapla JA, et al. Dabrafenib plus trametinib versus anti-PD-1 monotherapy as adjuvant therapy in BRAF V600-mutant stage III melanoma after definitive surgery: a multicenter, retrospective cohort study. *EClinicalMedicine*. (2023) 65:102290. doi: 10.1016/j.eclinm.2023.102290

9. Atkins MB, Lee SJ, Chmielowski B, Tarhini AA, Cohen GI, Truong TG, et al. Combination dabrafenib and trametinib versus combination nivolumab and ipilimumab for patients with advanced BRAF-mutant melanoma: the DREAMseq trial-ECOG-ACRIN EA6134. *J Clin Oncol*. (2023) 41:186–97. doi: 10.1200/JCO.22.01763

10. Kreuger IZM, Slieker RC, van Groningen T, van Doorn R. Therapeutic strategies for targeting CDKN2A loss in melanoma. *J Invest Dermatol*. (2023) 143:18–25 e1. doi: 10.1016/j.jid.2022.07.016

11. Sheppard KE, McArthur GA. The cell-cycle regulator CDK4: an emerging therapeutic target in melanoma. *Clin Cancer Res*. (2013) 19:5320–8. doi: 10.1158/1078-0432.CCR-13-0259

12. Schuler M, Zimmer L, Kim KB, Sosman JA, Ascierto PA, Postow MA, et al. Phase ib/II trial of ribociclib in combination with binimetinib in patients with NRAS-mutant melanoma. *Clin Cancer Res*. (2022) 28:3002–10. doi: 10.1158/1078-0432.CCR-21-3872

13. Ali LR, Garrido-Castro AC, Lenehan PJ, Bollenrucher N, Stump CT, Dougan M, et al. PD-1 blockade and CDK4/6 inhibition augment nonoverlapping features of T cell activation in cancer. *J Exp Med*. (2023) 220(4). doi: 10.1084/jem.20220729

14. Lelliott EJ, Sheppard KE, McArthur GA. Harnessing the immunotherapeutic potential of CDK4/6 inhibitors in melanoma: is timing everything? *NPJ Precis Oncol*. (2022) 6:26. doi: 10.1038/s41698-022-00273-9

15. Pandey K, Park N, Park KS, Hur J, Cho YB, Kang M, et al. Combined CDK2 and CDK4/6 inhibition overcomes palbociclib resistance in breast cancer by enhancing senescence. *Cancers (Basel)*. (2020) 12:3566. doi: 10.3390/cancers12123566

16. Young RJ, Waldeck K, Martin C, Foo JH, Cameron DP, Kirby L, et al. Loss of CDKN2A expression is a frequent event in primary invasive melanoma and correlates with sensitivity to the CDK4/6 inhibitor PD0332991 in melanoma cell lines. *Pigment Cell Melanoma Res*. (2014) 27:590–600. doi: 10.1111/pcmr.12228

17. Vilgelm AE, Saleh N, Shattuck-Brandt R, Riemenschneider K, Slesur L, Chen SC, et al. MDM2 antagonists overcome intrinsic resistance to CDK4/6 inhibition by inducing p21. *Sci Transl Med*. (2019) 11(505). doi: 10.1126/scitranslmed.aav7171

18. Yang J, Richmond A. Constitutive IkappaB kinase activity correlates with nuclear factor-kappaB activation in human melanoma cells. *Cancer Res*. (2001) 61:4901–9.

19. Eash KJ, Greenbaum AM, Gopalan PK, Link DC. CXCR2 and CXCR4 antagonistically regulate neutrophil trafficking from murine bone marrow. *J Clin Invest*. (2010) 120:2423–31. doi: 10.1172/JCI41649

20. Sharma B, Nannuru KC, Varney ML, Singh RK. Host Cxcr2-dependent regulation of mammary tumor growth and metastasis. *Clin Exp Metastasis*. (2015) 32:65–72. doi: 10.1007/s10585-014-9691-0

21. Greene S, Robbins Y, Mydlarz WK, Huynh AP, Schmitt NC, Friedman J, et al. Inhibition of MDSC trafficking with SX-682, a CXCR1/2 inhibitor, enhances NK-cell immunotherapy in head and neck cancer models. *Clin Cancer Res*. (2020) 26:1420–31. doi: 10.1158/1078-0432.CCR-19-2625

22. Sun L, Clavijo PE, Robbins Y, Patel P, Friedman J, Greene S, et al. Inhibiting myeloid-derived suppressor cell trafficking enhances T cell immunotherapy. *JCI Insight*. (2019) 4:e126853. doi: 10.1172/jci.insight.126853

23. Patel SP, Victor AI, Mooradian MJ, Buchbinder EI, Hernandez-Aya LF, Prieto P, et al. Safety and efficacy of first-in-class CXCR1/2 inhibitor SX-682 in combination with pembrolizumab (pem) in metastatic melanoma (mMEL) patients (pts) with disease progression on anti–PD-1 therap. *J Clin Oncol*. (2024) 42:16 suppl. doi: 10.1200/jco.2024.42.16.suppl.9508

24. Arora M, Moser J, Hoffman TE, Watts LP, Min M, Musteanu M, et al. Rapid adaptation to CDK2 inhibition exposes intrinsic cell-cycle plasticity. *Cell*. (2023) 186:2628–2643 e21. doi: 10.1016/j.cell.2023.05.013

25. Melnikova VO, Bolshakov SV, Walker C, Ananthaswamy HN. Genomic alterations in spontaneous and carcinogen-induced murine melanoma cell lines. *Oncogene*. (2004) 23:2347–56. doi: 10.1038/sj.onc.1207405

26. Petit V, Raymond J, Alberti C, Pouteaux M, Gallagher SJ, Nguyen MQ, et al. C57BL/6 congenic mouse NRAS(Q61K) melanoma cell lines are highly sensitive to the combination of Mek and Akt inhibitors *in vitro* and *in vivo*. *Pigment Cell Melanoma Res*. (2019) 32:829–41. doi: 10.1111/pcmr.12807

27. Yang J, Bergdorf K, Yan C, Luo W, Chen SC, Ayers GD, et al. CXCR2 expression during melanoma tumorigenesis controls transcriptional programs that facilitate tumor growth. *Mol Cancer*. (2023) 22:92. doi: 10.1186/s12943-023-01789-9

28. Saito Y, Xiao Y, Yao J, Li Y, Liu W, Yuzhalin AE, et al. Targeting a chemo-induced adaptive signaling circuit confers therapeutic vulnerabilities in pancreatic cancer. *Cell Discov*. (2024) 10:109. doi: 10.1038/s41421-024-00720-w

29. Chung M, Liu C, Yang HW, Koberlin MS, Cappell SD, Meyer T. Transient hysteresis in CDK4/6 activity underlies passage of the restriction point in G1. *Mol Cell*. (2019) 76:562–573 e4. doi: 10.1016/j.molcel.2019.08.020

30. Sherr CJ, Roberts JM. CDK inhibitors: positive and negative regulators of G1-phase progression. *Genes Dev*. (1999) 13:1501–12. doi: 10.1101/gad.13.12.1501

31. Malumbres M, Barbacid M. To cycle or not to cycle: a critical decision in cancer. *Nat Rev Cancer*. (2001) 1:222–31. doi: 10.1038/35106065

32. Fassl A, Geng Y, Sicinski P. CDK4 and CDK6 kinases: From basic science to cancer therapy. *Science*. (2022) 375:eabc1495. doi: 10.1126/science.abc1495

33. Italiano A, Miller WH Jr., Blay JY, Gietema JA, Bang YJ, Mileshkin LR, et al. Phase I study of daily and weekly regimens of the orally administered MDM2 antagonist idasanutlin in patients with advanced tumors. *Invest New Drugs*. (2021) 39:1587–97. doi: 10.1007/s10637-021-01141-2

34. Moschos SJ, Sandhu S, Lewis KD, Sullivan RJ, Puzanov I, Johnson DB, et al. Targeting wild-type TP53 using AMG 232 in combination with MAPK inhibition in Metastatic Melanoma; a phase 1 study. *Invest New Drugs*. (2022) 40:1051–65. doi: 10.1007/s10637-022-01253-3

35. Zhang X, Wen X, Peng R, Pan Q, Weng D, Ma Y, et al. A first-in-human phase I study of a novel MDM2/p53 inhibitor alrizomadlin in advanced solid tumors. *ESMO Open*. (2024) 9:103636. doi: 10.1016/j.esmoop.2024.103636

36. Peuget S, Selivanova G. MDM2-PROTAC versus MDM2 Inhibitors: Beyond p53 Reactivation. *Cancer Discov*. (2023) 13:1043–5. doi: 10.1158/2159-8290.CD-23-0229

37. O'Leary B, Finn RS, Turner NC. Treating cancer with selective CDK4/6 inhibitors. *Nat Rev Clin Oncol*. (2016) 13:417–30. doi: 10.1038/nrclinonc.2016.26

38. Narasimha AM, Kaulich M, Shapiro GS, Choi YJ, Sicinski P, Dowdy SF. Cyclin D activates the Rb tumor suppressor by mono-phosphorylation. *Elife*. (2014) 3:e02872. doi: 10.7554/eLife.02872

39. Fagundes R, Teixeira LK. Cyclin E/CDK2: DNA replication, replication stress and genomic instability. *Front Cell Dev Biol*. (2021) 9:774845. doi: 10.3389/fcell.2021.774845

40. Hwang HC, Clurman BE. Cyclin E in normal and neoplastic cell cycles. *Oncogene*. (2005) 24:2776–86. doi: 10.1038/sj.onc.1208613

41. Chu C, Geng Y, Zhou Y, Sicinski P. Cyclin E in normal physiology and disease states. *Trends Cell Biol*. (2021) 31:732–46. doi: 10.1016/j.tcb.2021.05.001

42. Herrera-Abreu MT, Palafox M, Asghar U, Rivas MA, Cutts RJ, Garcia-Murillas I, et al. Early adaptation and acquired resistance to CDK4/6 inhibition in estrogen receptor-positive breast cancer. *Cancer Res*. (2016) 76:2301–13. doi: 10.1158/0008-5472.CAN-15-0728

43. Guarducci C, Bonechi M, Benelli M, Biagioni C, Boccalini G, Romagnoli D, et al. Cyclin E1 and Rb modulation as common events at time of resistance to palbociclib in hormone receptor-positive breast cancer. *NPJ Breast Cancer*. (2018) 4:38. doi: 10.1038/s41523-018-0092-4

44. Taylor-Harding B, Aspuria PJ, Agadjanian H, Cheon DJ, Mizuno T, Greenberg D, et al. Cyclin E1 and RTK/RAS signaling drive CDK inhibitor resistance via activation of E2F and ETS. *Oncotarget*. (2015) 6:696–714. doi: 10.18632/oncotarget.2673

45. Groenland SL, Martinez-Chavez A, van Dongen MGJ, Beijnen JH, Schinkel AH, Huitema ADR, et al. Clinical pharmacokinetics and pharmacodynamics of the cyclin-dependent kinase 4 and 6 inhibitors palbociclib, ribociclib, and abemaciclib. *Clin Pharmacokinet*. (2020) 59:1501–20. doi: 10.1007/s40262-020-00930-x

46. Garutti M, Targato G, Buriolla S, Palmero L, Minisini AM, Puglisi F. CDK4/6 inhibitors in melanoma: A comprehensive review. *Cells*. (2021) 10(6):1334. doi: 10.3390/cells10061334

47. Zhu Z, Zhu Q. Differences in metabolic transport and resistance mechanisms of Abemaciclib, Palbociclib, and Ribociclib. *Front Pharmacol*. (2023) 14:1212986. doi: 10.3389/fphar.2023.1212986

48. Bandiera C, Locatelli I, Courlet P, Cardoso E, Zaman K, Stravodimou A, et al. Adherence to the CDK 4/6 inhibitor palbociclib and omission of dose management supported by pharmacometric modelling as part of the opTAT study. *Cancers (Basel)*. (2023) 15:316. doi: 10.3390/cancers15010316

49. Desai MP, Patil PH, Shenoy GG, Channabasavaiah JP. Estimation of CDK inhibitors by RP-HPLC: application for pharmacokinetic interactions studies with PPIs. *Bioanalysis*. (2024) 16:801–12. doi: 10.1080/17576180.2024.2372162

50. Teh JL, Purwin TJ, Greenawalt EJ, Chervoneva I, Goldberg A, Davies MA, et al. An *in vivo* reporter to quantitatively and temporally analyze the effects of CDK4/6 inhibitor-based therapies in melanoma. *Cancer Res*. (2016) 76:5455–66. doi: 10.1158/0008-5472.CAN-15-3384

51. Martin CA, Cullinane C, Kirby L, Abuhammad S, Lelliott EJ, Waldeck K, et al. Palbociclib synergizes with BRAF and MEK inhibitors in treatment naive melanoma but not after the development of BRAF inhibitor resistance. *Int J Cancer*. (2018) 142:2139–52. doi: 10.1002/ijc.31220

52. Barbash O, Diehl JA. SCF(Fbx4/alphaB-crystallin) E3 ligase: when one is not enough. *Cell Cycle*. (2008) 7:2983–6. doi: 10.4161/cc.7.19.6775

53. Ye X, Nalepa G, Welcker M, Kessler BM, Spooner E, Qin J, et al. Recognition of phosphodegron motifs in human cyclin E by the SCF(Fbw7) ubiquitin ligase. *J Biol Chem*. (2004) 279:50110–9. doi: 10.1074/jbc.M409226200

frontiers | Frontiers in Oncology

TYPE Original Research
PUBLISHED 01 September 2025
DOI 10.3389/fonc.2025.1641979

OPEN ACCESS

EDITED BY
Massimo Broggini,
Mario Negri Institute for Pharmacological Research (IRCCS), Italy

REVIEWED BY
Sivapar V. Mathan,
All India Institute of Medical Sciences, India
Jyoti Bala Kaushal,
University of Nebraska Medical Center, United States

*CORRESPONDENCE
Ruihan Zhang
zhangruihan@ynu.edu.cn
Weilie Xiao
xiaoweilie@ynu.edu.cn
Rong Liu
liurong@pkufh.com

†These authors have contributed equally to this work

RECEIVED 05 June 2025
ACCEPTED 05 August 2025
PUBLISHED 01 September 2025

CITATION
Chen X, Ni D, Cheng J, Liang B, Zhang R, Xiao W and Liu R (2025) Diaryl pyrimidine guanidine suppresses hepatocellular carcinoma cell stemness by targeting β-catenin signaling.
Front. Oncol. 15:1641979.
doi: 10.3389/fonc.2025.1641979

Diaryl pyrimidine guanidine suppresses hepatocellular carcinoma cell stemness by targeting β-catenin signaling

Xuechun Chen[1†], Dongxuan Ni[2†], Jinghui Cheng[1], Bin Liang[2], Ruihan Zhang[2*], Weilie Xiao[2,3*] and Rong Liu[1,3*]

[1]Translational Cancer Research Center, Peking University First Hospital, Beijing, China, [2]Key Laboratory of Medicinal Chemistry for Natural Resource of Ministry of Education, Yunnan Characteristic Plant Extraction Laboratory Co., Ltd., Yunnan Research and Development Center for Natural Products, School of Life Sciences and School of Pharmacy, Yunnan University, Kunming, China, [3]Southwest United Graduate School, Kunming, China

Background: Liver cancer remains a major global health burden, with hepatocellular carcinoma (HCC) accounting for approximately 80% of liver cancer cases. Cancer stem cells (CSCs) play a critical role in HCC initiation, progression, metastasis, and resistance to therapy, making them critical targets for novel therapeutic interventions. However, effective agents specifically targeting CSCs in HCC remain limited. The objective of this study was to identify and characterize novel small molecules that inhibit CSCs properties and overcome drug resistance in HCC.

Methods: Functional assays assessed the effects of C504244 on tumor sphere formation, cancer cell proliferation, and migration. RNA sequencing was conducted on C504244-treated HCC cells to investigate changes in gene expression profiles. Downstream targets of the Wnt signaling pathway were analyzed to determine pathway inhibition. Co-immunoprecipitation (Co-IP) was performed to assess whether C504244 disrupts the interaction between β-catenin and Transcription Factor 4 (TCF4) in HCC cells. Lenvatinib-resistant HCC cell lines were used to evaluate the combinatorial efficacy of C504244 and Lenvatinib *in vitro* and *in vivo*.

Results: C504244 significantly suppressed tumor sphere formation, proliferation, and migration of HCC cells. Transcriptome analysis revealed that C504244 treatment led to significant inhibition of the Wnt signaling pathway, with corresponding downregulation of downstream target gene expression. Mechanistically, C504244 disrupted the β-catenin/TCF4 complex formation, which may contribute to reduced transcriptional activity. Since β-catenin signaling is hyperactivated in Lenvatinib-resistant HCC cells, C504244 was tested in combination with Lenvatinib and found to markedly sensitize these resistant cells to Lenvatinib treatment both *in vitro* and *in vivo*.

Conclusions: C504244 represents a promising agent that effectively inhibits β-catenin signaling, thereby impairing CSCs properties and reversing Lenvatinib resistance in HCC cells. These findings suggest that C504244 may serve as a potential therapeutic agent for HCC.

KEYWORDS

diaryl pyrimidine guanidine, CSCs, HCC, β-catenin/TCF4, lenvatinib resistance, combination treatment

Introduction

HCC is one of the leading causes of cancer-related deaths worldwide, primarily due to late-stage diagnosis, metastasis, and the development of resistance to available therapies (1, 2). Treatment options available for early-stage HCC patients usually include surgical resection, liver transplantation, and radiofrequency ablation. However, in advanced-stage HCC patients, who are no longer eligible for resection interventions, systemic therapies, such as chemotherapy and target therapy, are the only treatment option that can benefit them (3, 4). Recently, targeted therapies such as tyrosine kinase inhibitors (TKIs) have become a major focus of clinical treatment for HCC (4–6). Lenvatinib, a multi-targeted TKI, is one of the approved and most effective first-line treatments for advanced HCC. It is able to target tyrosine kinases, such as vascular endothelial growth factor receptors (VEGFR), fibroblast growth factor receptors (FGFR), and platelet-derived growth factor receptors (PDGFR), KIT, and RET to inhibit tumor angiogenesis and growth (5, 7). Although Lenvatinib has shown promising effects in improving progression-free survival of HCC patients, the development of drug resistance remains a significant challenge. Preclinical *in vitro* and *in vivo* studies indicate that TKIs may have off-target effects, which might also contribute to tumor recurrence and metastasis (8). Clinically, only approximately 30% of HCC patients initially respond to TKIs, and nearly all responders develop resistance within six months (8, 9). Therefore, new therapeutic strategies are needed to overcome this resistance and improve long-term outcomes for HCC patients.

CSCs have emerged as a critical factor in the progression and recurrence of various cancers, including HCC (10, 11). CSCs are a small subpopulation of tumor cells with the ability to self-renew, differentiate, and initiate tumors. These cells are often more resistant to conventional therapies, contributing to relapse and metastasis (12, 13). In HCC, CSCs are thought to be responsible for tumor initiation, progression, and resistance to both chemotherapy and targeted therapies (14). Therefore, targeting CSCs represents a promising strategy for improving the effectiveness of current treatments.

Several signaling pathways are well-known to regulate CSCs properties, including the Wnt/β-catenin pathway (15, 16). It has been addressed that aberrant activation of the Wnt/β-catenin signaling axis contributes to the maintenance of CSCs, therefore promotes cancer proliferation and survival (16, 17). β-catenin, the key effector of the Wnt pathway, is a central player in regulating CSCs functions, and its stabilization in the nucleus leads to the activation of target genes that promote tumorigenesis and CSCs maintenance (17–19). In HCC, the Wnt/β-catenin signaling pathway is frequently dysregulated and is associated with aggressive disease progression (19–21). Therefore, targeting this pathway has become a major focus in the development of novel CSCs-targeting strategies for HCC. Drugs that inhibit the Wnt pathway have shown promise in preclinical models, and several small molecules and biologics have entered clinical trials (22, 23). However, there is still no approved therapy specifically targeting CSCs in HCC, and challenges still remain in translating these findings into clinical practice.

The tumor sphere formation assay has been developed as an *in vitro* surrogate method to study CSCs potential (24, 25), we therefore screened a series of compounds in our in-house library using HCC sphere model to identify potential CSCs inhibitors. During 34 compounds examined, we identified C504244 as the most potent inhibitor of tumor sphere formation in HCC cell line Huh7. Further investigation revealed that C504244 effectively suppresses HCC CSCs proportion, as well as cancer cell proliferation and migration. Mechanism study revealed C504244 was able to efficiently disrupt β-catenin/TCF4 complex formation and suppress β-catenin downstream targets' expression. Furthermore, we found that C504244 treatment could sensitize Lenvatinib-resistant HCC cells to Lenvatinib, suggesting C504244 could be a promising strategy to overcome Lenvatinib resistance. This discovery holds clinical potential, offering a new approach for HCC treatment.

Materials and methods

Cell lines

Huh7, SK-Hep1, Hep1–6 liver cancer cell lines were purchased from the American Type Culture Collection (ATCC) and authenticated by short tandem repeat (STR) profiling, which was performed by Qida Biotechnology (Shanghai, China). All liver

cancer cell lines were cultured in Dulbecco's Modified Eagle Medium (DMEM) (#10-013-CVRC, Corning, VA, United States) medium supplemented with 10% fetal bovine serum (FBS) (#10099-141, Gibco, NY, United States). All cells were maintained in a humidified incubator at 37°C with 5% CO_2.

Sphere formation assay

HCC cells were seeded in low-adhesion 96-well plate at a density of 1,000 cells/well, with fresh culture medium replenished every three days. 10 days after culture, tumor spheres with diameter greater than 100μm were counted under a microscope. F12/DMEM supplemented with 1×B27, 20 ng/mL 20 ng/mL epidermal growth factor (EGF), 10 ng/mL fibroblast growth factor 10 (FGF10), and 10 ng/mL hepatocyte growth factor (HGF) and 1% PS was used as culture medium for sphere formation.

Aldehyde dehydrogenase analysis

The ALDEFLUOR™ assay kit (#01700, STEMCELL Technologies, Vancouver, BC) was used for ALDH activity detection following the manufacturer's protocol. A total of 2×10^5 cells were centrifuged at 250g for 5 minutes, and the supernatant was discarded. The pellet was washed twice with the assay buffer. Cells was resuspended in 400μL of assay buffer mixed with 3μL activated ALDEFLUOR reagent, followed by dividing into 2 equal parts. 1 part were added with 3μL N, N-Diethylaminobenzaldehyde (DEAB) inhibitor to serve as the negative control, and the other part as the experimental one. Cells were incubated in dark at 37°C for 45 minutes. After incubation, cells were centrifuged at 250 g for 5 minutes, washed twice with the assay buffer, and resuspended in 300μL assay buffer for flow cytometry analysis within 4 hours on (#CytoFLEX S, Beckman Coulter Inc, CA, United States).

CD24 staining flow cytometry assay

2×10^5 cells were centrifuged at 250 g for 5 minutes, and the supernatant was discarded. Cells were washed twice with staining/washing buffer (1×Phosphate-Buffered Saline (PBS) with 2% FBS). Each sample was then resuspended in 300μL of buffer and incubated with 5μL of CD24 antibody (#PMG555428, Becton, Dickinson and Company, NJ, United States) on ice for 25 minutes. After incubation, cells were centrifuged at 250 g for 5 minutes, washed twice, resuspended and filtered for flow cytometry analysis within 4 hours on (#CytoFLEX S, Beckman Coulter Inc, CA, United States).

Western blot assays

Tumor cells were lysed using RIPA lysis buffer (#P0013B, Beyotime, Shanghai, China), and protein concentration was quantified using the BCA Protein Assay Kit (#A55865, Thermo Fisher Scientific, MA, United States). The lysates were then subjected to SDS-PAGE and transferred onto PVDF membranes (#ISEQ00010, Millipore, Boston, United States). The membranes were blocked with 5% BSA for 1 hour at room temperature and incubated with primary antibodies at 4°C overnight. Subsequently, the blots were incubated with the horseradish peroxidase conjugated secondary antibody and developed by enhanced chemiluminescence.

Primary antibodies used were listed as following: Nanog (#4903), OCT4 (#2750), Sox2 (#2738), Sox9 (#D8G9H), GAPDH (#14C10), p-β-catenin-34/37 (#9561), β-catenin (#9562), p-GSK-3β (#9336), CyclinD1 (#2922), and TCF4 (#2569) were purchased from CST (United States), c-Myc (#9E10) was from Santa Cruz (United States).

Reverse transcription quantitative polymerase chain reaction assays

Total RNA was extracted using TRI-Reagent (#TR118, Molecular Research Center, Inc, Cincinnati, OH, United States). Gene expression levels were measured using SYBR Premix Ex Taq II (Takara Bio, Shiga, Japan) on a 7,300 Real-Time PCR system (Applied Biosystems, Franklin Lakes, NJ, United States) with designed primers for target genes. The primers used in this study are listed in Supplementary Table S1.

Colony formation assay

Cells in the logarithmic growth phase were counted, and 1,000 cells were seeded into each well of a 6-well plate. The cells were cultured for 10–14 days, with fresh medium changed every 3days. Colonies were fixed with 1mL 4% paraformaldehyde for 15 minutes, followed by staining with 0.1% crystal violet at room temperature for 20 minutes. Subsequently, stained colonies were washed with water until no residual dye remained. After the plate dried, images were taken. Finally, 10% acetic acid solution was added to dissolve the crystal violet for absorbance measuring at 530 nm using a microplate reader (#Multiskan SkyHigh, Thermo Fisher Scientific, Massachusetts, United States).

Cell migration and invasion assay

Cells were trypsinized, washed with PBS, resuspended in serum-free medium, and adjusted to a density of 2×10^5/mL. 500 μL medium containing 20% FBS was added to the lower chamber, 100-200μL of cell suspension was added to the upper chamber, followed by incubation for desired time course. Afterward, the chambers were washed with PBS, and a cotton swab was used to remove non-migrated cells on the upper chamber side from the membrane. Migrated cells were fixed with 4% paraformaldehyde for 20 minutes, stained with 0.1% crystal violet for 30 minutes, and washed with PBS for three times. The chambers were dried at 37°C,

and microscopic images were captured, with the number of migrated cells counted.

For the cell invasion assay, 20% Matrigel (#353097; Corning, NY, United States) diluted with serum-free medium was added to the upper chambers to mimic the extracellular matrix before the assay.

Immunofluorescence assay

3.5×10^4 cells were seeded onto coverslips in 12-well plates and cultured for 48–72 hours until an appropriate confluence was achieved. After washing with 1×PBS, the cells were fixed with 1mL 4% paraformaldehyde for 15 minutes. Next, the cells were permeabilized with 0.2% Triton X-100 for 10 minutes, followed by three washes with PBS. The cells were then blocked with 3% BSA for 15 minutes, followed by incubating with the primary antibody overnight at 4°C. Then, the cells were washed and incubated with Alexa Fluor 488-conjugated goat anti-rabbit IgG (H + L) (#ZF-0511, ZSGB-Bio, Beijing, China) for 1 hour in the dark, after washing, cells were mounted in DAPI-containing mounting medium (#P36941, Thermo Fisher Scientific, Massachusetts, United States) for imaging on a fluorescence microscope (FV3000, Olympus Corporation, Japan).

Immunoprecipitation assay

The IP assay was performed using an IP kit (P2197M, Beyotime, Shanghai, China). First, 300 μL of IP lysis buffer and 40 μL of Protein A magnetic beads were added to a sterile, enzyme-free EP tube. The mixture was thoroughly mixed, and the beads were separated using a magnetic stand. After washing the beads with PBS, the supernatant was discarded. In the experimental group, 350 μL of diluted primary antibody was incubated with the magnetic beads, while the control group was incubated with IgG. The incubation was carried out at 4°C with rotation for 8 hours. After cell lysis, proteins were extracted using IP lysis buffer, and their concentrations were determined. Equal amounts of protein were incubated with the magnetic beads for 8 hours. The beads were washed 5–6 times to remove nonspecific proteins. After the final wash, the beads were transferred to a new microcentrifuge tube, and 40 μL of 1×loading buffer was added. The samples were heated at 100°C for 10 minutes to denature the proteins. The denatured samples were separated by SDS-PAGE and analyzed by Western blot to detect the expression of the target protein.

Chromatin immunoprecipitation assays

ChIP was performed using the ChIP kit (#P2080S, Beyotime, Shanghai, China) according to the manufacturer's manual. In brief, ells were crosslinked with 3.7% formaldehyde, and crosslinking was terminated with glycine. After washing with PBS, cells were lysed in SDS Lysis Buffer containing protease inhibitors and incubated on ice. Chromatin was then fragmented to 200–1000 bp by sonication, and the shearing efficiency was checked by agarose gel electrophoresis. After centrifugation to remove the pellet, the supernatant was collected and diluted with ChIP Dilution Buffer. The sample was incubated with antibody targeting designed antigen, followed by immunoprecipitation using Protein A/G magnetic beads to enrich DNA fragments bound to the target protein. The immunocomplexes underwent a series of stringent washing steps to remove nonspecific binding. Finally, the target DNA was eluted using elution buffer, and crosslinking was reversed under high-temperature conditions. The DNA was then extracted and analyzed by RT-qPCR. The primers used in this study are listed in Supplementary Table S1.

Xenograft assays

The animal protocols were approved by the Biomedical Ethics Committee, Subcommittee on Laboratory Animal Welfare, Peking University (PUIRB-LA2022626). All mice were purchased from Vital River Laboratory Animal Technology Co. (Beijing, China) and were subcutaneously implanted with Hepa1–6 cells at a concentration of 5×10^5 cells per site in 6-week-old BALB/c nude mice. Once tumors reached approximately 50 mm^3 in volume, the mice were randomly divided into four groups (six mice per group) for drug administration. Tumor volume and body weight were measured daily throughout the treatment period. Tumor volume was calculated using the formula: volume (mm^3) = $L \times W^2 \times 0.5$ (where L is the longest diameter and W is the shortest diameter). At the end of the treatment, mice were euthanized and tumors were harvested for further analysis.

Data and code availability

RNA sequencing data have been deposited at Genome Sequence Archive for Human HRA006499 and are publicly available as of the date of this publication.

Compound characterization

^1H and ^{13}C Nuclear Magnetic Resonance (NMR) spectra were recorded on a Bruker AM-400 MHz spectrometer using C_2D_6OS (Deuterated Dimethyl Sulfoxide (DMSO)-d_6) as the solvent and tetramethyl silane (TMS) as the internal standard. Chemical shifts (δ) were reported in parts per million (ppm), and coupling constants (J) were expressed in hertz (Hz). NMR spectroscopy was used for structural elucidation of the compounds, and the detailed spectral data are shown in Supplementary Table S2 and Supplementary Figures S1A, B.

High-resolution mass spectra were obtained using an Agilent Liquid Chromatography/Mass Selective Detector Time-of-Flight (LC/MSD TOF) mass spectrometer. The mass spectrometric analysis provided accurate molecular weight information, which

was used to confirm the molecular formula of the isolated compounds. The detailed High-Resolution Electrospray Ionization Mass Spectrometry (HRESIMS) data are presented in Supplementary Table S2 and Supplementary Figure S1C.

High-Performance Liquid Chromatography (HPLC) analysis was carried out using an Agilent 1260 instrument equipped with a Gemini-NX C18 110A column (4.6 × 250 mm, 5 μm). The elution was performed at a flow rate of 1 mL/min with a gradient from 5% mixed solvent (99.5% acetonitrile + 0.5% triethylamine in water) to 100% mixed solvent over 20 minutes, followed by 5 minutes at 100% mixed solvent. HPLC was used to assess the purity of the compounds, and the results are summarized in Supplementary Table S3 and Supplementary Figure S1D.

Statistical analysis

All experimental data were analyzed using GraphPad Prism 5 software. The results are presented as mean ± standard error of the mean (Mean ± SEM). For comparisons involving only two groups, a two-tailed Student's t-test was used to calculate the p-value. When comparing more than two groups, one-way analysis of variance (One-Way ANOVA) was applied to calculate the p-value. A p-value less than 0.05 was considered statistically significant. The significant differences in the results are indicated with an asterisk: $*p < 0.05$.

Results

Identification and validation of C504244 as a CSCs-inhibitory compound

To identify small molecules with potential inhibitory effects on CSCs stemness, we performed a primary screen using our in-house library containing 34 candidate compounds (5 μM) using sphere formation assay in Huh7 HCC cells. Among all compounds detected, compound 31 (C504244) exhibited the most potent suppression ability of sphere formation (Figure 1A; Supplementary Figure S2). Structurally, C504244 features a diaryl pyrimidine guanidine scaffold (Figure 1B). Its physicochemical properties were computationally evaluated using ADMETlab 3.0 (https://admetlab3.scbdd.com), and the results (Supplementary Table S4) indicate favorable ADMET parameters, supporting further investigation. To further validate the inhibitory effect of C504244 on CSCs stemness, we treated two HCC cell lines, Huh7 and SK-Hep1, with C504244 at indicated concentrations (Figure 1C). As the data shown in Figure 1C, C504244 exhibited strong suppression effects in a dosage-dependent manner in both cell lines, suggesting a robust and consistent inhibitory effect on CSCs properties. We further assessed the potential cytotoxicity of C504244 in four normal human cells, HUVEC (Human Umbilical Vein Endothelial Cells), HDF (Human Dermal Fibroblast), WI-38 (human embryonic lung fibroblast), and PBMC (Peripheral Blood Mononuclear Cell). As shown in Supplementary Figure S3, C504244 exhibited markedly lower toxicity in all four normal cells than in 2 HCC cells (Huh7 and SK-Hep1), supporting its tumor-selective activity.

C504244 inhibits CSCs stemness in HCC cells

We ALDH activity assay, CSCs marker CD24 flow cytometry analysis, and western blotting/qPCR analysis of CSCs markers, to further validate the inhibitory effect of C504244 on CSCs stemness. The results of both Huh7 and SK-Hep1 cells showed similar trends, with C504244 significantly reducing CSCs characteristics. As the data shown in Figure 2, compared to the control group, C504244 treatments significantly decreased the proportion of ALDH+ and CD24+ cells, further confirming its inhibitory effect on CSCs characteristics. Meanwhile, the expression of several well-known CSCs markers, such as Nanog, OCT4, Sox2, and Sox9, were noticeably suppressed in C504244 treated HCC cells at both protein and mRNA levels (Figures 2C, D). Additionally, C504244 also suppressed the mRNA expression of ALDH (Figure 2D), which might contribute to the reduced activity of ALDH in C504244-treated cells.

To further evaluate the CSC-targeting effects of C504244, we sorted Huh7 cells into $CD133^+$ (HCC stem cells) and $CD133^-$ (non-stem cells) subpopulations (26–28) and treated them with vehicle control or C504244 at indicated dosages. As shown in Figures 2E–H, $CD133^+$ cells were markedly more sensitive to C504244 treatment, with an IC50 of 1.927 μM, compared to 10.79 μM in $CD133^-$ cells (Figure 2F). Consistently, C504244 inhibited $CD133^+$ cell growth more severely than $CD133^-$ cells (Figure 2G). Also, sphere formation ability was significantly reduced in $CD133^+$ populations upon C504244 treatment, with no significant effects in $CD133^-$ cells (Figure 2H). Taken together, these results further implicated the selective inhibitory effects of C504244 on CSC-like subpopulations in HCC.

C504244 suppresses HCC cell growth and migration abilities

In order to detected the effects of C504244 on HCC malignant progression, we first checked the role of it on cell viability, and found C504244 suppressed Huh7 and SK-Hep1 cell survival with IC_{50} as 4.159 μM and 6.315 μM, respectively (Figure 3A). Since both decreased cell growth and increased cell death contribute to suppressed cell viability, we first evaluated the effect of C504244 on cell proliferation using both growth curve analysis and colony formation assays. As shown in Figures 3B, C, treatment with C504244 significantly inhibited cell proliferation and colony formation in both Huh7 and SK-Hep1 cells, compared to the control group, confirming its inhibitory effect on HCC cell growth. We also checked cell apoptosis using Annexin V flow cytometry analysis, and found C504244 did not induce HCC cell apoptosis significantly (data not shown), indicating C50244 induced cell loss might predominantly cause by cell proliferation

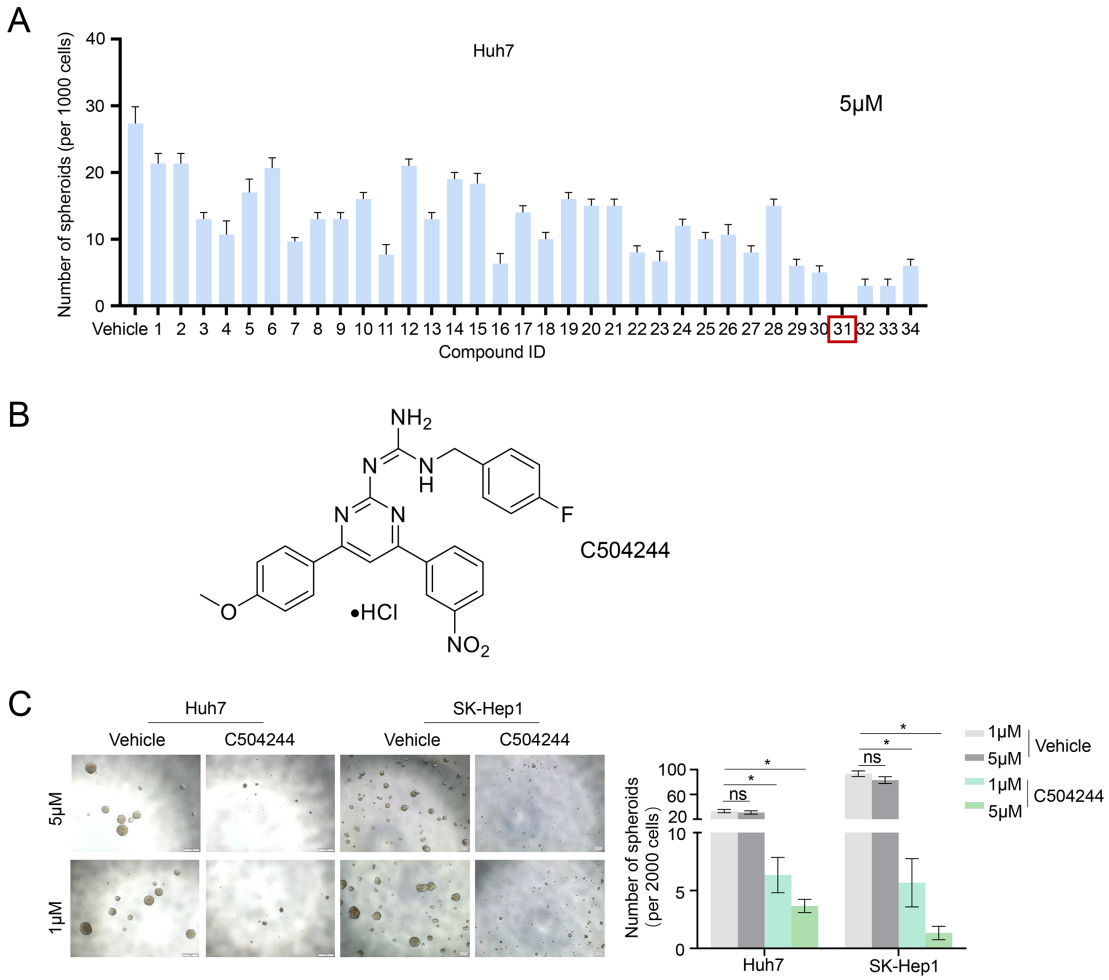

FIGURE 1
Identification of C504244 as a potent inhibitor of HCC sphere formation. **(A)** A panel of 34 small-molecule compounds from our in-house chemical library was screened in Huh7 spheres at a concentration of 5 μM. The number of tumor spheres with a diameter greater than 100 μm was counted. **(B)** The chemical structure of compound C504244. **(C)** Huh7 and SK-Hep1 cells were treated with vehicle Control (DMSO) or C504244 at indicated dosage for 6 days. Representative images of tumor spheres were captured, and the number of tumor spheres with a diameter greater than 100 μm was counted. All statistical analyses were performed using Student's *t*-test with significance indicated as $*p < 0.05$.

inhibition. We also examined the effects of C504244 on cell migration and invasion, the key characteristics of malignant progression. Transwell migration and Matrigel invasion assays (Figure 3D) revealed C504244 treatment significantly reduced both migration and invasion abilities of Huh7 and SK-Hep1 cells. Additionally, the wound healing assay (Figure 3E) showed impaired wound closure in C504244 treated cells, indicating slowed migration. In summary, C504244 effectively inhibits HCC cell proliferation, migration, and invasion, highlighting its potential as a therapeutic agent for targeting HCC progression.

C504244 suppresses Wnt signaling by disrupting β-catenin/TCF4 interaction

To elucidate the molecular mechanisms underlying the effects of C504244 in suppressing CSCs maintenance and malignant progression in HCC, we performed RNA sequencing using C504244-treated Huh7 cells, followed by Gene Ontology (GO) analysis. Among all the biological pathways affected by C504244, the Wnt signaling pathway (Figure 4A) particularly attracted our attention because the Wnt/β-catenin pathway is a central regulator of CSCs self-renewal and malignant progression in HCC. Activation of this pathway stabilizes β-catenin, facilitating its nuclear translocation and interaction with TCF4, which drives the transcription of downstream targets such as Cyclin D1 and c-Myc (17, 18, 29). To validate the sequencing results, we examined several downstream target genes of the Wnt pathway. Consistent with the RNA sequencing data, treatment with C504244 significantly inhibited the expression of 2 classic targets of Wnt signaling, c-Myc and CyclinD1 (Figure 4B). Unexpectedly, C504244 treatments did not alter total β-catenin levels or its phosphorylation at Ser33/37/Thr41 (which is targeted by GSK-3β for proteasomal degradation) (Figure 4B), nor the phosphorylation of GSK-3β (Ser9), a key kinase regulating β-catenin stability (Figure 4B), ruling out the possibility of upstream kinase modulation.

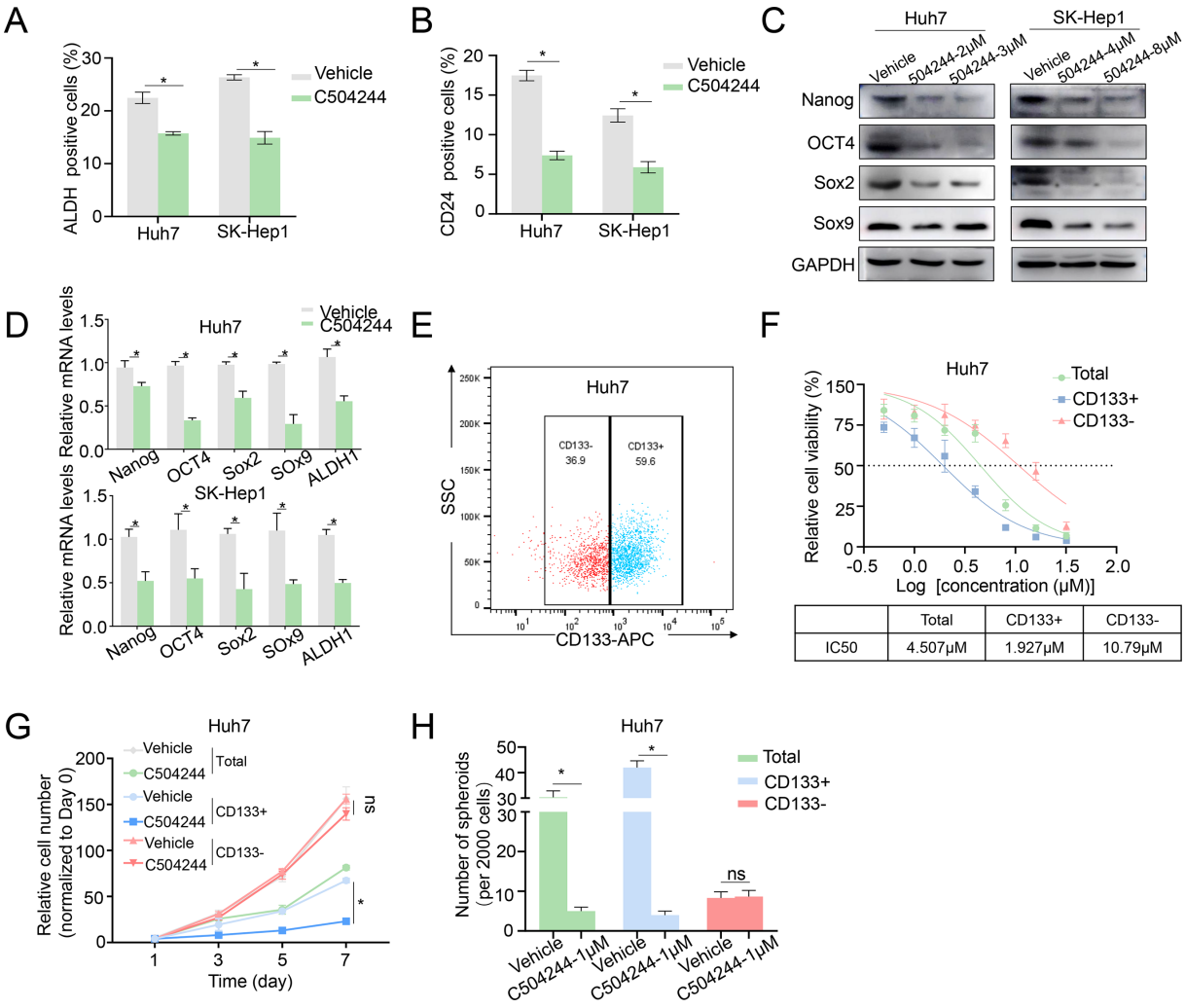

FIGURE 2
C504244 suppresses HCC CSCs maintenance. **(A-B)** DMSO or C504244 (2 μM) treated Huh7 and SK-Hep1 cells were collected for ALDH activity assay **(A)** and CD24 staining flow cytometry analysis**(B)**. The percentage of ALDH and CD24-positive cells was quantified in the bar graph. **(C-D)** Huh7 and SK-Hep1 cells treated with C504244 for 48 hours at indicated concentrations were collected for Western blot **(C)** and qPCRs **(D)** analysis. **(E)** Flow cytometric sorting of Huh7 cells to isolate $CD133^+$ and $CD133^-$ subpopulations. **(F)** Dose-response curves and IC50 values of C504244 in total, $CD133^+$, and $CD133^-$ Huh7 cells. **(G)** Huh7 cells plated in 96-well plates were treated with DMSO or C504244 at the day after seeding, cell numbers were counted every two days and monitored until day 7. Relative cell growth was normalized to day 1. **(H)** Huh7 cells were treated with vehicle Control (DMSO) or C504244 at indicated dosage for 6 days. Representative images of tumor spheres were captured, and the number of tumor spheres with a diameter greater than 100 μm was counted. All statistical analyses were performed using Student's *t*-test with significance indicated as $*p < 0.05$, ns, no statistical significance.

Moreover, immunofluorescence staining confirmed that the nuclear-cytoplasmic distribution of β-catenin was unchanged by C504244 treatments (Figure 4C). Given that the stability and localization of β-catenin were unaltered, we hypothesized that C504244 might interfere with its transcriptional activity. To test this possibility, we performed ChIP-qPCR to assess the binding of β-catenin/TCF complex to the promoters of its target genes. C504244 treatment led to a marked reduction in TCF4 occupancy at the c-Myc and Cyclin D1 promoter regions (Figure 4D), suggesting transcriptional repression. We further demonstrated that C504244 significantly impaired the formation of the β-catenin/TCF4 complex (Figure 4E), indicating that such compound disrupts their physical interaction. To further validate the inhibitory effect of C504244 on Wnt/β-catenin transcriptional activity, we performed qRT-PCR to assess the expression levels of key target genes. Consistent with previous results, treatment with C504244 significantly decreased c-Myc and Cyclin D1 mRNA expression (Figure 4F). These data provide evidences suggesting that C504244 represses Wnt signaling likely through inhibiting β-catenin/TCF4 interaction, thereby impairing the transcription of key oncogenic targets critical for HCC progression.

To determine whether the anti-tumor effects of C504244 are mainly dependent on β-catenin signaling or not, we checked the effects of C504244 on HCC cells under β-catenin knockdown

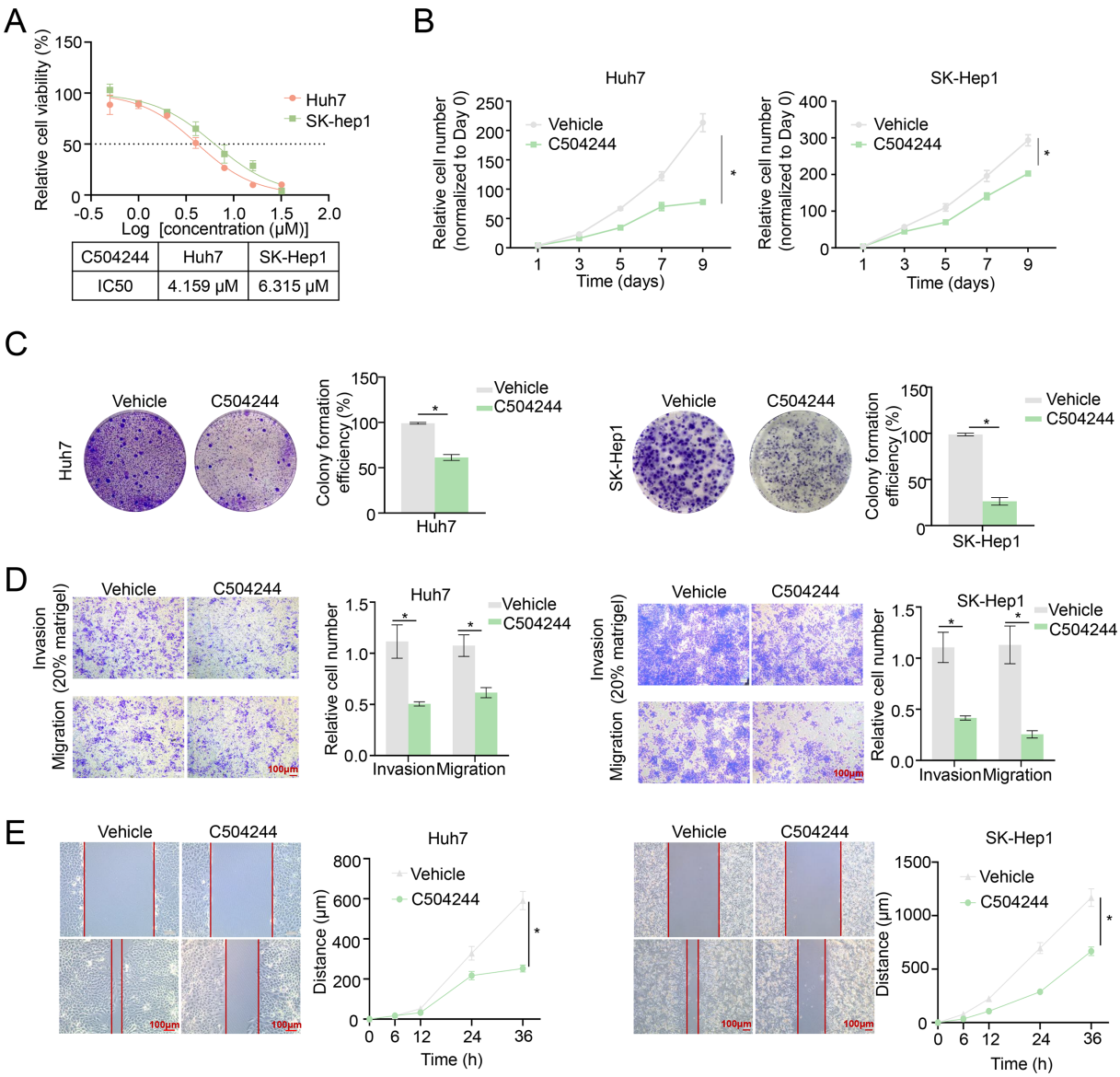

FIGURE 3
C504244 inhibits HCC cell proliferation and migration. **(A)** The IC_{50} values of C504244 in HCC cells were determined using cell viability assay. Huh7 and SK-Hep1 cells were treated with C504244 at indicated concentrations for 48 hours, followed by CCK-8 cell viability assay. **(B)** Huh7 and SK-Hep1 cells plated in 96-well plates were treated with DMSO or C504244 at the day after seeding, cell numbers were counted every two days and monitored until day 9. Relative cell growth was normalized to day 1. **(C)** Huh7 and SK-Hep1cells plated in 6-well plates were treated with DMSO or C504244 at the day after seeding. 14 days after drug treatment, the number of colonies formed was quantified, and representative images are shown. **(D)** DMSO or C504244 treated Huh7 and SK-Hep1 cells were collected for transwell migration and invasion assays. For invasion assays, 20% Matrigel was added to the transwell inserts. Cells that migrated or invaded through the membrane were stained with crystal violet and quantified by counting the number of cells. Scale bar = 100 μm. **(E)** Huh7 and SK-Hep1 cells treated with DMSO or C504244 for 24 hours were scratched for wound healing assay. Images were captured at 0- and 24-hours post-treatment. Scale bar = 100 μm. All statistical analyses were performed using Student's *t*-test, with significance indicated as $*p < 0.05$.

condition in Huh7 cells. In consistent with our previous results, we found C504244 alone significantly reduced the ALDH+ cell population, while β-catenin depletion (Supplementary Figure S4A) could slightly further enhance this reduction (Supplementary Figure S4B). We also found C504244 treatment markedly inhibited cell proliferation and migration, while β-catenin knockdown did not further suppress these phenotypes in HCC cells (Supplementary Figures S4C, D), indicating β-catenin plays vital roles in mediating C504244's functions in HCC cells.

C504244 synergizes with lenvatinib to overcome resistance in HCC

Multiple studies have confirmed that the Wnt/β-catenin signaling pathway is frequently aberrantly activated in HCC, contributing to disease progression and therapeutic resistance through various mechanisms (30–32). One critical mechanism is its role in maintaining CSCs stemness, which drives tumor resistance to anti-cancer therapies (22, 23). Consistently, analysis

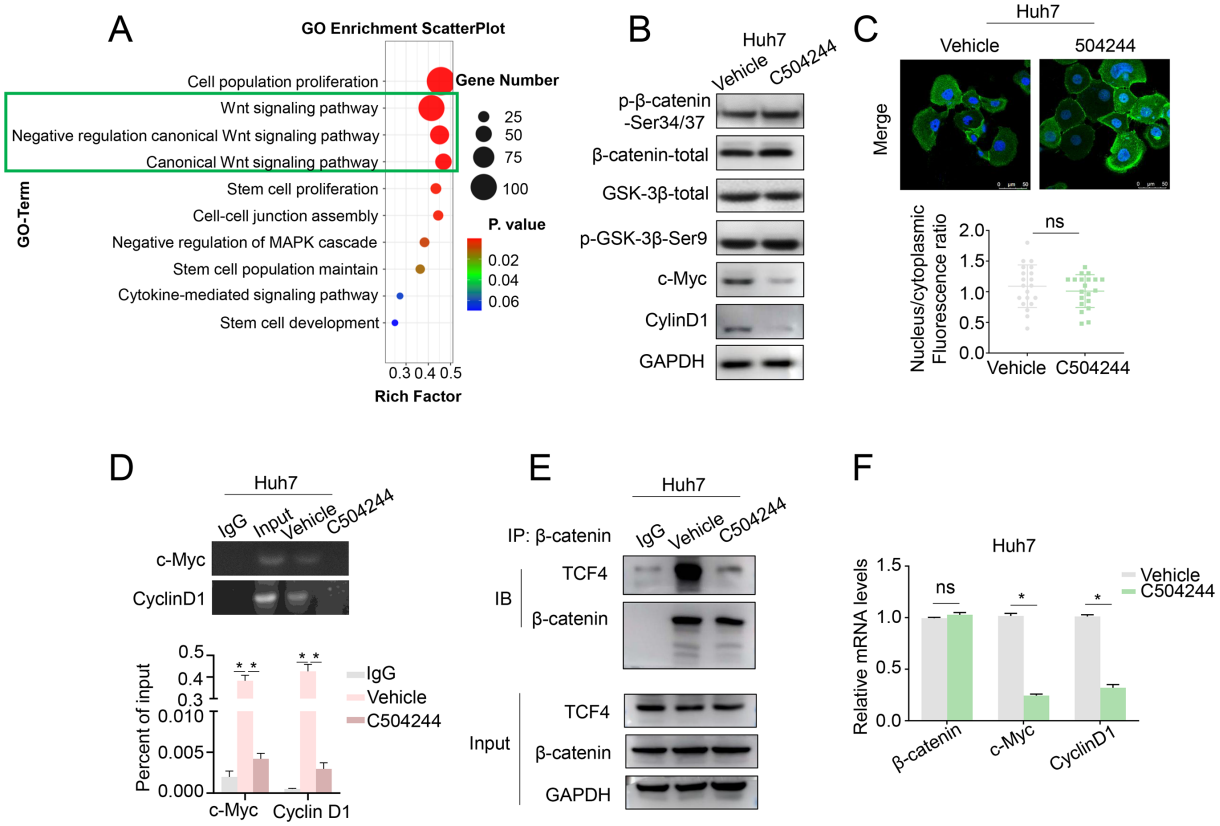

FIGURE 4
C504244 inhibits β-Catenin/TCF4 interaction. **(A)** GO analysis of C504244 treated compared to vehicle control Huh7 cell RNA sequencing data showing enrichment of the Wnt signaling pathway. **(B)** C504244 or DMSO treated Huh7 cells were collected for western blotting analysis, GAPDH was detected as the loading control. **(C)** Confocal immunofluorescence analysis of β-catenin in Huh7 cells treated with DMSO or C504244. The nucleocytoplasmic fluorescence ratio was quantified using ImageJ. Scale bar = 50 μm. **(D)** Binding of TCF4 to the promoter region of Cyclin D1 and c-Myc promoter was detected using chromatin immunoprecipitation (ChIP) assay in vehicle or C504244-treated Huh7 cells. **(E)** Co-immunoprecipitation (IP) analysis was performed to detect the interaction between TCF4 and β-catenin in vehicle or C504244-treated Huh7 cells. **(F)** mRNA expression levels of stemness-related genes were measured by qPCR in Huh7 cells treated with vehicle or C504244 (2 μM) for 48 hours. All statistical analyses were performed using Student's *t*-test, with significance indicated as $*p < 0.05$, ns, no statistical significance.

of our HCC organoids (with paired clinical samples) database (33) revealed significantly higher Wnt signaling activity in tumor tissues/organoids compared to adjacent normal liver tissues/organoids (Supplementary Figure S5A). Moreover, Wnt signaling is positively correlated with CSCs characteristics in HCC organoids (Supplementary Figure S5B), reinforcing its role in sustaining cancer stemness.

CSCs have been represented as the major source of therapy resistance (10, 12). Resistance to Lenvatinib, a first-line treatment for advanced HCC, has severely restricted the clinical benefits of this drug. Utilizing our HCC organoids drug-sensitivity database (33), we analyzed GSVA (Gene Set Variation Analysis) score of Wnt signaling in Lenvatinib resistant organoids compared to sensitive ones, the results revealed significantly higher Wnt pathway activation in the resistant organoids (Figure 5A). Furthermore, GSEA (Gene Set Enrichment Analysis) confirmed the enrichment of β-catenin target genes in the resistant organoids (Figure 5B). These findings suggest that aberrant Wnt activation may contribute to the development of Lenvatinib resistance.

Given these findings, we hypothesized that inhibiting Wnt/β-catenin signaling pathway could enhance the therapeutic efficacy of Lenvatinib. To test this possibility, we utilized Lenvatinib-resistant SK-Hep1 cells to assess whether combining C504244 with Lenvatinib could improve treatment response (8, 34, 35). Indeed, C504244 treatment significantly sensitize SK-Hep1 cells to Lenvatinib, with the synergy score (calculated using Synergy Finder 2.0) of 17 (Figure 5C), indicating a strong synergistic effect. Cell growth curve and colony formation assays confirmed the synergistic effects of C504244 and Lenvatinib (Figures 5D, E; Supplementary Figure S6A). Similarly, migration and wound healing assays showed that the combination treatment effectively suppressed cell migration (Figures 5F, G; Supplementary Figures S6B, C), indicating that C504244 enhances the sensitivity of Lenvatinib-resistant cells to Lenvatinib. We confirmed the effects of C504244 and Lenvatinib on HCC cells by checking the activation status of their target signaling pathways, including phosphorylation of VEGFR/Epidermal Growth Factor Receptor (EGFR) and expression of c-Myc and Cyclin D1.

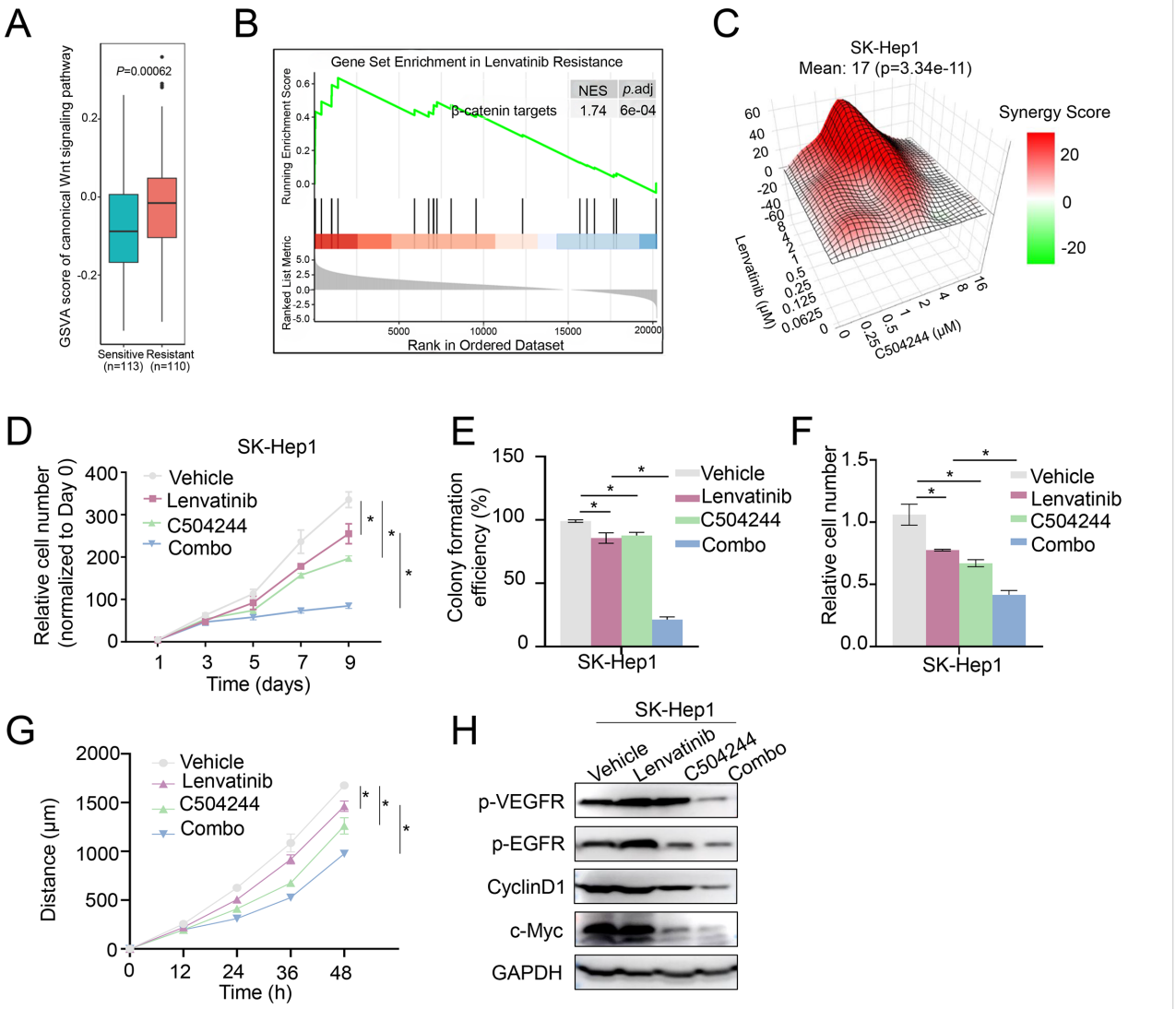

FIGURE 5
C504244 sensitize Lenvatinib resistant HCC cell to Lenvatinib. **(A)** GSVA of the canonical Wnt signaling pathway in Lenvatinib-sensitive (n=113) and Lenvatinib-resistant (n=110) organoids. **(B)** Gene Set Enrichment Analysis (GSEA) for β-catenin target genes in Lenvatinib-resistant organoids. The enrichment plot indicates significant upregulation of β-catenin target genes in resistant organoids. **(C)** Synergy map of SK-Hep1 cells treated with C504244 and Lenvatinib at indicated concentrations. **(D)** Cell proliferation was assessed by cell growth curve analysis of SK-Hep1 cells treated with DMSO, Lenvatinib (2 μM), C504244 (3 μM), or combination of both drugs. Cell numbers were counted every two days and monitored until day 9. Relative cell growth was normalized to day 0. **(E)** Colony formation assay was performed using SK-Hep1 cells treated with DMSO, Lenvatinib (2 μM), C504244 (3 μM), or combination of both drugs for 14 days. Colony formation efficiency was calculated by comparing colony numbers relative to the vehicle control. **(F)** SK-Hep1 cells treated with DMSO, Lenvatinib, C504244, or the combination for 24 hours were applied for cell migration assay. Scale bar = 100 μm. **(G)** SK-Hep1 cells treated with DMSO, Lenvatinib (2 μM), C504244 (3 μM), or the combination of both drugs were utilized for wound healing assay. Images were taken at 0- and 24-hours post-treatment. **(H)** SK-Hep1 cells treated with DMSO, Lenvatinib or C504244 were collected for western blotting analysis. GAPDH was detected as loading control. All statistical analyses were performed using Student's *t*-test, with significance indicated as $*p < 0.05$.

Lenvatinib inhibits VEGFR/EGFR signaling in Lenvatinib sensitive Huh7 cells as expected, and C504244 suppresses β-catenin signaling, thus combined application of both drugs blocks both VEGFR/EGFR and β-catenin signaling, which contributes the synergistic effects of these drugs in Huh7 cells (Supplementary Figure S7). While in Figure 5H, Lenvatinib failed to inhibit VEGFR/EGFR signalings in Lenvatinib resistant HCC cells, while C504244 suppresses β-catenin signaling, which meanwhile contributes to decreased EGFR activation (36), which might explain the synergistic effects of these drugs in HCC cells.

Combined lenvatinib and C504244 treatment inhibits tumor growth *in vivo*

To further confirm the synergistic anti-tumor effect of Lenvatinib and C504244, we employed the Hep1–6 cell line, which is also resistant to Lenvatinib (35). Similar to the results observed in SK-Hep1 cells, the combination of Lenvatinib and C504244 exhibited a strong synergistic effect in Hep1–6 cells (Supplementary Figure S8A). Consistently, the combination treatment also significantly inhibited Hep1–6 cell proliferation,

colony formation, and migration compared to either treatment alone (Supplementary Figures S8B-D).

To assess the therapeutic potential of combining Lenvatinib and C504244 *in vivo*, nude mice were implanted with Lenvatinib-resistant murine Hep1–6 tumor cells and treated with DMSO, Lenvatinib (4 mg/kg), C504244 (25 mg/kg), or the combination of both agents (35). Tumor volume was monitored over the treatment period, and the results demonstrated a significant reduction in tumor growth in the combination treatment group compared to the single-agent treatment groups (Figure 6A), without affecting the body weight, indicating that combination of Lenvatinib and C504244 did not cause obvious toxicity (Figure 6B). Moreover, Hematoxylin and Eosin (H&E) staining of major organs (heart, liver, kidney, spleen, and lung) showed no evident tissue damage, inflammation, or necrosis in mice treated with C504244 alone or in combination with Lenvatinib, further supporting the safety of C504244 and the combination regimen at the tested doses (Supplementary Figure S9). Tumor masses were weighed at the end of the treatment period, and the data revealed a significant decrease in tumor weight in the combination group compared to the individual treatment groups (Figures 6C, D). Meanwhile, we noticed that the Ki67 and c-Myc positive cells were severely reduced in the combination group, which further confirmed C504244, in combination with Lenvatinib, exhibits synergistic effects and can reverse Lenvatinib resistance in liver cancer cells. These results collectively demonstrate that the combination of Lenvatinib and C504244 effectively inhibits tumor growth and reduces tumor weight *in vivo*, supporting the potential of this combination therapy for enhanced anti-tumor efficacy.

Discussion

HCC remains a global health challenge worldwide, with late-stage diagnosis, aggressive metastasis, and therapeutic resistance significantly limiting patient survival benefits (1, 37). According to the 2024 American Society of Clinical Oncology (ASCO) guidelines, TKIs such as Lenvatinib or sorafenib remain key components of first-line therapy, typically in combination with immune checkpoint inhibitors (ICIs), such as PD-1/PD-L1 antibodies (4, 38, 39). As a multi-targeted TKI inhibiting VEGFR1-3, FGFR1-4, and PDGFRα, Lenvatinib demonstrated superior efficacy over sorafenib in the REFLECT phase III trial, with a median overall survival (OS) of 13.6 months (versus 12.3 months for sorafenib) and an objective response rate (ORR) of 24.1% (compared to 9.2% for sorafenib) (5, 6, 40). However, the therapeutic potential of Lenvatinib is still frequently hindered by acquired resistance mechanisms (8, 41). One of the critical contributors to Lenvatinib resistance is the enrichment of CSCs within the tumors (42, 43).

Extensive studies have established a close link between CSCs and HCC recurrence, metastasis, and drug resistance (12, 13). CSCs are a subset of tumor cells with self-renewal capacity, multilineage differentiation potential, and high tumorigenicity. Several keys signaling, such as Wnt/β-catenin, Notch and Hedgehog pathways, have been well-documented to play vital roles in maintaining stemness properties of CSCs (15, 16). Aberrant activation of the Wnt/β-catenin pathway in malignant tumors, often due to CTNNB1 gain-of-function or APC loss-of-function mutations, leads to the upregulation of crucial target genes, such as c-MYC, Cyclin D1, and SOX9, which are involved in promoting cancer cell proliferation, survival, and sustaining CSCs stemness (17, 22, 23). Accumulating evidences suggest that acquired resistance to TKIs is associated with the enrichment of CSCs populations (42, 43). In this context, Wnt/β-catenin signaling emerges as a key contributor, not only in maintaining CSCs stemness but also in driving TKI resistance (8). The aberrant activation of this pathway helps CSCs survive and proliferate despite treatment, making it an important factor in the development of resistance to therapies like TKIs (21, 29). Given the significant role of Wnt signaling in both CSCs maintenance and TKI resistance, targeting this pathway might provide a promising therapeutic strategy. Interestingly, a recent study showed that the combination of Lenvatinib with the CDK6 inhibitor palbociclib can overcome cell resistance to Lenvatinib by blocking the Wnt/β-catenin pathway (31). This approach highlights the potential for combination therapies to effectively target both CSCs stemness and the underlying mechanisms of drug resistance.

In this study, we identified C504244 as a novel compound that inhibits Wnt/β-catenin signaling and effectively suppresses malignant phenotypes of HCC cells. Functionally, C504244 treatment led to reduced cell proliferation, migration, and invasion, along with a marked decrease in CSCs-associated features (44). Mechanistically, we found that C504244 suppressed Wnt/β-catenin pathway by inhibiting the formation of β-catenin/TCF4 complex, thereby weakening the binding of such complex to target genes' promoter and inhibiting downstream genes' expression. It is worth noticing that although our data indicate reduced interaction between β-catenin and TCF4 upon C504244 treatment, we do not yet have direct evidence that C504244 physically disrupts the formation of the β-catenin/TCF4 complex. Importantly, our results also suggest that the inhibitory function of C504244 is largely dependent on β-catenin signaling, as β-catenin knockdown did not further enhance the anti-tumor effects of C504244. Further studies are needed to clarify the precise mechanism by which C504244 interferes with the β-catenin/TCF4 transcriptional complex, including whether it directly disrupts their interaction interface, induces conformational changes, or acts through other mechanisms.

Given the limited efficacy of Lenvatinib monotherapy, combination therapies are actively being explored (3, 4). Previous studies have reported that Lenvatinib combined with PD-1 inhibitors (e.g., pembrolizumab) benefits selected patients with high PD-L1 expression (7, 45). Additionally, Lenvatinib in combination with suberoylanilide hydroxamic acid (SAHA), a histone deacetylase inhibitor, has been shown to enhance therapeutic outcomes (35). For EGFR-positive HCC patients, the combination of Lenvatinib and the EGFR inhibitor gefitinib significantly improves ORR (46).

In our patient-derived organoid database (33), we observed that Wnt signaling is significantly upregulated in Lenvatinib-resistant HCC samples, suggesting that Wnt activation might contribute to

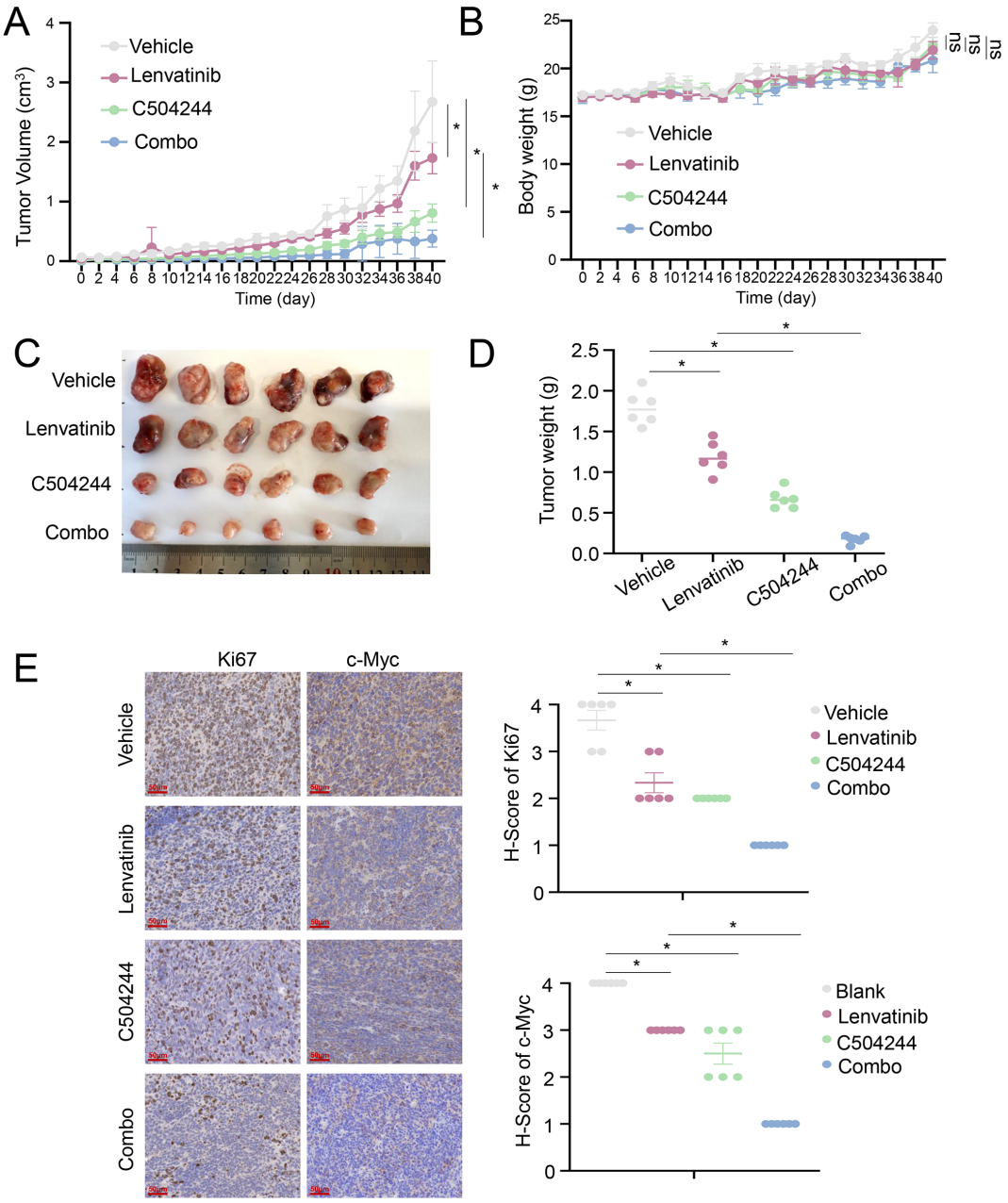

FIGURE 6
C504244 sensitize Lenvatinib resistant HCC cell to Lenvatinib *in vivo*. **(A-B)** Tumor growth curve of Hepa1–6 cells in nude mice treated with DMSO, Lenvatinib (4 mg/kg), C504244 (25 mg/kg), or the combination of both drugs. Tumor volume **(A)** and body weight **(B)** were measured daily, with every-other-day data displayed in the graphs for clarity. **(C-D)** Tumors excised at the end of the experiment **(C)** were weighed **(D)**. **(E)** Tumors from each group mentioned above were fixed and sectioned for IHC staining of Ki67 and c-Myc. Statistical significance was assessed by Student's *t*-test, with significance indicated as $*p < 0.05$.

Lenvatinib resistance. Thus, targeting Wnt signaling holds the possibility to overcome Lenvatinib resistance and improve therapeutic efficacy. Interestingly, both *in vitro* and *in vivo* studies revealed that C504244 enhances Lenvatinib sensitivity in resistant HCC cell lines. These findings suggest that C504244 not only suppresses CSCs stemness and malignant phenotypes in HCC cells but also potentiates Lenvatinib's therapeutic efficacy by counteracting Wnt-driven resistance mechanisms.

Compared to these approaches, C504244 offers a unique mechanism that integrates CSCs-targeting and anti-angiogenesis strategies, potentially overcoming the limitations of existing combination regimens. However, further validation in patient-derived organoids or humanized patient-derived xenograft models is necessary to translate these findings into clinical applications. Future studies should further investigate whether Wnt activation can be used as a predictive biomarker for Lenvatinib resistance and whether C504244's efficacy extends to a broader range of resistant models.

In conclusion, C504244, a novel compound that suppresses CSCs stemness, offers a potential strategy to overcome Lenvatinib

resistance in HCC. Its synergistic effect with Lenvatinib enhances treatment efficacy in resistant HCC models. Given Lenvatinib's current clinical positioning, this combination therapy may help bridge the gap between CSCs-targeting and anti-angiogenesis strategies, providing a new avenue for improving patient outcomes. However, further studies are needed to optimize its pharmacokinetic properties, validate its efficacy in patient-derived models, and explore its clinical translation potentials.

Data availability statement

The datasets presented in this study can be found in online repositories. The names of the repository/repositories and accession number(s) can be found in the article/Supplementary Material.

Ethics statement

Ethical approval was not required for the studies on humans in accordance with the local legislation and institutional requirements because only commercially available established cell lines were used. The animal study was approved by The animal protocols were approved by the Biomedical Ethics Committee, Subcommittee on Laboratory Animal Welfare, Peking University (PUIRB-LA2022626). The study was conducted in accordance with the local legislation and institutional requirements.

Author contributions

XC: Conceptualization, Data curation, Formal Analysis, Methodology, Software, Validation, Writing – original draft, Writing – review & editing. DN: Data curation, Resources, Writing – original draft. JC: Formal Analysis, Investigation, Resources, Writing – original draft. BL: Data curation, Visualization, Writing – original draft. RZ: Conceptualization, Project administration, Supervision, Writing – review & editing. WX: Methodology, Writing – review & editing, Funding acquisition, Conceptualization, Supervision. RL: Conceptualization, Funding acquisition, Methodology, Project administration, Supervision, Writing – original draft, Writing – review & editing.

Funding

The author(s) declare financial support was received for the research and/or publication of this article. This work was financially supported by the National Natural Science Foundation of China (U24A20805, 22477108, 82260694), the Yunnan Fundamental Research Projects (202501BC070005, 202301AW070003, 202201AT070297), the Project of Yunnan Characteristic Plant Screening and R&D Service CXO Platform (2022YKZY001), and the Yun Ling Scholar Project awarded to WX. The funders had no role in study design, data collection and analysis, decision to publish, or preparation of the manuscript.

Acknowledgments

The authors express their sincere gratitude to all individuals who participated in the study and to the research personnel for their invaluable assistance and cooperation throughout the duration of the research.

Conflict of interest

The authors declare that the research was conducted in the absence of any commercial or financial relationships that could be construed as a potential conflict of interest.

Generative AI statement

The author(s) declare that no Generative AI was used in the creation of this manuscript.

Any alternative text (alt text) provided alongside figures in this article has been generated by Frontiers with the support of artificial intelligence and reasonable efforts have been made to ensure accuracy, including review by the authors wherever possible. If you identify any issues, please contact us.

Publisher's note

Supplementary material

The Supplementary Material for this article can be found online at: https://www.frontiersin.org/articles/10.3389/fonc.2025.1641979/full#supplementary-material

SUPPLEMENTARY FIGURE 1
NMR, HRESIMS, and HPLC characterization of compound C504244. **(A)** ^{1}H NMR Spectrum (400MHz) of compound 504244 in DMSO-d6. **(B)** ^{13}C NMR Spectrum (100MHz) of compound 504244 in DMSO-d6. **(C)** HRESIMS Spectrum of compound 504244. **(D)** HPLC trace of compound 504244.

SUPPLEMENTARY FIGURE 2
Identification of C504244 as a potent inhibitor of tumor sphere formation. Representative images of spheroids formed under each treatment condition are shown. Compound 31 exhibited the strongest inhibitory effect.

SUPPLEMENTARY FIGURE 3
Cytotoxicity of C504244 in normal human cells. The IC_{50} values of C504244 in cells were determined using cell viability assay. Huh7, SK-Hep1, HUVEC, HDF, WI-38, and PBMC cells were treated with C504244 at indicated dosages for 48h, and cell viability was measured using the CCK-8 assay.

SUPPLEMENTARY FIGURE 4
C504244 functions mainly via suppressing β-catenin signaling in HCC cells. **(A)** Huh7 cells were transfected with siRNA targeting β-catenin (20 nM) or negative control, and treated with DMSO or C504244 (2 μM) for 48 hours. GAPDH was detected as the loading control. **(B)** ALDH activity was analyzed by flow cytometry, and the percentage of ALDH+ cells was quantified. **(C)** Cell proliferation was assessed by cell growth curve analysis in Huh7 cells. Cell numbers were detected every two days and monitored until day 9 after plating. Relative cell growth was normalized to day 1. **(D)** Cell migration was evaluated by wound healing assay in Huh7 cells. Images were captured at 0- and 24-hours post-scratching. Scale bar = 100 μm. All statistical analyses were performed using Student's t-test, with significance indicated as $*p < 0.05$.

SUPPLEMENTARY FIGURE 5
Canonical Wnt signaling correlates with stemness in HCC. **(A)** GSVA scores of the canonical Wnt signaling pathway were compared between tumor and adjacent liver tissue derived organoids and corresponding primary tissues. **(B)** A positive correlation was observed between canonical Wnt signaling activity and embryonic stem cell-like signatures in HCC organoids.

SUPPLEMENTARY FIGURE 6
Synergistic effects of Lenvatinib and C504244 in SK-Hep1 cells. **(A-C)** SK-Hep1 cells treated with DMSO, Lenvatinib, C504244, or the combination of both drugs were applied for colony formation **(A)**, migration **(B)**, and wound healing **(C)** assays.

SUPPLEMENTARY FIGURE 7
Synergistic effect of Lenvatinib and C504244 in Huh7 cells. **(A)** Huh7 cells treated with DMSO, Lenvatinib or C504244 were collected for western blotting analysis. GAPDH was detected as loading control. **(B)** SK-Hep1 and Hep1–6 cells treated with C504244 for 48 hours at indicated concentrations were collected for qPCRs analysis.

SUPPLEMENTARY FIGURE 8
Synergistic effect of Lenvatinib and C504244 in Hep1–6 cells. **(A)** Synergy map of Hep1–6 cells treated with indicated concentrations of C504244 and Lenvatinib. **(B)** Cell proliferation was assessed by cell growth curve analysis in Hep1–6 cells treated with DMSO, Lenvatinib (4 μM), C504244 (4 μM), or the combination. Cell numbers were counted every two days and monitored until day 9. Relative cell growth was normalized to day 0. **(C)** Colony formation assay was performed on Hep1–6 cells treated with DMSO, Lenvatinib (4 μM), C504244 (4 μM), or the combination for 14 days. Colony formation efficiency was quantified by counting colonies and expressing the results as a percentage relative to the vehicle control. **(D)** Cell migration was evaluated using a migration assay, where Hep1–6 cells were treated with DMSO, Lenvatinib, C504244, or the combination for 24 hours. Migrated cells were stained with crystal violet, and the relative number of cells that migrated through the membrane was quantified. Scale bar = 100 μm. All statistical analyses were performed using Student's *t*-test, with significance indicated as $*p < 0.05$.

SUPPLEMENTARY FIGURE 9
Evaluation of C504244 and combination treatment on organ histology. Histological analysis of major organs (heart, kidney, liver, spleen, and lung) from Hep1–6 tumor-bearing nude mice after treatment with vehicle, Lenvatinib, C504244, or the combination for 40 days. Representative H&E-stained sections from each group (n = 6) are shown. No evident tissue damage, inflammation, or necrosis was observed in any treatment group, indicating no overt systemic toxicity. Scale bar = 100 μm.

References

1. Toh MR, Wong EYT, Wong SH, Ng AWT, Loo L-H, Chow PK-H, et al. Global epidemiology and genetics of hepatocellular carcinoma. *Gastroenterology*. (2023) 164:766–82. doi: 10.1053/j.gastro.2023.01.033

2. Bray F, Laversanne M, Sung H, Ferlay J, Siegel RL, Soerjomataram I, et al. Global cancer statistics 2022: GLOBOCAN estimates of incidence and mortality worldwide for 36 cancers in 185 countries. *CA Cancer J Clin*. (2024) 74:229–63. doi: 10.3322/caac.21834

3. Yang C, Zhang H, Zhang L, Zhu AX, Bernards R, Qin W, et al. Evolving therapeutic landscape of advanced hepatocellular carcinoma. *Nat Rev Gastroenterol Hepatol*. (2023) 20:203–22. doi: 10.1038/s41575-022-00704-9

4. Huang A, Yang XR, Chung WY, Dennison AR, Zhou J. Targeted therapy for hepatocellular carcinoma. *Signal Transduct Target Ther*. (2020) 5:146. doi: 10.1038/s41392-020-00264-x

5. Al-Salama ZT, Syed YY, Scott LJ. Lenvatinib: A review in hepatocellular carcinoma. *Drugs*. (2019) 79:665–74. doi: 10.1007/s40265-019-01116-x

6. Rimassa L, Finn RS, Sangro B. Combination immunotherapy for hepatocellular carcinoma. *J Hepatol*. (2023) 79:506–15. doi: 10.1016/j.jhep.2023.03.003

7. Chen Y, Dai S, Cheng CS, Chen L. Lenvatinib and immune-checkpoint inhibitors in hepatocellular carcinoma: mechanistic insights, clinical efficacy, and future perspectives. *J Hematol Oncol*. (2024) 17:130. doi: 10.1186/s13045-024-01647-1

8. Ladd AD, Duarte S, Sahin I, Zarrinpar A. Mechanisms of drug resistance in HCC. *Hepatology*. (2024) 79:926–40. doi: 10.1097/HEP.0000000000000237

9. Gawi Ermi A, Sarkar D. Resistance to tyrosine kinase inhibitors in hepatocellular carcinoma (HCC): clinical implications and potential strategies to overcome the resistance. *Cancers (Basel)*. (2024) 16:3944. doi: 10.3390/cancers16233944

10. Lee TK, Guan XY, Ma S. Cancer stem cells in hepatocellular carcinoma - from origin to clinical implications. *Nat Rev Gastroenterol Hepatol*. (2022) 19:26–44. doi: 10.1038/s41575-021-00508-3

11. Lam KH, Ma S. Noncellular components in the liver cancer stem cell niche: Biology and potential clinical implications. *Hepatology*. (2023) 78:991–1005. doi: 10.1002/hep.32629

12. Batlle E, Clevers H. Cancer stem cells revisited. *Nat Med*. (2017) 23:1124–34. doi: 10.1038/nm.4409

13. Kreso A, Dick JE. Evolution of the cancer stem cell model. *Cell Stem Cell*. (2014) 14:275–91. doi: 10.1016/j.stem.2014.02.006

14. Zhao H, Ling Y, He J, Dong J, Mo Q, Wang Y, et al. Potential targets and therapeutics for cancer stem cell-based therapy against drug resistance in hepatocellular carcinoma. *Drug Resist Update*. (2024) 74:101084. doi: 10.1016/j.drup.2024.101084

15. Clara JA, Monge C, Yang Y, Takebe N. Targeting signalling pathways and the immune microenvironment of cancer stem cells - a clinical update. *Nat Rev Clin Oncol*. (2020) 17:204–32. doi: 10.1038/s41571-019-0293-2

16. Chu X, Tian W, Ning J, Xiao G, Zhou Y, Wang Z, et al. Cancer stem cells: advances in knowledge and implications for cancer therapy. *Signal Transduct Target Ther*. (2024) 9:170. doi: 10.1038/s41392-024-01851-y

17. Song P, Gao Z, Bao Y, Chen L, Huang Y, Liu Y, et al. Wnt/beta-catenin signaling pathway in carcinogenesis and cancer therapy. *J Hematol Oncol*. (2024) 17:46. doi: 10.1186/s13045-024-01563-4

18. Zhang Y, Wang X. Targeting the Wnt/beta-catenin signaling pathway in cancer. *J Hematol Oncol*. (2020) 13:165. doi: 10.1186/s13045-020-00990-3

19. Liu J, Xiao Q, Xiao J, Niu C, Li Y, Zhang X, et al. Wnt/beta-catenin signalling: function, biological mechanisms, and therapeutic opportunities. *Signal Transduct Target Ther*. (2022) 7:3. doi: 10.1038/s41392-021-00762-6

20. Perugorria MJ, Olaizola P, Labiano I, Esparza-Baquer A, Marzioni M, Marin JJG, et al. Wnt-beta-catenin signalling in liver development, health and disease. *Nat Rev Gastroenterol Hepatol*. (2019) 16:121–36. doi: 10.1038/s41575-018-0075-9

21. Russell JO, Monga SP. Wnt/beta-catenin signaling in liver development, homeostasis, and pathobiology. *Annu Rev Pathol*. (2018) 13:351–78. doi: 10.1146/annurev-pathol-020117-044010

22. Yang L, Shi P, Zhao G, Xu J, Peng W, Zhang J, et al. Targeting cancer stem cell pathways for cancer therapy. *Signal Transduct Target Ther*. (2020) 5:8. doi: 10.1038/s41392-020-0110-5

23. Takebe N, Miele L, Harris PJ, Jeong W, Bando H, Kahn M, et al. Targeting Notch, Hedgehog, and Wnt pathways in cancer stem cells: clinical update. *Nat Rev Clin Oncol*. (2015) 12:445–64. doi: 10.1038/nrclinonc.2015.61

24. Pastrana E, Silva-Vargas V, Doetsch F. Eyes wide open: a critical review of sp*here-formation as an assay for stem cells*. *Cell Stem Cell*. (2011) 8:486–98. doi: 10.1016/j.stem.2011.04.007

25. Tang DG. Understanding cancer stem cell heterogeneity and plasticity. *Cell Res*. (2012) 22:457–72. doi: 10.1038/cr.2012.13

26. Ma S, Chan KW, Hu L, Lee T-K, Wo JY-H, Ng I-O, et al. Identification and characterization of tumorigenic liver cancer stem/progenitor cells. *Gastroenterology*. (2007) 132:2542–56. doi: 10.1053/j.gastro.2007.04.025

27. Xue M, Dong L, Zhang H, Li Y, Qiu K, Zhao Z, et al. METTL16 promotes liver cancer stem cell self-renewal via controlling ribosome biogenesis and mRNA translation. *J Hematol Oncol*. (2024) 17:7. doi: 10.1186/s13045-024-01526-9

28. Liu F, Wu X, Jiang X, Qian Y, Gao J. Prolonged inhibition of class I PI3K promotes liver cancer stem cell expansion by augmenting SGK3/GSK-3beta/beta-catenin signalling. *J Exp Clin Cancer Res*. (2018) 37:122. doi: 10.1186/s13046-018-0801-8

29. Majumdar A, Curley SA, Wu X, Brown P, Hwang JP, Shetty K, et al. Hepatic stem cells and transforming growth factor beta in hepatocellular carcinoma. *Nat Rev Gastroenterol Hepatol*. (2012) 9:530–8. doi: 10.1038/nrgastro.2012.114

30. Wang J, Yu H, Dong W, Zhang C, Hu M, Ma W, et al. N6-methyladenosine-mediated up-regulation of FZD10 regulates liver cancer stem cells' Properties and lenvatinib resistance through WNT/beta-catenin and hippo signaling pathways. *Gastroenterology*. (2023) 164:990–1005. doi: 10.1053/j.gastro.2023.01.041

31. Leung CON, Yang Y, Leung RWH, So K-KH, Guo HJ, Lei MML, et al. Broad-spectrum kinome profiling identifies CDK6 upregulation as a driver of lenvatinib resistance in hepatocellular carcinoma. *Nat Commun*. (2023) 14:6699. doi: 10.1038/s41467-023-42360-w

32. Toh TB, Lim JJ, Hooi L, Abdul Rashid MBM, Chow EK-H. Targeting Jak/Stat pathway as a therapeutic strategy against SP/CD44+ tumorigenic cells in Akt/beta-catenin-driven hepatocellular carcinoma. *J Hepatol*. (2020) 72:104–18. doi: 10.1016/j.jhep.2019.08.035

33. Yang H, Cheng J, Zhuang H, Xu H, Wang Y, Zhang T, et al. Pharmacogenomic profiling of intra-tumor heterogeneity using a large organoid biobank of liver cancer. *Cancer Cell*. (2024) 42:535–551.e538. doi: 10.1016/j.ccell.2024.03.004

34. Tang Y, Fan S, Peng R, Liu H, Su B, Tu D, et al. TRIM29 reverses lenvatinib resistance in liver cancer cells by ubiquitinating and degrading YBX1 to inhibit the PI3K/AKT pathway. *Transl Oncol*. (2025) 53:102294. doi: 10.1016/j.tranon.2025.102294

35. Yan S, Chen L, Zhuang H, Yang H, Yang Y, Zhang N, et al. HDAC inhibition sensitize hepatocellular carcinoma to lenvatinib via suppressing AKT activation. *Int J Biol Sci*. (2024) 20:3046–60. doi: 10.7150/ijbs.93375

36. Hu T, Li C. Convergence between Wnt-beta-catenin and EGFR signaling in cancer. *Mol Cancer*. (2010) 9:236. doi: 10.1186/1476-4598-9-236

37. Llovet JM, Kelley RK, Villanueva A, Singal AG, Pikarsky E, Roayaie S, et al. Hepatocellular carcinoma. *Nat Rev Dis Primers*. (2021) 7:6. doi: 10.1038/s41572-020-00240-3

38. Yang H, Liu Y, Zhang N, Tao F, Yin G. Therapeutic advances in hepatocellular carcinoma: an update from the 2024 ASCO annual meeting. *Front Oncol*. (2024) 14:1453412. doi: 10.3389/fonc.2024.1453412

39. Gordan JD, Kennedy EB, Abou-Alfa GK, Beal E, Finn RS, Gade TP, et al. Systemic therapy for advanced hepatocellular carcinoma: ASCO guideline update. *J Clin Oncol*. (2024) 42:1830–50. doi: 10.1200/JCO.23.02745

40. Chan LL, Chan SL. The evolving role of lenvatinib at the new era of first-line hepatocellular carcinoma treatment. *Clin Mol Hepatol*. (2023) 29:909–23. doi: 10.3350/cmh.2023.0114

41. Vogel A, Qin S, Kudo M, Su Y, Hudgens S, Yamashita T, et al. Lenvatinib versus sorafenib for first-line treatment of unresectable hepatocellular carcinoma: patient-reported outcomes from a randomised, open-label, non-inferiority, phase 3 trial. *Lancet Gastroenterol Hepatol*. (2021) 6:649–58. doi: 10.1016/S2468-1253(21)00110-2

42. Si J, Ma Y, Bi JW, Xiong Y, Lv C, Li S, et al. Shisa3 brakes resistance to EGFR-TKIs in lung adenocarcinoma by suppressing cancer stem cell properties. *J Exp Clin Cancer Res*. (2019) 38:481. doi: 10.1186/s13046-019-1486-3

43. Del Re M, Arrigoni E, Restante G, Passaro A, Rofi E, Crucitta S, et al. Concise review: resistance to tyrosine kinase inhibitors in non-small cell lung cancer: the role of cancer stem cells. *Stem Cells*. (2018) 36:633–40. doi: 10.1002/stem.2787

44. Liu Y, Wang H. Biomarkers and targeted therapy for cancer stem cells. *Trends Pharmacol Sci*. (2024) 45:56–66. doi: 10.1016/j.tips.2023.11.006

45. Finn RS, Ikeda M, Zhu AX, et al. Phase ib study of lenvatinib plus pembrolizumab in patients with unresectable hepatocellular carcinoma. *J Clin Oncol*. 38:2960–70.

46. Jin H, Shi Y, Lv Y, et al. EGFR activation limits the response of liver cancer to lenvatinib. *Nature*. (2021) 595:730–4. doi: 10.1038/s41586-021-03741-7

frontiers | Frontiers in Oncology

TYPE Original Research
PUBLISHED 08 September 2025
DOI 10.3389/fonc.2025.1586531

OPEN ACCESS

EDITED BY
Giovanna Damia,
Mario Negri Institute for Pharmacological Research (IRCCS), Italy

REVIEWED BY
Afza Ahmad,
Babu Banarasi Das University, India
Ryo Morisue,
Harvard Medical School, United States

*CORRESPONDENCE
Lina Yang
yln1489@gzucm.edu.cn
Zhenjiang Yang
dzjysz@163.com

RECEIVED 03 March 2025
ACCEPTED 11 August 2025
PUBLISHED 08 September 2025

CITATION
Zhang M, Li X, Huang Z, Yang Z and Yang L (2025) Outstanding treatment success of pembrolizumab and bevacizumab combination therapy in first-line treatment of cervical sarcomatoid carcinoma: a rare case report. *Front. Oncol.* 15:1586531. doi: 10.3389/fonc.2025.1586531

Outstanding treatment success of pembrolizumab and bevacizumab combination therapy in first-line treatment of cervical sarcomatoid carcinoma: a rare case report

Mingzi Zhang[1], Xinbei Li[2], Zhonghua Huang[3], Zhenjiang Yang[4*] and Lina Yang[4*]

[1]Department of Pharmacy, Shenzhen Traditional Chinese Medicine Hospital, Shenzhen, China, [2]Department of Radiology, Shenzhen Traditional Chinese Medicine Hospital, Shenzhen, China, [3]Department of Pathology, Shenzhen Traditional Chinese Medicine Hospital, Shenzhen, China, [4]Department of Internal Medicine of Oncology and Hematology, Shenzhen Traditional Chinese Medicine Hospital, Shenzhen, China

Background: Cervical lesions of sarcomatoid carcinoma are very rare, and there are still no reports of any targeted drugs applied in this rare tumor. In this report, we document a patient with stage IVA sarcomatoid carcinoma of the cervix, according to the FIGO staging system. The genetic testing of the patient's tumor tissue indicated the expression of PD-L1. This finding is significant as it suggests that the patient may be a candidate for immunotherapy. In this manuscript, we report a case of a patient who achieved a transient recurrence-free survival period through combined therapy (although recurrence eventually occurred), with a progression-free survival exceeding 13 months and an overall survival exceeding 22 months (as of the last follow-up, the patient was receiving palliative care only).

Case presentation: After diagnostic confirmation, the patient was administered a first-line combination therapy consisting of pembrolizumab plus bevacizumab. After 2 cycles of treatment, there was a marked reduction in tumor volume and the patient did not experience any side effects. Since then, the patient has continued to receive the regimen and the tumor has continued to shrink. Ultimately, after 10 courses of treatment with immune checkpoint inhibitors and anti-angiogenic drugs, the PET-CT scan showed complete disappearance of the tumor, with no evidence of cancer throughout the body. Subsequently, the patient continued to receive maintenance therapy with the same regimen, with regular follow-up evaluations. No recurrence was detected until 13 months later, when a MRI scan revealed tumor recurrence.

Conclusions: The combination of a PD-1 inhibitor with a drug that promotes tumor vascular normalization has shown promise in treating advanced cervical sarcomatoid carcinoma. We are the first to report the use of this combination regimen in this rare tumor, where previously reported treatment has been with chemotherapy agents. In addition, the level of PD-L1 expression could serve as a

potential biomarker to predict the response to immunotherapy in patients with advanced sarcomatoid carcinoma of the cervix. Our case highlights the efficacy of immunotherapy in combination with anti-angiogenic targeted therapy for the treatment of sarcomatoid carcinoma of the cervix.

KEYWORDS

sarcomatoid carcinoma, cervix, pembrolizumab, bevacizumab, PD-L1

1 Introduction

The entity of sarcomatoid carcinoma is seldom encountered in the pathology of the uterine cervix (1, 2). Sarcomatoid carcinoma of the cervix (SCC) has both epithelial and sarcomatoid stromal tissue components, sarcomatoid tissue is usually dominant, squamous cell carcinoma is the main epithelial component (3, 4). Although the classification system of World Health Organization (WHO) for gynecological tumors does not formally acknowledge sarcomatoid carcinoma as a separate histological subtype of cervical cancer, it is noteworthy that this rare malignancy has been reported in a few case studies in the medical literature (5). These reports provide valuable insights into the clinical presentation, management challenges, and outcomes associated with this rare and aggressive form of cervical cancer.

Patients typically exhibit symptoms at later stages and experience a highly aggressive progression of the disease. Due to the rarity of the cervical sarcomatoid carcinoma, there is no standardized diagnostic and therapeutic protocol. The majority of these cases are managed as squamous cell carcinoma and treated with either surgery or radiotherapy or chemotherapy (1, 6, 7). Although a significant therapeutic response to the initial treatment is observed in the majority of cases, subsequent relapses tend to occur after a short period (2, 3, 6). SCC is an exceptionally rare malignancy, with fewer than 40 cases documented in the existing medical literature, resulting in a scarcity of long-term follow-up data. Currently, the landscape of treatment for SCC is characterized by a variety of approaches, including surgery, radiotherapy, and chemotherapy (1). SCC generally has a poor prognosis, especially in advanced stages. Therefore, there is an urgent need to explore new and reliable therapeutic options. However, there is a notable absence of a standardized therapeutic protocol, as well as a lack of a systematic treatment plan tailored to this rare condition. SCC is recognized for its heightened invasiveness compared to conventional cervical carcinomas, characterized by a propensity for rapid progression, a tendency to relapse shortly after treatment, and a generally poor response to pre-existing therapeutic interventions (6).

Historically, sarcomatoid carcinoma has demonstrated a lack of sensitivity to conventional radiotherapy and chemotherapy, which has posed significant challenges in its management (8). Given these factors, the mainstay of treatment has centered on early diagnosis and the complete surgical resection of the tumor (7). Despite its sarcomatous features, sarcomatoid carcinoma retains epithelial origins, which means that traditional chemotherapeutic agents may still be utilized in an adjuvant capacity to complement surgical intervention (1). However, for patients presenting with advanced stages or those experiencing recurrence, the effectiveness of current chemotherapy options remains limited, and no definitively effective regimen has been reported to date. Given these challenges, there is a pressing requirement for the innovation of new therapeutic agents or specially designed alternative treatment strategies.

There are currently no clinical studies to assess the combination of immune checkpoint inhibitors (ICIs) with anti-angiogenic therapies for the treatment of programmed death-ligand 1-positive (PD-L1-positive) SCC. Pembrolizumab is a type of immune checkpoint inhibitor (ICI) that functions by blocking the programmed cell death protein 1 (PD-1) on T cells, allowing them to recognize and attack cancer cells (9). Bevacizumab is a type of monoclonal antibody designed to target vascular endothelial growth factor (VEGF), a protein that is crucial for the development of blood vessels that nourish tumors. By inhibiting VEGF, bevacizumab not only exerts anti-angiogenic effects but also induces transient vascular normalization in tumor vasculature, thereby limiting its growth and spread (10). This paper reports a case study that analyses the efficacy and safety profile of the combination

Abbreviations: SCC, sarcomatoid carcinoma of the cervix; WHO, World Health Organization; ICIs, immune checkpoint inhibitors; PD-L1-positive, programmed death-ligand 1-positive; ICI, immune checkpoint inhibitor; PD-l, programmed cell death protein 1;VEGF, vascular endothelial growth factor; MRI, magnetic resonance imaging; FIGO, International Federation of Gynecology and Obstetrics; HE, hematoxylin and eosin; IHC, immunohistochemistry; CPS, Combined Positive Score; HPD, hyperprogressive disease; MSI, microsatellite instability; MSS, microsatellite stable; PD-L1, programmed death-ligand 1; PET-CT, positron emission tomography/computed tomography; CT, computed tomography; PFS, progression-free survival; OS, overall survival; VEGF-A, vascular endothelial growth factor A; VEGFR, vascular endothelial growth factor receptor; HPV, human papillomavirus; ALT, Alanine Aminotransferase; AST, Aspartate Aminotransferase; SCr, Serum creatinine; FBG, Fasting Blood Glucose; CRP, C-reactive protein; ESR, Erythrocyte Sedimentation Rate; CEA, Carcinoembryonic Antigen.

treatment using pembrolizumab, an ICI, together with bevacizumab, an anti-angiogenic agent, for an advanced case of PD-L1-positive SCC.

2 Case presentation

In 2023, a 73-year-old Chinese woman with a prior HPV-DNA test result positive for low-risk HPV type 70 presented to the Department of Internal Medicine of Oncology and Hematology at our hospital. She had been diagnosed with SCC at a local hospital approximately two weeks prior. The patient was in search of alternative treatment options, as she had declined the conventional approaches of radiotherapy and chemotherapy. The patient was admitted to a local hospital due to over 10 days of irregular vaginal bleeding without an immediately identifiable cause. Then, the patient underwent a pelvic magnetic resonance imaging (MRI) scan, which revealed an occupying mass in the anterior lip of the cervix, suggestive of cervical cancer, measuring 66 mm x 52.5 mm x 36 mm. The boundary with the anterior wall of the rectum and the posterior wall of the bladder is unclear (International Federation of Gynecology and Obstetrics (FIGO) stage IV4A) (Figure 1A). The patient subsequently underwent a colposcopic biopsy with hematoxylin and eosin (HE) staining and immunohistochemistry (IHC). The results of these tests were indicative of a predisposition to sarcomatoid carcinoma, leading to the diagnosis of SCC. The sarcomatoid component, as determined by comprehensive histopathological evaluation, accounted for 70% of the total tumor volume in this case (Figures 2, 3). The patient, who was not in favor of undergoing chemotherapy and radiotherapy, decided to seek alternative options and turned to our hospital for further assistance and potential treatment avenues.

SCC is extremely rare and has a poor prognosis in advanced stage patients, with no evidence of survival benefit from radiotherapy and chemotherapy. We advised the patient to undergo genetic testing to identify potential therapeutic targets that could inform a more personalized treatment approach. The genetic testing of the patient's tumor tissue revealed the following mutations and characteristics (1): Somatic tumor mutations:An NRAS Q61K mutation was detected at a frequency of 6%;A BRAF G464E mutation was identified at a frequency of 6.9%;An ABL1 K609del mutation was identified at a frequency of 6.0%; A

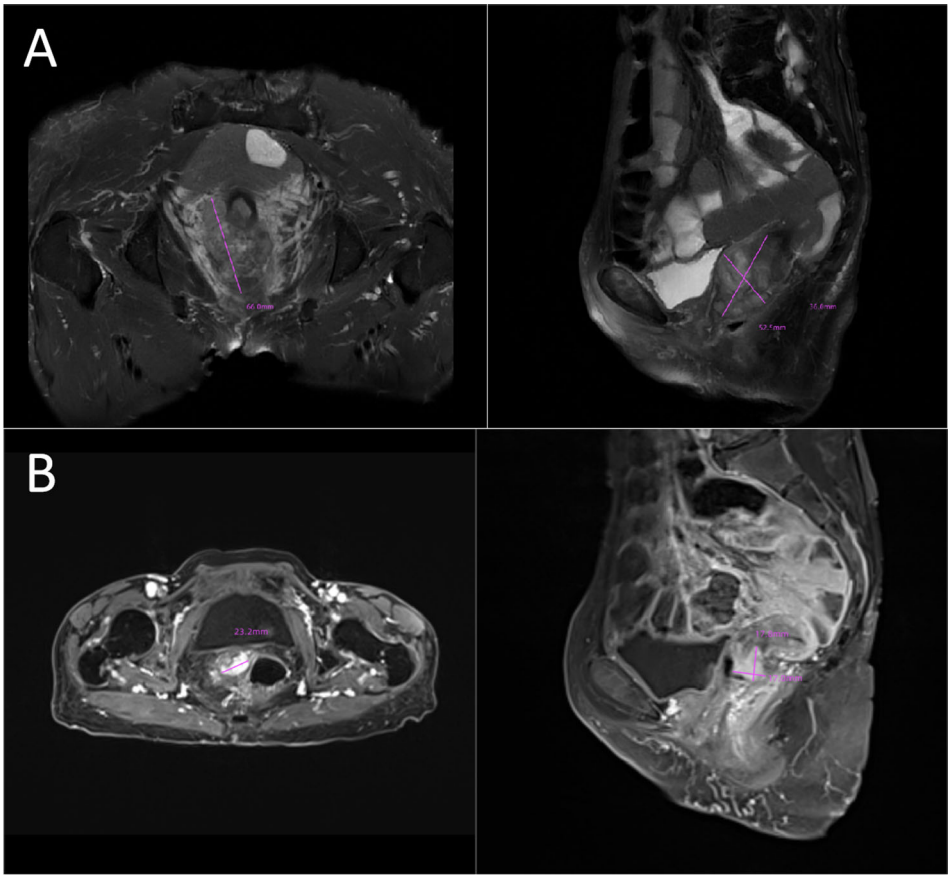

FIGURE 1
(A) Initial tumor mass:MRI image showing an occupying lesion in the anterior lip of the cervix, which is considered to be sarcomatoid carcinoma of the cervix (66mmx52.5mmx36mm). The boundary with the anterior wall of the rectum and the posterior wall of the bladder is unclear (FIGO stage IVA). **(B)** Post-treatment shrinkage:The pelvic MRI results showed a significant reduction in the size of the patient's tumor (23.2mmx17.8mmx17.0mm). MRI, magnetic resonance imaging.

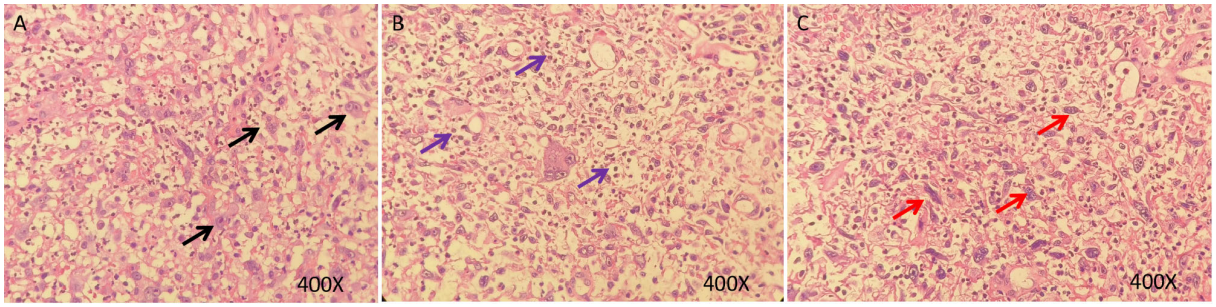

FIGURE 2
HE staining of sarcomatoid carcinoma of the cervix. **(A–C)**, H&E stain, original magnification ×400. HE staining of tumor showing a poorly differentiated malignant tumor with marked cellular atypia. The tumor cells exhibit epithelioid and myofibroblastic patterns, with abundant cytoplasm and prominent nucleoli. The background is mixed with granulation tissue and there is significant infiltration of inflammatory cells (Black arrows: Epithelioid carcinoma cells; Red arrows: Myofibroblast-like tumor cells; Purple arrows: Inflammatory infiltrates).

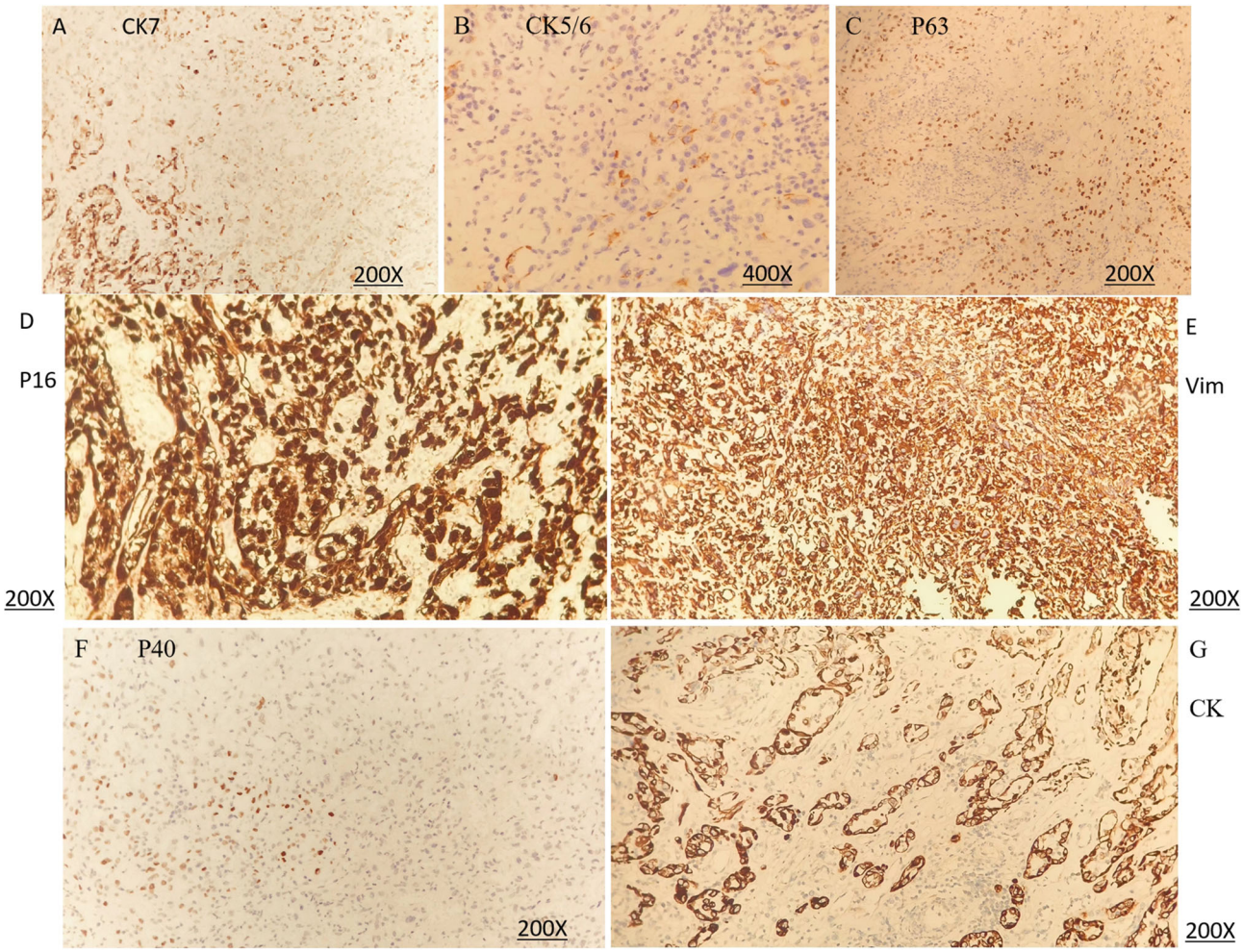

FIGURE 3
Immunohistochemical (IHC) staining of sarcomatoid carcinoma of the cervix. **(A)** CK7 (positivity), original magnification ×200. **(B)** CK5/6 (very rare positivity), original magnification ×400. **(C)** P63 (sparse positivity), original magnification ×200. **(D)** P16 (positivity), original magnification ×200. **(E)** Vimentin (positivity), original magnification ×200. **(F)** P40 (focal positivity), original magnification ×200. **(G)** CK (positivity, epithelioid component), original magnification ×200. **(A–F)** demonstrate protein expression in the sarcomatoid component, whereas **(G)** shows protein expression in the epithelioid component.

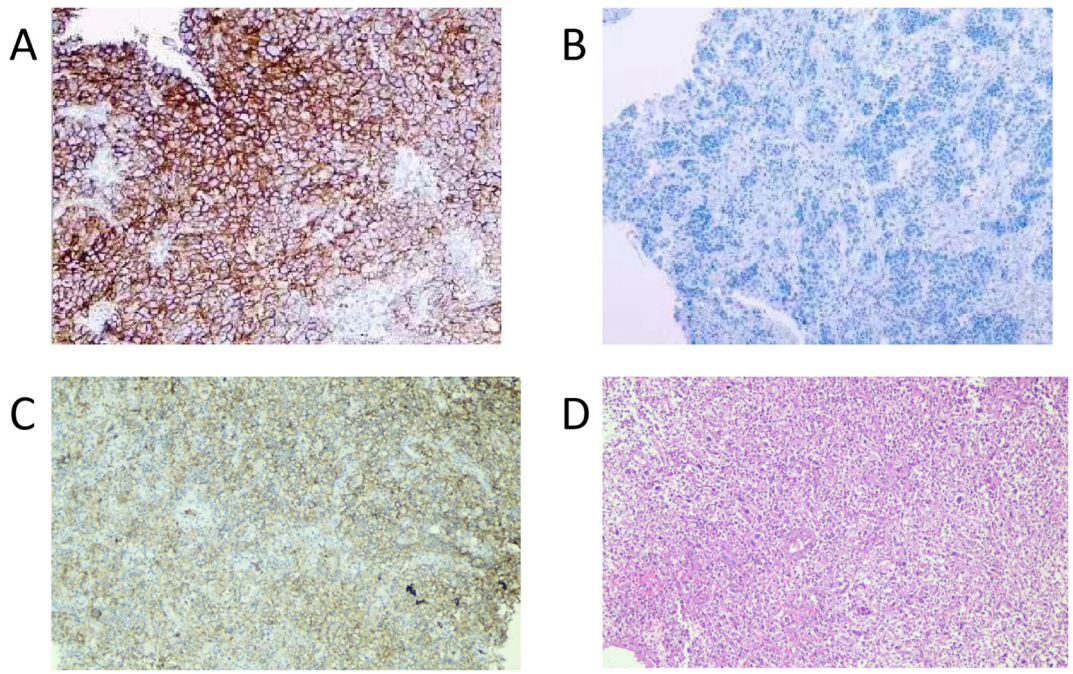

FIGURE 4
PD-L1 IHC of the tumor tissue. **(A)**, positive control (PD-L1-positive non-small cell lung cancer tissue), original magnification ×100. **(B)**, negative control (PD-L1-negative non-small cell lung cancer tissue), original magnification ×100. **(C)**, PD-L1 IHC of tissue from the patient in this case report (antibody 22C3 pharmDx), original magnification ×100. **(D)**, HE staining of tissue from the patient in this case report, original magnification ×100. Tumor Proportion Score (a TPS): 40% and Combined Positive Score (b CPS): 45. (a TPS is the percentage of living tumor cells that have partial or full PD-L1 membrane staining, assessed in a sample of at least 100 living tumor cells. b CPS is calculated by dividing the count of PD-L1 positive cells (such as tumor cells, lymphocytes, and macrophages) by the total tumor cell count, then multiplying the quotient by 100 to express it as a percentage.

DNMT3A S129G mutation was identified at a frequency of 48.2%; An EPCAM A82G mutation was identified at a frequency of 48.8%; A PALB2 A38G mutation was identified at a frequency of 42.5% (2). The tumor's Combined Positive Score (CPS) for PD-L1 expression was 45, indicating positive programmed death-ligand 1 (PD-L1) expression (Figure 4) (3). No genes associated with hyperprogressive disease (HPD) were found (4). No mutations were detected in either immunotherapy-positive associated genes (MMR-related genes, POLE, POLD1, DDR genes, KRAS, TP53) or immunotherapy-negative associated genes (B2M, DNMT3A, JAK1/2, ALK, ROS1, MET, VEGFA, PTEN, STK11) (5). The microsatellite instability (MSI) testing results indicate a microsatellite stable (MSS) status, with an MSI score of 0.0235 (values ≥0.4 classified as MSI-H, <0.4 as MSS). The CPS for PD-L1 expression indicates that the tumor is highly likely to be sensitive to ICIs, which could make immunotherapy a viable treatment option. Prior to initiating formal antitumor therapy, the patient underwent comprehensive biochemical testing. The baseline characteristics upon hospital admission are detailed in Table 1. As a result, the patient was administered a combination therapy consisting of bevacizumab (300 mg) plus pembrolizumab (200 mg) Q3W. After 2 cycles of the therapeutic regimen, the tumor shrank significantly, and the patient did not experience any side effects (Figure 1B). Since then, the patient has continued to receive the regimen and the tumor has continued to shrink. Ultimately, after completing 10 cycles of treatment with ICIs and anti-angiogenic drugs, the positron emission tomography/computed tomography (PET-CT) scan showed complete disappearance of the tumor, with no evidence of residual cancer in the body(Figure 5). Considering the patient's advanced stage and the high malignancy of cervical sarcomatoid carcinoma, which is highly prone to recurrence, we continued with the original treatment plan for maintenance therapy. During the maintenance therapy period, the patient underwent regular follow-up evaluations without evidence of recurrence. Treatment was maintained for 13 months until MRI demonstrated recurrence (Figure 6). Subsequently, the patient was transferred to the Department of Radiotherapy in our hospital and began radiotherapy. We still conducted regular follow-ups for the patient. Given the extremely high malignancy of this rare tumor, although the tumor eventually recurred unfortunately, the combination therapy initially achieved a transient recurrence-free survival period. Moreover, no significant adverse reactions were observed during the drug treatment. Radiotherapy was discontinued after 3 months due to concurrent tumor progression observed during treatment. The patient is currently receiving palliative care only. Our data demonstrate a progression-free

TABLE 1 Baseline characteristics of the patient.

Category	Details
Demographics	
Age/Sex	73-year-old, Female
Ethnicity	Han Chinese
ECOG Performance Status	1
Laboratory values	
HPV Status	Positive
p16 IHC	Positive
HPV DNA Typing Test	Positive for HPV type 70 (low-risk)
Albumin	34.0 g/L (Ref:40.0-55.0)
Alanine Aminotransferase (ALT)	11.6 U/L (Ref:7.0-40.0)
Aspartate Aminotransferase (AST)	14.7 U/L (Ref:13.0-35.0)
Serum creatinine (SCr)	39.0μmol/L (Ref:41-81)
Fasting Blood Glucose (FBG)	4.94 mmol/L (Ref:3.96-6.12)
C-reactive protein (CRP)	7.3 mg/L (Ref:0.0-6.0)
Erythrocyte Sedimentation Rate (ESR)	81.0 mm/h (Ref:0.0-20.0)
Carcinoembryonic Antigen (CEA)	6.2 ng/ml (Ref:0.0-5.0)

survival (PFS) exceeding 13 months and overall survival (OS) surpassing 22 months.

Notably, among all tumor markers monitored during treatment, only carcinoembryonic antigen (CEA) showed abnormal elevation, while other markers remained consistently within normal ranges. Although CEA levels were abnormally elevated during the clinical course, the fluctuations were relatively minimal (Table 2).

3 Discussion

In our report, we detail a rare instance of SCC that was successfully treated and achieved a clinical cure, highlighting the effectiveness of pembrolizumab combined with bevacizumab treatment. To our knowledge, PubMed records as of July 2025 indicate fewer than 40 reported cases of cervical sarcomatoid carcinoma worldwide, consequently no treatment guidelines are currently available for this malignancy (1–7, 11). Typically, the management of the disease involves a combination of surgery, chemotherapy, and radiation therapy, based on the stage of the disease and the patient's overall health status (6). At present, a standardized treatment protocol for SCC has not been established. In clinical practice, doctors will make professional judgments based on the main treatment methods for cervical cancer and sarcomatoid carcinoma. In the early stages of the disease, surgical treatment is given priority. For locally advanced cases that are resectable, a combination of surgery and chemoradiotherapy is used. For locally advanced cases that are unresectable and advanced-stage lesions, systemic drug treatment plans are adopted, with chemotherapy drugs for cervical cancer as the mainstay. While chemotherapy is frequently cited in the medical literature as the only class of therapeutic drugs, the overall prognosis for patients with this rare and aggressive form of cancer remains unfavorable (3, 6).

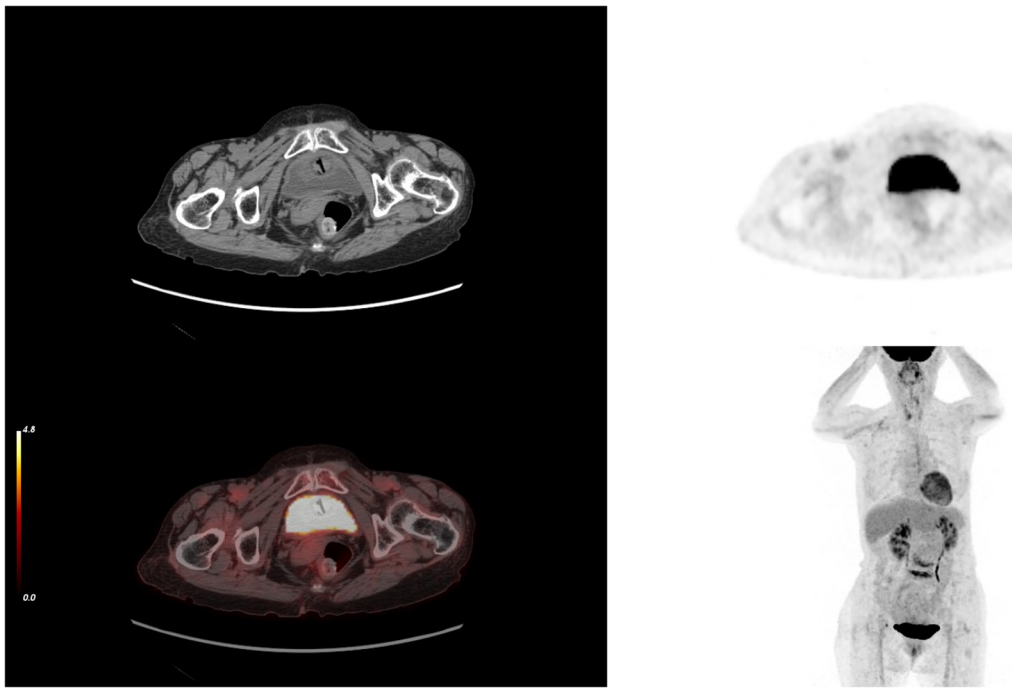

FIGURE 5
After 10 cycles of treatment, PET-CT results showing the complete disappearance of the tumor. PET-CT, positron emission tomography/computed tomography.

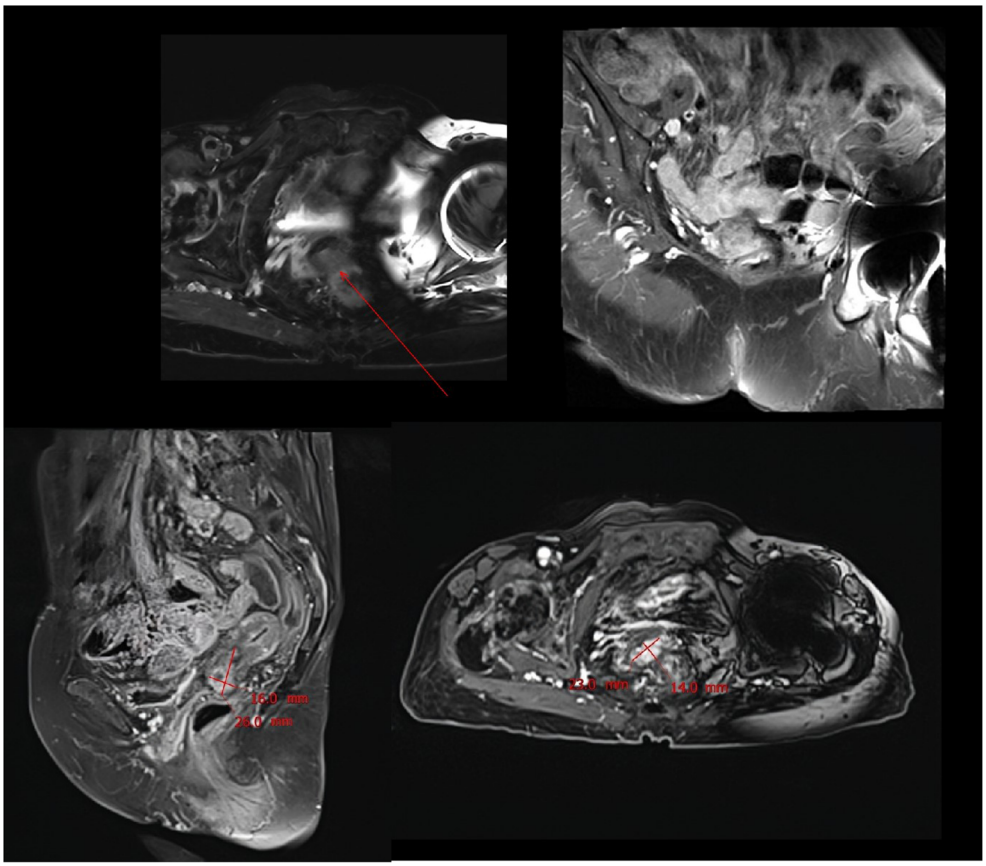

FIGURE 6
MRI scan performed after 13 months of combination therapy showed significant tumor recurrence.

TABLE 2 Dynamic monitoring of CEA levels.

Time point	CEA level (ng/mL)	Normal range (ng/mL)	Tumor response evaluation
Pre-treatment baseline	6.2	0.0-5.0	Diagnosed with SCC
After 2 treatment cycles	4.2	0.0-5.0	PR
After 10 treatment cycles	5.3	0.0-5.0	PET-CT showed the complete disappearance of the tumor
After 13 treatment cycles	5.5	0.0-5.0	MRI detected tumor recurrence
Final follow-up (22 months)	7.0	0.0-5.0	Bone metastasis confirmed

Because sarcomatoid carcinoma appears to be insensitive to radiotherapy and chemotherapy, and have limited therapeutic options, patients generally have a poor prognosis and a short survival time (2, 6, 11). Sarcomatoid carcinoma, despite limited literature, is described as an aggressive tumor with poor clinical outcome (12). The rarity of the disease complicates the development of standardized treatment protocols, and as such, treatment often relies on a combination of radiotherapy, surgery, and chemotherapy, tailored to the individual patient's condition and disease stage (1, 6). Despite the advent of novel treatments such as immunotherapy and targeted therapy, which have revolutionized the management of various gynecological malignancies, there remains a conspicuous absence of targeted drug applications specifically for this rare tumor. This underscores the urgent need for research and clinical trials to identify effective, personalized treatment strategies for patients afflicted with SCC.

The PD-1 is one of the checkpoints that regulates the immune response. The expression of PD-1 on effector T-cells and PD-L1 on neoplastic cells enables tumor cells to evade anti-tumor immunity. Blockade of PD-1 is an important immunotherapeutic strategy for

cancers. Pembrolizumab is a humanized monoclonal anti-PD-1 antibody that has been extensively investigated in numerous malignancies (9). Actually, the tumor microenvironment is a complex and interrelated environment, made up of various cell types such as endothelial cells, pericytes, immune cells, fibroblasts, and extracellularmatrix (13). Cancer cells manipulate their surrounding microenvironment by secreting extracellular signals that trigger tumor angiogenesis, boost cancer cell growth, and foster immune tolerance, thus evading detection by the immune system (14). Bevacizumab functions as a monoclonal antibody designed to target vascular endothelial growth factor A (VEGF-A), blocking its interaction with vascular endothelial growth factor receptor (VEGFR) and inhibiting angiogenesis, a process that supports tumor growth. As an early therapy aimed at the tumor microenvironment, incorporating bevacizumab into the standard treatment protocol introduces a new therapeutic strategy and provides an effective option for various advanced cancers that have a poor prognosis (10).

The growing availability of targeted drugs marks the advent of personalized medicine, while bevacizumab remains a mainstay in the treatment of various diseases. The collaboration of antiangiogenic therapy with ICIs can result in a synergistic therapeutic advantage (10, 14, 15). The synergistic antitumor effect of bevacizumab and pembrolizumab is primarily mediated through multi-level mechanisms (16). At the vascular level, VEGF blockade promotes tumor vascular normalization, improving vascular structure and function to facilitate immune cell infiltration (17). Regarding the tumor immune microenvironment, vascular normalization significantly enhances effector T cell infiltration while reducing the accumulation of various immunosuppressive cells, thereby effectively ameliorating the immunosuppressive state (18). On the metabolic level, the improved hypoxic condition alleviates the acidic tumor microenvironment and restores T cell function (19). Furthermore, VEGF inhibition downregulates immune checkpoint molecule expression and enhances T cell activation signaling pathways (20). A clinical study conducted in cervical cancer has confirmed that this combination regimen significantly improves the treatment response rate, demonstrating promising clinical translation potential (21). The combination therapy with pembrolizumab and bevacizumab has shown a synergistic effect in this patient, resulting in a significant tumor reduction without any adverse side effects. Meanwhile, anti-PD-1 immunotherapy activates immune cells, increases the secretion of IFN-γ, reduces the amount of VEGF, and thereby promotes vascular normalization (14). Hence, the marriage of antiangiogenic therapy with immunotherapy can interact to enhance the treatment's effectiveness on tumor cells.

Considering that the tumor was not sensitive to chemoradiotherapy, our patient in this case was in a locally advanced stage with a high recurrence and metastasis rate, along with the patient's advanced age and frailty, and the positive PD-L1 expression indicated by genetic testing, we opted for a treatment regimen similar to that used for pulmonary sarcomatoid cancer (22). The treatment involved a combination of pembrolizumab and bevacizumab.

The elderly female patient we admitted underwent 10 cycles of treatment with ICIs and anti-angiogenic drugs. Miraculously, the PET-CT scan data highlighted that the tumor had completely vanished, with no signs of cancer found throughout her body (Figures 5, 7). Considering the high malignancy of SCC, which is highly prone to recurrence, we continued with the original treatment plan for maintenance therapy.

During the maintenance therapy period, the patient received regular follow-up evaluations, with no signs of recurrence detected. This condition persisted until 13 months after combination therapy, when MRI indicated tumor recurrence. (Figure 6). Since this disease is a rare tumor with no established treatment guidelines available, we referred to the management guidelines for cervical cancer and consulted a radiation oncologist for evaluation (23). Considering the patient's advanced age and frail condition, the decision was made to refer her to the Department of Radiotherapy for the initiation of radiotherapy. The patient was then followed up regularly. Despite the eventual recurrence, we still consider this case a success worthy of reporting, as the patient achieved a PFS of over 13 months and an OS of over 22 months with the first-line combined treatment regimen. The success of this case suggests that for elderly and frail patients, traditional chemotherapy and radiotherapy may pose significant risks and side effects. In such scenarios, targeted therapy, being a relatively milder

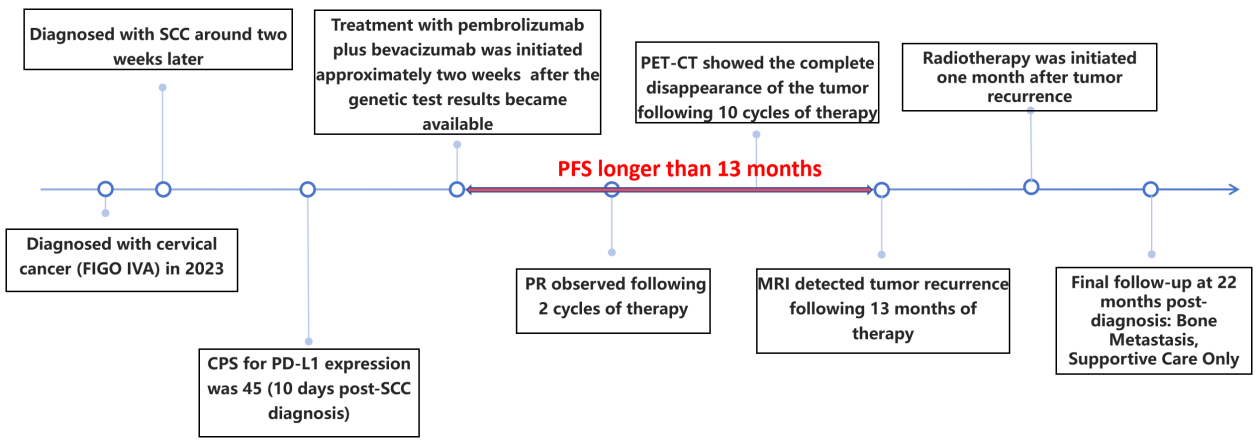

FIGURE 7
An overview of the patient's entire treatment process.

treatment modality, could potentially be a more suitable option for administering the care for these individuals.

The application of targeted therapy, which is designed to specifically attack cancer cells while sparing healthy ones, offers a less aggressive alternative to conventional treatments. This approach may be particularly beneficial for patients who may not tolerate the harsher effects of chemotherapy and radiation. By honing in on the molecular and cellular pathways that cancer cells rely on for growth and survival, targeted therapies like pembrolizumab and bevacizumab have shown promise in reducing tumor size and extending survival without the severe side effects often associated with more traditional cancer treatments.

4 Conclusion

Here we present an exceptionally rare case of SCC (initially staged as FIGO IV4A) exhibiting both low-risk HPV70 infection and p16 overexpression. The successful treatment of our patients demonstrates the efficacy and safety of targeted drugs applied in this rare tumor. Our case report confirms the therapeutic effectiveness of using ICIs in conjunction with antiangiogenic drugs to treat this PD-L1-positive and vascular-rich advanced rare tumor, providing evidence to support the clinical treatment of SCC. It also suggests that in rare tumors that are not sensitive to radiotherapy and chemotherapy, it is necessary to conduct genetic testing on tumor tissues to find effective therapeutic targets, at least the expression of PD-L1 is very meaningful. For elderly and frail patients with advanced tumors, blind pursuit of chemotherapy may not necessarily benefit patients, and may even shorten the survival period of patients. In the absence of sufficient chemotherapy evidence, seeking targeted therapy is a good strategy.

Data availability statement

The corresponding author can provide the datasets used or analyzed in this study upon receiving a reasonable request. The next-generation sequencing (NGS) data for this case report have been deposited into CNGB Sequence Archive (CNSA) of China National GeneBank DataBase (CNGBdb) with accession number CNP0006801.

Ethics statement

The requirement of ethical approval was waived by Ethics Committee of Shenzhen Traditional Chinese Medicine Hospital for the studies involving humans. The studies were conducted in accordance with the local legislation and institutional requirements. The participants provided their written informed consent to participate in this study. Written informed consent was obtained from the individual(s) for the publication of any potentially identifiable images or data included in this article.

Author contributions

MZ: Investigation, Project administration, Resources, Writing – original draft, Writing – review & editing. XL: Data curation, Formal analysis, Resources, Writing – review & editing. ZH: Data curation, Formal analysis, Resources, Writing – review & editing. ZY: Funding acquisition, Project administration, Supervision, Writing – review & editing. LY: Data curation, Formal analysis, Investigation, Project administration, Resources, Supervision, Writing – review & editing.

Funding

The author(s) declare financial support was received for the research and/or publication of this article. This research was financially backed by the Sanming Medical Project in Shenzhen, with the grant number SZZYSM202211003.

Acknowledgments

The authors thank the patient for her agreement to publication of the report.

Conflict of interest

The authors declare that the research was conducted in the absence of any commercial or financial relationships that could be construed as a potential conflict of interest.

Generative AI statement

The author(s) declare that no Generative AI was used in the creation of this manuscript.

Any alternative text (alt text) provided alongside figures in this article has been generated by Frontiers with the support of artificial intelligence and reasonable efforts have been made to ensure accuracy, including review by the authors wherever possible. If you identify any issues, please contact us.

Publisher's note

References

1. Kumar M, Bahl A, Sharma DN, Agarwal S, Halanaik D, Kumar R, et al. Sarcomatoid squamous cell carcinoma of uterine cervix: pathology, imaging, and treatment. *J Cancer Res Ther*. (2008) 4:39–41. doi: 10.4103/0973-1482.39604

2. Rodrigues L, Santana I, Cunha T, FelixA, FreireJ, CabralI. Sarcomatoid squamous cell carcinoma of the uterine cervix: case report. *Eur J Gynaecol Oncol*. (2000) 21:287–9.

3. Nageeti TH, Jastania RA. Sarcomatoid carcinoma of the cervix. *Ann Saudi Med*. (2012) 32:541–3. doi: 10.5144/0256-4947.2012.26.5.1110

4. Terada T. Sarcomatoid squamous cell carcinoma of the uterine cervix. *Arch Gynecol Obstet*. (2010) 282:231–2. doi: 10.1007/s00404-010-1409-1

5. Haight PJ, Castaneda AV, Savage JM, CopelandLJ. Cervical carcinoma with histologic components of sarcomatoid carcinoma and multiple basaloid variants: A case report and review of the literature. *Gynecol Oncol Rep*. (2021) 37:100797. doi: 10.1016/j.gore.2021.100797

6. Karapetyan L, Rai M, Dawani O, Laird-FickHS. Metastatic sarcomatoid squamous cell carcinoma of the cervix presenting with chest mass. *Case Rep Oncol Med*. (2017) 2017:5264564. doi: 10.1155/2017/5264564

7. Kong TW, Kim JH, Chang SJ, ChangKH, RyuHS, et al. Sarcomatoid squamous cell carcinoma of the uterine cervix successfully treated by laparoscopic radical hysterectomy: a case report. *J Reprod Med*. (2010) 55:445–8.

8. Ramesh K, Khatua A, Bhattacharjee A, TickuS. Sarcomatoid carcinoma: "A surgeons nightmare. *J Maxillofac Oral Surg*. (2019) 18:233–7. doi: 10.1007/s12663-018-1119-y

9. Kwok G, Yau TC, Chiu JW, TseE, KwongYL. Pembrolizumab (Keytruda). *Hum Vaccin Immunother*. (2016) 12:2777–89. doi: 10.1080/21645515.2016.1199310

10. Garcia J, Hurwitz HI, Sandler AB, MilesD, ColemanRL, DeurlooR, et al. Bevacizumab (Avastin(R)) in cancer treatment: A review of 15 years of clinical experience and future outlook. *Cancer Treat Rev*. (2020) 86:102017. doi: 10.1016/j.ctrv.2020.102017

11. Shrivastava S, Barmon D, Deka P, ChKA, ChoudharyBK. Sarcomatoid carcinoma of the cervix with foci of Malignant melanoma. *J Midlife Health*. (2014) 5:41–4. doi: 10.4103/0976-7800.127792

12. Ghosal R, Roychowdhury D, Chatterjee RP, SultanaM, SinhaS. Sarcomatoid carcinoma: A clinicopathological dichotomy. *Cureus*. (2024) 16:e53565. doi: 10.7759/cureus.53565

13. Xiao Y, Yu D. Tumor microenvironment as a therapeutic target in cancer. *Pharmacol Ther*. (2021) 221:107753. doi: 10.1016/j.pharmthera.2020.107753

14. Huang Y, Kim B, Chan CK, HahnSM, WeissmanIL. Improving immune-vascular crosstalk for cancer immunotherapy. *Nat Rev Immunol*. (2018) 18:195–203. doi: 10.1038/nri.2017.145

15. Xiang J, Si J, Hao Y, WeiJ, WangW, GuanY, et al. Efficacy and safety of immune checkpoint inhibitors (ICIs) combined with antiangiogenic therapy for thymic epithelial tumors (TETs): a retrospective study. *Transl Cancer Res*. (2023) 12:550–7. doi: 10.21037/tcr-22-2192

16. Jain RK. Normalizing tumor microenvironment to treat cancer: bench to bedside to biomarkers. *J Clin Oncol*. (2013) 31:2205–18. doi: 10.1200/JCO.2012.46.3653

17. Jain RK. Normalization of tumor vasculature: an emerging concept in antiangiogenic therapy. *Science*. (2005) 307:58–62. doi: 10.1126/science.1104819

18. Huang Y, Goel S, Duda DG, FukumuraD, JainRK. Vascular normalization as an emerging strategy to enhance cancer immunotherapy. *Cancer Res*. (2013) 73:2943–8. doi: 10.1158/0008-5472.CAN-12-4354

19. Jain RK. Antiangiogenesis strategies revisited: from starving tumors to alleviating hypoxia. *Cancer Cell*. (2014) 26:605–22. doi: 10.1016/j.ccell.2014.10.006

20. Fukumura D, Kloepper J, Amoozgar Z, DudaDG, JainRK. Enhancing cancer immunotherapy using antiangiogenics: opportunities and challenges. *Nat Rev Clin Oncol*. (2018) 15:325–40. doi: 10.1038/nrclinonc.2018.29

21. Oaknin A, Gladieff L, Martinez-Garcia J, VillacampaG, TakekumaM, De GiorgiU, et al. Atezolizumab plus bevacizumab and chemotherapy for metastatic, persistent, or recurrent cervical cancer (BEATcc): a randomised, open-label, phase 3 trial. *Lancet*. (2024) 403:31–43. doi: 10.1016/S0140-6736(23)02405-4

22. Li X, Wu D, Liu H, ChenJ. Pulmonary sarcomatoid carcinoma: progress, treatment and expectations. *Ther Adv Med Oncol*. (2020) 12:431402049. doi: 10.1177/1758835920950207

23. Restaino S, Pellecchia G, Arcieri M, BoganiG, TalientoC, GrecoP, et al. Management for cervical cancer patients: A comparison of the guidelines from the international scientific societies (ESGO-NCCN-ASCO-AIOM-FIGO-BGCS-SEOM-ESMO-JSGO). *Cancers (Basel)*. (2024) 16. doi: 10.3390/cancers16142541

frontiers | Frontiers in Oncology

TYPE Original Research
PUBLISHED 10 September 2025
DOI 10.3389/fonc.2025.1654491

OPEN ACCESS

EDITED BY
Giovanna Damia,
Mario Negri Institute for Pharmacological Research (IRCCS), Italy

REVIEWED BY
Sankar Jagadeeshan,
Ben-Gurion University of the Negev, Israel
Pingping Chen,
University of Miami, United States

*CORRESPONDENCE
Serena Pillozzi
serena.pillozzi@unifi.it

†These authors contributed equally to this work and share first authorship

‡These authors contributed equally to this work and share senior authorship

RECEIVED 26 June 2025
ACCEPTED 26 August 2025
PUBLISHED 10 September 2025

CITATION
Tubita A, Fancelli S, Anela L, Petroni G, Caliman E, Mazzoni F, Scolari F, Napolitano B, Menicacci B, Comin CE, Voltolini L, Pillozzi S and Antonuzzo L (2025) KRAS G12C inhibition enhances efficacy to conventional chemotherapy in KRAS-mutant NSCLC. *Front. Oncol.* 15:1654491. doi: 10.3389/fonc.2025.1654491

KRAS G12C inhibition enhances efficacy to conventional chemotherapy in KRAS-mutant NSCLC

Alessandro Tubita[1†], Sara Fancelli[2†], Lorenzo Anela[1], Giulia Petroni[1], Enrico Caliman[2], Francesca Mazzoni[2], Federico Scolari[3], Brunella Napolitano[2], Beatrice Menicacci[4], Camilla Eva Comin[1], Luca Voltolini[1], Serena Pillozzi[3*‡] and Lorenzo Antonuzzo[1,2‡]

[1]Department of Experimental and Clinical Medicine, University of Florence, Florence, Italy, [2]Oncology Unit, Careggi University Hospital, Florence, Italy, [3]Department of Experimental and Clinical Biomedical Sciences, University of Florence, Florence, Italy, [4]Department of Health Sciences, University of Florence, Florence, Italy

Despite recent therapeutic advances, the adjuvant treatment of non-small cell lung cancer (NSCLC) remains a challenge. Reducing the risk of recurrence is still a concern, especially in the KRAS G12C population, for which platinum-based adjuvant chemotherapy (CT) remains the gold standard. In this study, we evaluated the efficacy, in terms of cell viability and volumetric reduction, of adding KRAS inhibitors (KRASi) sequentially or concurrently to CT in both parental (PR) and gemcitabine-resistant (GR) KRAS mutated NSCLC cell lines (SW1573 and H23). We demonstrated that KRASi added to CT (both sequential and concurrent treatment strategies) reduced cell viability in SW1573-PR and H23-PR and this effect is less evident in GR cell lines. Interestingly, in the 3D model, the concomitant use of KRASi+CT reduced spheroid volume in both PR and GR spheroids. Our results indicate that KRASi enhances the efficacy of CT in both NSCLC PR and GR cells, suggesting a potential therapeutic strategy to overcome chemoresistance in the adjuvant setting of NSCLC.

KEYWORDS

NSCLC, KRAS mutations, chemoresistance, KRAS inhibitors (KRASi), adjuvant chemotherapy

Introduction

Lung cancer is the leading cause of cancer-related mortality worldwide, with non-small cell lung cancer (NSCLC) accounting for approximately 85% of all lung cancer cases (1–3). The prognosis for NSCLC patients is often poor, even in early stages with a five-year survival rate between 26%-60% (4). 25% of NSCLC patients are diagnosed with an early-

stage resectable disease, and for these patients surgery remains the primary therapeutic approach with curative intent. However, approximately 35-60% of these patients experience disease recurrence after surgery alone. Despite significant advancements in treatment modalities over the past decades, the management of post-operative NSCLC has been based on traditional chemotherapy (CT) platinum-based regimens with nucleoside analogs (e.g., gemcitabine) (5). Adjuvant CT provides only a 5.4% improvement in 5-year overall survival (OS) regardless of the choice of platinum-based treatments (6). The discovery of molecular alterations and oncogenic drivers in NSCLC has paved the way for targeted therapies, offering a new paradigm in cancer treatment. Recently, the integration of immunotherapy into the adjuvant setting for NSCLC with programmed death-ligand 1 (PD-L1) expression ≥50% (7), as well as targeted therapies for epidermal growth factor receptor (EGFR)-mutated disease (8) and anaplastic lymphoma kinase (ALK) fusions (9), has significantly improved survival outcomes in patients undergoing surgical treatment.

Currently, not all oncogene alterations known to have a therapeutic target in the metastatic setting have a treatment counterpart in earlier settings, including the adjuvant one. Among these, kirsten rat sarcoma viral oncogene homolog (KRAS) gene mutations are prevalent in approximately 30% of NSCLC cases and represent a critical therapeutic target (10–12). The majority of these mutations results in the replacement of glycine (G) in codon 12 with cysteine (C) (G12C), occurring in approximately 50% of KRAS mutant tumors. KRAS G12C mutations are strongly associated with tobacco exposure and KRAS G12C-mutant NSCLCs have been consistently reported to have a higher tumor mutational burden (TMB) and a high rate of concurrent mutations such as *STK11*, *KEAP1*, *SMARCA4* and *ATM* compared to NSCLCs carrying other KRAS isoforms or KRAS wild-type (WT) (13). However, the prognostic role of KRAS mutations is still unclear, although recent experience may suggest an unfavorable role compared to WT disease and when mutant KRAS NSCLC are associated with co-occurring mutations in advanced disease treated with chemo/chemoimmunotherapy (14, 15). The demonstrated efficacy of sotorasib and adagrasib, the first mutant-selective covalent KRAS G12C inhibitors (KRASi) in KRAS G12C pretreated NSCLC, with response rates of 30-40%, led to approval by the European Medicines Agency (EMA) and the Food and Drug Administration (FDA), marking a breakthrough for this drug category (16–19). However, there are currently no data on the efficacy of KRASi in the adjuvant setting, and the few available clinical trials are in early stages of enrollment (NAUTIKA-1, NCT04302025).

Given the poor efficacy of traditional adjuvant CT and the advent of KRAS-targeted therapies, there is a growing interest in exploring combination approaches with KRASi in early settings to enhance the therapeutic efficacy and overcome resistance mechanisms, thereby improving clinical outcomes for NSCLC patients. The present study investigates the potential of combining KRASi with standard chemotherapeutic agents in both parental (PR) and gemcitabine-resistant (GR) NSCLC cell lines. By harnessing 2D and 3D preclinical cellular models, we aim to elucidate the effects of these combinations, to determine whether the sequential or concomitant use of KRASi with CT modifies cell viability, and thus establish their potential for advancement in the therapeutic landscape of NSCLC.

Materials and methods

Patients

Patients with NSCLC who underwent surgery between 2019 and 2023 at the Clinical Oncology Unit of the Azienda Ospedaliero-Universitaria Careggi in Florence in Italy were enrolled. We collected data of patients stage II to IIIB per the Union Internationale Contre le Cancer and American Joint Committee on Cancer staging system (8th edition-2017) treated with adjuvant CT. We recorded demographic characteristics, type of surgery and adjuvant CT performed, stage, and biomolecular characteristics when available. Finally, we collected data on relapse-free survival (RFS) and overall survival (OS).

The study was conducted in accordance with good clinical practice (GCP) guidelines, the ethical principles of the Declaration of Helsinki, and regulatory requirements and local laws. The protocol was approved by the local ethics committee (CEAVC n.22712). All patients provided written informed consent.

Adjuvant treatment and follow-up

Patients who were able to receive cisplatin-based CT underwent 4 cycles of cisplatin 75 mg/mq or carboplatin AUC5 IV D1 Q3W and gemcitabine 1250 mg/mq days IV D1,8 Q3W. Radiologic evaluation was performed according to the clinical practice schedule at baseline and then every 3 months with a whole body CT scan.

Cell lines and culture

NSCLC cell lines (SW1573 and H23) with a KRAS G12C mutation were kindly provided by Dr. Azucena Esparís-Ogando (IBMCC-CIC, IBSAL, CIBERONC, Salamanca, Spain). NSCLC cell lines were cultured in Roswell Park Memorial Institute (RPMI)-1640 medium (Life technologies, Carlsbad, CA, USA) supplemented with 10% fetal bovine serum, L-glutamine (2mM), penicillin/streptomycin (50 U/ml) (Euroclone, Milan, Italy) at 37°C and 5% CO2. To generate GR-cells, SW1573 and H23 cells were transiently exposed to gemcitabine twice a week with increasing concentrations of gemcitabine weekly for more than 2 months.

Drug treatments

The chemotherapeutic agents used in this study were carboplatin, gemcitabine, pemetrexed, and paclitaxel. The KRASi

used were sotorasib and adagrasib. gemcitabine, sotorasib, adagrasib, pemetrexed and paclitaxel were purchased from MedChemExpress (Monmouth Junction, NJ, USA). carboplatin was provided by the Azienda Ospedaliera Universitaria Careggi's galenic pharmacy (AOUC, Firenze, Italy).

Cell viability assay

Cell viability was measured using Prestoblue™ Cell Viability reagent (Invitrogen, Waltham, MA, USA) according to the manufacturer's protocol. The optical density (OD) was measured using a 560 nm excitation filter and 590 nm emission filter using the BioTek Synergy™ H1 hybrid multi-mode microplate reader (Agilent, CA, USA). Half-maximal inhibitory concentration (IC_{50}) values were derived by a sigmoidal dose-response (variable slope) curve fitted using a four-parameter logistic regression model (log (inhibitor) vs. normalized response Variable slope (four parameters)) as described in the software documentation of Graph Pad Prism v6.0.

Analysis of cell cycle

A total of 150–000 cells/well were seeded in 6-multiwell plates. After medium removal, 500 µl of solution containing 50 µg/mL propidium iodide, 0.1% w/v trisodium citrate and 0.1% NP40 was added. Samples were then incubated for 1 hour at 4°C in the dark and nuclei analyzed with FACSCanto flow cytometer (Becton Dickinson, Franklin Lakes, New Jersey, USA).

Cell lysis and western blotting

Total cell lysates were obtained using Laemmli buffer (62.5 mM Tris-HCl-pH 6.8, 10% glycerol, 0.005% bromophenol blue, SDS 2%). Culture plates were placed on ice and cell monolayers were rapidly washed three times with ice-cold PBS containing 100 mM orthovanadate (Merck Millipore, Billerica, MA, USA). Cells were lysed by scraping in Laemmli buffer and incubating at 95°C for 10 min. Lysates were then clarified by centrifugation (13000 rpm for 10 min at room temperature). Proteins were separated on Bolt BisTris Plus gels 4–12% precast polyacrylamide gels (Life Technologies, Monza, Italy). Then, proteins were transferred from the gel to a polyvinylidene difluoride (PVDF) membrane using the iBlot 2 System (Thermo Fischer Scientific, Milan, Italy). Blots were blocked for 5 min, at room temperature, with the EveryBlot Blocking Buffer (BioRad, Hercules, CA, USA). Subsequently, the membrane was probed at 4°C overnight with primary antibodies diluted in a solution of 1:1 Immobilon® Block–FL/T-PBS buffer (Merck Millipore, Billerica, MA, USA). The primary antibodies were as follows: Rabbit anti-p21Waf1/Cip1, rabbit anti-pRb-S807/811, mouse anti-Vinculin, rabbit anti-pERK1/2-T202/Y204, rabbit anti-pAKT-S473, rabbit anti-Beclin-1, rabbit anti-E-Cadherin, rabbit anti-Actin, mouse anti-p21, rabbit anti-cleaved-caspase 3, mouse anti-PCNA (1:1000, Cell Signaling Technology, Danvers, MA, USA), mouse anti-N-Cadherin (1:1000, DAKO Agilent, Milan, Italy), rabbit anti-CyclinB, mouse anti-CyclinD1 and mouse anti-Tubulin (1:1000, Santa Cruz Biotechnology, Santa Cruz, CA, USA). The membrane was washed in T-PBS buffer, incubated for 1 h with goat anti-rabbit IgG Alexa Fluor 750 antibody (1:30000) or with goat anti-mouse IgG Alexa Fluor 680 antibody (1:30000; Invitrogen, Monza, Italy), and then visualized at the Odyssey Infrared Imaging System (LI-COR Bioscience, Lincoln, NE, USA). Mouse anti-Vinculin or rabbit anti-Actin antibodies were used to assess an equal amount of protein loaded in each lane.

Spheroid formation assay

SW1573-PR/GR and H23-PR/GR cells were seeded in RPMI 10% FBS in 96-well plate (2000 cells/well) precoated with 1.5% agarose (Condalab, Madrid, Spain) in water. After 72 hours, photos of time 0 were taken and spheroids were left untreated (CTRL) or treated with drugs. Photos were taken after 3 and 7 days of treatment by using Leica DM1 Inverted Microscope (Leica, Wetzlar, Germany) and the volume of SW1573-PR/GR or H23-PR/GR spheroids was quantified with ImageJ [Volume = 0.5*L*W2, L=length (major axis) W=width (minor axis)].

RNA extraction and bulkRNAseq

Total RNA was extracted from NSCLC cell lines using the RNeasy Mini kit (Qiagen, Manchester, UK). The quantity and the quality of RNA were evaluated using a Nanodrop spectrophotometer (Thermo Fischer Scientific, Milan, Italy). RNA-seq was performed by Novogene using the Novaseq PE150 pipeline.

Transcriptomic analysis

Raw sequencing data were assessed for quality. Reads were trimmed and aligned to the GRCh38 reference genome using HISAT2 (20). Alignment files were converted, sorted, and indexed using Samtools (21). Gene-level expression was quantified with featureCounts (22) and raw counts were loaded in an R environment. Differential expression analysis (DEA) was performed on raw counts using DESeq2 (23). Gene Set Enrichment Analysis (GSEA) was performed on the DEA results sorted by the Wald statistic using clusterProfiler (24). Pathways' gene expression scores were calculated on normalized, log-scaled and variance-stabilized counts as the average expression of the pathway genes. P-values were corrected for multiple testing when necessary using the BH method.

Statistical analysis

Cell viability and spheroid volumes are reported as mean ± SD of values obtained from at least three independent experiments.

Clinical data are reported as absolute numbers and percentages. P values were calculated using the appropriate statistical test based on the distribution of the data and multiple testing corrections were applied when necessary using the Bonferroni method. Survival data were reported using the Kaplan-Meier estimator and comparison of survival times between groups were performed using a log-rank test.

Results

Population characteristics and survivorship

We identified a total of 47 patients with NSCLC who received adjuvant platinum- and gemcitabine-based CT (Table 1). 57.4% (n=27) of patients were aged 70 years or younger, and 74.5% (n=35) were male. Surgery consisted of lobectomy in 78.7% (n=37) and included lymphadenectomy in almost all cases (95.7%; n=45). Histological examination revealed that 91.5% (n=43) were adenocarcinomas, while the remaining 8.5% (n=4) were squamous cell carcinomas. The most common stages were IIB (57.4%; n=27) and IIIA (31.9%; n=15). 53.2% of patients had PD-L1 greater than or equal to 1 and 44.7% (n=21) had KRAS mutations. The most common KRAS mutations were G12C (42.9%; n=9), G12V (19%; n=4) and G12A (14.3%; n=3). 51.1% of patients (n=24) experienced a recurrence, which involved lung in 50% of cases (n=12), lymph nodes in 33.3% (n=8), and the central nervous system (CNS) in 16.7% (n=4).

Comparing the two subgroups of KRAS mutated and KRAS WT patients for demographic and disease characteristics, we found that WT patients are more likely to be female (83.4%; n=10, Fisher's Exact Test p=0.042), stage IIB (59.3%; n=16) or IIIA (53.4%; n=8, p=0.806), and are PD-L1 <1% (68.2%; n=15, p=0.171). In contrast, the KRAS mutated subgroup has a similar distribution of male and stage of disease presentation, but is more likely to be PD-L1 ≥1% (56%; n=14). Moreover, although not statistically significant (p=0.054), WT patients are more likely to have positive lymph nodes pN1 (80%; n=12) and pN2 (53.9%; n=7) than mutated patients pN1 (20%; n=3) and pN2 (46.1%; n=6). Finally, both groups have the same probability of recurrence with a higher incidence of CNS metastases in the WT subgroup (75%; n=3) (p=0,59).

To define the predictive and prognostic value of KRAS mutations, we compared the mutated and WT patient populations of our cohort for RFS and OS. Although they did not reach statistical significance, we observed a slight trend in favor of the WT subgroup with median RFS (mRFS) of 31.99 months (95% CI: 16.34-NA) compared to 25.84 months (95% CI: 10.16-NA) of the mutated group (*p=0.23*). Similarly, OS also tends to favor the WT population over the mutated population (mOS 44.38 months 95% CI: 28.93-NA vs. 41.82 months 95% CI: 41.46-NA, *p=0.21*) (Figure 1A). Finally, within the subgroup of patients with KRAS mutations, we evaluated the RFS and OS of G12C compared to the other mutations, showing a non-statistically significant advantage for both endpoints. In particular, mRFS was 26.5 months (95% CI: 6.02-NA) for G12C compared to 10.78 months (95% CI: 10.78-NA) for the others (*p=0.47*). For the G12C mutation, mOS was not reached (95% CI: 28.93-NA), while it was 34.78 months (95% CI: 21.73-NA) for the remaining mutations (p=0.25; Figure 1B).

Enhanced efficacy of carboplatin and gemcitabine combined with KRASi in reducing viability in KRAS-mutated NSCLC cell lines

To define the optimal combination of chemotherapeutic agents, among those commonly used in NSCLC in adjuvant settings, that are capable of maximizing sensitivity to KRASi treatment, we developed two experimental protocols: one based on sequential treatments and the other based on concurrent treatments. Chemosensitivity was quantified as the IC_{50} value, representing the drug concentration required to achieve a 50% reduction in cell viability. The IC_{50} values for chemotherapeutic agents and KRASi (sotorasib or adagrasib) were derived from dose-response curves (Table 2; Supplementary Figure S1). Of note, SW1573 cell line has been reported to be more resistant to sotorasib compared to the H23 cell line (25). In general, with the exception of gemcitabine, our experiments demonstrate that the SW1573 cells exhibit significantly higher IC_{50} values for all other drugs tested, highlighting their increased resistance profile. Using the sequential treatment scheme (Figure 2A), KRAS-G12C-mutated NSCLC cell lines (SW1573 and H23) were seeded and after 24 hours were treated with a combination of chemotherapeutics, including gemcitabine (IC50 H23: 3.3nM-SW1573: 4nM) plus carboplatin (IC50 H23: 30μM-SW1573: 64μM) (Gem+Carbo), pemetrexed (IC50 H23: 2.3nM-SW1573: 37μM) plus carboplatin (Peme+Carbo), and paclitaxel (IC50 H23: 134μM-SW1573: 245μM) plus carboplatin (Pacli +Carbo), for 48 hours at their IC_{50}. Control cells (CTRL) were maintained without any chemotherapeutic agents or KRASi for 72 hours. After 48 hours of treatment, the chemotherapeutics were removed, and the cells were subsequently exposed to KRASi (sotorasib or adagrasib; IC50 sotorasib H23: 540nM-SW1573: 65μM; IC50 adagrasib H23: 200nM-SW1573: 4μM) for an additional 24 hours at their IC_{50}.

The results were expressed as the percentage change in cell viability (Δ%) relative to the control or between the indicated samples. Significant differences were observed in cell viability across different treatment groups, with variations between the responses of SW1573 and H23 cell lines. Importantly, although the Gem+Carbo condition did not achieve the highest percentage of growth inhibition among all tested chemotherapeutic combinations as compared to untreated cells (SW1573: Gem+Carbo Δ=61% vs Peme+Carbo Δ=58% and Pacli+Carbo Δ=72%; H23: Gem+Carbo Δ=65% vs Peme+Carbo Δ=58% and Pacli+Carbo Δ=72%), it proved to be the most effective combination respect to the other combined treatments in sensitizing SW1573 and H23 cells to sotorasib (Δ=49% and Δ=29%, respectively compared to Gem+Carbo-treated cells) and adagrasib (Δ=72% and Δ=40%, respectively compared to Gem+Carbo-treated cells) (Figure 2B).

For the experimental design in which treatments were administered concurrently, firstly we tested the best combination of

10.3389/fonc.2025.1654491

TABLE 1 Patient clinical, and molecular characteristics stratified by KRAS mutation status.

		TOT	KRAS		P-value
		N=47	mut (n=21)	wt (n=26)	
Age	<70	27 (57.4%)	12 (44.4%)	15 (55.6%)	
	≥70	20 (42.6%)	9 (45%)	11 (55%)	1
Gender	F	12 (25.5%)	2 (16.6%)	10 (83.4%)	
	M	35 (74.5%)	19 (54.3%)	16 (45.7%)	0.042
Lymphadenectomy	NO	2 (4.3%)	2 (100%)	0 (0%)	
	YES	45 (95.7%)	19 (42.2%)	26 (57.8%)	0.194
Resection type	Lobectomy	37 (78.7%)	13 (35.1%)	24 (64.9%)	
	Pyramidotomy	1 (2.1%)	1 (100%)	0 (0%)	
	Pneumonectomy	2 (4.3%)	2 (100%)	0 (0%)	
	Atypical resection	3 (6.4%)	2 (66.6%)	1 (33.4%)	
	Segmentectomy	4 (8.5%)	3 (75%)	1 (25%)	0.071
Histology	Squamous cell carcinoma	4 (8.5%)	1 (25%)	3 (75%)	
	Adenocarcinoma	43 (91.5%)	20 (46.5%)	23 (53.5%)	0.617
pT	pT1	9 (19.1%)	2 (22.2%)	7 (77.8%)	
	pT2	14 (29.8%)	6 (42.8%)	8 (57.2%)	
	pT3	19 (40.4%)	10 (47.6%)	9 (52.4%)	
	pT4	5 (10.6%)	3 (60%)	2 (40%)	0.443
pN	pN0	17 (36.2%)	10 (58.8%)	7 (41.2%)	
	pN1	15 (31.9%)	3 (20%)	12 (80%)	
	pN2	13 (27.7%)	6 (46.1%)	7 (53.9%)	
	pNx	2 (4.3%)	2 (100%)	0 (0%)	0.054
pM	pM0	47 (100%)	21 (44.7%)	26 (55.3%)	
Stage	IIA	1 (2.1%)	1 (100%)	0 (0%)	
	IIB	27 (57.4%)	11 (40.7%)	16 (59.3%)	
	IIIA	15 (31.9%)	7 (46.7%)	8 (53.3%)	
	IIIB	4 (8.5%)	2 (50%)	2 (50%)	0.806
PD-L1	<1%	22 (46.8%)	7 (33.3%)	15 (57.7%)	
	≥1%	25 (53.2%)	14 (66.7%)	11 (42.3%)	0.171
KRAS status	mut	21 (44.7%)	21 (100%)	0 (0%)	
	wt	26 (55.3%)	0 (0%)	26 (100%)	
Adjuvant therapy	plat + gem	47 (100%)	21 (44.7%)	26 (55.3%)	
First line therapy	NO	23 (48.9%)	9 (39.1%)	14 (60.9%)	
	YES	24 (51.1%)	12 (50%)	12 (50%)	0.649
Relapse site	Distance	10 (41.7%)	5 (50%)	5 (50%)	
	Local	13 (54.2%)	7 (53.9%)	6 (46.1%)	
	Both	1 (4.2%)	0 (0%)	1 (100%)	
	NA	23	9	14	1

(Continued)

10.3389/fonc.2025.1654491

TABLE 1 Continued

		TOT	KRAS		P-value
		N=47	mut (n=21)	wt (n=26)	
Metastasis CNS	NO	20 (83.3%)	11 (55%)	9 (45%)	
	YES	4 (16.7%)	1 (25%)	3 (75%)	
	NA	23	9	14	0.59
Nodal metastasis	NO	16 (66.7%)	8 (50%)	8 (50%)	
	YES	8 (33.3%)	4 (50%)	4 (50%)	
	NA	23	9	14	1
Lung metastasis	NO	12 (50%)	4 (33.3%)	8 (66.7%)	
	YES	12 (50%)	8 (66.7%)	4 (33.3%)	
	NA	23	9	14	0.22
Bone metastasis	NO	21 (87.5%)	10 (47.6%)	11 (52.4%)	
	YES	3 (12.5%)	2 (66.7%)	1 (33.3%)	
	NA	23	9	14	1
Other metastasis	NO	18 (75%)	10 (55.5%)	8 (45.5%)	
	YES	6 (25%)	2 (33.3%)	4 (66.7%)	
	NA	23	9	14	0.64
KRAS mutation types	G12A	3 (14.3%)			
	G12C	9 (42.9%)			
	G12D	1 (4.8%)			
	G12S	1 (4.8%)			
	G12V	4 (19%)			
	Q61L	1 (4.8%)			
	UNK	2 (9.5%)			

The table summarizes the distribution of age, gender, surgical procedures, histological subtypes, tumor staging (pT, pN, pM, and overall stage), PD-L1 expression, and KRAS mutation details. Statistical analyses, including p-values by Fisher's Exact Test, are provided to indicate significant differences between KRAS-mut and KRAS-wt groups. Additional columns report treatment modalities, metastasis locations, and KRAS mutation types. Abbreviations: CNS, Central nervous system; UNK, Unknown.
The bold values were those significant in the table.

chemotherapeutic agents (Gem+Carbo) and KRASi at the IC_{25} or at the IC_{50} concentrations for 72 hours in SW1573 and H23 cell lines (Supplementary Figure S2). Importantly, using this experimental design at the IC_{25} concentrations, for the Gem+Carbo treatment we achieved a similar reduction in cell viability, comparable to the sequential treatment scheme, at least in the H23 cell line. Specifically, in H23 cells the viability reduction due to gem+carbo combined treatment was substantial ($\Delta = 65\%$), while in SW1573 cells, the decrease was more moderate ($\Delta = 46\%$). A higher decrease was obtained when the chemotherapeutic agents and KRASi were administered together at the IC_{50}, and with a smaller, but significant, reduction when the drugs were administered at the IC_{25} for 72 hours in both cell lines (Supplementary Figure S2).

In view of these results, we decided to use the best chemotherapeutic combination Gem+Carbo at the IC_{25} combined with KRASi at the IC_{50}, for 72 hours in both cell lines (Figure 2C) since we obtained similar effects when the chemotherapeutic agents and KRASi were administered together (SW1573: Gem+Carbo +Soto Δ=82% and Gem+Carbo+Ada Δ=77%; H23: Gem+Carbo +Soto Δ=72% and Gem+Carbo+Ada Δ=67%), while reducing the toxicity of chemotherapeutic agents. As expected, the administration of Gem+Carbo (this combination will be indicated as "CI" from here on) induced a slighter reduction of cell viability compared to the previous experiment (SW1573: CI Δ=47%; H23: CI Δ=48%), but determined a robust decrease of cell viability when used in combination with KRASi in SW1573 and H23 NSCLC cell lines (SW1573: CI+sotorasib Δ=66%, CI+adagrasib Δ=56%; H23: CI +sotorasib Δ=46% CI+adagrasib Δ=36%; compared to CI alone. Figure 2D). Thus, the combination of Gem+Carbo effectively enhances the sensitivity of KRAS-G12C-mutated NSCLC cell lines to KRASi, with both sequential and concurrent treatment strategies, achieving significant reductions in cell viability.

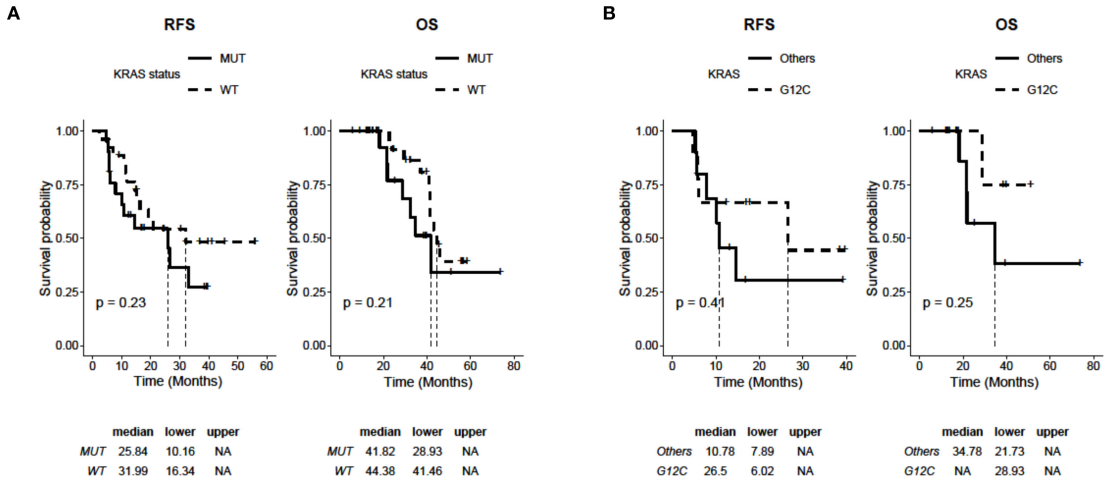

FIGURE 1
Kaplan-Meier analysis of RFS and OS depending on the status of KRAS in 47 NSCLC patients (WT: n=26; mutated: n=21). **(A)** RFS and OS curves of patients with WT and mutated KRAS (KRAS mutations: G12C, G12A, G12D, G12S, G12V, Q61L). **(B)** RFS and OS curves of patients with KRASG12C mutation (n=9) and KRAS mutated in other isoforms (i.e., G12A, G12D, G12S, G12V, Q61L; n=12). P values were calculated with a log-rank test.

TABLE 2 IC_{50} values for chemotherapeutic agents and KRAS inhibitors in NSCLC cell lines.

	SW1573 (μM)	H23 (μM)
Carboplatin	64h4.4	30 ± 6
Gemcitabine	0.004 ± 0.0006	0.0033 ± 0.00025
Sotorasib	65 ± 4.9	0.540 ± 0.014
Adagrasib	4 ± 0.5	0.200 ± 0.015
Pemetrexed	37 ± 0.6	0.0023 ± 0.003
Paclitaxel	245 ± 7.2	134 ± 0.021

Effect of chemotherapeutic agents and KRASi on spheroid volume reduction in parental KRAS mutated cell lines

Three-dimensional tumor spheroids grown *in vitro* are extensively utilized as 3D cell culture models for anticancer drug evaluation because they closely mimic the physiological conditions of tumor tissue compared to 2D models (26). SW1573 and H23 spheroids were generated following this procedure: firstly cells were seeded to allow the formation of spheroids and after 72 hours, photos of time 0 (T0) were taken and spheroids were then treated with drugs or left untreated (CTRL). Photos were taken after 3 and 7 days of treatment and the volume of SW1573 or H23 spheroids was quantified (Figure 3A). We used SW1573 and H23 spheroids to test whether using the combination of CI and the KRASi adagrasib, which has demonstrated greater efficiency in reducing cell viability compared to sotorasib (Figure 2), at the IC_{50} concentrations leads to a similar response with respect to 2D models. At 3 days, the combination of CI and adagrasib showed a reduction between 45% and 65% in SW1573 spheroid volumes and a reduction between 30% and 63% in H23 spheroid volumes compared to the respective single-agent treatments or CI (Figure 3B). At 7 days, the effect was maintained (Figures 3C, D).

These findings confirm the data obtained from the 2D assay, and further demonstrate that the CI+adagrasib combination exhibits superior efficacy even when the cells are cultured in a 3D model.

Generation and characterization of gemcitabine resistant cells

Our experiments showed that gemcitabine is the most promising platinum partner in SW1573 and H23 cell lines inhibition, especially in sensitizing NSCLC cells to treatment with KRASi (Figure 2B). Notably, tumor cells often develop multidrug resistance after CT; therefore, to investigate the impact of acquired resistance to gemcitabine to the efficacy of KRASi, we generated NSCLC cell lines (SW1573 and H23) resistant to gemcitabine by chronic and repeated exposure to increasing gemcitabine concentrations (Figure 4A). We observed evident morphological differences between parental (PR) and resistant (GR) NSCLC cells. The SW1573-GR cells acquired a long spindle shape compared to the round shape of the PR cells. Furthermore, the SW1573-GR show a larger volume compared to PR cells. The H23-GR cells have developed pseudopodia and these are also larger than the PR counterpart (Figure 4B). GR cells were validated using cell viability assay, comparing PR and GR cell proliferation after a 72h of gemcitabine treatment. Compared to parental cells, H23-GR and SW1573-GR cells showed a slight decrease in cell viability upon treatment with increasing doses of gemcitabine (Figure 4C). To investigate the impact of gemcitabine resistance on cell proliferation, we performed a cell cycle analysis. In the H23-GR cell line, we observed a slight increase in the proportion of cells in

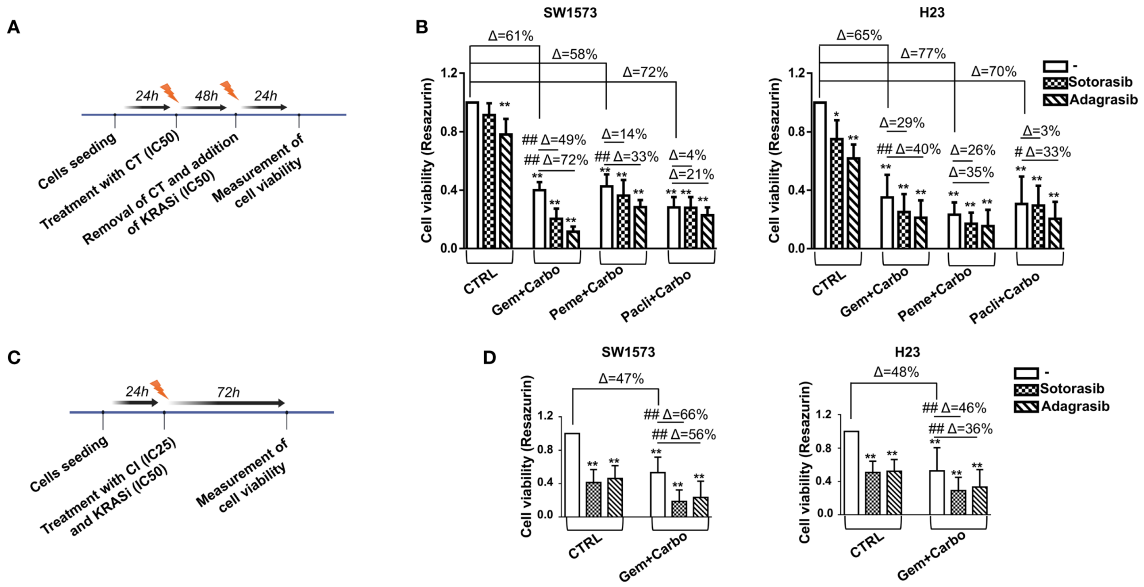

FIGURE 2
Chemotherapeutic agents sensitized NSCLC cells to KRASi in 2D cell viability assay. **(A)** The cartoon indicates the sequential treatment schedule used for the cell viability assay. Initially the cells were seeded and after 24 hours they were treated with chemotherapeutic (CT) agents for 48 hours at their IC_{50}. After this amount of time, these agents were removed and a KRAS inhibitor was administered for additional 24 hours at their IC_{50}. **(B)** Cell viability assay was performed in SW1573 or H23 cells treated with combination of chemotherapeutic agents (gemcitabine+carboplatin or pemetrexed+carboplatin or paclitaxel+carboplatin) and KRASi (sotorasib or adagrasib) following the time schedule reported in **(A)**. Data shown are mean ± SD from three independent experiments. *P < 0.05; **P < 0.01 refer to differences vs untreated cells (CTRL) as determined by Student t test; #P < 0.05; ##P < 0.01 refer to differences between the indicated samples as determined using one-way ANOVA. Δ indicates the percentage change in cell viability relative to CTRL cells or between the indicated samples. **(C)** The cartoon indicated the concomitant treatment schedule used for the cell viability assay. Initially the cells were seeded and after 24 hours they were treated with a combination of Gem+Carbo (CI) at their IC_{25} and KRASi at their IC_{50} for 72 hours. **(D)** Cell viability assay was performed in SW1573 or H23 cells treated with combination of chemotherapeutic agents Gem+Carbo and KRASi adagrasib following the schedule reported in **(C)** Data shown are mean ± SD from three independent experiments. **P < 0.01 refer to differences with respect to control (CTRL) as determined by Student t test; ##P < 0.01 refer to differences between the indicated samples as determined using one-way ANOVA. Δ indicates the percentage change in cell viability relative to the control (CTRL) or between the indicated samples.

the G0/G1 phase, and consequently a reduction in the S and G2/M phases, with respect to H23-PR. Consistently, in the H23-GR cell line we observed reduced levels of pRB, cyclin D1 and B1. We also found an increased expression of the cyclin-dependent kinase inhibitor (CDKi) p21, confirming the slight slowdown of the cell cycle in the gemcitabine-resistant cell line (Figure 4D). Then, we performed a comprehensive analysis of differentially expressed genes (DEGs) and KEGG pathway enrichment in H23 cell lines, including both PR and GR variants, under two conditions: untreated and treated with gemcitabine. This dual comparison enabled us to identify specific genes and pathways associated with the development and maintenance of gemcitabine resistance. By analyzing RNA-seq data from H23-PR and -GR cells in untreated and treated conditions, we identified 166 upregulated and 268 downregulated genes in untreated GR vs. PR cells, while 196 upregulated and 326 downregulated genes were observed in treated GR vs. PR cells ($|log2FC| > 1$; p-value < 0.05). These DEGs are visualized in volcano plots (Figure 4E). The top 10 genes that were consistently up-regulated in both untreated and treated GR cells were SLC4A4, TNFSF15, IGFBP3, ZNF711, CD36, CHRNA9, PLXDC2, GALNT13, PLCH1, UBE2QL1. While the top 10 genes that were consistently down-regulated in both untreated and treated GR cells were MYCN, SFRP5, DOK5, CRTAC1, TRPA1, CSMD2, GOLGA7B, RGS6, CYP24A1, TMEM179. To explore the functional implications of these transcriptional changes, we conducted a KEGG pathway analysis, identifying key pathways involved in mechanisms driving or contributing to drug resistance in both treated and untreated conditions (Figure 4F). In both conditions, the most enriched pathways are largely centered around protein synthesis (ribosome biogenesis, ribosome, RNA polymerase), RNA processing (spliceosome, mRNA surveillance), DNA metabolism (DNA replication, chromatin remodeling) and cell cycle regulation (Figure 4F). This upregulation shifts towards enhanced transcriptional and translational machinery, which may support an adaptation of resistant cells to survive DNA damage caused by gemcitabine. To delve deeper and to identify the main pathways involved in the mechanism of resistance to gemcitabine, we performed a gene set enrichment analysis on Gene Ontology pathways comparing H23-PR- and H23-GR-cells. This allowed us to identify multiple cellular pathways associated with gemcitabine resistance, including autophagy, PI3K/AKT signaling, epithelial-mesenchymal transition (EMT), and hypoxia response (Figure 4G). To confirm these findings at protein level, we performed Western blot analysis. In the H23-GR cell line, we observed a decrease in E-cadherin expression and an increase in N-cadherin expression, a common characteristic of EMT. Additionally, this resistant cell line exhibited an increase in Beclin-1, a marker of autophagy, as well as enhanced AKT phosphorylation, accompanied by a decrease in

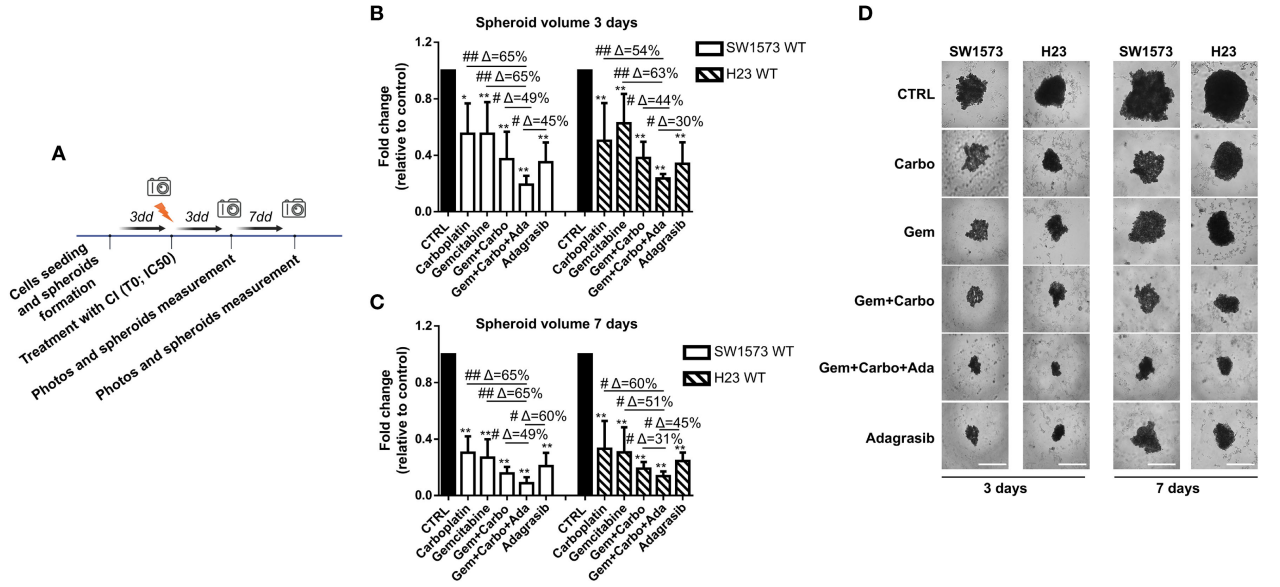

FIGURE 3
Chemotherapeutic agents sensitized NSCLC cells to KRASi adagrasib in a 3D spheroids model. **(A)** The cartoon indicated the treatment schedule used for the spheroid assay. Initially the cells were seeded and we waited 72 hours for spheroid formation. Then after this time, photos of time 0 were taken and spheroids were treated with chemotherapeutic agents or KRASi at their IC50. After that, photos were taken also after 3 and 7 days and spheroid volume was quantified each time. **(B)** SW1573 or H23 spheroids were treated with different combinations of chemotherapeutic agents and KRASi adagrasib at their IC_{50} for 3 days. **(C)** SW1573 or H23 spheroids were treated with different combinations of chemotherapeutic agents and KRASi adagrasib at their IC_{50} for 7 days. Graphs **(A, B)** show the quantification of spheroid volumes ± SD at different time points (3 and 7 days) normalized for the time point 0 (n = 3 independent experiments). **(D)** Representative images of spheroids taken at day 3 and 7 are shown. *P < 0.05; **P < 0.01 refer to differences with respect to control (CTRL) as determined by Student t test; #P < 0.05; ##P < 0.01 refer to differences between the indicated samples as determined using one-way ANOVA. Scale bar: 400 µm.

ERK1/2 phosphorylation (Figure 4G). Moreover, we observed that combined treatments of CI and CI+adagrasib result in modulation of the pERK1/2 pathway. Regarding AKT phosphorylation, which is more active in the gemcitabine-resistant cell line, was not modulated by the combined treatments (Supplementary Figure S3A). Given all of that, these findings suggest that gemcitabine resistance is associated with adaptive mechanisms that promote cell survival and therapy resistance.

Effect of chemotherapeutic agents and adagrasib on GR NSCLC cells

Next, we evaluated whether NSCLC cells, with different gemcitabine sensitivities (PR and GR), exhibit a different response to KRASi adagrasib. Firstly, we used SW1573-GR and H23-GR to assess cell viability after a 72 h treatment using CI at IC_{25} and KRASi adagrasib at IC_{50} (values determined in parental cell lines, see Table 2), following the same experimental schedule of Figure 2C (Figure 5A). While both GR cell lines showed resistance to gemcitabine as expected, the combination of CI+adagrasib was more effective respect to CI treatment alone and more significant accentuated in SW1573-GR (Δ=45%) compared to H23-GR (Δ=36%; Figure 5B). Importantly we observed a significant reduction in cell viability of PR and GR cell lines with the combination of CI and adagrasib although this effect is less evident in GR cell lines (SW1573GR vs PR: Gem +Carbo+Ada Δ=42%; H23GR vs PR: Gem+Carbo+Ada Δ=53%) (Figure 5C). To investigate the mechanisms underlying the reduction in cell viability, we observed a modulation of the Cleaved-Caspase-3 in the PR cell line following treatment with Gem+Carbo, as well as with the triple combination of CI+KRAS inhibitor. Interestingly, a similar modulation was also detected in the GR cell line, although to a lesser extent, suggesting a differential apoptotic response between the two models. We also evaluated the expression of additional proliferation- and cell cycle-related markers, including PCNA and p21. We observed a reduction in PCNA signal following treatment with Adagrasib alone and in combination with Gem+Carbo in both cell lines, indicating decreased proliferative activity. Additionally, p21 expression was upregulated upon treatment with Gem+Carbo, both in the presence and absence of the KRAS inhibitor, indicating activation of cell cycle arrest mechanisms. Notably, the increase was more pronounced in GR cell line compared to their parental counterparts, especially with CI+Adagrasib combination treatment, as confirmed by densitometric analysis (Figure 5D). These findings support the impact of the treatments on both apoptotic and proliferative pathways.

Effect of chemotherapeutic agents and adagrasib on spheroid volume reduction of GR NSCLC cell lines

Then, we studied the effect of combination therapies with CI and adagrasib to inhibit viability in GR NSCLC tumor spheroids

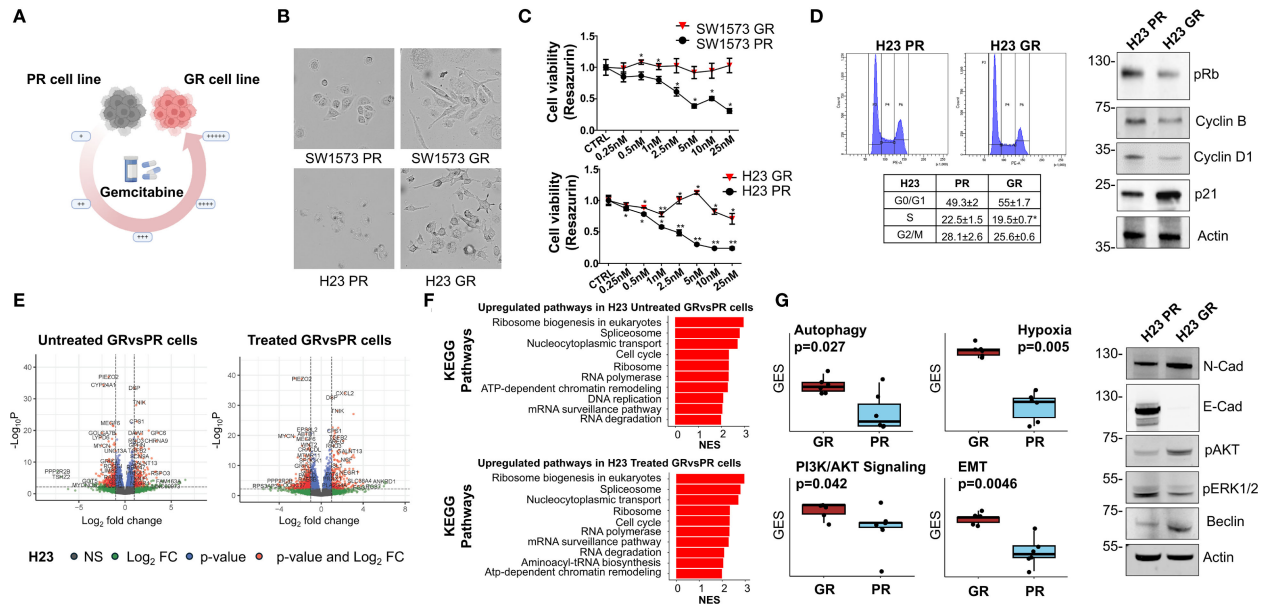

H23	PR	GR
G0/G1	49.3±2	55±1.7
S	22.5±1.5	19.5±0.7*
G2/M	28.1±2.6	25.6±0.6

FIGURE 4
Characterization of gemcitabine resistance NSCLC cells **(A)** Schematic representing the generation of gemcitabine-resistant (GR) NSCLC cells from parental NSCLC cells, using incrementally increasing concentrations of gemcitabine in culture over time. **(B)** Representative images of PR and GR NSCLC cells. Cells were grown to 50% confluency and then photographed under 10× magnification. **(C)** Determination of cell viability for gemcitabine in PR and GR SW1573 and H23 NSCLC cells. Cells were treated with gemcitabine at the indicated concentrations for 72 h and viability was determined. Data were normalized to control and presented as mean ± SD from three independent experiments. *P < 0.05; **P < 0.01 refers to differences with respect to control (CTRL) as determined by Student t test. **(D)** Cell cycle phase distribution plots and values (tables) of GR NSCLC cells and of PR NSCLC cells (H23). Cells were analyzed after 48 h from cell seeding. Data shown are mean ± SD from three independent experiments. *p < 0.05 as determined by Student's t-test (left). Immunoblot showing the expression or phosphorylation status of cell cycle regulators in H23-PR and H23-GR cells cultured for 48h (right). Actin was used as a loading control. **(E)** Volcano plot of differentially expressed genes (DEG) between H23-PR and H23-GR cells. H23-PR and H23-GR cells were treated with gemcitabine for 72 hours. Data are from three independent experiments. **(F)** KEGG pathways Gene Set Enrichment analysis of the DEGs between H23-PR and H23-GR cells. Only the ten most significantly upregulated pathways in H23-GR cells are shown. NES: Normalized Enrichment Score. **(G)** Differences in the expression of gemcitabine resistance-associated pathways in H23-PR and H23-GR cells (left). GES: Gene Expression Score. P-values have been computed with a Wilcoxon rank-sum test. Immunoblot showing the expression or phosphorylation status of resistance markers in H23-PR and H23-GR cells cultured for 72h (right). Actin was used as loading control.

using the same experimental schedule of Figure 3A (Figure 6A). Importantly, the spheroids generated from H23 PR and GR cells exhibit the same volume at all time points, whereas the spheroids derived from SW1573 PR and GR cells show a significant difference at 7 days (Figure 6B). As shown in Figures 6C, D, we observed a substantial and significant reduction in spheroid volume with different treatments in both cell lines (Figures 6C, D). At 3 days, the combination of CI and adagrasib led to reductions in spheroid volumes ranging from 8% to 61% for SW1573 and from 22% to 70% for H23 when compared to the corresponding single-agent treatments or CI alone (Supplementary Figure S3B, Figure 6C). By 7 days, these effects became more pronounced, with the SW1573 cell line showing a marked response to combination therapy, achieving up to an 89% reduction in spheroid volume, while the H23 cell line demonstrated a maximum reduction of 75% under similar conditions (Figure 6D).

Finally, at 7 days in GR spheroids the percentages of inhibition (Δ) of the combined treatment CI+adagrasib were the same as the parental type 3D models and the reduction of the volumes were similar with respect to parental cells (Supplementary Figure S3C). These findings are crucial as they provide evidence that the CI +adagrasib combination is effective also in resistant cells.

Discussion

Adjuvant CT in NSCLC has a limited impact on survival, and for decades has been the only treatment available for stage II and III patients undergoing radical surgery. This lack of benefit is notable for EGFR mutations and ALK fusions, for which it has recently introduced targeted agents into clinical practice with significant survival benefits over CT alone (8, 9). However, with the exception of the mutations listed above, therapies for other known targets in the metastatic setting are not currently available in NSCLC early stages, including KRAS.

KRAS is one of the isoforms, along with HRAS and NRAS, that belong to the RAS oncogene family. KRAS is the most frequently mutated and is found in approximately 15-20% of patients with NSCLC (27). The KRAS protein has a characteristic action, depending on a GTP-GDP mechanism, it oscillates between an active phase "ON" and an inactive phase "OFF", allowing signal transduction to promote various cellular processes such as differentiation, growth, chemotaxis and apoptosis. This particular activation mechanism gathers the absence of well-defined hydrophobic pockets on the surface, picomolar affinity of GTP and GDP making mutations in KRAS difficult targets (28) as proved

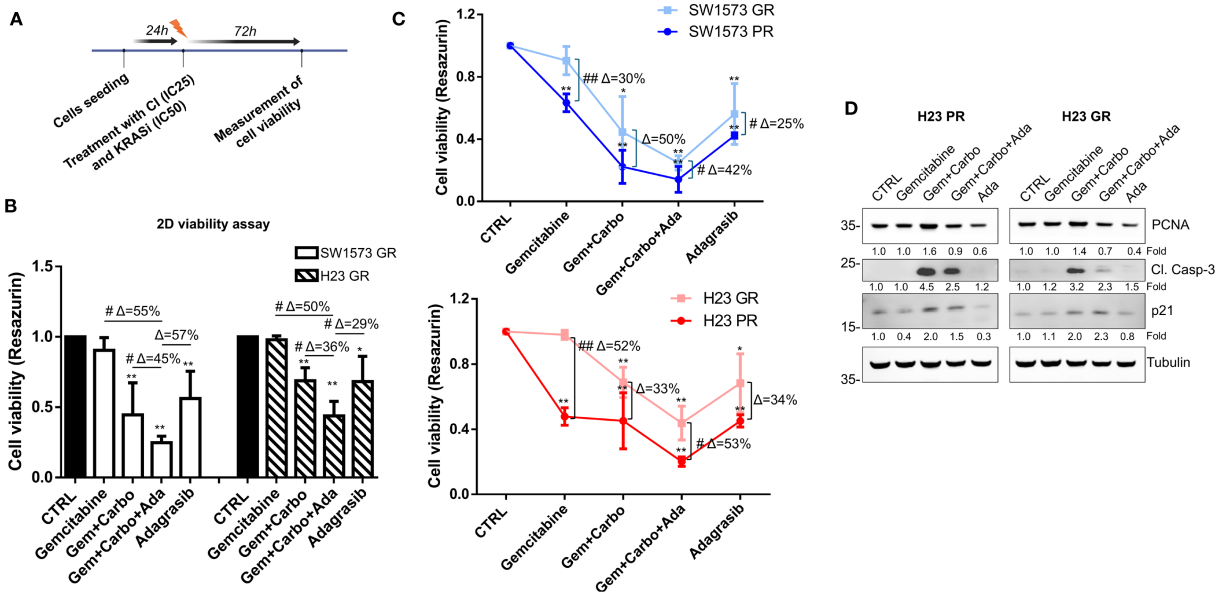

FIGURE 5
Chemotherapeutic agents sensitized gemcitabine resistant NSCLC cells to KRASi adagrasib in 2D cell viability assay. **(A)** The cartoon indicated the treatment schedule used for the cell viability assay. Initially the cells were seeded and after 24 hours they were treated with a combination of chemotherapeutic agents at their IC_{25} and KRASi at their IC_{50} for 72 hours. **(B)** Cell viability assay was performed in SW1573 or H23 cells treated with combination of chemotherapeutic agents gemcitabine and carboplatin and KRASi adagrasib following the time schedule of Figure 2C. Data shown are mean ± SD from three independent experiments. *P < 0.05; **P < 0.01 refer to differences with respect to control (CTRL) as determined by Student t test; #P < 0.05; ##P < 0.01 refer to differences between the indicated samples as determined using one-way ANOVA. Δ indicates the percentage change in cell viability relative to the control (CTRL) or between the indicated samples. **(C)** Determination of cell viability for gemcitabine comparing parental and GR SW1573 and H23 NSCLC cells. Cells were treated as indicated in Figure 4B. Data were normalized to control and presented as mean ± SD from three independent experiments. *P < 0.05; **P < 0.01 refers to differences with respect to control (CTRL) as determined by Student t test. #P < 0.05; ##P < 0.01 refer to differences between the indicated samples as determined using one-way ANOVA. **(D)** Expression of cleaved-caspase 3, PCNA and p21 in H23-PR and H23-GR cell line treated with the indicated drug combination for 72h detected by western blotting. Tubulin was used as loading control.

by the RR and PFS data in the metastatic setting with the selective inhibitors sotorasib and adagrasib (29, 30). Literature data have shown that KRAS mutations have a negative impact on prognosis (31), leading to resistance to most treatments, including checkpoint inhibitors, particularly when co-occurring with mutations like *STK11/LKB1* in metastatic setting (32). On the other hand, the available data on KRAS in the adjuvant setting come from the analysis of the LACE-bio trial and an old but large meta analysis, which showed no statistically significance in OS compared to wild-type and few data confirm no difference in OS between single hotspot mutation probably due to the small sample size (33, 34).

In our cohort of patients, 47 underwent radical surgery and were administered adjuvant CT with platinum-based therapy with gemcitabine. KRAS mutations exhibited a higher prevalence of PD-L1≥1% (56%; n=14), the most common mutations were G12C, G12V and G12A findings that align with the existing literature (11).

A subsequent analysis of survival data revealed a trend in favor of the WT population (mOS: 44.38 months 95% CI: 28.93-NA vs. 41.82 months 95% CI: 41.46-NA, *p=0.2*). However, when we analyzed the G12C subgroup compared to the other mutations, we did not find statistical significance in survival (mOS NR 95% CI: 28.93-NA vs. 34.78 months 95% CI: 21.73-NA, *p=0.25*).

This work aims to explore the potential of adding KRASi sequentially or concurrently to CT in two KRAS G12C mutated NSCLC cell lines. In this study, the CI with Gem+Carbo exerts the best viability reduction in SW1573-PR and H23-PR cell lines when KRASi are added sequentially or concurrently in 2D model and similar results were confirmed in spheroid models. The combination therapy was particularly effective in reducing the viability of SW1573-PR and H23-PR, outperforming other tested chemotherapeutic regimens such as Peme+Carbo and Pacli+Carbo. However, the efficacy of these agents is frequently compromised by the development of chemoresistance, a major obstacle in the successful management of the disease. In our cohort more than half of the patients (n=24) experienced a recurrence. RFS was shorter in KRAS mutated patients without a statistical significance (mRFS 25.84 months vs. 31.99 months; *p=0.23*) suggesting that the KRAS mutation may have a deleterious effect and that the tumor cells may be inherently resistant to adjuvant therapies. Gemcitabine resistance, in particular, poses a significant challenge, limiting the effectiveness of this widely used chemotherapeutic agent (35). Gemcitabine resistance in NSCLC involves multiple mechanisms as per autophagy suppression via impaired JNK-mediated Bcl-2 phosphorylation that limits autophagy-dependent cell death (36), enhancing activation of the PI3K/AKT/NF-κB pathway and reducing ROS-driven ERK signaling, with survival and proliferation boost as direct results (37). Another mechanism of resistance involves hypoxia-inducible

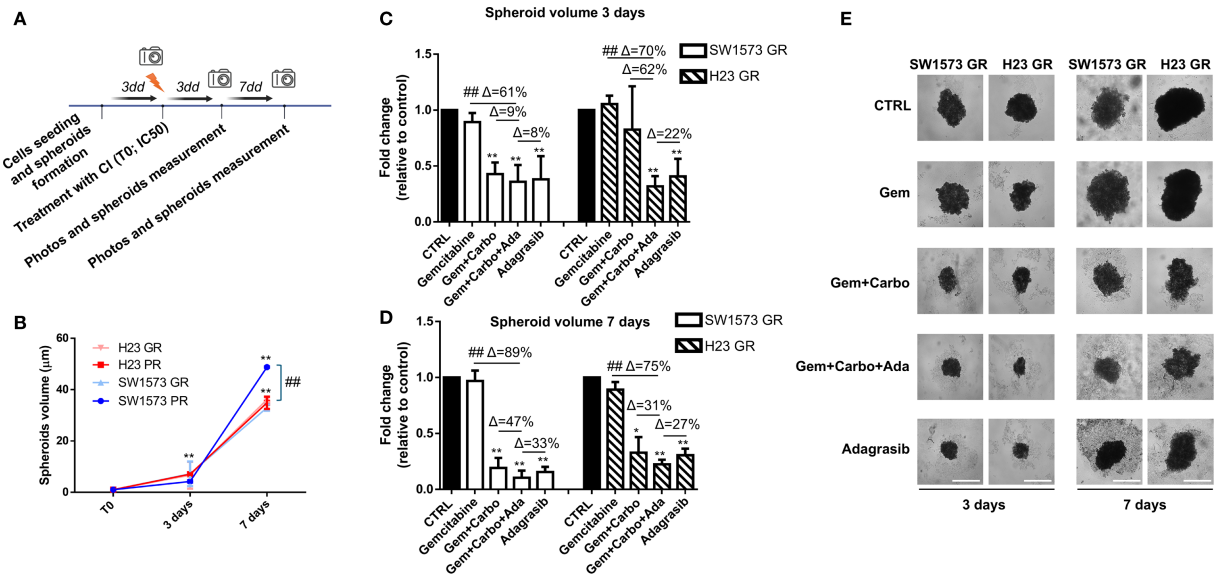

FIGURE 6
Chemotherapeutic agents sensitized gemcitabine resistant NSCLC cells to KRASi adagrasib in a 3D spheroids model. **(A)** The cartoon indicated the treatment schedule used for the spheroid assay. Initially the cells were seeded and spheroids were allowed to form for 72 hours. After this time, photos of time 0 were taken and spheroids were treated with chemotherapeutic agents or KRASi at their IC50. Photos were then taken after 3 and 7 days and spheroid volume was quantified each time. **(B)** Quantification of spheroid volumes ± SD at different time points (3 and 7 days) normalized for the time point 0 (n = 3) in PR and GR NSCLC cell lines. *P < 0.05; **P < 0.01 refers to differences with respect to control (CTRL) as determined by Student t test. ##, P < 0.01 refers to the difference between SW1573 GR and SW1573 PR as determined by Student t test. **(C)** SW1573 or H23 spheroids were treated with different combinations of chemotherapeutic agents and KRASi adagrasib at their IC_{50} for 3 days **(D)** GR SW1573 or H23 spheroids were treated with different combinations of chemotherapeutic agents and KRASi adagrasib at their IC_{50} for 7 days. Graphs **(A, B)** show the quantification of spheroid volumes ± SD at different time points (3 and 7 days) normalized for the time point 0 (n = 3). **(E)** Representative images of spheroids taken at day 3 and 7 are shown. *P < 0.05; **P < 0.01 refers to differences with respect to control (CTRL) as determined by Student t test. ##P < 0.01 refer to differences between the indicated samples as determined using one-way ANOVA. Scale bar: 400 µm.

factor-1α (HIF-1α) that upregulates ABCB6 expression, reprogramming heme metabolism to reduce reactive oxygen species (ROS) and conferring resistance (38). Similarly, targeting mTORC2, rather than mTORC1, sensitizes cells to gemcitabine by inducing apoptosis (39). The FOXO3-regulated TRIM22 axis promotes autophagy to protect cells from gemcitabine-induced apoptosis, further reducing drug sensitivity (40). Additionally, exosomal transfer of miR-222-3p drives gemcitabine resistance and malignancy by targeting SOCS3 (41). To better understand the mechanism behind gemcitabine chemoresistance in KRAS mutated cells we developed H23-GR and SW1573-GR cell lines, highlighting that chronic gemcitabine exposure induces significant transcriptional and cellular adaptations in NSCLC cells, promoting the development of resistance. Key resistance mechanisms include enhanced DNA damage repair, altered cell cycle dynamics, and an upregulation of transcriptional and translational machinery. The observed increase in the G0/G1 cell population in H23-GR cells, coupled with enrichment of pathways related to ribosome biogenesis, RNA processing, and chromatin remodeling, supports the hypothesis that resistant cells reprogram their metabolic and replicative machinery to adapt to therapeutic stress.

To determine whether gemcitabine resistance was reversible with the addition of a KRASi, we next replicated the analysis of cell viability on the two resistant cell lines H23-GR and SW1573-GR. Based on our previous results, we decided to treat both the 2D model and the spheroids directly with the CI+adagrasib combination, the most promising of the combination tested. Interestingly, both H23-GR and SW1573-GR exhibited similar sensibility to adagrasib used as a single agent or in combination with CI in 2D and 3D models. This finding suggests that KRASi may mitigate the adaptive resistance mechanisms in GR cells as already reported in preclinical PDAC models (42–44). Our 2D and 3D models demonstrated that the combination of CI+adagrasib was consistently more effective than CI or adagrasib alone in both PR and GR cells. The significant reduction in spheroid volume over extended treatment periods underscores the potential for combination regimens to achieve durable antitumor effects, even in the context of chemoresistance.

Importantly, while previous preclinical studies have investigated KRASi such as adagrasib and sotorasib in combination with CT (17, 19), our study provides several novel contributions. First, we employed both 2D and 3D spheroid models, the latter of which better mimics tumor architecture and drug penetration than conventional monolayer cultures (45). Second, we evaluated the effects of KRASi+CT combinations in chemoresistant cell lines—a clinically relevant context that remains underexplored in current literature. Third, we analyzed both concurrent and sequential treatment strategies, offering insights into potential therapeutic scheduling strategies that could optimize efficacy. These aspects collectively differentiate our work and underscore its translational relevance in a setting where therapeutic options for KRAS-mutant NSCLC remain limited in the adjuvant context.

Conclusion

The results of this study highlight the potential impact of combination therapies in the early treatment of operated NSCLC, particularly for KRAS G12C tumors. The ability of KRASi to potentiate cytotoxic effects when combined with conventional chemotherapeutic agents provides a rationale for the integration of these agents into adjuvant treatment regimens. In addition, the efficacy observed in GR cell models suggests that KRASi may have a role to play in the treatment of chemoresistant disease. However, given the adverse event profile of individual agents, further *in vivo* safety evaluations are needed.

Data availability statement

The original contributions presented in the study are included in the article/Supplementary Material. Further inquiries can be directed to the corresponding author.

Ethics statement

The protocol was approved by the local ethics committee (CEAVC n.22712). The studies were conducted in accordance with the local legislation and institutional requirements. The participants provided their written informed consent to participate in this study.

Author contributions

AT: Writing – original draft, Conceptualization, Methodology, Data curation, Investigation, Validation. SF: Writing – original draft, Data curation, Investigation, Formal Analysis. LA: Investigation, Data curation, Writing – review & editing, Methodology. GP: Methodology, Writing – review & editing. EC: Formal Analysis, Writing – review & editing, Investigation. FM: Conceptualization, Data curation, Writing – review & editing. FS: Data curation, Writing – review & editing, Investigation. BN: Data curation, Writing – review & editing. BM: Investigation, Writing – review & editing. CC: Writing – review & editing, Data curation. LV: Data curation, Writing – review & editing. SP: Funding acquisition, Supervision, Writing – original draft, Conceptualization. LAnt: Writing – review & editing, Conceptualization, Funding acquisition, Supervision.

Funding

The author(s) declare financial support was received for the research and/or publication of this article. Departments of Excellence award 2023-2027, Ministry of University and Research to Serena Pillozzi.

Acknowledgments

We thank Dr. Azucena Esparís-Ogando (IBMCC-CIC, IBSAL, CIBERONC, Salamanca, Spain) for kindly providing NSCLC cell lines.

Conflict of interest

The authors declare that the research was conducted in the absence of any commercial or financial relationships that could be construed as a potential conflict of interest.

Generative AI statement

The author(s) declare that no Generative AI was used in the creation of this manuscript.

Any alternative text (alt text) provided alongside figures in this article has been generated by Frontiers with the support of artificial intelligence and reasonable efforts have been made to ensure accuracy, including review by the authors wherever possible. If you identify any issues, please contact us.

Publisher's note

Supplementary material

The Supplementary Material for this article can be found online at: https://www.frontiersin.org/articles/10.3389/fonc.2025.1654491/full#supplementary-material

SUPPLEMENTARY FIGURE 1
Dose-response curves (using GraphPad Prism) tested for chemotherapeutic agents and KRAS inhibitors in NSCLC cell lines with cell viability assay.

SUPPLEMENTARY FIGURE 2
Cell viability assay was performed in SW1573 or H23 cells treated for 72 hours with different combinations of chemotherapeutic agents and KRASi. Black bars indicated treatments at IC25 of the indicated drugs. Grey bars indicated treatments at IC50 of the indicated drugs. Data shown are mean ± SD from three independent experiments. *, $P < 0.05$; **, $P < 0.01$ refer to differences with respect to control (CTRL) as determined by Student t test; #, $P < 0.05$; ##, $P < 0.01$ refers to differences between the indicated samples as determined using one-way ANOVA. Δ indicates the percentage change in cell viability relative to the control (CTRL) or between the indicated samples.

SUPPLEMENTARY FIGURE 3
(A) Combined treatment of H23-PR and H23-GR NSCLC cells showing the effect of Gemcitabine, Carboplatin and Adagrasib or their combination on the

phosphorylation of ERK1/2 and AKT. Vinculin was used as loading control. The graph below shows densitometric values of pERK1/2 and pAKT normalized for Vinculin content. Data shown are mean ± SD from two independent experiments. **(B, C)** Determination of spheroid volumes ± SD at different time points (3 and 7 days) normalized for the time point 0 (n = 3) comparing parental and GR SW1573 and H23 NSCLC cells. Cells were treated with different combinations of chemotherapeutic agents and KRASi Adagrasib at their IC50. Data were normalized to control and presented as mean ± SD from three independent experiments. *, $P < 0.05$; **, $P < 0.01$ refer to differences with respect to control (CTRL) as determined by Student t test.

References

1. PDQ® Adult Treatment Editorial Board. PDQ Non-Small Cell Lung Cancer Treatment. Bethesda, MD: National Cancer Institute. (2025) Available online at: https://www.cancer.gov/types/lung/hp/non-small-cell-lung-treatment-pdq (Accessed September 02, 2025)

2. Duma N, Santana-Davila R, Molina JR. Non-small cell lung cancer: epidemiology, screening, diagnosis, and treatment. *Mayo Clin Proc*. (2019) 94:1623–40. doi: 10.1016/j.mayocp.2019.01.013

3. de Sousa VML, Carvalho L. Heterogeneity in lung cancer. *Pathobiology*. (2018) 85:96–107. doi: 10.1159/000487440

4. Goldstraw P, Chansky K, Crowley J, Rami-Porta R, Asamura H, Eberhardt WE, et al. The IASLC lung cancer staging project: proposals for revision of the TNM stage groupings in the forthcoming (Eighth) edition of the TNM classification for lung cancer. *J Thorac Oncol*. (2016) 11:39–51. doi: 10.1016/j.jtho.2015.09.009

5. Bao R, Chan P. Novel compounds in the treatment of lung cancer: current and developing therapeutic agents. *J Exp Pharmacol*. (2011) 3:21–34. doi: 10.2147/JEP.S7804

6. Pignon JP, Tribodet H, Scagliotti GV, Douillard JY, Shepherd FA, Stephens RJ, et al. Lung adjuvant cisplatin evaluation: a pooled analysis by the LACE Collaborative Group. *J Clin Oncol*. (2008) 26:3552–9. doi: 10.1200/JCO.2007.13.9030

7. Felip E, Altorki N, Zhou C, Vallières E, Martínez-Martí A, Rittmeyer A, et al. Overall survival with adjuvant atezolizumab after chemotherapy in resected stage II-IIIA non-small-cell lung cancer (IMpower010): a randomised, multicentre, open-label, phase III trial. *Ann Oncol*. (2023) 34:907–19. doi: 10.1016/j.annonc.2023.07.001

8. Tsuboi M, Herbst RS, John T, Kato T, Majem M, Grohé C, et al. Overall survival with osimertinib in resected EGFR-mutated NSCLC. *N Engl J Med*. (2023) 389:137–47. doi: 10.1056/NEJMoa2304594

9. Wu YL, Dziadziuszko R, Ahn JS, Barlesi F, Nishio M, Lee DH, et al. Alectinib in resected ALK-positive non-small-cell lung cancer. *N Engl J Med*. (2024) 390:1265–76. doi: 10.1056/NEJMoa2310532

10. Fancelli S, Petroni G, Pillozzi S, Antonuzzo L. Unconventional strategy could be the future: From target to KRAS broad range treatment. *Heliyon*. (2024) 10:e29739. doi: 10.1016/j.heliyon.2024.e29739

11. Judd J, Abdel Karim N, Khan H, Naqash AR, Baca Y, Xiu J, et al. Characterization of KRAS mutation subtypes in non-small cell lung cancer. *Mol Cancer Ther*. (2021) 20:2577–84. doi: 10.1158/1535-7163.MCT-21-0201

12. Riely GJ, Marks J, Pao W. KRAS mutations in non-small cell lung cancer. *Proc Am Thorac Soc*. (2009) 6:201–5. doi: 10.1513/pats.200809-107LC. Moore MJ, et al. gemcitabine: a review of the pharmacokinetics, pharmacodynamics, and clinical efficacy of gemcitabine. Clin Ther. 1997;19(5):1041-1053.

13. Skoulidis F, Byers LA, Diao L, Papadimitrakopoulou VA, Tong P, Izzo J, et al. Co-occurring genomic alterations define major subsets of KRAS-mutant lung adenocarcinoma with distinct biology, immune profiles, and therapeutic vulnerabilities. *Cancer Discov*. (2015) 5:860–77. doi: 10.1158/2159-8290.CD-14-1236

14. West HJ, McCleland M, Cappuzzo F, Reck M, Mok TS, Jotte RM, et al. Clinical efficacy of atezolizumab plus bevacizumab and chemotherapy in KRAS-mutated non-small cell lung cancer with STK11, KEAP1, or TP53 comutations: subgroup results from the phase III IMpower150 trial. *J Immunother Cancer*. (2022) 10:e003027. doi: 10.1136/jitc-2021-003027

15. Fancelli S, Caliman E, Mazzoni F, Paglialunga L, Gatta Michelet MR, Lavacchi D, et al. KRAS G12 isoforms exert influence over up-front treatments: A retrospective, multicenter, Italian analysis of the impact of first-line immune checkpoint inhibitors in an NSCLC real-life population. *Front Oncol*. (2022) 12:968064. doi: 10.3389/fonc.2022.968064

16. Skoulidis F, Li BT, Dy GK, Price TJ, Falchook GS, Wolf J, et al. sotorasib for lung cancers with KRAS p.G12C mutation. *N Engl J Med*. (2021) 384:2371–81. doi: 10.1056/NEJMoa2103695

17. Canon J, Rex K, Saiki AY, Mohr C, Cooke K, Bagal D, et al. The clinical KRAS (G12C) inhibitor AMG 510 drives anti-tumour immunity. *Nature*. (2019) 575:217–23. doi: 10.1038/s41586-019-1694-1

18. Jänne PA, Riely GJ, Gadgeel SM, Heist RS, Ou SI, Pacheco JM, et al. Adagrasib in non-small-cell lung cancer harboring a *KRASG12C* mutation. *N Engl J Med*. (2022) 387:120–31. doi: 10.1056/NEJMoa2204619

19. Fell JB, Fischer JP, Baer BR, Blake JF, Bouhana K, Briere DM, et al. Identification of the clinical development candidate MRTX849, a covalent KRASG12C inhibitor for the treatment of cancer. *J Med Chem*. (2020) 63:6679–93. doi: 10.1021/acs.jmedchem.9b02052

20. Kim D, Paggi JM, Park C, Bennett C, Salzberg SL. Graph-based genome alignment and genotyping with HISAT2 and HISAT-genotype. *Nat Biotechnol*. (2019) 37:907–15. doi: 10.1038/s41587-019-0201-4

21. Danecek P, Bonfield JK, Liddle J, Marshall J, Ohan V, Pollard MO, et al. Twelve years of SAMtools and BCFtools. *Gigascience*. (2021) 10:giab008. doi: 10.1093/gigascience/giab008

22. Liao Y, Smyth GK, Shi W. featureCounts: an efficient general purpose program for assigning sequence reads to genomic features. *Bioinformatics*. (2014) 30:923–30. doi: 10.1093/bioinformatics/btt656

23. Love MI, Huber W, Anders S. Moderated estimation of fold change and dispersion for RNA-seq data with DESeq2. *Genome Biol*. (2014) 15:550. doi: 10.1186/s13059-014-0550-8

24. Yu G, Wang LG, Han Y, He QY. clusterProfiler: an R package for comparing biological themes among gene clusters. *OMICS*. (2012) 16:284–7. doi: 10.1089/omi.2011.0118

25. Mohanty A, Nam A, Srivastava S, Jones J, Lomenick B, Singhal SS, et al. Acquired resistance to KRAS G12C small-molecule inhibitors via genetic/nongenetic mechanisms in lung cancer. *Sci Adv*. (2023) 9:eade3816. doi: 10.1126/sciadv.ade3816

26. Lv D, Hu Z, Lu L, Lu H, Xu X. Three-dimensional cell culture: A powerful tool in tumor research and drug discovery. *Oncol Lett*. (2017) 14:6999–7010. doi: 10.3892/ol.2017.7134

27. Chevallier M, Borgeaud M, Addeo A, Friedlaender A. Oncogenic driver mutations in non-small cell lung cancer: Past, present and future. *World J Clin Oncol*. (2021) 12:217–37. doi: 10.5306/wjco.v12.i4.217

28. Prior IA, Lewis PD, Mattos C. A comprehensive survey of Ras mutations in cancer. *Cancer Res*. (2012) 72:2457–67. doi: 10.1158/0008-5472.CAN-11-2612

29. de Langen AJ, Johnson ML, Mazieres J, Dingemans AC, Mountzios G, Pless M, et al. Sotorasib versus docetaxel for previously treated non-small-cell lung cancer with KRASG12C mutation: a randomised, open-label, phase 3 trial. *Lancet*. (2023) 401:733–46. doi: 10.1016/S0140-6736(23)00221-0

30. Mok TSK, Yao W, Duruisseaux M, Doucet L, Azkárate Martínez A, Gregorc V, et al. KRYSTAL-12: Phase 3 study of adagrasib versus docetaxel in patients with previously treated advanced/metastatic non-small cell lung cancer (NSCLC) harboring a KRASG12C mutation. *J Clin Oncol*. (2024) 42:LBA8509. doi: 10.1200/JCO.2024.42.17_suppl.LBA8509

31. Sun JM, Hwang DW, Ahn JS, Ahn MJ, Park K. Prognostic and predictive value of KRAS mutations in advanced non-small cell lung cancer. *PloS One*. (2013) 8:e64816. doi: 10.1371/journal.pone.0064816

32. Skoulidis F, Goldberg ME, Greenawalt DM, Hellmann MD, Awad MM, Gainor JF, et al. STK11/LKB1 mutations and PD-1 inhibitor resistance in KRAS-mutant lung adenocarcinoma. *Cancer Discov*. (2018) 8:822–35. doi: 10.1158/2159-8290.CD-18-0099

33. Shepherd FA, Domerg C, Hainaut P, Jänne PA, Pignon JP, Graziano S, et al. Pooled analysis of the prognostic and predictive effects of KRAS mutation status and KRAS mutation subtype in early-stage resected non-small-cell lung cancer in four trials of adjuvant chemotherapy. *J Clin Oncol*. (2013) 31:2173–81. doi: 10.1200/JCO.2012.48.1390

34. Mascaux C, Iannino N, Martin B, Paesmans M, Berghmans T, Dusart M, et al. The role of RAS oncogene in survival of patients with lung cancer: a systematic review of the literature with meta-analysis. *Br J Cancer*. (2005) 92:131–9. doi: 10.1038/sj.bjc.6602258

35. Jia Y, Xie J. Promising molecular mechanisms responsible for gemcitabine resistance in cancer. *Genes Dis*. (2015) 2:299–306. doi: 10.1016/j.gendis.2015.07.003

36. Chiu CH, Ramesh S, Liao PH, Kuo WW, Chen MC, Kuo CH, et al. Phosphorylation of Bcl-2 by JNK confers gemcitabine resistance in lung cancer cells by reducing autophagy-mediated cell death. *Environ Toxicol*. (2023) 38:2121–31. doi: 10.1002/tox.23836

37. Chiu CH, Lin YJ, Ramesh S, Kuo WW, Chen MC, Kuo CH, et al. Gemcitabine resistance in non-small cell lung cancer is mediated through activation of the PI3K/AKT/NF-κB pathway and suppression of ERK signaling by reactive oxygen species. *J Biochem Mol Toxicol*. (2023) 37:e23497. doi: 10.1002/jbt.23497

38. Xiang L, Wang Y, Lan J, Na F, Wu S, Gong Y, et al. HIF-1-dependent heme synthesis promotes gemcitabine resistance in human non-small cell lung cancers via

enhanced ABCB6 expression. *Cell Mol Life Sci*. (2022) 79:343. doi: 10.1007/s00018-022-04360-9

39. Chawsheen MA, Dash PR. mTOR modulates resistance to gemcitabine in lung cancer in an MTORC2 dependent mechanism. *Cell Signal*. (2021) 81:109934. doi: 10.1016/j.cellsig.2021.109934

40. Wang Y, Liang HX, Zhang CM, Zou M, Zou BB, Wei W, et al. FOXO3/TRIM22 axis abated the antitumor effect of gemcitabine in non-small cell lung cancer via autophagy induction. *Transl Cancer Res*. (2020) 9:937–48. doi: 10.21037/tcr.2019.12.33

41. Wei F, Ma C, Zhou T, Dong X, Luo Q, Geng L, et al. Exosomes derived from gemcitabine-resistant cells transfer Malignant phenotypic traits via delivery of miRNA-222-3p. *Mol Cancer*. (2017) 16:132. doi: 10.1186/s12943-017-0694-8

42. Lee JE, Woo MG, Jung KH, Kang YW, Shin SM, Son MK, et al. Combination therapy of the active KRAS-targeting antibody inRas37 and a PI3K inhibitor in pancreatic cancer. *Biomol Ther (Seoul)*. (2022) 30:274–83. doi: 10.4062/biomolther.2021.145

43. Lee JE, Kang YW, Jung KH, Son MK, Shin SM, Kim JS, et al. Intracellular KRAS-specific antibody enhances the anti-tumor efficacy of gemcitabine in pancreatic cancer by inducing endosomal escape. *Cancer Lett*. (2021) 507:97–111. doi: 10.1016/j.canlet.2021.03.015

44. Huang YK, Cheng WC, Kuo TT, Yang JC, Wu YC, Wu HH, et al. Inhibition of ADAM9 promotes the selective degradation of KRAS and sensitizes pancreatic cancers to chemotherapy. *Nat Cancer*. (2024) 5:400–19. doi: 10.1038/s43018-023-00720-x

45. Friedrich J, Seidel C, Ebner R, Kunz-Schughart LA. Spheroid-based drug screen: considerations and practical approach. *Nat Protoc*. (2009) 4:309–24. doi: 10.1038/nprot.2008.226

frontiers | Frontiers in Oncology

TYPE Case Report
PUBLISHED 17 September 2025
DOI 10.3389/fonc.2025.1632133

OPEN ACCESS

EDITED BY
Giovanna Damia,
Mario Negri Institute for Pharmacological Research (IRCCS), Italy

REVIEWED BY
Ran Wang,
Anhui Medical University, China
Qinglin Shen,
Jiangxi Provincial People's Hospital, China

*CORRESPONDENCE
Tong Zhang
ashtray7654@126.com

RECEIVED 18 June 2025
ACCEPTED 28 August 2025
PUBLISHED 17 September 2025

CITATION
Sun Y, Bian J, Wang L and Zhang T (2025) Etoposide and cisplatin in combination with anlotinib for lung NUT carcinoma: a case report.
Front. Oncol. 15:1632133.
doi: 10.3389/fonc.2025.1632133

Etoposide and cisplatin in combination with anlotinib for lung NUT carcinoma: a case report

Yuxing Sun[1], Jiangyu Bian[1], Linfeng Wang[2] and Tong Zhang[1]*

[1]Department of Oncology, Xiyuan Hospital of China Academy of Chinese Medical Sciences, Beijing, China, [2]China Three Gorges University, Yichang, Hubei, China

Lung NUT carcinoma is a rare malignant tumor, which is highly aggressive, poorly differentiated, and difficult to recognize at an early stage, and is associated with very rare reports and extremely poor prognosis, with some reports showing a mOS of only 2.2 months. In this paper, we report the treatment of a rare case of primary lung NUT cancer. After surgery, chemotherapy and targeted therapy, the patient's progression-free survival is now more than 4 months, which provides a feasible treatment option for lung NUT cancer.

KEYWORDS

lung NUT carcinoma, NUT midline carcinoma, chemotherapy, anlotinib, targeted therapy, case report

1 Introduction

Pulmonary NUT carcinoma belongs to a type of Nuclear protein of the testis carcinoma (NC).NC also known as NUT midline carcinoma (NMC), is a rare and highly aggressive malignant tumor that can occur anywhere in the body but most tumors are located in the midline anatomy or mediastinum and are characterized by chromosomal rearrangements (1). Due to its rarity, no studies have been conducted to clarify the specific incidence values and the pattern of disease incidence distribution, and only partial evidence-based evidence suggests that the onset of the disease involves patients of all age groups and is more common in younger patients (2–4). Cases of pulmonary NUT carcinoma are reported to be rare and have a poor prognosis, with a median overall survival (OS) of only 2.2 months in a real-world retrospective study (5). In this paper, we report a case of pulmonary NUT carcinoma with a long survival after comprehensive treatment including surgery and chemotherapy combined with antivascular targeted therapy, which provides a reference for the clinical management of pulmonary NUT carcinoma.

2 Case presentation

A 54-year-old male presented to the local hospital in September 2024 with a cough. No family history of genetic predisposition. Chest CT (Figure 1) showed a right lower lobe occupancy of about 47*41 mm with multiple tiny nodules in both lungs. PET/CT showed a

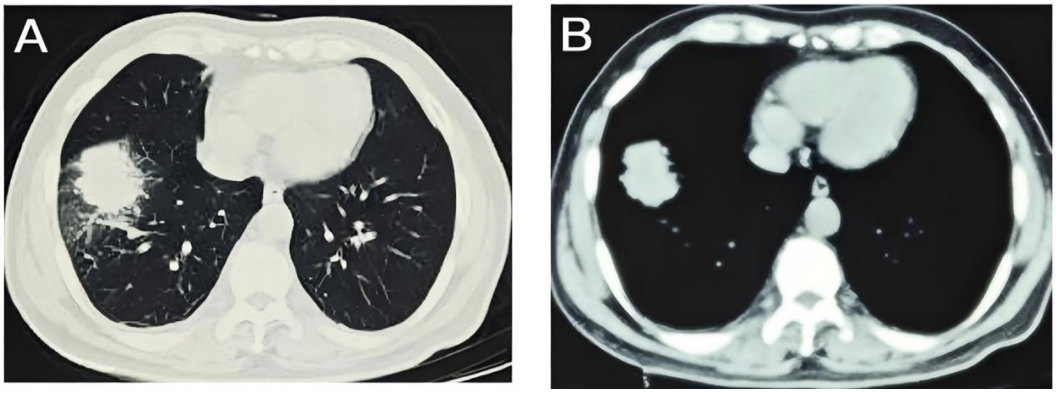

FIGURE 1
Baseline imaging characteristics: CT imaging on September 18, 2024, established the initial diagnosis of pulmonary NUT carcinoma; **(A)** lung window; **(B)** mediastinal window.

right lower lobe hypermetabolic occupancy of about 47*41 mm with SUVmax: 11.1 and right hilar hypermetabolic lymph node with SUVmax: 8.3.The patient underwent video-assisted thoracic surgery for partial lower lobectomy of the right lung along with excision of a diaphragmatic mass at Dezhou Hospital of Shandong University Qilu Hospital on September 27, 2024.Postoperative pathology: NUT carcinoma (right lung lower lobe mass). Immunohistochemistry: NUT (1+), P40 (2+), INSM1 (-), CK5/6 foci (+), CgA (-), Syn (-), CD56 (-), ALK (-), HER2 (0), Ki67 (70%+). Genetic testing (PAN116) showed no driver mutations and Microsatellite Stability (MSS). Lung NUT carcinoma was considered in combination with immunohistochemistry. No postoperative treatment was performed and chest CT was repeated in November 2024 and Progressive Disease (PD) was evaluated according to Response Evaluation Criteria in Solid Tumors 1.1 (RECIST 1.1) efficacy. Genetic testing was performed to see APC, ATM, BRCA1, BRCA2, CSFIR, GNA11, KIT, MLH1, EGFR, and ROS1 mutations, TMB 2mut/Mb, and MSS. One cycle of treatment was performed in December 2024 at outside hospital, with the following specific regimen: anlotinib (8mg qd), afatinib (30mg qd), and olaparib (150mg bid). Review CT in January 2025 suggested (Figure 2) postoperative changes in the lower lobe of the right lung, peripheral strips of soft-tissue shadows, which increased in size compared with the range of 2024-11, fullness of the right lung hilar, no significant changes were seen, thickening and adhesion of the right pleura, and a small amount of effusion in the right thoracic cavity. Efficacy evaluation of PD. Four cycles of etoposide (1.8g d1-3), cisplatin (60mg d1-2), and anlotinib (8mg po d1-14,q21d) were performed on 2025-1-16, 2-6, 2-26, and 3-18.A repeat CT (Figure 3) on 2025-4–7 suggested postoperative changes in the right lower lobe of the lungs, with striated solid changes in the operative area, and a slightly enlarged lymph node in the right hilar region, with a large one 8mm in short diameter. Right pleural thickening and adhesion, right pleural cavity little effusion roughly the same as before, compare 2025-3–18 did not see obvious changes. The current tumor measures 18.28*11.62 mm, with a 25% reduction in the sum of the longest diameters of target lesions compared to the January 15, 2025 baseline without new lesions, meeting the criteria for partial response (PR) according to RECIST 1.1. At present, the patient is still in the second-line chemotherapy combined with targeted therapy, the current PFS has been more than 3 months,

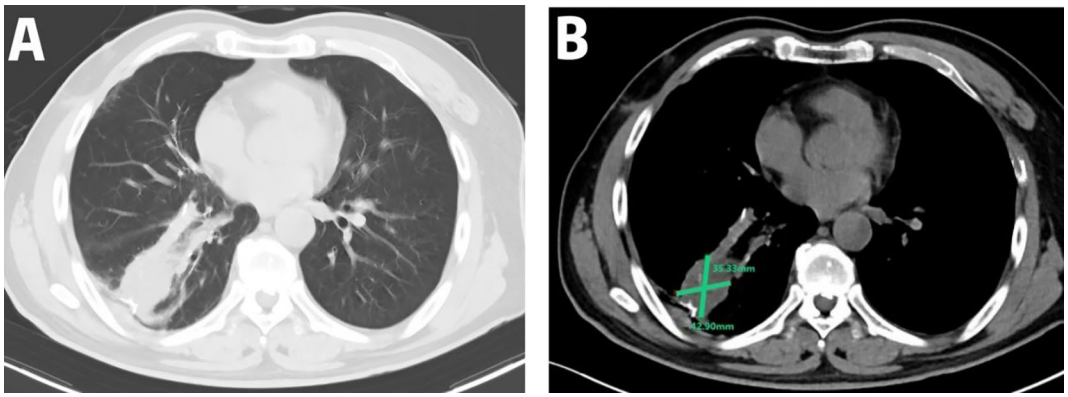

FIGURE 2
Disease progression on targeted therapy: CT imaging on January 15, 2025, demonstrated a peripheral soft tissue opacity in the right lower lobe (42.90 × 35.33 mm) showing interval enlargement compared to pre-treatment baseline; **(A)** lung window; **(B)** mediastinal window.

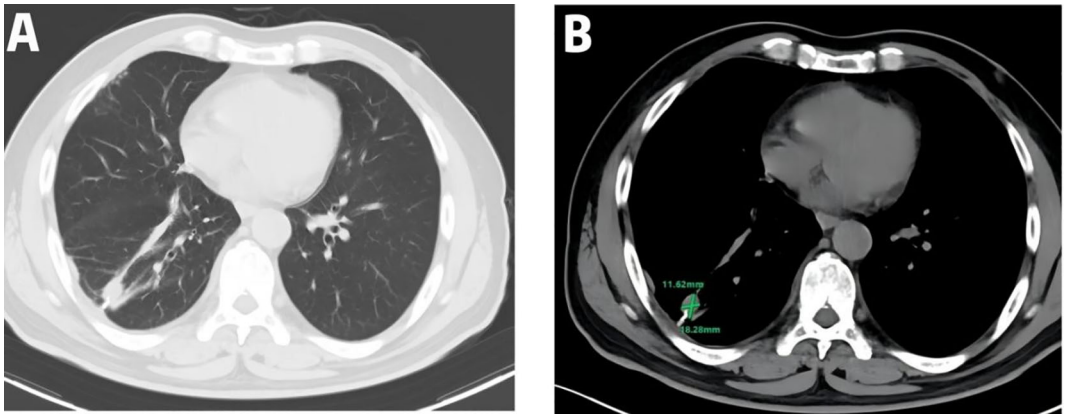

FIGURE 3
Therapeutic response to EP plus anlotinib: Post-treatment CT on April 7, 2025 (after 4 cycles) showed a 25% reduction in the target lesion (18.28 × 11.62 mm) compared to the January 15, 2025 assessment with no new metastatic lesions observed; **(A)** lung window; **(B)** mediastinal window.

the patient's treatment was well tolerated, and the symptoms of cough and fatigue were once significantly improved compared with the pre-treatment period. The patient's treatment history is shown in Table 1.

3 Discussion

Diagnosing NUT midline carcinoma (NMC) poses significant challenges due to non-specific clinical manifestations and histopathological features lacking pathognomonic morphology. Current diagnostic approaches rely on immunohistochemical (IHC) staining demonstrating nuclear NUT overexpression or molecular confirmation of NUTM1 rearrangement through fluorescence *in situ* hybridization, next-generation sequencing, or reverse transcription polymerase chain reaction (6). In this case, the diagnosis of primary pulmonary NUT carcinoma was established based on poorly differentiated carcinoma identified via core needle biopsy, combined with NUT overexpression on IHC, and further supported by clinical presentation and imaging findings.

Pulmonary NUT carcinoma exhibits non-specific clinical manifestations unrelated to smoking, with cough being the most frequent symptom (7). The poorly differentiated or undifferentiated nature of the tumor complicates histomorphological identification and necessitates broad differential diagnoses. Focal squamous differentiation is frequently observed in pulmonary NUT carcinoma histology, where immunomarkers P63 and P40 may show positivity—features overlapping with pulmonary squamous cell carcinoma (SCC). Consequently, primary pulmonary NUT carcinoma was historically classified as an SCC subtype (8) but was reclassified under 'other epithelial tumors' in the 2015 and 2021 WHO classifications of thoracic tumors.

For thoracic NUT carcinoma, CT imaging delineates primary lesion size, location, lymph node involvement, and extent of local invasion. CT typically reveals a solitary lobulated mass without site predilection, characterized by large dimensions, relatively well-defined margins, and heterogeneous mild enhancement. Distant metastases to bone or lymph nodes are common (9, 10). In this case, initial CT demonstrated a 47×41 mm right lower lobe mass with bilateral pulmonary micronodules. PET/CT confirmed absence of distant metastasis.

The pathologic features, imaging manifestations, and standard treatment options for NUT cancers originating in the lung are currently unknown. Synchronized radiotherapy or sequential radiotherapy plays an important role, followed by surgery

TABLE 1 The patient's treatment history.

Timepoint	Intervention	PFS months	Assessment	Key outcomes
2024-09-27	Video-assisted thoracic surgery for partial lower lobectomy of the right lung along with excision of a diaphragmatic	3	Postoperative pathology and IHC	Pathologically confirmed NUT carcinoma
2024-12	Anlotinib (8 mg qd) Afatinib (30 mg qd) Olaparib (150 mg bid)	1	RECIST 1.1, PET/CT, CT	Target lesion: Metabolic hyperintensity 31*26*44mm, SUVmax6.9
2025-01-16	EP + Anlotinib (Cycle 1)	4+	RECIST 1.1, CT	Target lesions stable, no new metastases
2025-03-18	EP + Anlotinib (Cycle 4)		RECIST 1.1, CT	25% reduction in sum of longest diameters of target lesions vs. January 15, 2025 baseline; no new lesions; partial response (PR) per RECIST 1.1

combined with neoadjuvant therapy or adjuvant radiotherapy. Surgery alone or chemotherapy alone also prolongs patient survival to some extent. The clinical efficacy of immunotherapy is unknown, and it is mainly used as a backline treatment. Chemotherapy regimens usually use platinum-containing dual agents (mainly TP). Anthracyclines, cyclophosphamide, isocyclophosphamide and other chemotherapeutic agents are also used (11). The EP regimen was selected for this case based primarily on germ cell tumor (GCT)-like characteristics: Involvement of testis-specific protein genes suggests potential germ cell tumor origin, and EP serves as the chemotherapeutic backbone for GCTs (12). Additionally, strong co-expression of P40 and CK5/6 indicates squamous differentiation. Studies have demonstrated EP application in SCC carcinomas under specific clinical circumstances (13). A Ki-67 index of 70% reflects aggressive tumor biology. Etoposide preferentially targets rapidly proliferating cells by stabilizing topoisomerase II-DNA complexes during S/G2 phase, while high Ki-67 tumors exhibit heightened mitotic activity, potentially indicating increased susceptibility to etoposide (14).

Angiogenesis plays an important role in tumor growth, and recent studies have shown that blocking angiogenesis has become a successful alternative strategy in cancer treatment (15). Anlotinib is a novel oral multi-target tyrosine kinase inhibitor that targets receptors involved in tumor proliferation, angiogenesis, and microenvironment modulation. It potently inhibits vascular endothelial growth factor receptor 2/3, fibroblast growth factor receptor 1-4, platelet-derived growth factor receptor α/β, stem cell factor receptor, and rearranged during transfection (16). This multi-kinase blockade confers broad antitumor activity against angiogenesis and growth in diverse solid tumors through three core mechanisms:Anti-angiogenesis: Suppresses VEGF-mediated endothelial cell proliferation, migration, and tube formation, significantly reducing tumor microvessel density. Direct antiproliferative action: Inhibits FGFR-dependent signaling pathways, induces G1/S cell cycle arrest, and triggers caspase-3-dependent apoptosis. Microenvironment modulation: Blocks PDGFR-β phosphorylation and downstream ERK signaling, inhibiting cancer-associated fibroblast activation and reducing interstitial fluid pressure (16). Anlotinib is currently approved as a third-line treatment for refractory advanced NSCLC, and recent studies have demonstrated that anrotinib increases the sensitivity of pneumoblastoma to *in vivo* chemotherapy (17). Therefore, we hypothesized that anlotinib may play an active role in overcoming chemotherapy resistance, and from imaging observations, chemotherapy combined with anlotinib as a second-line treatment for patients achieved PR, but the efficacy of this regimen remains to be further validated due to insufficient sample size.

4 Conclusion

Our first use of EP in combination with anlotinib significantly prolonged progression-free survival and significantly improved clinical symptoms in patients with lung NUT cancer, providing a therapeutic option for the treatment of lung NUT cancer.

Data availability statement

The original contributions presented in the study are included in the article/supplementary material. Further inquiries can be directed to the corresponding author.

Ethics statement

Written informed consent was obtained from the individual(s) for the publication of any potentially identifiable images or data included in this article.

Author contributions

YS: Conceptualization, Writing – original draft, Writing – review & editing. TZ: Conceptualization, Writing – review & editing. JB: Writing – review & editing. LW: Writing – review & editing.

Funding

The author(s) declare that no financial support was received for the research and/or publication of this article.

Conflict of interest

The authors declare that the research was conducted in the absence of any commercial or financial relationships that could be construed as a potential conflict of interest.

Generative AI statement

The author(s) declare that no Generative AI was used in the creation of this manuscript.

Any alternative text (alt text) provided alongside figures in this article has been generated by Frontiers with the support of artificial intelligence and reasonable efforts have been made to ensure accuracy, including review by the authors wherever possible. If you identify any issues, please contact us.

Publisher's note

References

1. Chau NG, Hurwitz S, Mitchell CM, Aserlind A, Grunfeld N, Kaplan L, et al. A. Intensive treatment and survival outcomes in NUT midline carcinoma of the head and neck. *Cancer*. (2016) 122:3632–40. doi: 10.1002/cncr.30242

2. French CA, Ramirez CL, Kolmakova J, Hickman TT, Cameron MJ, Thyne ME, et al. BRD-NUT oncoproteins: a family of closely related nuclear proteins that block epithelial differentiation and maintain the growth of carcinoma cells. *Oncogene*. (2008) 27:2237–42. doi: 10.1038/sj.onc.1210852

3. Stelow EB. A review of NUT midline carcinoma. *Head Neck Pathol*. (2011) 5:31–5. doi: 10.1007/s12105-010-0235-x

4. Bellizzi AM, Bruzzi C, French CA, Stelow EB. The cytologic features of NUT midline carcinoma. *Cancer*. (2009) 117:508–15. doi: 10.1002/cncy.20044

5. Sholl LM, Nishino M, Pokharel S, Mino-Kenudson M, French CA, Janne PA, et al. Primary pulmonary NUT midline carcinoma: clinical, radiographic, and pathologic characterizations. *J Thorac Oncol*. (2015) 10:951–9. doi: 10.1097/JTO.0000000000000545

6. Chau NG, Ma C, Danga K, Al-Sayegh H, Nardi V, Barrette R, et al. An anatomical site and genetic-based prognostic model for patients with nuclear protein in testis (NUT) midline carcinoma: analysis of 124 patients. *JNCI Cancer Spectr*. (2019) 4: pkz094. doi: 10.1093/jncics/pkz094

7. Chen J, Li M, Lu H. Nuclear protein in testis carcinoma of the lung. *Transl Oncol*. (2023) 30:101640. doi: 10.1016/j.tranon.2023.101640

8. Bauer DE, Mitchell CM, Strait KM, Lathan CS, Stelow EB, Lüer SC, et al. Clinicopathologic features and long-term outcomes of NUT midline carcinoma. *Clin Cancer Res*. (2012) 18:5773–9. doi: 10.1158/1078-0432.CCR-12-1153

9. 李 飞. 崔光彬.肺NUT癌的临床特征及CT影像学分析. 中国*CT*和*MRI*杂志. (2024) 22:55–8. doi: 10.3969/j.issn.1672-5131.2024.10.018

10. Chang AI, Kim TS, Han J, Kim TJ, Choi JY. NUT midline carcinoma of the lung: computed tomography findings in 10 patients. *J Comput Assist Tomogr*. (2021) 45:330–6. doi: 10.1097/RCT.0000000000001133

11. Yuan J, Xu Z, Guo Y. Diagnosis, treatment and prognosis of primary pulmonary NUT carcinoma: A literature review. *Curr Oncol*. (2022) 29:6807–15. doi: 10.3390/curroncol29100536

12. Hu Z, Yu J, Gui G, Chen Y, Huang R, Jiang L, et al. Cisplatin for testicular germ cell tumors: a rapid review. *J Evid Based Med*. (2016) 9:144–51. doi: 10.1111/jebm.12210

13. Ardizzoni A, Antonelli G, Grossi F, Tixi L, Cafferata M, Rosso R. The combination of etoposide and cisplatin in non-small-cell lung cancer (NSCLC). *Ann Oncol*. (1999) 10 Suppl 5:S13–7. doi: 10.1093/annonc/10.suppl_5.s13

14. Mollaei M, Hassan ZM, Khorshidi F, Langroudi L. Chemotherapeutic drugs: Cell death- and resistance-related signaling pathways. Are they really as smart as the tumor cells? *Transl Oncol*. (2021) 14:101056. doi: 10.1016/j.tranon.2021.101056

15. Haefliger S, Tzankov A, Frank S, Bihl M, Vallejo A, Stebler J, et al. NUT midline carcinomas and their differentials by a single molecular profiling method: a new promising diagnostic strategy illustrated by a case report. *Virchows Arch*. (2021) 478:1007–12. doi: 10.1007/s00428-020-02869-7

16. Shen G, Zheng F, Ren D, Du F, Dong Q, Wang Z, et al. Anlotinib: a novel multi-targeting tyrosine kinase inhibitor in clinical development. *J Hematol Oncol*. (2018) 11 (1):120. doi: 10.1186/s13045-018-0664-7

17. Luo Z, Cao C, Xu N, Ying K. Classic biphasic pulmonary blastoma: a case report and review of the literature. *J Int Med Res*. (2020) 48(10):300060520962394. doi: 10.1177/0300060520962394

frontiers | Frontiers in Oncology

TYPE Case Report
PUBLISHED 20 October 2025
DOI 10.3389/fonc.2025.1590497

OPEN ACCESS

EDITED BY
Giovanna Damia,
Mario Negri Institute for Pharmacological Research (IRCCS), Italy

REVIEWED BY
Jelena Milasin,
University of Belgrade, Serbia
Satoshi Kano,
Hokkaido University, Japan

*CORRESPONDENCE
Jiyuan Ding
jiyuanding@163.com

RECEIVED 09 March 2025
ACCEPTED 07 October 2025
PUBLISHED 20 October 2025

CITATION
Zhang L, Xu X, Gao L and Ding J (2025) HER2 inhibitor-based combination therapy for recurrent and metastatic salivary duct carcinoma in an elderly patient: a case report and literature review.
Front. Oncol. 15:1590497.
doi: 10.3389/fonc.2025.1590497

HER2 inhibitor-based combination therapy for recurrent and metastatic salivary duct carcinoma in an elderly patient: a case report and literature review

Luxin Zhang[1], Xiaofeng Xu[2], Liujie Gao[2] and Jiyuan Ding[2]*

[1]Second Clinical Medical College, Zhejiang Chinese Medical University, Hangzhou, Zhejiang, China, [2]Department of Oncology and Hematology, Hangzhou Red Cross Hospital, Hangzhou, Zhejiang, China

Salivary duct carcinoma (SDC) is a rare and highly aggressive malignancy with limited treatment options, particularly in elderly patients. HER2 overexpression has emerged as a potential therapeutic target in this disease. This study reports the case of an 86-year-old male with HER2-positive submandibular gland SDC who underwent surgical resection on June 19, 2020. Six months postoperatively, follow-up revealed lymph node metastasis and local recurrence at the left submandibular region. Ultrasound-guided radiofrequency ablation was performed, but local recurrence persisted. The patient subsequently received trastuzumab combined with low-dose nab-paclitaxel, achieving a partial response according to RECIST 1.1 criteria. Maintenance therapy with trastuzumab monotherapy was then initiated, resulting in disease stability for over 20 months. In October 2023, the disease progressed to the left sublingual region. After targeted monotherapy and local radiotherapy by April the following year, disease control was achieved. At the most recent follow-up, the patient remains in stable condition. This case highlights the efficacy and safety of HER2-targeted combination therapy in elderly SDC patients, offering valuable insights into biomarker-driven personalized treatment strategies for this population.

KEYWORDS

HER2, salivary duct carcinoma, submandibular gland, elderly patients, case report

1 Introduction

Salivary duct carcinoma (SDC) is one of the most aggressive subtypes of salivary gland carcinomas (SGCs), a rare group of malignancies accounting for less than 5% of all head and neck neoplasms (1). Clinically, SDC most frequently arises in the parotid gland, followed by the submandibular gland and minor salivary glands. It typically presents as a by rapidly enlarging neck masses, often accompanied by facial nerve paralysis and cervical lymph node metastasis. Owing to its highly invasive nature and propensity for early metastasis, SDC generally carries a poor prognosis, with a 5-year disease-specific survival rate of only 40-60%. Furthermore, the majority of cases are diagnosed at advanced stages, which further compromises treatment outcomes (2).

SDC has an aggressive clinical course and poor prognosis, making therapeutic strategies challenging, especially in elderly patients with reduced tolerance to conventional treatments. Molecular targeted therapies, particularly HER2 inhibitors, have emerged as a promising approach. However, evidence for their use in elderly populations remains limited (3). This study presents a case report of an 86-year-old man with HER2-positive submandibular gland SDC who underwent HER2 inhibitor-based combination therapy following postoperative recurrence. Follow-up evaluations revealed sustained disease stability over four years with treatment-related toxicity remaining within manageable limits. This case highlights the efficacy and safety of HER2-targeted combination therapy in elderly SDC patients, offering valuable insights into biomarker-driven personalized treatment strategies for this population.

2 Case report

An 86-year-old man patient was admitted to our hospital on June 17, 2020, presenting with a ten-year history of a left submandibular mass and newly developed left-sided lingual numbness and paresthesia persisting for one week. The patient had been previously asymptomatic and had not sought medical attention for the mass until the recent onset of symptoms. On physical examination a firm, approximately 3.5 cm mass was palpated in the left submandibular region, exhibiting fixation to the overlying skin and restricted mobility. The tongue was midline at rest with preserved mobility.

Initial diagnostic imaging included magnetic resonance imaging (MRI) of the head and neck, which identified a 1.5×1.3×1.1 cm calcified lesion within the left submandibular gland (Figure 1). Subsequent contrast-enhanced ultrasonography revealed a heterogeneous hypoechoic nodule with prominent internal vascularity in the left submandibular gland. Fine-needle aspiration biopsy (FNAB) confirmed the presence of infiltrating atypical glandular tissue, suggestive of submandibular gland malignancy.

The patient underwent left submandibular gland excision on June 19, 2020, for definitive diagnosis. Histopathological examination confirmed ductal carcinoma (pT2NxM0) with perineural and vascular invasion. Immunohistochemical analysis demonstrated positive staining for CK7, AR, and HER2 (3+) (Figure 2), with strong p53 expression (+++) and a Ki-67 proliferation index of 35%. Negative markers included CK5/6, GCDFP-15, SMA, p40, p63, CD117, and Calponin (Table 1). The patient was followed up regularly without any adjuvant therapy.

By April 2021, the patient developed progressive lingual sensory disturbance, dysarthria, and leftward tongue deviation. Cervical ultrasonography revealed lymph node metastasis and local recurrence at the left submandibular region, confirmed by biopsy. The recurrent lesion was then treated with ultrasound-guided radiofrequency ablation.

In October 2021, the patient experienced progressive worsening of symptoms and was subsequently transferred to our department for further management. Contrast-enhanced CT of the tongue demonstrated an irregular soft tissue density lesion (2.1×5.0 cm) in the left submandibular region with heterogeneous enhancement (Figure 3). Biopsy confirmed poorly differentiated invasive carcinoma with immunohistochemical profile consistent with the primary lesion (Table 1), confirming SDC origin.

Based on HER2 overexpression, advanced age, and poor performance status, the patient started trastuzumab (loading dose 8 mg/kg, maintenance dose 6 mg/kg q3w) combined with nab-paclitaxel (80 mg/m^2 on days 1 and 8, q3w) in November 2021. After four cycles, contrast-enhanced CT scan of the tongue showed a partial response (PR), with a reduction in the size of the submandibular lesion. Two additional cycles were administered as consolidation therapy, achieving radiological stability. Maintenance therapy with trastuzumab (6 mg/kg q3w) began in April 2022, with imaging follow-up scheduled every 12 weeks (every 4 treatment cycles). However, due to poor patient compliance, only four cycles were intermittently completed between April 2022 and June 2023.Imaging evaluations during this period confirmed stable disease (SD) according to RECIST 1.1 criteria (Figure 3).

In October 2023, follow-up contrast-enhanced MRI of the head and neck revealed a lesion in the left sublingual region. Combined with clinical findings, this was assessed as disease progression according to RECIST 1.1 criteria. Targeted monotherapy was recommended but the patient did not adhere to the treatment regimen.

By March 2024, enhanced MRI of the mandible showed enlargement of the left sublingual mass (maximum diameter 4.1 cm) accompanied by progressive worsening of symptoms. Following comprehensive assessment, radiotherapy to the submandibular region was initiated on 9th April 2024 (total dose 60 Gy/30 fractions, 2 Gy/fraction), resulting in symptom relief. The patient remained in stable condition at the most recent follow-up in January 2025.

3 Discussion

SDC is a rare, highly aggressive malignancy characterized by high rates of local recurrence, poor prognosis, and significant mortality (4).Standard treatment involves complete surgical

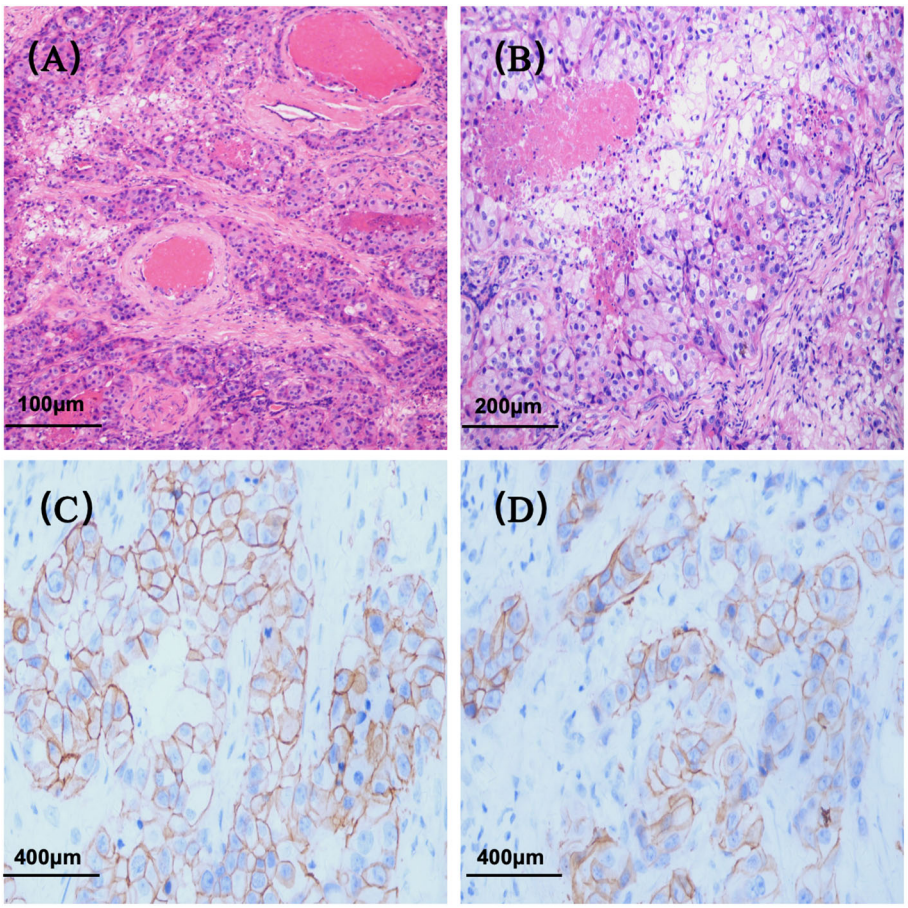

FIGURE 1
Histopathological features of salivary duct carcinoma. **(A)** Hematoxylin and eosin (H&E) staining (original magnification ×100); **(B)** H&E staining (original magnification ×200); **(C)** Immunohistochemical staining for HER2 (original magnification ×400); **(D)** HER2 immunohistochemistry (original magnification ×400).

resection followed by postoperative radiotherapy (5). For inoperable, recurrent, or metastatic disease, chemotherapy is the mainstay, though no standardized regimen exists. Given the limitations of single-modality treatments, a multimodal approach is often optimal.

In recent years, molecular profiling has gained increasing importance in SDC, and HER2-targeted therapy has attracted growing interest. Several international guidelines now recommend HER2 status assessment in the diagnostic workup of recurrent or metastatic SDC (6). This approach is supported by the notable morphological and molecular similarities between SDC and high-grade breast ductal carcinoma. Trastuzumab, a humanized monoclonal antibody targeting the extracellular domain of HER2, inhibits downstream signaling and suppresses proliferation of HER2-overexpressing tumor cells (7). Its efficacy, well-established in breast cancer through large-scale randomized trials, provides a rationale for its application in SDC.

Building on the success in breast cancer therapy and supported by clinical evidence in SDC, several phase II trials have evaluated the efficacy of trastuzumab-based targeted therapy combined with

TABLE 1 Immunohistochemical Staining Control.

Immunohistochemical staining	Jun-20	Oct-21
Positive marker		
CK7	(+)	
AR	(+)	(+)
HER2	(3+)	(3+)
p53	(+++)	
Ki-67	35%	
GCDFP-15	(-)	(+)
CAM5.2		(+)
MSH2		(+)
MSH6		(+)
PMS2		(+)
MLH1		(+)

(Continued)

TABLE 1 Continued

Immunohistochemical staining	Jun-20	Oct-21
Negative Marker		
CK5/6	(-)	
SMA	(-)	
p40	(-)	(-)
p63	(-)	(-)
CD117	(-)	
Calponin	(-)	
PSA		(-)
TTF-1		(-)
NapsinA		(-)
CK20		(-)
CDX2		(-)
PD-1		(-)
ER		(-)

Blank spaces indicate items not assessed in the current examination.

chemotherapy in SDC, demonstrating promising outcomes with objective response rates (ORR) ranging from 58% to 70% and median progression-free survival (MPFS) ranging from 6.9 to 11.7 months (8–11). Notably, this approach has shown promising clinical efficacy even in patients with recurrent or metastatic disease, For example, a recent phase II clinical trial conducted by Lee et al. reported a 70% ORR for trastuzumab combined with taxane therapy in metastatic SDC, which is consistent with the partial response observed in our case. Notably, while the combination of trastuzumab and docetaxel has become a recommended regimen for salivary duct carcinoma (SDC), it is associated with a high incidence (approximately 50%) of grade ≥3 treatment-related adverse events (12). Data in frail elderly patients are scarce. Our use of low-dose nab-paclitaxel aimed to optimize tolerability.

This trastuzumab-based, low-dose nab-paclitaxel regimen represents a deviation from standard therapy, aiming to balance efficacy and safety. In our case, the clinical outcome was consistent with previous studies. Despite suboptimal treatment compliance during the maintenance phase due to the patient's frail condition, local disease control was sustained for over 20 months. This suggests that a HER2-targeted, low-intensity chemotherapy combination can yield durable efficacy even in elderly, vulnerable patients, though its definitive value requires confirmation in prospective studies. Therefore, comprehensive molecular testing is recommended for this population.

The optimal duration of HER2 inhibitor maintenance therapy remains undefined. In numerous cases of SDC treatment, the duration of targeted maintenance therapy varies significantly, with some patients achieving favorable outcomes after only one year of trastuzumab maintenance therapy (13, 14). In our case, disease progression occurred after one year of maintenance therapy, which may be related to irregular treatment adherence. The outcome appears slightly inferior compared to other reported cases, suggesting that maintenance therapy should be stratified according to disease stage. However, specific protocols require further investigation through larger sample sizes. Ultimately, treatment decisions should be based on comprehensive assessment of patient status and treatment goals, incorporating the best available evidence.

Adjuvant radiotherapy has demonstrated significant efficacy in the management of head and neck cancers. Current evidence suggests substantial clinical benefits of postoperative radiotherapy in SDC patients, particularly those with high-risk features such as extracapsular extension and/or positive margins. This approach has been shown to improve overall survival and enhance locoregional control. And there are Studies have consistently identified the omission of postoperative radiotherapy as a significant risk factor for disease recurrence (15).

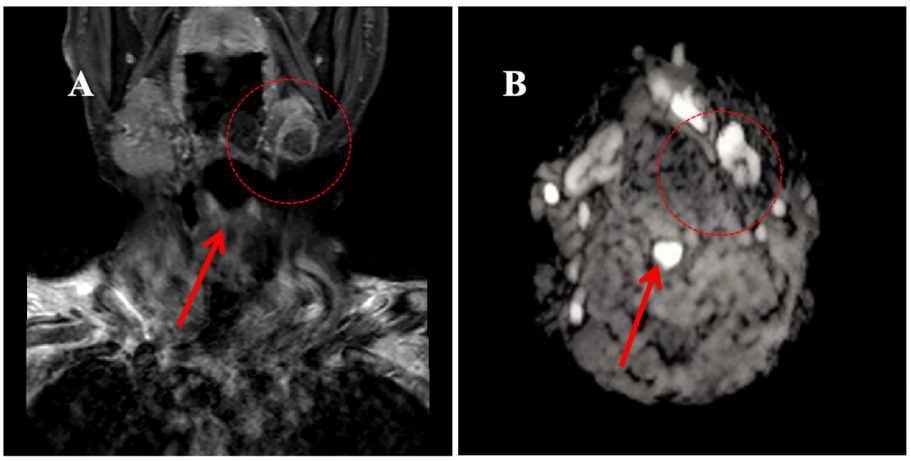

FIGURE 2
Magnetic Resonance Imaging (MRI) of the neck region in June 2020. **(A)** T1-weighted image showing a hypointense lesion in the left submandibular gland (approximately 1.5×1.3×1.1 cm); **(B)** Diffusion-weighted image demonstrating a hyperintense signal in the left submandibular gland.

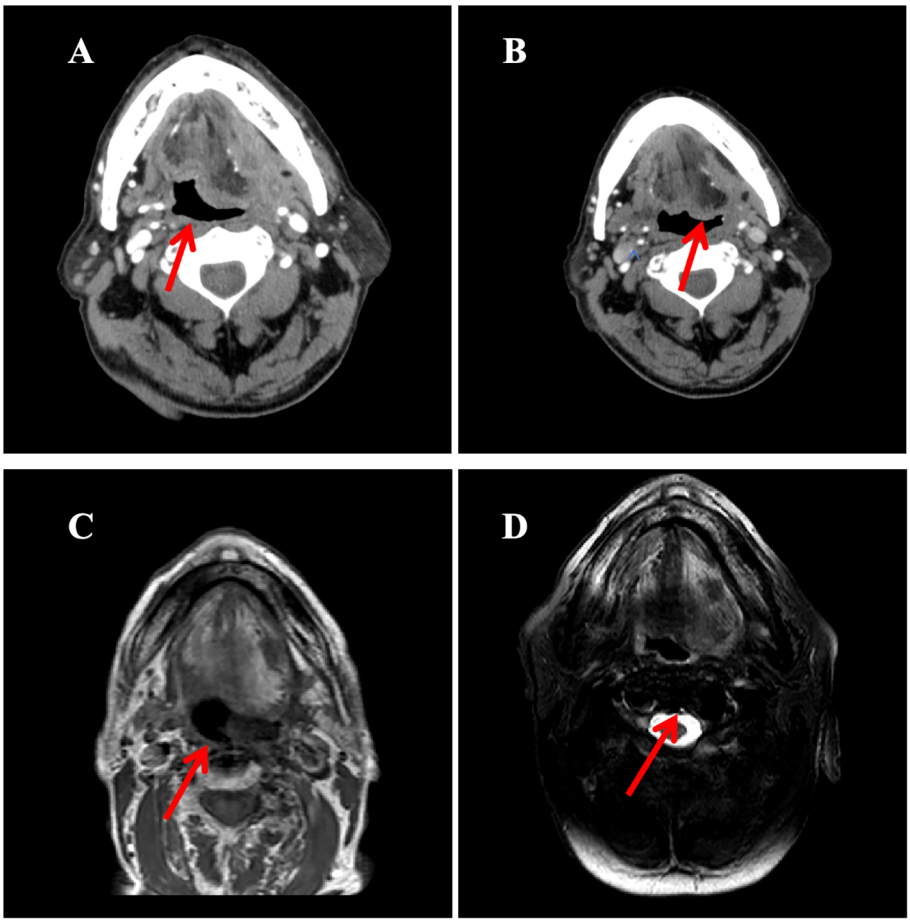

FIGURE 3
The imaging evolution of a left submandibular mass in a patient during the treatment period from November 2021 to October 2023. **(A)** Contrast-enhanced neck CT (October 2021): Demonstrates an enhancing mass in the left submandibular region (maximum diameter: 5.0 cm); **(B)** Contrast-enhanced neck CT (February 2022, After 4 cycles of treatment): Shows significant reduction in the size of the mass compared to A (maximum diameter: 3.2 cm); **(C)** Contrast-enhanced MRI of the submandibular gland (axial T1-weighted image; March 2023): Reveals a mass in the sublingual region (maximum diameter: 1.7 cm); **(D)** MRI of the submandibular gland (axial T1-weighted image; June 2023): The mass measures 1.8 cm in maximum diameter, indicating size stability compared to C.

Unfortunately, the patient did not receive standard postoperative radiotherapy initially, due to comorbid conditions and patient preference. Subsequently, the patient developed lymph node metastasis within six months after surgery, suggesting that the omission of adjuvant radiotherapy may have compromised disease control.

It is worth noting that radiotherapy may still play an important role within multimodal therapy even in recurrent or metastatic settings. For example, Rencui Qua et al. reported a case of SDC with postoperative lymph node metastasis treated with trastuzumab, chemotherapy, and concurrent regional radiotherapy, achieving a complete response lasting five years (16). Had our patient received concurrent radiotherapy during HER2-targeted treatment—if medically feasible—it might have provided additional benefit, potentially improving disease control and prognosis.

Other therapeutic avenues for recurrent/metastatic SDC include androgen deprivation therapy (ADT) and immunotherapy (17, 18). Approximately 70% of SDCs express androgen receptor (AR), and ADT is gaining traction due to its favorable toxicity profile and efficacy (19). Although our patient was AR-positive, ADT was not initially considered due to limitations in clinical consensus and therapeutic depth at the time. Current evidence suggests that targeted therapy should take precedence, but combination with ADT may prolong survival (20). For selected patients, adjuvant ADT or ADT-based combination therapy may represent a promising strategy, further refining personalized treatment approaches.

In conclusion, SDC is a rare and highly aggressive malignancy with significant therapeutic challenges, particularly in elderly patients. Identifying unique biomarkers, such as HER2, and implementing personalized treatment strategies are crucial. HER2 inhibitor-based combination therapy has shown efficacy and manageable toxicity in elderly SDC patients with local recurrence and metastasis. However, further clinical studies are needed to refine and optimize treatment protocols.

Data availability statement

The raw data supporting the conclusions of this article will be made available by the authors, without undue reservation.

Ethics statement

Written informed consent was obtained from the individual(s) for the publication of any potentially identifiable images or data included in this article. Written informed consent was obtained from the participant/patient(s) for the publication of this case report.

Author contributions

LZ: Writing – original draft, Writing – review & editing, Methodology. XX: Data curation, Methodology, Writing – review & editing. LG: Data curation, Writing – review & editing, Methodology, Resources. JD: Writing – review & editing, Supervision.

Funding

The author(s) declare financial support was received for the research and/or publication of this article. This work was supported by the Zhejiang Provincial Traditional Chinese Medicine Science and Technology Project (Grant number 2022ZA140).

Conflict of interest

The authors declare that the research was conducted in the absence of any commercial or financial relationships that could be construed as a potential conflict of interest.

Generative AI statement

The author(s) declare that no Generative AI was used in the creation of this manuscript.

Any alternative text (alt text) provided alongside figures in this article has been generated by Frontiers with the support of artificial intelligence and reasonable efforts have been made to ensure accuracy, including review by the authors wherever possible. If you identify any issues, please contact us.

Publisher's note

All claims expressed in this article are solely those of the authors and do not necessarily represent those of their affiliated organizations, or those of the publisher, the editors and the reviewers. Any product that may be evaluated in this article, or claim that may be made by its manufacturer, is not guaranteed or endorsed by the publisher.

References

1. Kleinsasser O, Klein HJ, Hübner G. Salivary duct carcinoma. A group of salivary gland tumors analogous to mammary duct carcinoma. *Arch Klin Exp Ohren Nasen Kehlkopfheilkd.* (1968) 192:100–5. Speichelgangearcinome. Ein den Milchgangcarcinomen der Brustdrüse analoge Gruppe von Speichldrüsentumoren. ger. doi: 10.1007/BF00301495

2. Schmitt NC, Kang H, Sharma A. Salivary duct carcinoma: An aggressive salivary gland Malignancy with opportunities for targeted therapy. *Oral Oncol.* (2017) 74:40–8. doi: 10.1016/j.oraloncology.2017.09.008

3. Nakaguro M, Tada Y, Faquin WC, Sadow PM, Wirth LJ, Nagao T. Salivary duct carcinoma: Updates in histology, cytology, molecular biology, and treatment. *Cancer Cytopathol.* (2020) 128:693–703. doi: 10.1002/cncy.22288

4. Stodulski D, Mikaszewski B, Majewska H, Kuczkowski J. Parotid salivary duct carcinoma: a single institution's 20-year experience. *Eur Arch Otorhinolaryngol.* (2019) 276:2031–8. doi: 10.1007/s00405-019-05454-0

5. Colevas AD, Cmelak AJ, Pfister DG, Spencer S, Adkins D, Birkeland AC, et al. NCCN guidelines® Insights: head and neck cancers, version 2.2025. *J Natl Compr Canc Netw.* (2025) 23:2–11. doi: 10.6004/jnccn.2025.0007

6. Prost D, Iseas S, Gatineau M, Adam J, Cavalieri S, Bergamini C, et al. Systemic treatments in recurrent or metastatic salivary gland cancer: a systematic review. *ESMO Open.* (2024) 9:103722. doi: 10.1016/j.esmoop.2024.103722

7. Raghav KPS, Moasser MM. Molecular pathways and mechanisms of HER2 in cancer therapy. *Clin Cancer Res.* (2023) 29:2351–61. doi: 10.1158/1078-0432.Ccr-22-0283

8. Uijen MJM, Lassche G, van Engen-van Grunsven ACH, Driessen CML, van Herpen CML. Case series of docetaxel, trastuzumab, and pertuzumab (DTP) as first line anti-HER2 therapy and ado-trastuzumab emtansine (T-DM1) as second line for recurrent or metastatic HER2-positive salivary duct carcinoma. *Oral Oncol.* (2022) 125:105703. doi: 10.1016/j.oraloncology.2021.105703

9. Takahashi H, Tada Y, Saotome T, Akazawa K, Ojiri H, Fushimi C, et al. Phase II trial of trastuzumab and docetaxel in patients with human epidermal growth factor receptor 2-positive salivary duct carcinoma. *J Clin Oncol.* (2019) 37:125–34. doi: 10.1200/jco.18.00545

10. Hanna GJ, Bae JE, Lorch JH, Haddad RI, Jo VY, Schoenfeld JD, et al. The benefits of adjuvant trastuzumab for HER-2-positive salivary gland cancers. *Oncologist.* (2020) 25:598–608. doi: 10.1634/theoncologist.2019-0841

11. Lee J, Park S, Jung HA, Lee SH, Seo S, Kim SB, et al. A phase 2 multicenter study of docetaxel-PM and trastuzumab-pkrb combination therapy in recurrent or metastatic salivary gland carcinomas. *Cancer.* (2023) 129:2966–74. doi: 10.1002/cncr.34892

12. Kano S, Kiyota N, Kinoshita I, Tada Y, Ijichi K, Yamazaki T, et al. Multicenter phase II trial of trastuzumab and docetaxel for HER2-positive salivary gland cancer. *Jpn J Clin Oncol.* (2025) 55(10):1131–1140. doi: 10.1093/jjco/hyaf106

13. Iqbal MS, Shaikh G, Chatterjee S, Cocks H, Kovarik J. Maintenance therapy with trastuzumab in her2 positive metastatic parotid ductal adenocarcinoma. *Case Rep Oncol Med.* (2014) 2014:162534. doi: 10.1155/2014/162534

14. Çolak R, Kapar C, Yilmaz M. Complete response with trastuzumab in heavily pretreated HER2-positive metastatic salivary duct carcinoma. *Anticancer Drugs.* (2025) 36:675–7. doi: 10.1097/cad.0000000000001733

15. Haderlein M, Scherl C, Semrau S, Lettmaier S, Hecht M, Erber R, et al. Impact of postoperative radiotherapy and HER2/new overexpression in salivary duct carcinoma: A monocentric clinicopathologic analysis. *Strahlenther Onkol.* (2017) 193:961–70. doi: 10.1007/s00066-017-1196-8

16. Wu S, Quan R, Han L. Trastuzumab-based therapy is effective for salivary duct carcinoma: Case report and review of the literature. *Oral Oncol.* (2019) 91:121–2. doi: 10.1016/j.oraloncology.2019.02.015

17. Bugia L, Jungbauer F, Zaubitzer L, Hörner C, Merx K, Yasser AM, et al. Nivolumab as a promising treatment option for metastatic salivary duct carcinoma. *J Immunother.* (2024) 47:258–62. doi: 10.1097/cji.0000000000000513

18. Poxleitner P, Shoumariyeh K, Steybe D, Hupfer V, Voss PJ, Rawluk J, et al. Combined androgen deprivation therapy in recurrent androgen-receptor-positive salivary duct carcinoma - a case report and review of the literature. *J Stomatol Oral Maxillofac Surg.* (2020) 121:599–603. doi: 10.1016/j.jormas.2019.12.012

19. Matiku S, Murenzi G, Rugengamanzi E, Liwa E, Shaban I, Orgenes A, et al. Androgen receptor overexpression by immunohistochemistry in Malignant salivary gland tumors in Tanzania. *BMC Cancer*. (2025) 25:29. doi: 10.1186/s12885-024-13368-2

20. Kanno M, Kano S, Imamura Y, Kawakita D, Narita N, Tada Y, et al. Palliative systemic therapy for locally advanced or metastatic salivary duct carcinoma: A comprehensive review. *Cancer Treat Rev*. (2025) 139:102993. doi: 10.1016/j.ctrv.2025.102993

frontiers | Frontiers in Oncology

TYPE Case Report
PUBLISHED 22 October 2025
DOI 10.3389/fonc.2025.1587752

OPEN ACCESS

EDITED BY
Giovanna Damia,
Mario Negri Institute for Pharmacological Research (IRCCS), Italy

REVIEWED BY
Omkar Ijare,
Houston Methodist Research Institute, United States
Young Zoon Kim,
Sungkyunkwan University, Republic of Korea

*CORRESPONDENCE
John Villano
jlvillano@uky.edu

RECEIVED 04 March 2025
ACCEPTED 04 August 2025
PUBLISHED 22 October 2025

CITATION
Reusch E, Peh KH, Morgan R, Momo H, Orren D, Rock S, Pittman T, Neltner J, Kolesar J and Villano J (2025) Case Report: Advanced grade 2 meningioma with *PBRM1* inactivation with prolonged response to immunotherapy.
Front. Oncol. 15:1587752.
doi: 10.3389/fonc.2025.1587752

Case Report: Advanced grade 2 meningioma with *PBRM1* inactivation with prolonged response to immunotherapy

Ellen Reusch[1], Keng Hee Peh[1,2], Rachael Morgan[1,2], Harry Momo[1], David Orren[3], Stephanie Rock[4], Thomas Pittman[5], Janna Neltner[6], Jill Kolesar[1,2] and John Villano[1,3,5,6]*

[1]Markey Cancer Center, University of Kentucky, Lexington, KY, United States, [2]College of Pharmacy, University of Kentucky, Lexington, KY, United States, [3]College of Medicine, University of Kentucky, Lexington, KY, United States, [4]Molecular Science Liaison Group, Caris Life Sciences, Phoenix, AZ, United States, [5]Department of Neurosurgery, University of Kentucky, Lexington, KY, United States, [6]Department of Pathology and Laboratory Medicine, University of Kentucky, Lexington, KY, United States

Meningiomas are the most common primary tumor in the central nervous system, yet an effective systemic treatment remains a challenge. We present a grade 2 meningioma that resulted in a positive and prolonged response to pembrolizumab. Our case had polybromo-1 (*PBRM1*) and *BAP1* functional loss, tumor mutational burden of 4 Muts/Mb, stable microsatellite status, and a PD-L1 tumor proportion score of <1%. We add to the limited literature regarding *PBRM1* mutations in meningiomas. We discuss our findings in relation to the ongoing investigation of immune checkpoint inhibitor therapy in treating higher-grade refractory meningiomas.

KEYWORDS

atypical meningioma, immunotherapy, PBRM1, grade 2 meningioma, PD-1/L1

Introduction

Meningioma incidence is increasing in the US population. Meningioma is one of the rare tumors whose incidence continues to rise with advancing age (1, 2). They arise from arachnoid cells of the leptomeninges and are the most common primary tumor in the central nervous system (CNS) (1, 3). Although there are widespread asymptomatic cases in 1%–2% of the general adult population, nearly all are non-malignant grade 1 tumors (1, 4, 5). In 2016, the World Health Organization defined grade 2 meningiomas as atypical, exhibiting mitotic rates of 4–19 per 10 high power fields (HPFs), brain invasion, or at least three of five defined histological features (necrosis, sheet-like growth, prominent nucleoli, high cellularity, or high nuclear:cytoplasmic ratio within cells). Grade 3 meningiomas were considered anaplastic or malignant and were described as having mitotic rates >20 per 10 HPFs or papillary or rhabdoid histological features (6, 7). More recently, the 2021 WHO guidelines emphasize that, regardless of any underlying pathologic characteristics, atypical and anaplastic

meningiomas should be classified as grade 2 and grade 3, respectively (5). Additionally, where rhabdoid and papillary features previously would be automatically classified as a grade 3 meningioma, the WHO CNS5 now recommends that meningiomas be classified based on criteria outside of those cytologic features (5). There are several molecular biomarkers that can be utilized in the classification of meningiomas. BAP1 is associated with the rhabdoid and papillary subtypes, SMARCE1 is consistent with the clear cell subtype, and KLF4/TRAF7 mutations are associated with the secretory subtype. Furthermore, meningiomas with *CDKN2A/B* homozygous deletions and/or *TERT* promoter mutations are classified as grade 3. Prognosis can be estimated through methylome profiling, and some mutations (H2K27me3 loss of nuclear expression) may be associated with poorer prognoses (5). From surgically resected cases, higher-grade meningiomas remain a minority: atypical or borderline malignant grade 2 tumors occur in 5%–15% and malignant grade 3 tumors in 1%–3% of cases (1, 4). The recurrence rates following surgery are low for grade 1 tumors but increase to 30% to 40% for grade 2 and 50% to 80% for grade 3 (1, 4).

Regarding immune access, recent anatomical discoveries demonstrate that the central nervous system is no longer considered a strictly immune-privileged organ (8). Lymphatic vessels, adjacent to the blood vascular system, are the primary means by which bodily tissues can eliminate excess fluid and proteins (9). Tissues with higher metabolic rates typically contain denser lymphatic systems. Interestingly, despite the high rate of metabolic byproduct formation, the brain and spinal cord do not contain a lymphatic tree (9, 10). Instead, waste products from the CNS are removed through the exchange of cerebrospinal fluid (CSF) and interstitial fluid (ISF) within the para-arterial interstitial space (9, 11). ISF then drains out of the CNS into the subarachnoid lymphatic-like membrane (SLYM). This recently identified structure present under the dura separates the subarachnoid space into outer and inner compartments and limits the exchange of most peptides and proteins between the two subarachnoid compartments. The recent discovery of the SLYM adds to the suggestion that CSF transport is more sophisticated than previously acknowledged (12).

We report one of the first pathologically proven cases of meningioma having a significant and prolonged response to a single agent pembrolizumab. This patient's tumor had a truncation in the polybromo-1 (*PBRM1*) gene, which is a tumor suppressor gene involved in the control of the cell cycle, the promotion of genomic stability, and centromeric cohesion (8). Overall, *PBRM1* is mutated in nearly 40% of all clear cell renal cell carcinoma (RCC) occurrences, as well as some papillary RCCs and bladder carcinoma (13). *PBRM1* mutations are relatively uncommon in meningiomas, but when present, they are associated with papillary subtypes and often have overlapping *BAP1* mutations (14).

The occurrence of meningiomas has undergone only limited formal investigation in regard to therapies, and they currently remain among the few relatively common tumors without a Food and Drug Administration (FDA)-approved therapy. Meningiomas are chemotherapy resistant, and both targeted and immune-based therapies have been actively investigated (15–18). As discussed previously, there is evidence of an immune-based role in higher-grade meningiomas, including containing a significantly greater intra-tumoral T-cell infiltrate, inducing known local and systemic immunosuppression, a recent case of possible immune-mediated abscopal effect from radiation therapy, and several case reports of activity for immune checkpoint inhibitors (ICIs) (19, 20). With our case study, we have begun to further explore the occurrence of *PBRM1* mutations and subsequent outcomes in patients with meningiomas.

Caris genomics study

Genomics data from patient tumors that were sent to Caris Life Sciences for next-generation sequencing were utilized for this analysis. A total of 399 patients with meningiomas were identified, and 2.5% (n = 10) had alterations in *PBRM1*. Of the 10 patients with PBRM1 alterations, one patient had a known pathogenic point mutation variant (R1027X). Overall survival (OS) was estimated using the Kaplan–Meier method. The median OS was 797 days (95% CI 270 to ∞ days) for patients with *PBRM1* alteration and 1,862 days for those without (95% CI 1,547–2,009 days) (Figure 1). Of note, the patient having the *PBRM1* R1027X mutation had a survival of 797 days. The Kaplan–Meier plots and p-values were not generated due to a low sample size of *PBRM1* alterations.

Clinical case

In 1993, at age 19, our patient was diagnosed with atypical meningioma, grade 2, located around the right mastoid region. Her treatment plan included two closely spaced surgeries and proton therapy, followed by surveillance for more than a decade. She lacked a family history of neurofibromatosis 2 (NF2) or cancer, as well as clinical or imaging evidence of NF2. Referral for genetic counseling was refused. In March 2017, at age 43, she developed progressive

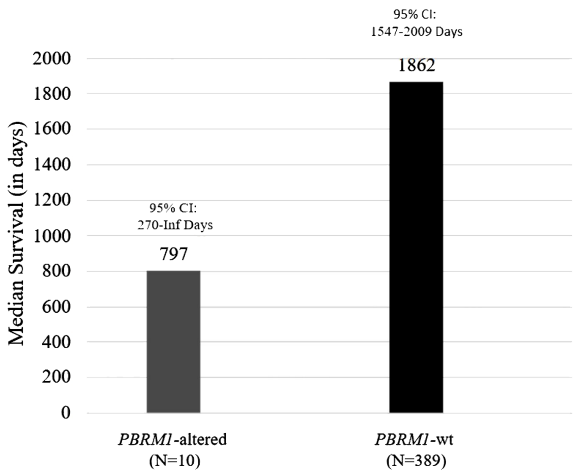

FIGURE 1
Overall survival estimates of meningioma patients with and without *PBRM1* alterations.

headaches, and imaging demonstrated an enhancing right upper neck mass with erosion of C1–C2 and extension into the posterior fossa (Figure 2A). Her first surgical resection (R1) following recurrence was performed in April 2017, and pathology demonstrated atypical meningioma lacking immune infiltrates. The post-surgery MRI and histopathology (H&E) images are depicted in Figures 2B, 3A, respectively.

She initiated somatostatin analog injections in July 2017, which she continued monthly for 22 months until imaging in November 2018 demonstrated progression (21–23). She also developed mild headaches, tearing in her right eye, and decreased movement in the right side of her face. The decision was made to undertake a large cancer-based surgery, R2 (Figures 2C, D), in April 2019. Pathology from this surgery was similar to that of the R1 specimen (Figure 3B).

After recovery (June 2019), she enrolled in a phase I clinical trial of BXQ-350, a synthetic form of the human glycoprotein saposin C (NCT02859857). Unfortunately, she soon progressed in August 2019 with the growth of the right skull base tumor and began to have increased symptoms of headaches, dysphagia with liquids, and weight loss. To identify possible targeted therapies, next-generation sequencing (NGS) testing was performed on the R2 specimen (right cerebellar tumor) with FoundationOne. This demonstrated a non-elevated tumor mutational burden (TMB) of 4 Muts/Mb, stable microsatellite status, and no recommended therapies or trials. There were alterations including *FBXW7* G419, *BAP1* loss, and *PBRM1* loss of exons 2 to 12. The tumor was also found to have a PD-L1 tumor proportion score of <1% on PD-L1 22C3 IHC testing.

Having the *PBRM1* mutation, a mutation possibly associated with immune therapy response in RCC, pembrolizumab was administered at standard flat dosing of 200 mg every 3 weeks starting in September 2019 (30 months from R1). The patient soon reported improvement in her symptoms and, after three cycles, returned to full-time work. She experienced no significant adverse effects from therapy. Repeat imaging demonstrated a reduction in size with near resolution of mass effect (Figures 4A, B), and she continued ICI therapy. At the time of manuscript writing, the

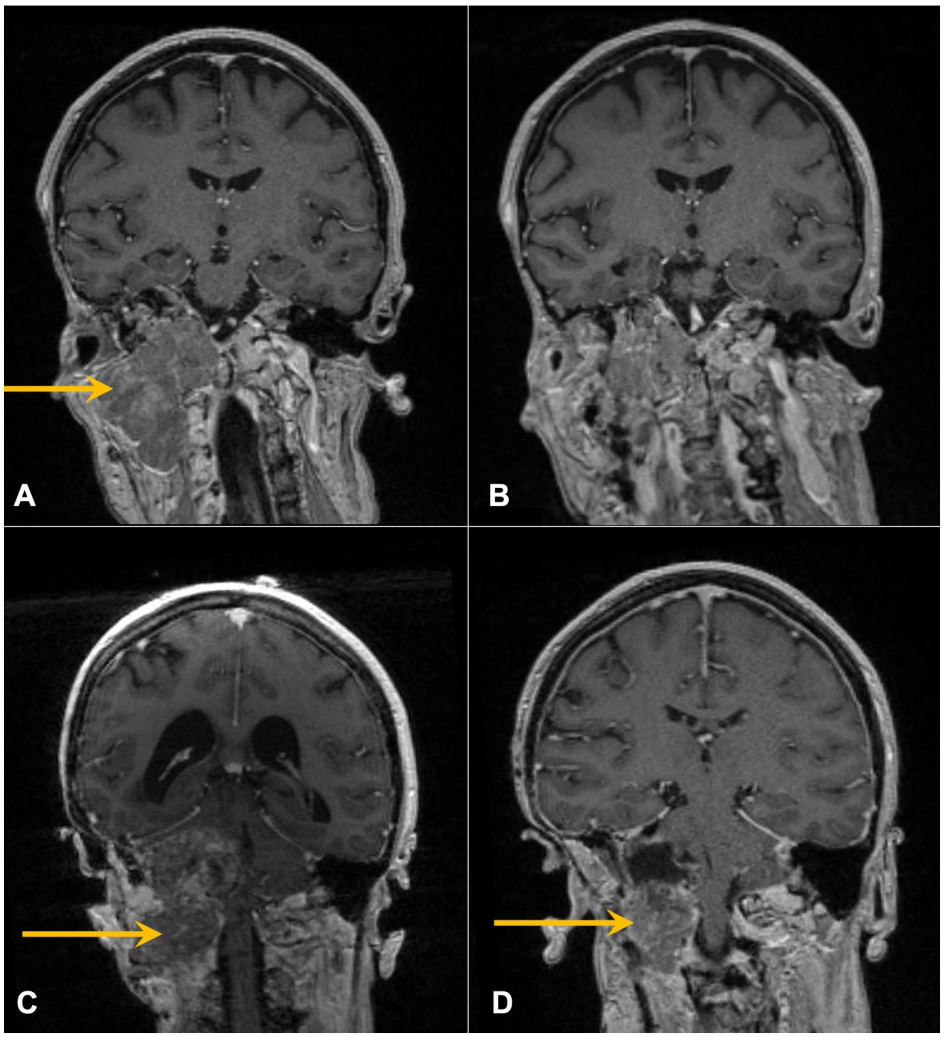

FIGURE 2
Contrast-enhanced coronal T1 MRI of the brain following recent surgeries. Arrows mark enhancing skull base mass prior to R1 **(A)** and R2 **(C)** and resulting post-operative images following R1 **(B)** and R2 **(D)**.

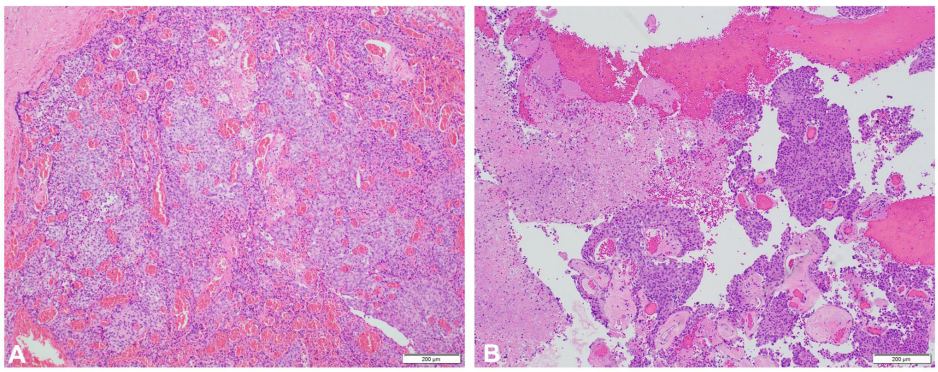

FIGURE 3
H&E, ×100 **(A, B)**. Specimens from R1 and R2 demonstrating recurrent atypical meningioma.

patient had completed 66 cycles of pembrolizumab 200 mg every 3 weeks since R2. She continues to work and enjoys high performance status and has no evidence of disease on her most recent imaging (Figures 4C, D), approximately 3 years 9 months from the initiation of ICI therapy and 50 months from R2.

Other cases benefiting from ICI therapy include an advanced lung cancer patient co-diagnosed with imaging-based meningioma (lacking tissue confirmation) in which both tumors continued growing on standard chemotherapy prior to seeing a positive response to nivolumab (24). Another case with atypical meningioma (grade 2)—with mismatch repair deficiency and disease extending extra-axially from a frontal convexity tumor to involving the scalp—had prior treatment with bevacizumab, temozolomide, two radiosurgeries, and seven surgical debulking procedures, but exhibited benefit from nivolumab (25). In a 1997 study, six patients with unresectable or malignant meningiomas were treated with interferon alpha-2B, with five patients showing a positive response to treatment. Of those five patients, four experienced tumor stabilization with a range of 6 to 14 months (26, 27). Furthermore, a study published in 2022 documented a slight trend in increased PD-L1 expression correlating with better outcomes and growth stabilization in pembrolizumab-treated meningioma patients (20). Twelve patients achieved a median progression-free survival (PFS) of 7.6 months, which was a favorable comparison to previous trials that had only reported PFS of 4–26 weeks (20, 28). The findings of this study also suggested that T-cell or myeloid-cell phenotypic dynamics, as well as the level of histological aggression, may dictate whether a clinical benefit or disease response is achieved from ICI therapy (20). Although limited in scope, these cases collectively support the exploration of immunotherapy as an option for the treatment of advanced meningiomas.

Discussion

PBRM1 is a tumor suppressor gene that codes for BAF180, a component of the chromatin remodeling complex (29). Thus, its loss of function impacts chromatin structure and downstream transcriptional and DNA repair processes (30, 31). *In vivo* experiments have demonstrated increased tumorigenesis in mice with downregulated *PBRM1*, with the greatest difference in gene expression being seen in the chemokine/chemokine receptor interaction pathway, suggesting a possible mechanism by which *PBRM1* alters cell cycle progression and proliferation (32). Other recent studies have shown that a lack of *PBRM1* subsequently results in DNA damage and dynamic chromosome instability (33).

In patients with clear cell RCC, loss-of-function mutations in *PBRM1* are common and are associated with clinical benefit from immune checkpoint inhibitors (13, 34). Braun and colleagues reported consistent results: in 189 patients with metastatic clear cell RCC receiving nivolumab or everolimus as part of a clinical trial, 55 patients had a *PBRM1* mutation, which was associated with both clinical benefit and longer PFS in nivolumab-treated patients. There was no effect noted in those treated with everolimus only.

In contrast, in a retrospective analysis conducted at three Chinese institutions, presumably in Asian patients, *PBRM1* mutations were infrequent in patients with non-small cell lung cancer (84/2,767, 3%). This analysis demonstrated that *PBRM1* may be potentially associated with poorer survival in patients treated with immunotherapy, despite previous reports suggesting a correlation between *PBRM1* mutations and increased neoantigens (35, 36).

PBRM1 genetic alterations are infrequent (2.8%) in meningiomas, and alterations are usually associated with high-grade meningiomas (37). Unfortunately, the genomics data we obtained from Caris Life Sciences did not contain information regarding the tumor grade of the included patients. However, in a recent case series of 850 patients with meningiomas that were grade 1 (220/850, 26%), grade 2 (441/850, 52%), and grade 3 (176/850, 20%) (13 cases were not graded due to inadequate specimens), only 16 had an inactivating mutation in *PBRM1* (1.9%) (14). The majority of the 16 *PBRM1* meningioma cases (11) had papillary histologic features that were higher grade (2/16 grade 1, 8/16 grade 2, and 6/16 grade 3), all were microsatellite stable and had a low median TMB of 2.1 Muts/Mb, and five cases had an overlap mutation with *BAP1*. Our analyses of 399 meningioma patients undergoing NGS testing demonstrated that patients with *PBRM1*

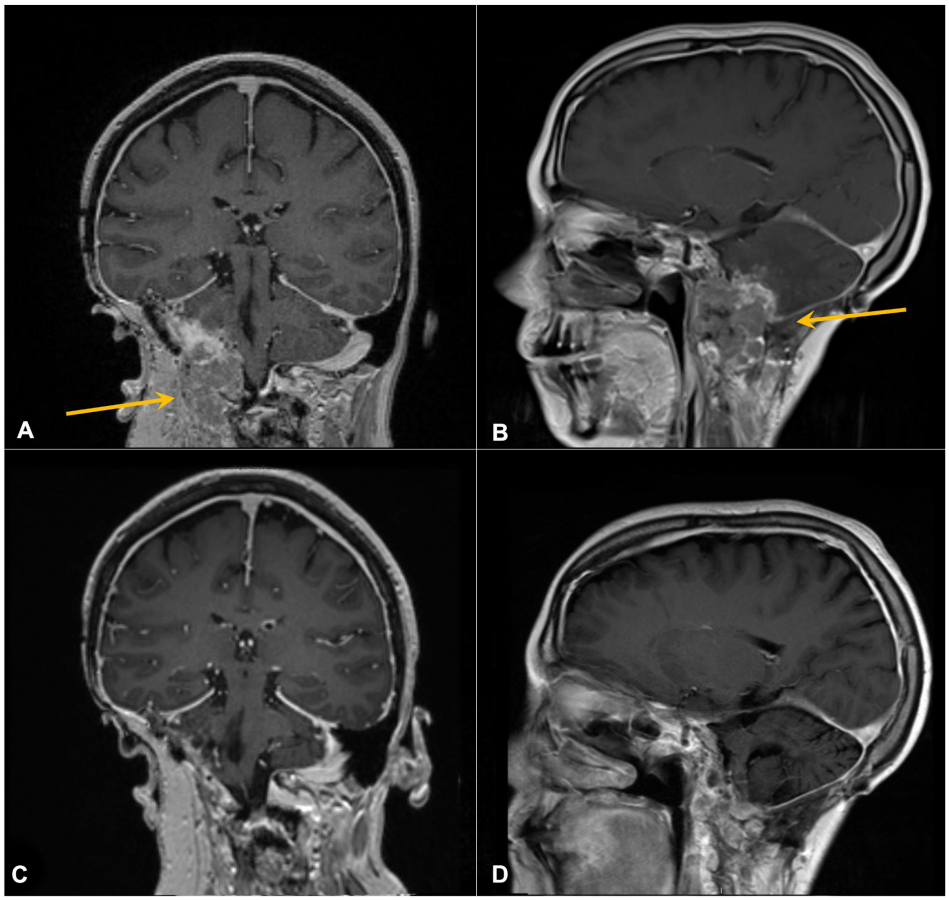

FIGURE 4
Contrast-enhanced coronal **(A, C)** and sagittal **(B, D)** T1 MRI of the brain. Arrows in panels A and B mark enhancing right cerebellar/skull base prior to pembrolizumab. **(C, D)** Following six cycles of therapy, demonstrating response.

alterations had likely lower overall survival. The frequency (2.5%) of *PBRM1* alterations in meningiomas in our analysis matches published literature. Despite PBRM1 mutations rarely occurring in meningioma, this represents a potential therapeutic investigation.

BAP1 was originally identified as a *BRCA1*-interacting protein and encodes a de-ubiquitinating enzyme that is involved in many processes (38). *BAP1* can act as a subunit of the Polycomb Repressive De-ubiquitinase complex (PR-DUB), which reverses the ubiquitinating activity of Polycomb Repressive Complex 1 (PRC1); one key PR-DUB substrate is histone H2A ubiquitinated at lysine 119, so *BAP1* normally acts to modulate chromatin structure and cellular epigenetic status (39, 40). Thus, loss of *BAP1* function is thought to affect DNA repair and transcription processes that are affected by chromatin state. Mutations in *BAP1* have been reported to correlate with positive response to immunotherapy (41), perhaps by similar mechanisms as for *PBRM1*, but *BAP1* alterations are even rarer (<1%) (37).

This report details our experiences with a patient with advanced meningiomas and illustrates the challenges associated with treating these malignancies. Our patient received proton therapy and aggressive multi-team surgery, underwent a first-in-human early-phase clinical trial, and was treated with a somatostatin analog for many years. Our patient's meningioma demonstrated stable microsatellite status and PD-L1 negativity, but with a TMB of 4 Muts/Mb, which is higher than reported for atypical meningioma (mean 1.8 Muts/Mb) but lower than TMBs in other tumors (melanomas, many lung cancers, and microsatellite instability (MSI)-high cancers) (25) for which ICIs have FDA labeling. Thus, it seems unlikely that PD-L1 or TMB levels explain the positive response to immunotherapy.

The genomics report demonstrated probable loss-of-function alterations (large deletions) in the tumor suppressor gene *PBRM1* on chromosome 3p21. Our patient had a *PBRM1* deletion involving exons 2 through 12. Missense mutations in the bromodomain regions have been shown to result in the tumor suppressor activity of *PBRM1*, especially in the bromodomain 2 (42). Further, the bromodomains have also been found to be essential in the chromatin complex interaction (42, 43). Even though it is tempting to suggest that loss of function of *PBRM1* and/or BAP1 plays a role in the positive response of our patient to pembrolizumab, the role of mutations in *PBRM1* has yet to be well-characterized. Our genomics analysis on meningioma patients demonstrated 90% (9/10) patients having *PBRM1* mutations with unknown oncogenic significance. The patient in our case report had

a reported exon loss in *PBRM1*, which may result in truncating mutations leading to a loss of function as a tumor suppressor. Truncating or splice site mutations appear to be the majority of reported *PBRM1* oncogenic alterations based on the cBioPortal database (44, 45). This suggests that despite *PBRM1* being a potential biomarker for immunotherapy, heterogeneity in tumors may present challenges when validating biomarkers as a response to immunotherapy.

The current therapeutic landscape remains limited in meningioma, but treatments targeted to actionable mutations are promising. In addition to immunotherapy, ongoing clinical trials are under investigation involving FAK inhibition in patients based on preclinical synthetic lethality seen with NF2 loss and FAK inhibition (46). Despite evidence of *PBRM1* loss contributing to genomic instability or neoantigen production, a majority of the reported literature is preclinical in nature, and the concept requires further research to validate *PBRM1* as a marker for immunotherapy response. Our experience with immunotherapy in treating meningioma patients mirrors that observed in patients with other malignancies—i.e., while a substantial percentage of patients may have a positive or even exceptional response, others may not respond even though their tumors may possess a marker that would potentially predict a positive response. Our findings expand this paradigm to aggressive meningiomas from the positive outcome of our patient case, which adds to the limited previous literature demonstrating positive responses of these malignancies to immunotherapy.

Data availability statement

The original contributions presented in the study are included in the article/supplementary material. Further inquiries can be directed to the corresponding author.

Ethics statement

Written informed consent was obtained from the individual(s) for the publication of any potentially identifiable images or data included in this article.

Author contributions

ER: Formal analysis, Validation, Writing – original draft, Writing – review & editing. KP: Formal analysis, Validation, Writing – review & editing. RM: Validation, Writing – review & editing. HM: Validation, Writing – review & editing. DO: Supervision, Validation, Writing – review & editing. SR: Data curation, Validation, Writing – review & editing. TP: Validation, Writing – review & editing. JN: Validation, Writing – review & editing. JK: Validation, Writing – review & editing. JV: Funding acquisition, Investigation, Supervision, Writing – review & editing.

Funding

The author(s) declare financial support was received for the research and/or publication of this article. The Research Communications Office of the University of Kentucky Markey Cancer Center (P30CA177558) supported the publication of the manuscript but did not contribute to the writing of the manuscript.

Acknowledgments

We would like to thank our patient.

Conflict of interest

The authors declare that the research was conducted in the absence of any commercial or financial relationships that could be construed as a potential conflict of interest.

Generative AI statement

The author(s) declare that no Generative AI was used in the creation of this manuscript.

Any alternative text (alt text) provided alongside figures in this article has been generated by Frontiers with the support of artificial intelligence and reasonable efforts have been made to ensure accuracy, including review by the authors wherever possible. If you identify any issues, please contact us.

Publisher's note

References

1. Louis D, Perry A, Reifenberger G, von Deimling A, Figarella-Branger D, Cavenee W, et al. *WHO classification of tumours of the central nervous system. 4th edition*. Lyon: International Agency For Research On Cancer (2016).

2. Saraf S, McCarthy BJ, Villano JL. Update on meningiomas. *Oncologist*. (2011) 16:1604–13. doi: 10.1634/theoncologist.2011-0193

3. Nakasu S, Hirano A, Shimura T, Llena J. Incidental meningiomas in autopsy study. *Surg Neurol*. (1987) 27:319–22. doi: 10.1016/0090-3019(87)90005-X

4. Perry A, Stafford SL, Scheithauer BW, Suman V, Lohse C. Meningioma grading: an analysis of histologic parameters. *Am J Surg Pathol*. (1997) 21:1455–65. doi: 10.1097/00000478-199712000-00008

5. Louis DN, Perry A, Wesseling P, Brat D, Cree I, Figarella-Branger D, et al. The 2021 WHO classification of tumors of the central nervous system: a summary. *Neuro Oncol*. (2021) 23:1231–51. doi: 10.1093/neuonc/noab106

6. Maggio I, Franceschi E, Tosoni A, Di Nunno V, Gatto L, Lodi R, et al. Meningioma: not always a benign tumor. A review of advances in the treatment of meningiomas. *CNS Oncol*. (2021) 10:Cns72. doi: 10.2217/cns-2021-0003

7. Louis DN, Perry A, Reifenberger G, von Deimling A, Figarella-Branger D, Cavenee W, et al. The 2016 world health organization classification of tumors of the central nervous system: a summary. *Acta Neuropathol*. (2016) 131:803–20. doi: 10.1007/s00401-016-1545-1

8. Gao W, Li W, Xiao T, Liu X, Kaelin W Jr. Inactivation of the PBRM1 tumor suppressor gene amplifies the HIF-response in VHL-/- clear cell renal carcinoma. *Proc Natl Acad Sci U.S.A*. (2017) 114:1027–32. doi: 10.1073/pnas.1619726114

9. Nedergaard M. Neuroscience. Garbage truck of the brain. *Science*. (2013) 340:1529–1530. doi: 10.1126/science.1240514

10. Loukas M, Bellary SS, Kuklinski M, Ferrauiola J, Yadav A, Shoja M, et al. The lymphatic system: a historical perspective. *Clin Anat*. (2011) 24:807–16. doi: 10.1002/ca.21194

11. Nagelhus EA, Mathiisen TM, Ottersen OP. Aquaporin-4 in the central nervous system: cellular and subcellular distribution and coexpression with KIR4. *1. Neurosci*. (2004) 129:905–13. doi: 10.1016/j.neuroscience.2004.08.053

12. Mollgard K, Beinlich FRM, Kusk P, Miyakoshi L, Delle C, Pla V, et al. A mesothelium divides the subarachnoid space into functional compartments. *Science*. (2023) 379:84–8. doi: 10.1126/science.adc8810

13. Braun DA, Ishii Y, Walsh AM, Van Allen E, Wu C, Shukla S, et al. Clinical validation of PBRM1 alterations as a marker of immune checkpoint inhibitor response in renal cell carcinoma. *JAMA Oncol*. (2019) 5:1631–3. doi: 10.1001/jamaoncol.2019.3158

14. Caruso G, Ferrarotto R, Curcio A, Metro L, Pasqualetti F, Gaviani P, et al. Frequent inactivating mutations of the PBAF complex gene PBRM1 in meningioma with papillary features. *Acta Neuropathol*. (2020) 140:89–93. doi: 10.1007/s00401-020-02161-7

15. Nayak L, Iwamoto FM, Rudnick JD, Norden A, Lee E, Drappatz J, et al. Atypical and anaplastic meningiomas treated with bevacizumab. *J Neurooncol*. (2012) 109:187–93. doi: 10.1007/s11060-012-0886-4

16. Norden AD, Raizer JJ, Abrey LE, Lamborn K, Lassman A, Chang S, et al. Phase II trials of erlotinib or gefitinib in patients with recurrent meningioma. *J Neurooncol*. (2010) 96:211–7. doi: 10.1007/s11060-009-9948-7

17. Dunn IF, Du Z, Touat M, Sisti M, Wen P, Umeton R, et al. Mismatch repair deficiency in high-grade meningioma: a rare but recurrent event associated with dramatic immune activation and clinical response to PD-1 blockade. *JCO Precis Oncol*. (2018) 2018. doi: 10.1200/PO.18.00190

18. Wen PY, Yung WK, Lamborn KR, Norden A, Cloughesy T, Abney L, et al. Phase II study of imatinib mesylate for recurrent meningiomas (North American Brain Tumor Consortium study 01-08). *Neuro Oncol*. (2009) 11:853–60. doi: 10.1215/15228517-2009-010

19. Louveau A, Plog BA, Antila S, Alitalo K, Nedergaard M, Kipnis J. Understanding the functions and relationships of the glymphatic system and meningeal lymphatics. *J Clin Invest*. (2017) 127:3210–9. doi: 10.1172/JCI90603

20. Brastianos PK, Kim AE, Giobbie-Hurder A, Lee E, Wang N, Eichler A, et al. Phase 2 study of pembrolizumab in patients with recurrent and residual high-grade meningiomas. *Nat Commun*. (2022) 13:1325. doi: 10.1038/s41467-022-29052-7

21. Chamberlain MC, Glantz MJ, Fadul CE. Recurrent meningioma. *Salvage Ther long-acting somatostatin analogue*. (2007) 69:969–73. doi: 10.1212/01.wnl.0000271382.62776.b7

22. Norden AD, Ligon KL, Hammond SN, Muzikansky A, Reardon D, Kaley T, et al. Phase II study of monthly pasireotide LAR (SOM230C) for recurrent or progressive meningioma. *Neurology*. (2015) 84:280–6. doi: 10.1212/WNL.0000000000001153

23. Schulz C, Mathieu R, Kunz U, Mauer U. Treatment of unresectable skull base meningiomas with somatostatin analogs. *Neurosurg Focus*. (2011) 30:E11. doi: 10.3171/2011.1.FOCUS111

24. Garzon-Muvdi T, Bailey D, Pernik M, Pan E. Regression of intracranial meningioma following treatment with nivolumab: Case report and review of the literature. *J Clin Neurosci*. (2017) 37:51–3. doi: 10.1016/j.jocn.2016.11.011

25. Bi WL, Greenwald NF, Abedalthagafi M, Wala J, Gibson W, Agarwalla P, et al. Genomic landscape of high-grade meningiomas. *NPJ Genom Med*. (2017) 2:15. doi: 10.1038/s41525-017-0014-7

26. Sioka C, Kyritsis AP. Chemotherapy, hormonal therapy, and immunotherapy for recurrent meningiomas. *J Neuro-Oncology*. (2009) 92:1–6. doi: 10.1007/s11060-008-9734-y

27. Kaba SE, DeMonte F, Bruner JM, Kyritsis A, Jaeckle K, Levin V, et al. The treatment of recurrent unresectable and Malignant meningiomas with interferon alpha-2B. *Neurosurgery*. (1997) 40:271–5. doi: 10.1097/00006123-199702000-00007

28. Kaley T, Barani I, Chamberlain M, McDermott M, Panageas K, Raizer J, et al. Historical benchmarks for medical therapy trials in surgery- and radiation-refractory meningioma: a RANO review. *Neuro Oncol*. (2014) 16:829–40. doi: 10.1093/neuonc/not330

29. Gerlinger M, Horswell S, Larkin J, Rowan A, Salm M, Varela I, et al. Genomic architecture and evolution of clear cell renal cell carcinomas defined by multiregion sequencing. *Nat Genet*. (2014) 46:225–33. doi: 10.1038/ng.2891

30. Hodges C, Kirkland JG, Crabtree GR. The many roles of BAF (mSWI/SNF) and PBAF complexes in cancer. *Cold Spring Harb Perspect Med*. (2016) 6. doi: 10.1101/cshperspect.a026930

31. Hopson S, Thompson MJ. BAF180: its roles in DNA repair and consequences in cancer. *ACS Chem Biol*. (2017) 12:2482–90. doi: 10.1021/acschembio.7b00541

32. Wang H, Qu Y, Dai B, Zhu Y, Shi G, Zhu Y, et al. PBRM1 regulates proliferation and the cell cycle in renal cell carcinoma through a chemokine/chemokine receptor interaction pathway. *PLoS One*. (2017) 12:e0180862. doi: 10.1371/journal.pone.0180862

33. Miao D, Margolis CA, Gao W, Voss M, Li W, Martini D, et al. Genomic correlates of response to immune checkpoint therapies in clear cell renal cell carcinoma. *Science*. (2018) 359:801–6. doi: 10.1126/science.aan5951

34. Carril-Ajuria L, Santos M, Roldán-Romero JM, Rodriguez-Antona C, de Velasco G. Prognostic and predictive value of PBRM1 in clear cell renal cell carcinoma. *Cancers (Basel)*. (2019) 12. doi: 10.3390/cancers12010016

35. Zhou H, Liu J, Zhang Y, Huang Y, Shen J, Yang Y, et al. PBRM1 mutation and preliminary response to immune checkpoint blockade treatment in non-small cell lung cancer. *NPJ Precis Oncol*. (2020) 4:6. doi: 10.1038/s41698-020-0112-3

36. Park LC, Chang S, Ko T, Rhee K, Anker J, Bhave M, et al. P1.04–01 impact of chromatin remodeling genes including SMARCA2 and PBRM1 on neoantigen and immune landscape of NSCLC. *J Thorac Oncol*. (2018) 13:S525. doi: 10.1016/j.jtho.2018.08.716

37. Birzu C, Peyre M, Sahm F. Molecular alterations in meningioma: prognostic and therapeutic perspectives. *Curr Opin Oncol*. (2020) 32:613–22. doi: 10.1097/CCO.0000000000000687

38. Louie BH, Kurzrock R. BAP1: Not just a BRCA1-associated protein. *Cancer Treat Rev*. (2020) 90:102091. doi: 10.1016/j.ctrv.2020.102091

39. Scheuermann JC, de Ayala Alonso AG, Oktaba K, Ly-Hartig N, McGinty R, Fraterman S, et al. Histone H2A deubiquitinase activity of the Polycomb repressive complex PR-DUB. *Nature*. (2010) 465:243–7. doi: 10.1038/nature08966

40. Campagne A, Lee M-K, Zielinski D, Michaud A, Le Corre S, Dingli F, et al. BAP1 complex promotes transcription by opposing PRC1-mediated H2A ubiquitylation. *Nat Commun*. (2019) 10:348. doi: 10.1038/s41467-018-08255-x

41. Ladanyi M, Sanchez Vega F, Zauderer M. Loss of BAP1 as a candidate predictive biomarker for immunotherapy of mesothelioma. *Genome Med*. (2019) 11:18. doi: 10.1186/s13073-019-0631-0

42. Porter EG, Dykhuizen EC. Individual bromodomains of polybromo-1 contribute to chromatin association and tumor suppression in clear cell renal carcinoma. *J Biol Chem*. (2017) 292:2601–10. doi: 10.1074/jbc.M116.746875

43. Slaughter MJ, Shanle EK, McFadden AW, Hollis E, Suttle L, Strahl B, et al. PBRM1 bromodomains variably influence nucleosome interactions and cellular function. *J Biol Chem*. (2018) 293:13592–603. doi: 10.1074/jbc.RA118.003381

44. Cerami E, Gao J, Dogrusoz U, Gross B, Sumer S, Aksoy B, et al. The cBio cancer genomics portal: an open platform for exploring multidimensional cancer genomics data. *Cancer Discov*. (2012) 2:401–4. doi: 10.1158/2159-8290.CD-12-0095

45. Gao J, Aksoy BA, Dogrusoz U, Dresdner G, Gross B, Sumer S, et al. Integrative analysis of complex cancer genomics and clinical profiles using the cBioPortal. *Sci Signal*. (2013) 6:pl1. doi: 10.1126/scisignal.2004088

46. Shapiro IM, Kolev VN, Vidal CM, Kadariya Y, Ring J, Wright Q, et al. Merlin deficiency predicts FAK inhibitor sensitivity: a synthetic lethal relationship. *Sci Transl Med*. (2014) 6:237ra268. doi: 10.1126/scitranslmed.3008639

frontiers | Frontiers in Oncology

TYPE Original Research
PUBLISHED 19 November 2025
DOI 10.3389/fonc.2025.1626301

OPEN ACCESS

EDITED BY
Giovanna Damia,
Mario Negri Institute for Pharmacological Research (IRCCS), Italy

REVIEWED BY
Alessandra Brambati,
University of Colorado Anschutz Medical Campus, United States
Oriol Mirallas,
The University of Texas MD Anderson Cancer Center, United States

*CORRESPONDENCE
Intidhar Labidi-Galy
intidhar.labidi-galy@hug.ch

†These authors have contributed equally to this work

RECEIVED 10 May 2025
ACCEPTED 28 October 2025
PUBLISHED 19 November 2025

CITATION
Zouggari N, Trugenberger C, Du Bois V, Wang W, Rossetti GG, Halazonetis TD and Labidi-Galy I (2025) CldU sensitizes *BRCA2* reverse-mutated cells to PARP inhibitors. *Front. Oncol.* 15:1626301. doi: 10.3389/fonc.2025.1626301

CldU sensitizes *BRCA2* reverse-mutated cells to PARP inhibitors

Nawel Zouggari[1,2†], Camilla Trugenberger[1,2†], Valentine Du Bois[1], Wenwen Wang[1], Giacomo G. Rossetti[2], Thanos D. Halazonetis[2] and Intidhar Labidi-Galy[1,3*]

[1]Department of Medicine and Center of Translational Research in Onco-Hematology, Faculty of Medicine, University of Geneva, Geneva, Switzerland, [2]Department of Molecular and Cellular Biology, Faculty of Sciences, University of Geneva, Geneva, Switzerland, [3]Department of Oncology, Geneva University Hospitals, Geneva, Switzerland

PARP inhibitors are widely used class of drugs for the treatment of homologous recombination deficient cancers, including *BRCA* mutated ones. These drugs led to substantial improvement in survival, particularly for patients with *BRCA* mutated tumors. However, many patients eventually develop resistance to PARP inhibitors, mainly due to *BRCA* reversion mutations. Overcoming resistance to PARP inhibitors is an unmet medical need. Recently, it has been shown that *BRCA*-deficient cells are hypersensitive to the thymidine analogue 5-chloro-2'-deoxyuridine (CldU), either alone or in combination with PARP inhibitors. In this study, we show, across multiple BRCA*2* mutated cell lines, that CldU sensitizes PARP inhibitor-resistant cells to PARP inhibitors. This synergy was also present in cell lines with BRCA*2* reversion mutations and was associated with high levels of DNA damage and arrest in S phase. This effect, which is specific to thymidine analogue CldU, may open new avenues for the treatment of *BRCA* mutated cancers resistant to PARP inhibitors.

KEYWORDS

BRCA mutation, PARP inhibitor, resistance, reversion mutation, thymidine analogue, CldU, cancer

1 Introduction

Poly(ADP-ribose) polymerase (PARP) inhibitors (PARPi) induce cell death by exploiting the absence of homologous recombination in cancer cells harboring mutations in the *BRCA1/BRCA2* genes (1). More precisely, cancer cells lacking the repair proteins BRCA1 and BRCA2 rely more heavily on PARP to repair their damaged DNA. Hence, inhibiting PARP leads to cell death as these cells are no longer able to repair the damage to their DNA. Studies have shown that loss of *BRCA2* leads to cells being 100 to 1000 times more sensitive to PARPi, this led to their exploitation in the clinic in the context of *BRCA1/2*-mutated cancer (2, 3). Other mechanisms whereby PARPi induce cell death include regulation of fork reversal and non-homologous end joining (NHEJ) at collapsed

forks (4). It is also thought that inhibition of PARP activity causes a delay in single-strand breaks, which will accumulate and become toxic double-strand breaks upon encounters with the replication fork (5). PARPi are the first successful example of therapy exploiting synthetic lethality in cancer. They showed survival benefit across multiple cancers with *BRCA* mutations (6, 7).

Despite the substantial impact that PARPi have made in the clinic, most patients with metastatic disease do eventually develop resistance, creating a major unmet medical need. For instance, the SOLO2 phase III trial exemplified how 78% of *BRCA*-mutated patients with relapsed ovarian cancer eventually experienced disease progression on Olaparib, indicating the development of resistance to PARPi (8). Another example is the ARIEL2 study, which showed that 60% of *BRCA*-mutated, high-grade ovarian carcinoma patients treated with Rucaparib ultimately experienced disease progression (9). Patients that become resistant to PARPi have poor outcome and develop cross-resistance with other DNA damage agents such as platinum (10, 11).

There are various described mechanisms to render cancer cells resistance to PARPi. The first is the restoration of the homologous recombination pathway, either through reversion mutations that restore activity to the BRCA proteins (12, 13) or via loss of 53BP1 and other resection-associated proteins (14), which will, in turn, restore the homologous recombination capacity of the cell (15). Recent analyses reported that up to 80% of prostate cancer patients with *BRCA2* mutations who developed resistance to PARPi had undergone reversion mutations (16). Mutations in PARP itself can also lead to resistance to inhibitors by reducing the binding of the drug (17). Finally, loss of Poly(ADP-ribose) Glycohydrolase results in defective removal of PAR chains, potentially conferring resistance to PARPi (18).

It is expected that this resistance issue will affect approximately 40-70% of metastatic patients with *BRCA* mutations (19). Strategies aiming to combine PARPi with other drugs to overcome the hurdle of resistance have not yet proven to be successful. Strategies aiming to combine different PARPi with various chemotherapeutic drugs, such as PI3K inhibitors (20), ATR inhibitors (21, 22) or Polθ inhibitors (23, 24) have been explored but are yet to deliver impactful results with manageable toxicities. This illustrates the major need for strategies to overcome resistance to PARPi. Recently, it was shown that *BRCA*-defective cells are sensitive to treatment with the thymidine analogue CldU either alone or in combination with PARPi olaparib (5). In this study, we found that the thymidine analogue CldU conferred specific sensitivity to PARPi in *BRCA2* mutated cell lines that were previously resistant, including those with reversion mutations. We show that this combination of treatments induced high levels of DNA damage in PARP inhibitor-resistant cell lines.

2 Material and methods

2.1 Cell lines

PEO1 and PEO4 serous ovarian cancer cell lines were purchased from Sigma-Aldrich. They are derived from peritoneal ascites of the same patient with a poorly differentiated serous ovarian adenocarcinoma. PEO1 cells were collected from the patient at first relapse (cisplatin-sensitive). PEO4 cells were collected after the patient demonstrated resistance to cisplatin (25). PEO1 has *BRCA2* non-sense mutation (5193C>G, Y1655X) and PEO4 harbors *BRCA2* reversion mutation (5193C>T, Y1655Y). C4–02 and C4–13 clones were derived *in vitro* from PEO1 cells through continuous exposure to cisplatin for 4 weeks (25). C4–02 exhibited *BRCA2* reversion mutation (5192A>T). PEO1 and its 3 clones were cultured in RPMI1640 medium (+) l-glutamine supplemented with 2mM Sodium Pyruvate and 10% fetal bovine serum (FBS).

CAPAN-1 is a *BRCA2* mutant (6174delT) pancreatic cancer cell line. Its clones C2-5, C2–8 and C2–13 were derived *in vitro* through continuous exposure to cisplatin for 4 weeks. C2–5 exhibited *BRCA2* reversion mutation (6006_6308del303) while C2–08 and C2–13 do not have reversion mutations (13). CAPAN-1 and its 3 clones were cultured in RPMI1640 medium (+) l-glutamine supplemented with 2mM Sodium Pyruvate and 10% fetal bovine serum (FBS). PEO1 derived clones (C4–02 and C4-13), CAPAN-1 and its clones (C2-05, C2–08 and C2-13) were generously provided by Prof. Toshiyasu Taniguchi (Tokai University school of medicine).

2.2 Drugs and chemicals

Olaparib (HY-10162), CldU (Merck, C6891) and Saruparib (HY-132167) were purchased from MedChemExpress (LUCERNA-CHEM). Thymidine (T1895) was purchased from Sigma-Aldrich, EdU (A10044) from ThermoFisher Scientific and BrdU (B23151 from Invitrogen). The stock solutions of PARPi and chemical compounds were prepared from powders dissolved in 100% dimethyl sulfoxide (DMSO) for a stock solution concentration of 10mM except for thymidine that was dissolved in water, aliquoted, and stored at −80°C for up to a maximum of 12 months. In order to minimize the cytotoxic effect of DMSO dilution solution on the cells, several intermediate dilutions were prepared to dispense 2µL of inhibitors in 2mL medium per well of a 6-well plate. The same volume of DMSO was added to control wells.

2.3 Clonogenic assay

The cytotoxic activity of drugs and their influence on cell growth, survival and their ability to form colonies were assessed using the colony formation assay. Briefly, cells were seeded in 6-well plates in 2 mL of culture medium in triplicate (1500 cells per well for CAPAN-1 and its clones, and 3000 cells for PEO1 and its clones) and incubated for 24 h (37°C, 5% CO2). Drugs were added to the medium 24h after cell seeding with pre-selected doses of tested compounds (0.001 – 10µM olaparib, 10 - 100–1000 nM saruparib, 0.05 - 5 µM CldU or their combinations) by adding 2µL of 1000 × concentrated drugs prepared in DMSO. The same volume of DMSO was added to control wells. After 48h, the medium was changed, and cells were

allowed to grow and proliferate in a drug-free medium for 14–21 days until non-overlapping colonies were formed in control wells. Colonies were fixed with paraformaldehyde (PFA) 4% for 20 min, stained with 0.5% crystal violet in 20% ethanol for 20 min, thoroughly rinsed with deionized water to remove residual dye, and air-dried at room temperature. Each well was photographed using the FUSION FX6 EDGE Imaging System and number of colonies was quantified using ImageJ software® with colony counting extension. A colony of at least a size of 20 pixel^2 was scored as one survivable colony and considered for the count. Results were expressed as relative survival (percentage of colonies) as the number of colonies per treatment versus colonies that appeared in the DMSO control (mean colony counts ± standard errors are reported). Graphs were generated using GraphPad Prism®, 9 software (v.9.4.1).

2.4 Flow cytometry

Following drug treatment, cells were harvested by trypsin and fixed in 70% ethanol in PBS1X overnight at −20°C. Detection of γH2AX phosphorylation was performed using the Guava Histone H2AX Phosphorylation Assay Kit (Luminex, catalogue no. FCCS100182) according to the manufacturer's instructions. Genomic DNA was stained by incubating the cells in PBS containing RNase (Roche, catalogue no. 11119915001) and propidium iodide (Sigma-Aldrich catalogue no. 81845). DNA-γH2AX profiles were acquired by flow cytometry (CytoFLEX LX flow cytometer); more than 5,000 cells were analyzed per sample using Kaluza® software (Beckman Coulter).

2.5 Statistical analysis

Statistical analysis was performed using GraphPad Prism 9 software (v.9.4.1). Detailed description of means or medians, error bars and the number replicates and/or cells analyzed is reported in the figure legends. For comparison of more than two groups, the two-way ANOVA with Tukey's multiple comparisons test was used Values are presented as mean ± SEM. $p<0.05$ was considered significant. Detailed description of means or medians, error bars and the number replicates and/or cells analyzed is reported in the figure legends. Statistical analysis was reported on Supplementary Tables.

3 Results

3.1 BRCA2-mutant cells' sensitivity to CldU resembles the sensitivity to PARP inhibitor

Recent findings have demonstrated that BRCA1-deficient cells exhibit marked sensitivity to chlorodeoxyuridine (CldU), both as a monotherapy and in combination with the PARP inhibitor olaparib (4). In this study, we assessed the sensitivity to CldU across eight *BRCA2*-mutant cancer cell lines. These included: (1) PEO1, an ovarian cancer-derived cell line, and its isogenic derivatives resistant to cisplatin, either with (PEO4; C4-02) or without *BRCA2* reversion mutation (25); and (2) CAPAN-1, a pancreatic cancer-derived cell line, along with its cisplatin-resistant clones due to either *BRCA2* reversion mutations (C2–05 and C2-13) or other mechanisms (C2-08) (13). Our results revealed that sensitivity to CldU partially reflected sensitivity to PARP inhibitor olaparib. Notably, PEO1 displayed pronounced sensitivity to olaparib (Figures 1A–C) and CldU (Figure 1E), whereas PEO4, C4-02, CAPAN-1, C2-05, C2-08, and C2–13 exhibited reduced sensitivity to both olaparib (Figures 1C, D) and CldU (Figures 1E, F).

3.2 CldU sensitizes PARP inhibitor-resistant cells to PARP inhibitors

We next investigated whether the combination of CldU and PARPi exerts a synergistic effect in *BRCA2*-mutant cancer cells. Remarkably, the co-treatment with low doses of olaparib (1 μM) and CldU (0.5 μM) proved to be lethal in *BRCA2*-mutant PEO1 cells, as well as in its olaparib-resistant isogenic derivatives, including revertant clones PEO4 and C4-02 (Figure 2A, Supplementary Table 1 and Supplementary Figure 1A). This synergistic effect was further validated using saruparib (AZ5305), a second-generation, highly potent and PARP1-selective inhibitor with approximately 500-fold selectivity for PARP1 over PARP2 (18). Low-dose saruparib (10 nM) combined with CldU resulted in >80% cell death across the three PEO1-derived clones, all of which were resistant to saruparib monotherapy (Figure 2C, Supplementary Table 3, Supplementary Figure 1C and Supplementary Figures 2A–D). Consistently, the combination of CldU with olaparib (Figure 2B, Supplementary Table 2 and Supplementary Figure 1B) elicited a synergistic response in the *BRCA2*-mutant CAPAN-1 cell line and its PARP inhibitor-resistant isogenic derivatives, including the reversion-bearing C2–05 clone. Interestingly, the synergistic response between saruparib and CldU in CAPAN-1 cells was less significant (Figure 2D, Supplementary Table 4, Supplementary Figure 1D and Supplementary Figures 2E–H). This could reflect the high intrinsic resistance of these cells to both agents, in addition to saruparib being a PARP1 specific inhibitor with lower trapping potential than olaparib (26). Collectively, these findings demonstrate that CldU and PARPi act synergistically in *BRCA2*-mutant cancer cells, even in the context of acquired PARP inhibitor resistance, including resistance mediated by *BRCA2* reversion mutations.

3.3 The synergistic effect of CldU and PARP inhibitor is specific

CldU is a thymidine analogue with a chemical structure closely resembling that of native thymidine. It is commonly used in molecular biology to label newly synthesized DNA, as it is incorporated into DNA but not RNA. Other thymidine analogues, such as 5-ethynyl-2′-deoxyuridine (EdU) and 5-bromo-2′-deoxyuridine (BrdU), serve similar roles in tracking DNA synthesis (Figure 3A). To determine

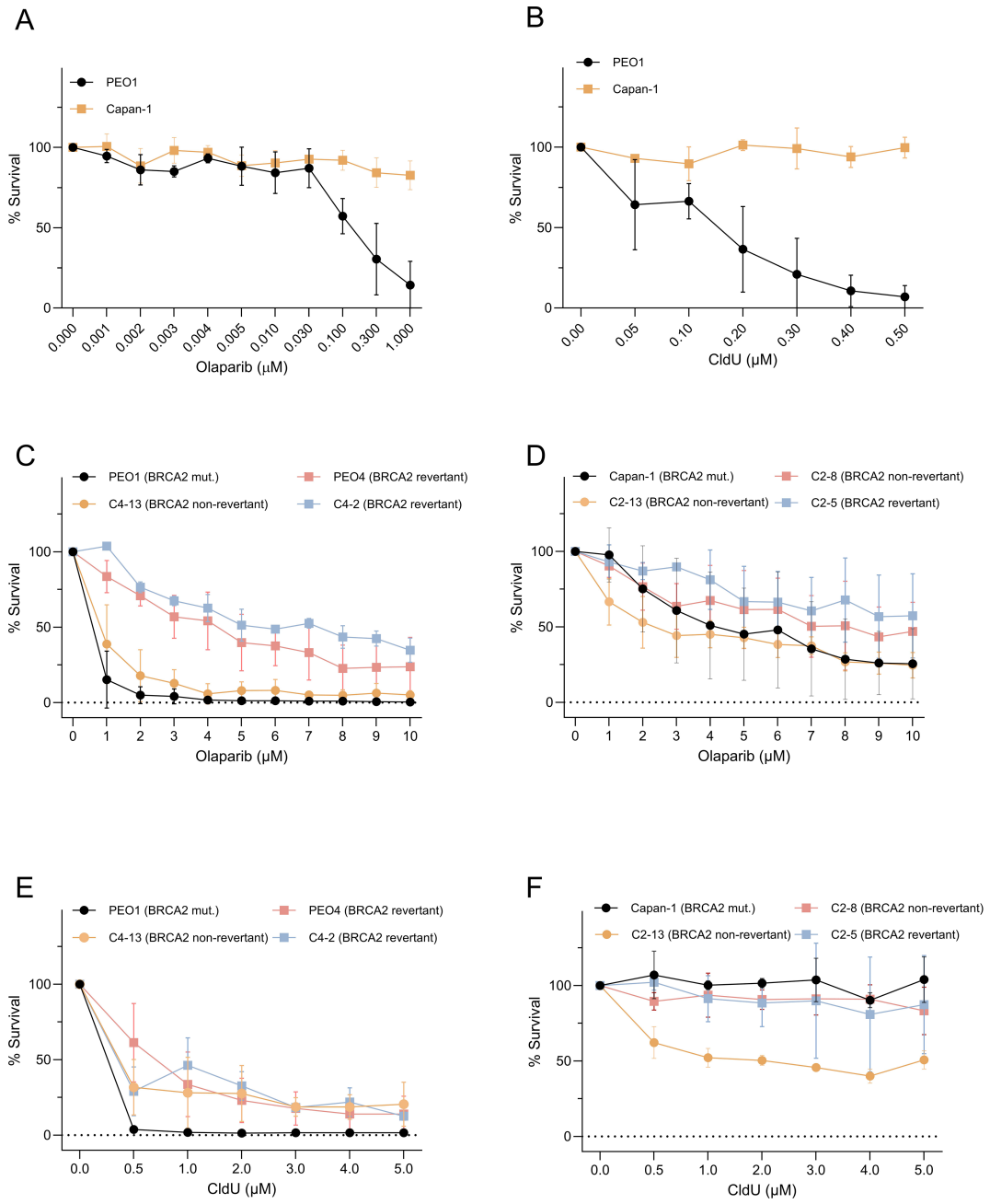

FIGURE 1
Clonogenic sensitivity to olaparib and CldU in BRCA2-mutant cancer cells and their PARPi-resistant derivatives. **(A, B)** Dose–response of BRCA2-deficient PEO1 and Capan-1 cells treated for 48 h with increasing concentrations of **(A)** the PARP inhibitor olaparib (0.0001–1 μM) or **(B)** chlorodeoxyuridine (CldU; 0.05–0.5 μM). Survival is expressed as percent of untreated control. **(C, D)** Olaparib sensitivity in BRCA2-mutant parental lines versus isogenic PARPi-resistant clones. **(C)** PEO1 (BRCA2-mutant) compared to C4-13 (non-revertant resistant) and two BRCA2-reversion derivatives (PEO4, C4-2). **(D)** Capan-1 (BRCA2-mutant) compared to C2-13 (non-revertant) and two BRCA2-reversion clones (C2-8, C2-5). **(E, F)** Corresponding clonogenic survival following 48 h CldU treatment in the same sets of PEO1-derived [**(E)** PEO1, PEO4, C4-2, C4-13] and Capan-1-derived [**(F)** Capan-1, C2-8, C2-13, C2-5] cell lines. In all panels, data are mean ± SD of three independent biological replicates; curves are normalized to untreated controls.

whether the observed synergy between CldU and PARPi is unique to CldU or shared among thymidine analogues, we evaluated the cytotoxic effects of olaparib (1 μM) in combination with thymidine or its analogues (CldU, BrdU, and EdU) at an equivalent concentration (0.5 μM) in PEO1 and PEO4 cell lines. Our results demonstrated that the synergistic interaction with olaparib was specific to CldU (Figures 3B-E and Supplementary Figure 3). In contrast, EdU exhibited intrinsic cytotoxicity across all conditions, independent of olaparib co-treatment (Figures 3B–E and Supplementary Figure 3). This result is consistent with a recent report showing that EdU induces DNA damage in mammalian cells, that is repaired by nucleotide excision repair (27). Neither

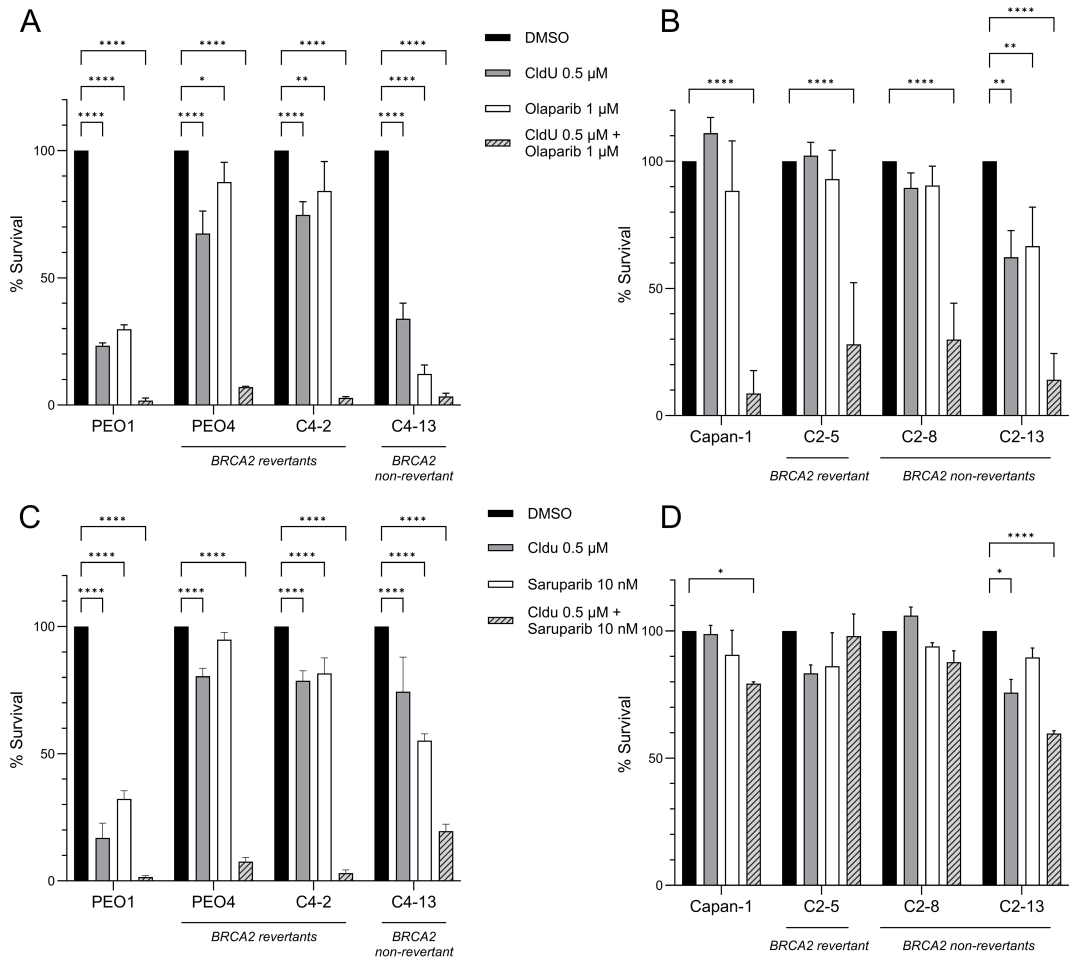

FIGURE 2
Synergistic cytotoxicity of CldU and PARP inhibitors in BRCA2-deficient and PARPi-resistant cell lines. **(A, B)** Clonogenic survival of parental BRCA2-mutant cells and their isogenic PARPi-resistant derivatives after 48 h treatment with vehicle (DMSO), CldU (0.5 µM), olaparib (1 µM), or the combination. **(A)** PEO1 (BRCA2-mutant), PEO4 and C4-2 (BRCA2-revertant resistant), and C4-13 (non-revertant resistant). Data are mean ± SD of three technical replicates from one representative experiment (n = 3 independent repeats). **(B)** Capan-1 (BRCA2-mutant), C2–5 and C2-8 (BRCA2-revertant resistant), and C2-13 (non-revertant resistant). Data are mean ± SD of three independent biological replicates. **(C, D)** Clonogenic survival of the same cell panels treated for 48 h with CldU (0.5 µM), the PARP-1 selective inhibitor saruparib (10 nM), or their combination. **(C)** PEO1 lineage (PEO1, PEO4, C4-2, C4-13); mean ± SD of three technical replicates from one representative experiment (n = 3). **(D)** Capan-1 lineage (Capan-1, C2-5, C2-8, C2-13); mean ± SD of three technical replicates from one representative experiment (n=3). Statistical significance was assessed using GraphPad Prism 10.5.0 software by two-way ANOVA with Tukey's multiple comparisons test. *P < 0.05, **P < 0.01, ***P < 0.001, ****P < 0.0001. In all panels, the striped bars (combination) reveal pronounced loss of clonogenic survival in both parental and PARPi-resistant clones, indicating strong synergy between CldU and either olaparib or saruparib.

thymidine nor BrdU alone, nor in combination with olaparib, exhibited significant cytotoxic effects. These findings suggest that the synergy between CldU and PARPi is not a general property of thymidine analogues, but rather a specific feature of CldU.

3.4 CldU combination with PARP inhibitor induce DNA damage

Finally, we sought to determine whether the combination of CldU and PARP inhibition induces DNA damage in *BRCA2*-mutant cancer cells. As expected, treatment with olaparib alone triggered DNA damage in PARP-sensitive PEO1 cells (Figure 4A). In contrast, olaparib monotherapy did not elicit substantial DNA damage in PARP-resistant PEO4 and C4–02 cells (Figure 4B and Supplementary Figure 4). Notably, co-treatment with CldU and olaparib resulted in marked DNA damage in these resistant cell lines (Supplementary Figure 4). Furthermore, the combination of CldU and olaparib induced early S-phase cell cycle arrest in both PEO1 and PEO4 cells (Supplementary Figure 4), consistent with replication stress-associated DNA damage. In parallel, EdU treatment led to DNA damage across all conditions (Figures 4A, B), independent of *BRCA2* status, underscoring its inherent cytotoxicity. Collectively, these findings demonstrate that CldU and olaparib cooperate to induce DNA damage in PARPi-resistant cells, supporting a synergistic mechanism of action.

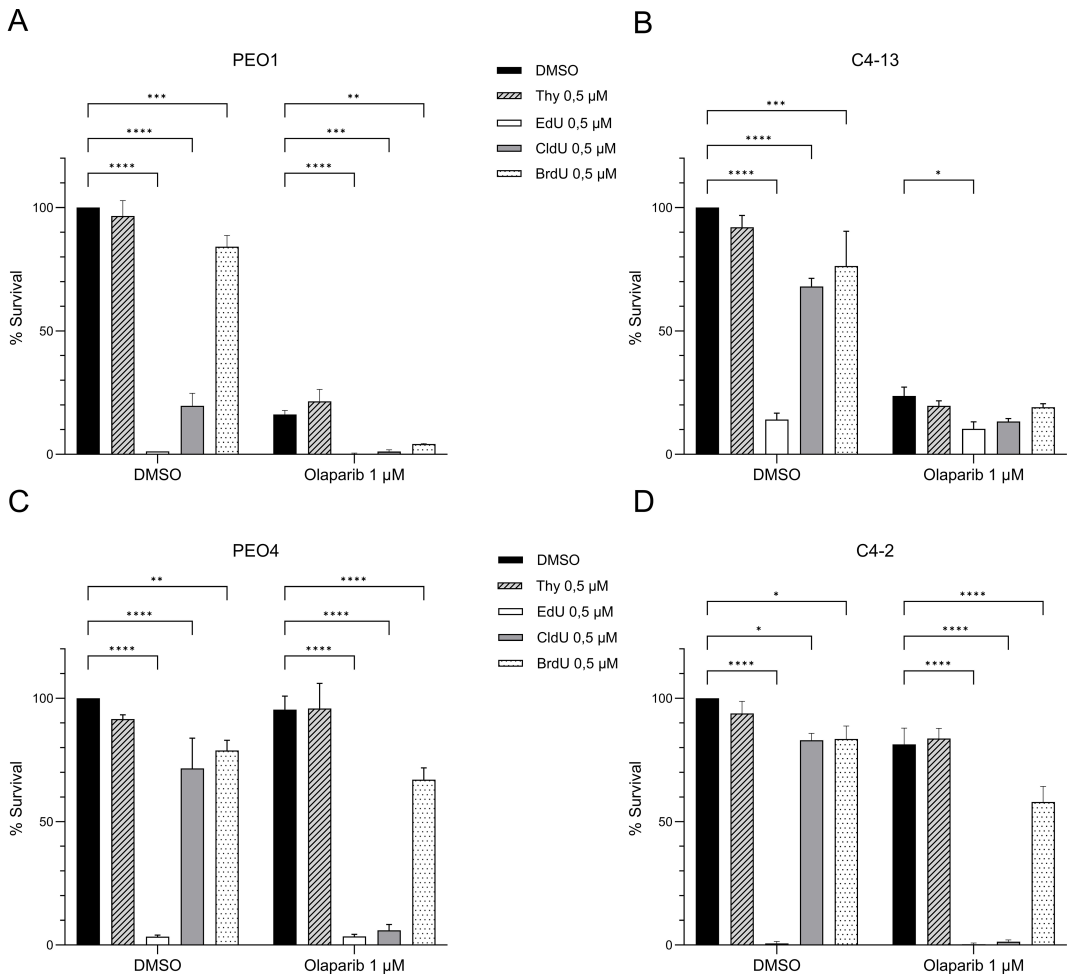

FIGURE 3
CldU is the most potent and selective thymidine analogue for synergizing with PARP inhibition. **(A–D)** Clonogenic survival of BRCA2-mutant PEO1 cells and isogenic derivatives following 48-hour treatment with thymidine analogues (Thymidine, EdU, CldU, or BrdU; 0.5 µM) alone or combined with olaparib (1 µM). **(A)** PEO1 parental cells. **(B)** C4-13 (PARPi-resistant, BRCA2 non-revertant). **(C)** PEO4 (PARPi-resistant, BRCA2-revertant). **(D)** C4-2 (PARPi-resistant, BRCA2-revertant). Data represent the mean ± SD of three technical replicates from one representative experiment (n=3). Statistical significance was assessed using GraphPad Prism 10.5.0 software by two-way ANOVA with Tukey's multiple comparisons test. *P < 0.05, **P < 0.01, ***P < 0.001, ****P < 0.0001. Experiments were repeated independently three times for panels **(A, C)**, and twice for panels **(B, D)**.

4 Discussion

PARP inhibitors (PARPi) have significantly advanced the treatment of cancers harboring *BRCA1* or *BRCA2* mutations by exploiting deficiencies in homologous recombination-mediated DNA repair. However, resistance to PARPi remains a major clinical challenge. Reversion mutations in *BRCA1/BRCA2*—observed in up to 80% of patients who develop resistance to PARPi—can restore protein function, thereby reinstating DNA repair capability and leading to therapeutic resistance and poor outcomes (16, 17). Strategies to overcome PARPi resistance are actively being explored. In this study, we demonstrate that the thymidine analogue chlorodeoxyuridine (CldU) sensitizes PARPi-resistant cancer cells to PARP inhibition. This cytotoxic effect is thought to result from the accumulation of single-stranded DNA gaps initiated by uracil DNA glycosylase-mediated base excision repair. When combined with PARPi-induced replication stress and compromised fork protection in *BRCA*-deficient cells, this leads to lethal levels of DNA damage. Notably, even cells harboring *BRCA* reversion mutations, which partially restore homologous recombination, remain sensitive to the combination of CldU and PARPi. This suggests that the mechanism of cytotoxicity may bypass conventional *BRCA*-mediated repair pathways. Although the exact mechanism of cell death remains to be fully elucidated, our findings point to a potentially novel vulnerability in PARPi-resistant cancers. Of note, we observed that the combination of CldU and olaparib was synergetic across all cell lines derived from both PEO1 and CAPAN-1, while the synergistic effect between saruparib and CldU in CAPAN-1 cells was less significant. Elucidating whether this is due to intrinsic differences in DNA repair between cell lines, replication stress response, or PARP trapping efficiency (26) need to be addressed in the future.

Importantly, while CldU is not approved for clinical use and is currently limited to research applications as a DNA synthesis

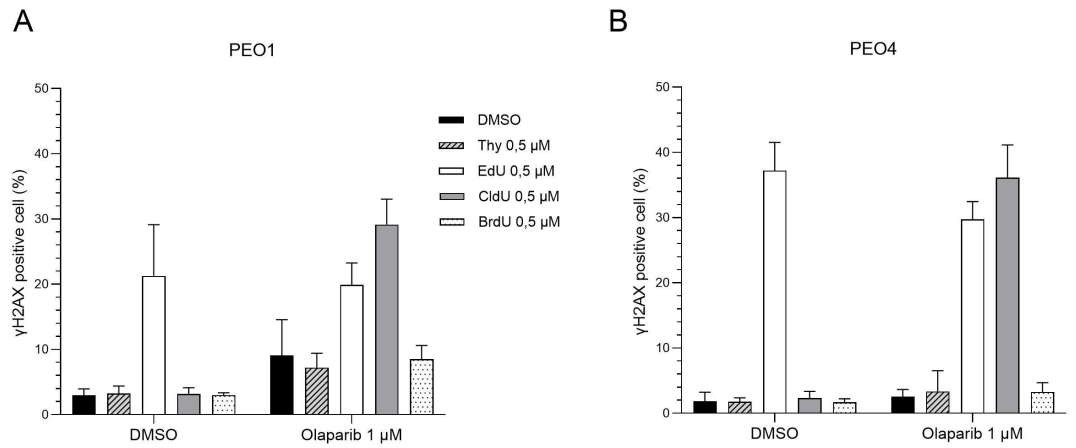

FIGURE 4
The chlorine group in CldU drives enhanced DNA damage in BRCA2-mutant cells under PARP inhibition. Quantification of γH2AX-positive cells (marker of DNA damage) by flow cytometry after 48-hour treatment with thymidine analogues (Thymidine, EdU, CldU, or BrdU; 0.5 μM), alone or combined with olaparib (1 μM). **(A)** PEO1 (BRCA2-mutant parental line). **(B)** PEO4 (PARPi-resistant, BRCA2-revertant). Data show the percentage of γH2AX-positive cells from three independent experiments. Increased DNA damage in CldU-treated groups highlights the role of the chlorine modification under PARP inhibition.

marker, clinically approved nucleoside analogues such as gemcitabine, cytarabine, and trifluridine share structural similarities. Some of these, particularly gemcitabine, have shown synergistic activity with PARPi in preclinical models of non-small-cell lung cancer (28) and in a clinical trial that enrolled pancreatic cancer patients (29). Next-generation antibody drug conjugates combining dual payloads that target DNA damage, for instance topoisomerase 1 inhibitor and PARPi, are currently investigated (30) and could be a therapeutic approach to reduce the toxicities of such combinations. Our work also confirmed that another thymidine analogue, EdU, is cytotoxic and induces DNA damage in mammalian cancer cells (27, 31), independent of *BRCA2* status. Overall, our findings prompt further investigation into nucleotide analogues for the treatment of PARPi-resistant cancers.

Data availability statement

The raw data supporting the conclusions of this article will be made available by the authors, without undue reservation.

Author contributions

NZ: Conceptualization, Formal analysis, Investigation, Methodology, Project administration, Visualization, Writing – original draft, Writing – review & editing. CT: Data curation, Formal analysis, Investigation, Methodology, Validation, Visualization, Writing – original draft. VD: Data curation, Project administration, Visualization, Writing – review & editing. WW: Data curation, Writing – review & editing. GR: Writing – original draft, Writing – review & editing, Data curation, Supervision, Conceptualization, Investigation, Visualization. TH: Conceptualization, Funding acquisition, Resources, Supervision, Writing – review & editing. IL: Conceptualization, Funding acquisition, Methodology, Project administration, Resources, Supervision, Validation, Writing – original draft, Writing – review & editing.

Funding

The author(s) declare financial support was received for the research and/or publication of this article. The study was supported by la ligue genevoise contre le cancer (#LGC-2205) and the Office of the Assistant Secretary of Defense for Health Affairs through the Ovarian Cancer Research Program under Award No. W81XWH-22-1-0558 to I.L.-G. Opinions, interpretations, conclusions, and recommendations are those of the author and are not necessarily endorsed by the Department of Defense.

Acknowledgments

The authors thank Prof. Toshiyasu Taniguchi, Tokai University School of Medicine, for giving access to cell lines established in his lab derived from CAPAN-1 (clones C2-5, C2–8 and C2-13) and PEO1 (clones C4–02 and C4-13).

Conflict of interest

The authors declare that the research was conducted in the absence of any commercial or financial relationships that could be construed as a potential conflict of interest.

Generative AI statement

The author(s) declare that no Generative AI was used in the creation of this manuscript.

Any alternative text (alt text) provided alongside figures in this article has been generated by Frontiers with the support of artificial intelligence and reasonable efforts have been made to ensure accuracy, including review by the authors wherever possible. If you identify any issues, please contact us.

Publisher's note

Supplementary material

The Supplementary Material for this article can be found online at: https://www.frontiersin.org/articles/10.3389/fonc.2025.1626301/full#supplementary-material

SUPPLEMENTARY FIGURE 1
Representative colony formation assays showing the effects of combined CldU and PARP inhibition on BRCA2-mutant and PARPi-resistant cell lines. **(A, B)** Representative images from clonogenic survival assays following 48-hour treatment with olaparib (1 μM) plus CldU (0.5 μM) in: **(A)** PEO1 (BRCA2-mutant) and its isogenic derivatives (PEO4, C4-2, C4-13) **(B)** Capan-1 (BRCA2-mutant) and its isogenic derivatives (C2-8, C2-13, C2-5) **(C, D)** Representative images from clonogenic survival assays following 48-hour treatment with saruparib (10 nM) plus CldU (0.5 μM) in: **(C)** PEO1 and its isogenic derivatives (PEO4, C4-2, C4-13) **(D)** Capan-1 and its isogenic derivatives (C2-8, C2-13, C2-5). For each condition, one well from triplicate experiments is shown.

SUPPLEMENTARY FIGURE 2
Effect of saruparib and CldU combination treatment on clonogenic survival in BRCA2-mutant and PARPi-resistant cell lines. Clonogenic survival of BRCA2-mutant PEO1 and Capan-1 cells, and their isogenic derivatives (PEO4, C4-2, C4-13, C2-5, C2-8, C2-13), after 48-hour treatment with saruparib alone (10 nM, 100 nM, or 1 μM) or in combination with CldU (0.5 μM). Data represent one experiment with a single well per treatment condition.

SUPPLEMENTARY FIGURE 3
Representative colony formation assays showing the effects of thymidine analogues combined with PARP inhibition. **(A)** Chemical structures of the thymidine analogues used in this study (sourced from PubChem, public domain). **(B–E)** Representative images from clonogenic survival assays following 48-hour treatment with thymidine analogues (Thymidine, EdU, CldU, or BrdU; 0.5 μM), alone or in combination with olaparib (1 μM), in: **(A)** PEO1 (BRCA2-mutant parental line) **(B)** C4-13 (PARPi-resistant, BRCA2 non-revertant) **(C)** PEO4 (PARPi-resistant, BRCA2-revertant) (D) C4-2 (PARPi-resistant, BRCA2-revertant). For each condition, one well from triplicate experiments is shown.

SUPPLEMENTARY FIGURE 4
Representative flow cytometry analysis of cell cycle distribution and DNA damage following treatment with thymidine analogues and PARP inhibition. **(A–D)** Representative flow cytometry plots showing cell cycle distribution and γH2AX staining after 48-hour treatment with thymidine analogues (Thymidine, EdU, CldU, or BrdU; 0.5 μM), alone or combined with olaparib (1 μM), in: **(A)** PEO1 (BRCA2-mutant parental line) **(B)** PEO4 (PARPi-resistant, BRCA2-revertant) **(C)** C4.13 (PARPi resistant, BRCA2 non-revertant) **(D)** C4.2 (PARPi resistant, BRCA2-revertant) Data represent the percentage of γH2AX-positive cells from one representative independent experiment.

SUPPLEMENTARY TABLE 1
statistical tests of Figure 2A. Test used: Two-way ANOVA with Tukey's multiple comparisons test.

SUPPLEMENTARY TABLE 2
statistical tests of Figure 2B. Test used: Two-way ANOVA with Tukey's multiple comparisons test.

SUPPLEMENTARY TABLE 3
statistical tests of Figure 2C. Test used: Two-way ANOVA with Tukey's multiple comparisons test.

SUPPLEMENTARY TABLE 4
statistical tests of Figure 2D. Test used: Two-way ANOVA with Tukey's multiple comparisons test.

References

1. Helleday T. The underlying mechanism for the PARP and BRCA synthetic lethality: clearing up the misunderstandings. *Mol Oncol.* (2011) 5:387–93. doi: 10.1016/j.molonc.2011.07.001

2. Farmer H, McCabe N, Lord CJ, Tutt AN, Johnson DA, Richardson TB, et al. Targeting the DNA repair defect in BRCA mutant cells as a therapeutic strategy. *Nature.* (2005) 434:917–21. doi: 10.1038/nature03445

3. Bryant HE, Schultz N, Thomas HD, Parker KM, Flower D, Lopez E, et al. Specific killing of BRCA2-deficient tumors with inhibitors of poly(ADP-ribose) polymerase. *Nature.* (2005) 434:913–7. doi: 10.1038/nature03443

4. Liptay M, Barbosa JS, Rottenberg S. Replication fork remodeling and therapy escape in DNA damage response-deficient cancers. *Front Oncol.* (2020) 10:670. doi: 10.3389/fonc.2020.00670

5. Serrano-Benitez A, Wells SE, Drummond-Clarke L, Russo LC, Thomas JC, Leal GA, et al. Unrepaired base excision repair intermediates in template DNA strands trigger replication fork collapse and PARP inhibitor sensitivity. *EMBO J.* (2023) 42: e113190. doi: 10.15252/embj.2022113190

6. Hussain M, Mateo J, Fizazi K, Saad F, Shore N, Sandhu S, et al. Survival with olaparib in metastatic castration-resistant prostate cancer. *N Engl J Med.* (2020) 383:2345–57. doi: 10.1056/NEJMoa2022485

7. Geyer CE Jr., Garber JE, Gelber RD, Yothers G, Taboada M, Ross L, et al. Overall survival in the OlympiA phase III trial of adjuvant olaparib in patients with germline pathogenic variants in BRCA1/2 and high-risk, early breast cancer. *Ann Oncol.* (2022) 33:1250–68. doi: 10.1016/j.annonc.2022.09.159

8. Poveda A, Floquet A, Ledermann JA, Asher R, Penson RT, Oza AM, et al. Olaparib tablets as maintenance therapy in patients with platinum-sensitive relapsed ovarian cancer and a BRCA1/2 mutation (SOLO2/ENGOT-Ov21): a final analysis of a double-blind, randomzsed, placebo-controlled, phase 3 trial. *Lancet Oncol.* (2021) 22:620–31. doi: 10.1016/S1470-2045(21)00073-5

9. Swisher EM, Lin KK, Oza AM, Scott CL, Giordano H, Sun J, et al. Rucaparib in relapsed, platinum-sensitive high-grade ovarian carcinoma (ARIEL2 Part 1): an international, multicenter, open-label, phase 2 trial. *Lancet Oncol.* (2017) 18:75–87. doi: 10.1016/S1470-2045(16)30559-9

10. Cecere SC, Giannone G, Salutari V, Arenare L, Lorusso D, Ronzino G, et al. Olaparib as maintenance therapy in patients with BRCA 1–2 mutated recurrent platinum sensitive ovarian cancer: Real world data and post progression outcome. *Gynecol Oncol*. (2020) 156:38–44. doi: 10.1016/j.ygyno.2019.10.023

11. Harter P, Marth C, Mouret-Reynier MA, Cropet C, Lorusso D, Guerra-Alia EM, et al. Efficacy of subsequent therapies in patients with advanced ovarian cancer who relapse after first-line olaparib maintenance: results of the PAOLA-1/ENGOT-ov25 trial. *Ann Oncol*. (2025) 36:185–96. doi: 10.1016/j.annonc.2024.10.828

12. Li H, Liu ZY, Wu N, Chen YC, Cheng Q, Wang J. PARP inhibitor resistance: the underlying mechanisms and clinical implications. *Mol Cancer*. (2020) 19:107. doi: 10.1186/s12943-020-01227-0

13. Sakai W, Swisher EM, Karlan BY, Agarwal MK, Higgins J, Friedman C, et al. Secondary mutations as a mechanism of cisplatin resistance in BRCA2-mutated cancers. *Nature*. (2008) 451:1116–20. doi: 10.1038/nature06633

14. Jaspers JE, Kersbergen A, Boon U, Sol W, van Deemter L, Zander SA, et al. Loss of 53BP1 causes PARP inhibitor resistance in Brca1-mutated mouse mammary tumors. *Cancer Discov*. (2013) 3:68–81. doi: 10.1158/2159-8290.CD-12-0049

15. Kim DS, Camacho CV, Kraus WL. Alternate therapeutic pathways for PARP inhibitors and potential mechanisms of resistance. *Exp Mol Med*. (2021) 53:42–51. doi: 10.1038/s12276-021-00557-3

16. Seed G, Beije N, Yuan W, Bertan C, Goodall J, Lundberg A, et al. Elucidating acquired PARP inhibitor resistance in advanced prostate cancer. *Cancer Cell*. (2024) 42:2113–2123 e4. doi: 10.1016/j.ccell.2024.10.015

17. Mweempwa A, Wilson MK. Mechanisms of resistance to PARP inhibitors - an evolving challenge in oncology. *Cancer Drug Resist*. (2019) 2:608–17. doi: 10.20517/cdr.2019.50

18. Gogola E, Duarte AA, de Ruiter JR, Wiegant WW, Schmid JA, de Bruijn R, et al. Selective loss of PARG restores PARylation and counteracts PARP inhibitor-mediated synthetic lethality. *Cancer Cell*. (2018) 33:1078–1093 e12. doi: 10.1016/j.ccell.2018.05.008

19. Kim D, Nam HJ. PARP inhibitors: clinical limitations and recent attempts to overcome them. *Int J Mol Sci*. (2022) 23:1–18. doi: 10.3390/ijms23158412

20. Konstantinopoulos PA, Barry WT, Birrer M, Westin SN, Cadoo KA, Shapiro GI, et al. Olaparib and alpha-specific PI3K inhibitor alpelisib for patients with epithelial ovarian cancer: a dose-escalation and dose-expansion phase 1b trial. *Lancet Oncol*. (2019) 20:570–80. doi: 10.1016/S1470-2045(18)30905-7

21. Mahdi H, Hafez N, Doroshow D, Sohal D, Keedy V, Do KT, et al. Ceralasertib-mediated ATR inhibition combined with olaparib in advanced cancers harboring DNA damage response and repair alterations (Olaparib combinations). *JCO Precis Oncol*. (2021) 5:1432–42. doi: 10.1200/PO.20.00439

22. Kim H, Xu H, George E, Hallberg D, Kumar S, Jagannathan V, et al. Combining PARP with ATR inhibition overcomes PARP inhibitor and platinum resistance in ovarian cancer models. *Nat Commun*. (2020) 11:3726. doi: 10.1038/s41467-020-17127-2

23. Zatreanu D, Robinson HMR, Alkhatib O, Boursier M, Finch H, Geo L, et al. Poltheta inhibitors elicit BRCA-gene synthetic lethality and target PARP inhibitor resistance. *Nat Commun*. (2021) 12:3636. doi: 10.1038/s41467-021-23463-8

24. Zhou J, Gelot C, Pantelidou C, Li A, Yucel H, Davis RE, et al. A first-in-class Polymerase Theta Inhibitor selectively targets Homologous-Recombination-Deficient Tumors. *Nat Cancer*. (2021) 2:598–610. doi: 10.1038/s43018-021-00203-x

25. Sakai W, Swisher EM, Jacquemont C, Chandramohan KV, Couch FJ, Langdon SP, et al. Functional restoration of BRCA2 protein by secondary BRCA2 mutations in BRCA2-mutated ovarian carcinoma. *Cancer Res*. (2009) 69:6381–6. doi: 10.1158/0008-5472.CAN-09-1178

26. Petropoulos M, Karamichali A, Rossetti GG, Freudenmann A, Iacovino LG, Dionellis VS, et al. Transcription-replication conflicts underlie sensitivity to PARP inhibitors. *Nature*. (2024) 628:433–41. doi: 10.1038/s41586-024-07217-2

27. Wang L, Cao X, Yang Y, Kose C, Kawara H, Lindsey-Boltz LA, et al. Nucleotide excision repair removes thymidine analog 5-ethynyl-2'-deoxyuridine from the mammalian genome. *Proc Natl Acad Sci U.S.A*. (2022) 119:e2210176119. doi: 10.1073/pnas.2210176119

28. Jiang Y, Dai H, Li Y, Yin J, Guo S, Lin SY, et al. PARP inhibitors synergize with gemcitabine by potentiating DNA damage in non-small-cell lung cancer. *Int J Cancer*. (2019) 144:1092–103. doi: 10.1002/ijc.31770

29. Bendell J, O'Reilly EM, Middleton MR, Chau I, Hochster H, Fielding A, et al. Phase I study of olaparib plus gemcitabine in patients with advanced solid tumors and comparison with gemcitabine alone in patients with locally advanced/metastatic pancreatic cancer. *Ann Oncol*. (2015) 26:804–11. doi: 10.1093/annonc/mdu581

30. Yin G, Calarese D, Yam A, Rubas W, Bajjuri K, Li X, et al., in: *Enhancing Topo1i ADC efficacy: development of homogeneous dual-payload ADCs combining Topo1i with microtubule inhibitors or PARP inhibitors in AACR annual meeting*, Cancer Res. Chicago (2025) 85(8_Supplement_1):2870. doi: 10.1158/1538-7445.AM2025-2870

31. Ross HH, Rahman M, Levkoff LH, Millette S, Martin-Carreras T, Dunbar EM, et al. Ethynyldeoxyuridine (EdU) suppresses *in vitro* population expansion and *in vivo* tumor progression of human glioblastoma cells. *J Neurooncol*. (2011) 105:485–98. doi: 10.1007/s11060-011-0621-6

Frontiers in Oncology

Advances knowledge of carcinogenesis and tumor progression for better treatment and management

The third most-cited oncology journal, which highlights research in carcinogenesis and tumor progression, bridging the gap between basic research and applications to imrpove diagnosis, therapeutics and management strategies.

Discover the latest Research Topics

See more →

Frontiers

Avenue du Tribunal-Fédéral 34
1005 Lausanne, Switzerland
frontiersin.org

Contact us

+41 (0)21 510 17 00
frontiersin.org/about/contact